การประกอบตัวเองและการเกิดผลึกของสตาร์ชข้าวตัดกิ่งในความสัมพันธ์กับการย่อยด้วยเอนไซม์

นางสาววรวิกัลยา เกียรติ์พงษ์ลาภ

วิทยานิพนธ์นี้เป็นส่วนหนึ่งของการศึกษาตามหลักสูตรปริญญาวิทยาศาสตรดุษฎีบัณฑิต
สาขาวิชาเทคโนโลยีอาหาร
มหาวิทยาลัยเทคโนโลยีสุรนารี
ปีการศึกษา 2557

SELF-ASSEMBLY AND CRYSTALLIZATION OF DEBRANCHED RICE STARCHES IN RELATION TO ENZYME DIGESTIBILITY

Worawikunya Kiatponglarp

A Thesis Submitted in Partial Fulfillment of the Requirements for the

Degree of Doctor of Philosophy in Food Technology

Suranaree University of Technology

Academic Year 2014

SELF-ASSEMBLY AND CRYSTALLIZATION OF DEBRANCHED RICE STARCHES IN RELATION TO ENZYME DIGESTIBILITY

Suranaree University of Technology has approved this thesis submitted in partial fulfillment of the requirements for the Degree of Doctor of Philosophy.

Thesis Examining Committee

_____
(Assoc. Prof. Dr. Jirawat Yongsawatdigul)
Chairperson

_____
(Asst. Prof. Dr. Sunanta Tongta)
Member (Thesis Advisor)

_____
(Prof. Dr. Alain Buléon)
Member

_____
(Asst. Prof. Dr. Supagorn Rugmai)
Member

_____
(Dr. Kuakoon Piyachomkwan)
Member

_____
(Prof. Dr. Sukit Limpijumnong)
Vice Rector for Academic Affairs and Innovation

_____
(Asst. Prof. Dr. Suwayd Ningsanond)
Dean of Institute of Agricultural Technology

วรวิกัลยา เกียรติ์พงษ์ลาภ : การประกอบตัวเองและการเกิดผลึกของสตาร์ชข้าวตัดกิ่งในความสัมพันธ์กับการย่อยด้วยเอนไซม์ (SELF-ASSEMBLY AND CRYSTALLIZATION OF DEBRANCHED RICE STARCHES IN RELATION TO ENZYME DIGESTIBILITY) อาจารย์ที่ปรึกษา : ผู้ช่วยศาสตราจารย์ ดร. สุนันทา ทองทา, 233 หน้า.

งานวิจัยนี้มีวัตถุประสงค์เพื่อพัฒนาความเข้าใจพื้นฐานของการเกิดผลึก และการประกอบตัวเองแบบสเฟียรูไลท์ของโพลิเมอร์แป้งในสารละลายน้ำ สตาร์ชข้าวจากข้าวไทยสี่สายพันธุ์ที่แตกต่างกันนำมาศึกษาการตัดกิ่ง การเกิดผลึกที่สภาวะอุณหภูมิคงที่ การเกิดผลึกที่สภาวะการรักษาความร้อนชื้น และการเกิดผลึกแบบสเฟียรูไลท์ในสารละลายน้ำ

สตาร์ชตัดกิ่งตกผลึกเป็นผลึกมวลรวม (polycrystalline aggregate) ภายใต้สภาวะอุณหภูมิคงที่ การเกิดผลึกที่ความเข้มข้นต่ำและอุณหภูมิต่ำสนับสนุนการก่อตัวของโครงสร้างผลึกชนิดบี (B-type) ในขณะที่การเกิดผลึกที่ความเข้มข้นสูงและอุณหภูมิสูงทำให้เกิดโครงสร้างผลึกชนิดเอ (A-type) ที่มีอุณหภูมิการหลอมเหลวที่สูงขึ้น (100-120 องศาเซลเซียส) และปริมาณแป้งต้านทานที่สูงขึ้น (ร้อยละ 52) การดัดแปรต่อมาด้วยการอบอ่อนหรือความร้อนชื้นแสดงให้เห็นการเพิ่มขึ้นของปริมาณแป้งต้านทาน ปริมาณผลึกสัมพัทธ์ และอุณหภูมิการหลอมเหลว แต่แสดงการลดลงในค่าเอนทาลปี นอกจากนั้น การดัดแปรด้วยความร้อนชื้นแสดงการเปลี่ยนแปลงโครงสร้างผลึกชนิดบีเป็นชนิดเอที่มีปริมาณผลึกสูงขึ้น ในทางตรงกันข้ามกับโครงสร้างผลึกชนิดบี ปริมาณผลึกร่วมชนิดเอลดลงโดยการดัดแปรด้วยการอบอ่อน ผลเหล่านี้ชี้ให้เห็นถึงการทำลายผลึกที่ไม่สมบูรณ์ การก่อตัวของผลึกใหม่ และการเจริญเติบโตหรือความสมบูรณ์ของนิวเคลียสหรือผลึกที่เกิดขึ้นในระหว่างการรักษาความร้อนชื้นที่มีผลในการเพิ่มการเกิดแป้งต้านทาน

พฤติกรรมการเกิดผลึกของสตาร์ชในช่วงการตัดกิ่งและการบ่มที่มีปริมาณของแข็งและอุณหภูมิแตกต่างกันได้ตรวจสอบโดยเทคนิคการกระเจิงรังสีเอกซ์มุมกว้างจากแหล่งกำเนิดแสงซินโครตรอนเชิงเวลา (Time-resolved synchrotron radiation wide-angle x-ray scattering) แบบจำลองสมการอัฟรามี (Avrami) นำมาใช้ในเพื่อวิเคราะห์ค่าพารามิเตอร์ของการเกิดผลึก ค่าเอ็กโปเนนเชียลเอ็นและค่าเค (exponent n and k) พบว่า การเกิดผลึกในช่วงการตัดกิ่งได้รับการสนับสนุนโดยสายโซ่ยาวพิเศษ และรูปแบบของการเกิดผลึกเป็นการเจริญเติบโตของผลึกลักษณะคล้ายแท่งยาว (rod-like) จากนิวเคลียสแบบกระจายไม่แน่นอน (sporadic nuclei) ในขณะที่การเกิดผลึกในช่วงการบ่มได้รับการสนับสนุนโดยสายโซ่สั้นที่มีการเจริญเติบโตของผลึกเป็นรูปทรงเรขาคณิตคล้ายแท่งยาวหรือคล้ายจาน (disc-like) เมื่อตกผลึกที่อุณหภูมิต่ำหรือสูงตามลำดับ

สุดท้ายได้ทำการศึกษาความสามารถของสตาร์ชตัดกิ่งในการประกอบเป็นสเฟียรูไลท์ สเฟียรูไลท์สมบูรณ์ที่แสดงลักษณะมอลทีสครอส (Maltese cross) พบในสตาร์ชตัดกิ่งซึ่งมีสัดส่วน

ของสายโซ่ยาวพิเศษสูง โดยอนุภาคเหมือนซินเตอร์ (sintered-like) ที่มีพื้นผิวหยาบ มีลักษณะไบรฟริงเจนท์แบบบวก (positive birefringence) และการจัดเรียงสายโซ่ในแนวรัศมี (radial orientation) เกิดจากสตาร์ชตัดกิ่งอะมิโลสสูง สเฟียรูไลท์ขนาดใหญ่ที่มีพื้นผิวเรียบ มีไบรฟริงเจนท์แบบลบ (negative birefringence) และการจัดเรียงสายโซ่ในแนววง (tangential orientation) สร้างจากสตาร์ชตัดกิ่งข้าวเหนียว สเฟียรูไลท์ทั้งสองชนิดแสดงโครงสร้างผลึกชนิดบีที่มีปริมาณผลึกสูงและมีพฤติกรรมการหลอมเหลวแบบเดียวกัน อย่างไรก็ตาม สเฟียรูไลท์จากสตาร์ชตัดกิ่งข้าวเหนียวแสดงการต้านทานการย่อยจากเอนไซม์สูงกว่าสเฟียรูไลท์จากสตาร์ชตัดกิ่งอะมิโลสสูงซึ่งอาจสัมพันธ์กับการจัดเรียงสายโซ่ในแนววง ความแน่นและความเรียบของพื้นผิวของสเฟียรูไลท์

สาขาวิชาเทคโนโลยีอาหาร
ปีการศึกษา 2557

ลายมือชื่อนักศึกษา_____
ลายมือชื่ออาจารย์ที่ปรึกษา_____
ลายมือชื่ออาจารย์ที่ปรึกษาร่วม_____

WORAWIKUNYA KIATPONGLARP : SELF-ASSEMBLY AND CRYSTALLIZATION OF DEBRANCHED RICE STARCHES IN RELATION TO ENZYME DIGESTIBILITY. THESIS ADVISOR : ASST. PROF. SUNANTA TONGTA, Ph.D., 233 PP.

CRYSTALLIZATION/SELF-ASSEMBLY/DEBRANCHED STARCH/RESISTANT STARCH/SPHERULITES

The purpose of this research was to develop a fundamental understanding of the crystallization and spherulitic self-assembly of starch polymers in aqueous solution. The rice starches from four different Thai rice varieties were used to study debranching, isothermal crystallization, hydrothermal crystallization and spherulitic crystallizations in aqueous solution.

Debranched starch was crystallized into polycrystalline aggregates under isothermal crystallization. The crystallization at low concentration and low temperature favored the formation of B-type structure, whereas the crystallization at high concentration and high temperature led to an A-type structure with a higher melting temperature (100-120 °C) and higher resistant starch (RS) content (52%). Subsequent annealing or heat moisture treatment (HMT) showed an increased RS content, relative crystallinity and melting temperatures, but decreased enthalpy. Furthermore, HMT showed a transition from B to A-type structure with a higher crystallinity. In contrast to B-type crystallinity, the coexisted A-type crystallinity was reduced by annealing. These suggested the disruption of imperfect crystallites, the formation of new crystallites and growth or perfection of nuclei/crystallites formed during

hydrothermal treatment resulting in the enhancement of RS formation.

Crystallization behavior of starches during debranching and incubation with different solid contents and temperatures was investigated using time-resolved synchrotron radiation wide-angle x-ray scattering. The Avrami model was applied to determine the crystallization parameters, *n* and *k*. It was found that crystallization during debranching was favored by extra-long chains and the mode of crystallization was rod-like growth from sporadic nuclei, whereas crystallization during incubation was favored by short chains with a preferential growth into rod-like or disc-like geometry when crystallization at low or high temperature respectively.

Finally, the ability of debranched starches to form spherulites was investigated. Well-formed spherulites exhibiting a Maltese cross pattern were obtained in debranched starches which contained a high proportion of extra-long chains. Sintered-like particles with rough surface, positive birefringence and radial orientation were formed in debranched high-amylose rice starches (DBCN1). Larger spherulites with smooth surface, negative birefringence and tangential orientation were obtained in debranched waxy starch (DBRD6). Both spherulites showed a B-type crystalline structure with an exceptionally high crystallinity and a similar melting behavior. However, DBRD6 spherulites exhibited higher resistance to enzymatic hydrolysis than DBCN1 spherulites. This probably associated with tangential orientation, compactness and smooth surface of spherulites.

School of Food Technology Student's Signature_____

Academic Year 2014 Advisor's Signature_____

Co-advisor's Signature_____

ACKNOWLEDGEMENTS

First of all, I express my gratitude to my advisor Asst. Prof. Dr. Sunanta Tongta, who along with teaching me a great deal about starch chemistry and technology, also contributed significantly towards my overall professional development. Her guidance, patience and encouragement throughout my doctoral work are instrumental in its completion. Without her contribution, this thesis would not have achieved and completed.

I also wish to express my gratitude towards Prof. Alain Buléon, Biopolymères Interaction Assemblages (BIA), INRA, Nantes, France for giving me a wonderful opportunity to learn more about crystallization and crystalline structures in starch, for being able to work with his research group and for serving as my co-advisor. His inputs and support were critical in the successful completion of this work.

I am grateful to Asst. Prof. Dr. Supagorn Rugmai and Dr. Siriwat Soontaranon from BL1.3W beamline, Synchrotron Light Research Institute, Thailand for all the invaluable assistance and guidance on Synchrotron SAXS and WAXS measurements.

I warmly thank Dr. Agnès Rolland-Sabaté, BIA-INRA, Nantes, France for her excellent guidance and invaluable help in starch structure analysis. Many thanks go to Dr. Cedric Gaillard, BIA-INRA, Nantes, France for his assistance in AFM and TEM studies, Bruno Pontoire for helping with WAXD and SAXS analysis, Sophie Guilois for kind assistance with chromatography experiments, Anne-Laure Reguerre, and Marion de Carvalho for their assistance in the BIA-MC2 lab and Dr. Nicolas Stephant from Jean Rouxel Institute of Materials at University of Nantes for the use of SEM instrument.

I also express my gratitude towards Assoc. Prof. Dr. Jirawat Yongsawadigul and Dr. Kuakoon Piyachomkwan for their comments and invaluable suggestions and for serving on my committee.

I would like to thank Udonthani Rice Research Centre under Bureau of Rice Research and Development (BRRD), Thailand for raw material support.

Furthermore, I would like to thank the Royal Golden Jubilee (RGJ) Ph.D. program (Grant No. PHD/0197/2551) and the French Embassy, Thailand for funding support. I am also thankful for Suranaree University of Technology, Biopolymères Interaction Assemblages (BIA), INRA, Nantes, France and Synchrotron Light Research Institute, Thailand for supporting the laboratory facilities.

I would like to acknowledge a number of friends and colleagues, without whom, this experience would have not been incomplete. First, special thanks to my friends at the Suranaree University of Technology, who have made my life and study here an unforgettable experience. Special thanks to all members of Asst. Prof. Dr. Sunanta Tongta and all members of BIA-MC2 and BIA-NANO for their assistance, thier friendship and excellent working atmosphere.

Finally, my most important acknowledgments are towards my families who have been the single biggest motivating force in my life. I thank my parents, my sister, my brother and my husband for their encouragement, advice and for the many sacrifices. This dissertation is dedicated to them.

Worawikunya Kiatponglarp

CONTENTS

CONTENTS (Continued)

Page

CONTENTS (Continued)

Page

CONTENTS (Continued)

Page

CONTENTS (Continued)

Page

CONTENTS (Continued)

Page

LIST OF TABLES

LIST OF FIGURES

LIST OF FIGURES (Continued)

Figure **Page**

LIST OF FIGURES (Continued)

Figure **Page**

LIST OF FIGURES (Continued)

Figure **Page**

LIST OF FIGURES (Continued)

Figure **Page**

LIST OF FIGURES (Continued)

Figure **Page**

LIST OF FIGURES (Continued)

Figure **Page**

LIST OF FIGURES (Continued)

Figure **Page**

LIST OF FIGURES (Continued)

Figure **Page**

LIST OF ABBREVIATIONS

ΔH	=	Enthalpy
2θ	=	Bragg's angle
α	=	Thickness for the alternating crystalline
Å	=	Angstrom
ACC	=	Apparent amylose
AE	=	Amylose equivalent
AFM	=	Atomic force microscopy
Ann	=	Annealing
ANOVA	=	Analysis of variance
°C	=	Degree celsius
CL	=	Average chain length
CN1	=	Chainat1
D	=	Bragg distance
db.	=	Dry basis
DBCN1	=	Debranched starch from Chainat1 rice starch
DBPS1	=	Debranched starch from Phitsanulok1 rice starch
DBPS2	=	Debranched starch from Phitsanulok2 rice starch
DBRD6	=	Debranched starch from RD6 rice starch
DP	=	Degree of polymerization
DP_{max}	=	The maximum degree of polymerization
DP_n	=	The number-average degree of polymerization

LIST OF ABBREVIATIONS (Continued)

DP_w	=	The weight-average degree of polymerization
DSC	=	Differential scanning calorimetry
ECL	=	Average external chain length
ELC	=	Extra-long chains
g	=	Gram
GPC	=	Gel permeation chromatography
h	=	Hour
ΔH	=	Enthalpy
ΔH_T	=	Total enthalpy
HMT	=	Heat moisture treatment
HPAEC-PAD	=	High-performance anion exchange chromatography with pulsed amperometric detection
HPSEC-MALLS-DRI	=	High-performance size-exclusion chromatography coupled to multiangle laser light scattering and differential refractive index detection
HT	=	High temperature
IAU	=	Isoamylase activity unit
K	=	Rate constant of crystallization ($time^{-1}$)
λ_{max}	=	Maximum wave length
L	=	Litter
LC	=	Long chains
L_{crl}	=	Crystalline lamella thickness

LIST OF ABBREVIATIONS (Continued)

LT	=	Low temperature
M	=	Molar
mM	=	Millimolar
mL	=	Milliliter
μL	=	Microlitter
min	=	Minute
mg	=	Milligram
nm	=	Nanometer
MW	=	Molecular weight
n	=	Avrami exponent
nm	=	Nanometer
P	=	Polydispersity index
PS1	=	Phitsanulok1
PS2	=	Phitsanulok2
RDS	=	Rapidly digested starch
r^2	=	Coefficient of determination
RS	=	Resistant starch
RS_1	=	Resistant starch type I
RS_2	=	Resistant starch type II
RS_3	=	Resistant starch type III
RS_4	=	Resistant starch type IV
SAXS	=	Small angle X-ray scattering

LIST OF ABBREVIATIONS (Continued)

SC	=	Short chains
SCLCP	=	Side-chain liquid-crystalline polymer
SDS	=	Slowly digestible starch
SEM	=	Scanning electron microscopy
$t_{1/2}$	=	Haft-time of crystallization
T_g	=	Glass transition temperature
T_m	=	Melting temperature
T_{p1}	=	The main endothermic peaks
T_{p2}	=	The second endothermic peak
T_o	=	Onset temperature
WAXD	=	Wide Angle X-ray diffraction
WAXS	=	Wide-angle x-ray scattering
w/v	=	Weight: volume
X(t)	=	The normalized crystallinity
$X_{c\infty}$	=	The maximum crystallinity at the end of incubation period
X_{c0}	=	The crystallinity at time 0
X_{ct}	=	The crystallinity at time t
σ	=	Mean square deviation

CHAPTER I

INTRODUCTION

1.1 Background and significance of the study

Starch is the most abundant food biopolymer which is the main source of energy in both human diet and animal feed. Starch consists mainly of two carbohydrate polymers, amylose and amylopectin, that differ in molecular size and degree of branching. Amylose is essentially linear with a few relatively long branches (less than 1%) whereas amylopectin is highly branched macromolecule consisting of 5–6% α-(1, 6) linkages (Buléon, Colonna, Planchot and Ball, 1998). There is more amylopectin than amylose in normal starch granules. Chain length and branching characteristics are major parameters in determining functional and physical properties of starch (Hoover, 2001). Starch is a very useful biomaterial which is used in a wide range of food and non-food (pharmaceutics, papers, adhesives, packaging, biofuels, etc) applications (Ellis et al., 1998). Since the starch generally has a granular structure, most use of starch requires the disruption or modification of the starch granules through chemical, enzymatic and/or hydrothermal treatments (Buléon and Colonna, 2007; Singh, Kaur and McCarthy, 2007). The enzymatic and hydrothermal treatments, which are optimized in order to improve functional characteristics of starch, can be used to tailor starch to specific food application. This leads to achieve specific textures of food (consistency, softness, or crispness), to design biodegradable materials with suitable mechanical properties, and to optimize the susceptibility to

to enzymatic hydrolysis by amylases, in terms of nutritional quality, biodegradability, or ferment ability (Buléon, Véronèse and Putaux, 2007). An interest in understanding the relationships between digestion of starch and its impacts on human health is growing (Aarathi, Urooj and Puttaraj, 2003; Parada and Aguilera, 2009). The fundamental knowledge with respect to the relationship of starch structure and digestion is of particular interest to the food industry and has been reviewed in the literature. Despite its relatively extensive researches, it is necessary to better understand the unique properties of this complex biopolymer in order to more efficiently utilize the available starch resource e.g. rice which is abundant natural resources in Thailand and has more than 80 rice varieties with difference in structural and physicochemical properties. Since the structure and components of starches are found to be diverse at different structural levels, depending on its botanic origin, the research in this area is still continuously conducted for many years due to its complexity. Understanding of the roles of structural parameters on unique phenomenon such as self-assembly and crystallization is of fundamental importance necessary for the development of new starch-based products and further improvement of current starch processing technology.

Starch crystallization, which follows starch gelatinization, is a non-equilibrium process as well known as retrogradation. It occurs when an aqueous starch solution is cooled or the water evaporated. The crystallization of starch gel is attributed to gelation involving phase separation of the polymers to form a network structure and crystallization of amylose fraction and subsequent crystallization of amylopectin fraction during storage (Miles, Morris and Ring, 1985; Sievert and Wursch, 1993). However, crystallization can occur without gelation, and phase separation can occur

without crystallization or gel network formation that is described as liquid-liquid demixing (Creek, Ziegler and Runt, 2006). Starch and amylose could be crystallized into A, B, and V crystalline forms with various morphologies (gel, precipitates, aggregates, crystal, spherulites, etc) which depend on factors such as solvent, molecular weight, branching, concentration, or temperature (Buléon et al., 2007; Conde-Petit, Handschin, Heinemann and Escher, 2007; Nordmark and Ziegler, 2002a; Shamai, Bianco-Peled and Shimoni, 2003). The structural features of recrystallized starch such as the morphology and crystal structure, further influences the thermal stability and physiological functionality.

One of starch crystallization technology was applied to produce a functional starch called resistant starch type III, a starch derivative whose physiological activity resembles that of dietary fibers. RS is desirable for the human diet because of its prebiotic effects and associated health benefits for the colon (Fuentes-Zaragoza, Riquelme-Navarrete, Sánchez-Zapata and Pérez-Álvarez, 2010; Haralampu, 2000; Topping and Clifton, 2001). It is also considered to be beneficial for the dietary management of metabolic and lifestyle disorders, including obesity, type-II diabetes and hyperlipidemia (Akerberg, Liljeberg and Bjorck, 1998; Brennan, 2005; Dongowski, Jacobasch and Schmiedl, 2005; Lynch et al., 2007; Wisker, 2000; Yin et al., 2004). It is generally accepted that RS type III contains mainly retrograded amylose which requires an amylose chain length of 10 - 35 glucose units to form heat-stable and butyrogenic RS (Eerlingen, Deceuninck and Delcour, 1993; Lehmann, Jacobasch and Schmiedl, 2002; Schmiedl, Bäuerlein, Bengs and Jacobasch, 2000). Therefore, RSIII is generally produced from native starch by gelatinization, debranching, followed by crystallization process (isothermal, or hydrothermal

treatments, i.e., autoclaving-cooling cycles and temperature cycling. Enzymatic debranching using pullulanase or isoamylase has been applied to produce linear starch chains, providing for more mobility of chains and ordered alignment; thus, the chains aggregate into perfectly crystalline structures (Cai, Shi, Rong and Hsiao, 2010; Ozturk, Koksel, Kahraman and Ng, 2009). The properties of RS from debranched product are dependent on the chain length distribution, the degree of debranching, and the debranching and crystallization conditions. Crystallized debranched products from amylose-containing starch generally have better thermal stability than those from waxy rice starch; however, the broad chain length distribution of debranched products containing amylose inhibits the formation of products with low crystallinity (Birkett, Cui, Shi and Thatcher, 2006). High concentration, high temperature, and short chains are known to induce A-type crystallization, whereas low concentration, low temperature and long chains favor the formation of B-type crystals (Buléon et al., 2007; Cai and Shi, 2014). Consequently, a variety of ordered structures are formed, depending on the predominant crystallization process, the molecular conformation, intermolecular associations or a combination of these factors, which, in turn, impact the thermal stability and the enzyme susceptibility of the RS (Cai and Shi, 2010; Cai et al., 2014). However, there is limited available information regarding structural properties and starch digestibility deriving from the combined effects of crystallization conditions. It still needs for information on the combination of factors affecting starch crystallization and the relationship between the properties of resulting products and RS formation.

More recently, it has been demonstrated that starch, amylose and short amylose chain can form spherulites on crystallization from a high concentrated

aqueous solution (Cai and Shi, 2013; Creek et al., 2006; Nordmark et al., 2002a; Nordmark and Ziegler, 2002b; Singh, Lelane, Stewart and Singh, 2010; Ziegler, Creek and Runt, 2005; Ziegler, Nordmark and Woodling, 2003) or on the formation of helical amylose inclusion complexes with small ligands (Conde-Petit et al., 2007; Fanta, Felker, Shogren and Salch, 2006; Fanta, Felker, Shogren and Salch, 2008; Heinemann, Escher and Conde-Petit, 2002; Shogren, Fanta and Felker, 2006). The spherulitic crystallization of native starches was obtained when aqueous starch dispersions were heated to 160-180 °C, which was termed "clearing temperature" (Creek et al., 2006), followed by rapid cooling. This mode of spherulitic crystallization has been proposed as a model for in-vivo starch granule initiation (Ziegler et al., 2005). On the other hand, spherulitic crystallization occurred during the slow cooling of amylose-ligand mixtures after heating at 140 °C (Fanta, Felker and Shogren, 2002; Shogren et al., 2006) and the process has been termed 'high temperature retrogradation' (Davies, Miller and Procter, 1980). There are many factors can affect the spherulitic crystallization of starch. For example, Ziegler el al. (2003) reported that a heating treatment above 170 °C and fast cooling are necessary for the formation of well developed round spherulites. Creek el al. (2006) hypothesized that this temperature is necessary to go through a helix → coil transition in order to avoid gel formation during cooling caused by the presence of helical nuclei. Spherulite formation also depends on the starch source (Ziegler et al., 2003), amylose concentration (Ma, Floros and Ziegler, 2011; Singh et al., 2010), cooling rate and quench temperature (Ziegler, Creek and Runt, 2005; Creek et al., 2006). Well-developed starch spherulites were found to be easily formed in mung bean starch, potato starch, acid modified maize starch and high amylomiaze starch, respectively

(Ziegler et al., 2003). Similarly, Ma et al. (2011) reported that a higher ratio of amylose to amylopectin resulted in the formation of large amount of spherulites and better developed spherulites. These authors reported that spherulite formation is favored by linear material (amylose) and that spherulites were practically absent in amylopectin samples (waxy maize). Nordmark and Ziegler (2002a) suggested that the lightly branched intermediate material may be ideal for spherulite formation. However, the spherulite formation from debranched starch which contains essentially linear glucan chains has never been studied. The study on molecular structure of debranched starch, such as chain length distribution influencing on the spherulitic crystallization is of interesting and perhaps surprising issues.

In terms of spherulites morphology, two different spherulites morphologies i.e. large spherical/lobed and small torus/disc shape particles were obtained, depending on starch concentration, fatty acid, pH of the dispersion and cooling condition (Bhosale and Ziegler, 2010; Byars, Fanta and Felker, 2003; Fanta et al., 2006; Heinemann, Escher and Conde-Petit, 2003). Heinemann et al. (2003) reported that these types of spherulites are slowly hydrolyzed at low concentrations of α-amylase, while breakdown of spherulites occurs at high α-amylase concentration. Bhosale and Ziegler (2010) reported that resistant starch content of spherulites from the two spherulitic morphologies, i.e. spherical and torus was 28% and 39%, respectively. Therefore, the spherulites can be slowly degraded in the mouth and slowly degraded in the gastrointestinal tract. The investigations of spherulites morphology and their crystal, thermal and enzymatic digestibility will be included to provide a basis for future investigation of end-use applications.

The crystallization of starch in micromaterials creates the innovative solutions that have a potential to generate radically new products and processes. The starch micro- and nanoparticles could be use as a filler to improve mechanical and barrier properties of biocomposites (Le Corre, Bras and Dufresne, 2010). Another innovation of starch is its application in the encapsulation technology of controlled release which more effectively and efficiently delivers nutrients, proteins and antioxidants to the body. In the future, food will not only need to be a good source of nutrient with good sensory appeal, but also need to contribute to well-being of individuals. It has a significant role for the development of functional food industry which targets a delivery of food components that have an impact on health status of consumers. Understanding the self-assembly characteristic of starch into micromaterials is essential and it is a requirement to control bioaccessibility of target release food component during gastrointestinal transit, whilst maintaining food texture, structure and sensory appeal.

1.2 Research objectives

The objectives of this study were:

1. To investigate the combined effects of polymer chain length, solid concentration and incubation temperature on resistant starch formation and their physicochemical properties from four different debranched rice starches.

2. To study the effects of hydrothermal treatments on improving resistant starch content and thermal property.

3. To investigate the effect of crystallization conditions (chain length distribution, concentration and temperature) on crystallization behaviors during debranching and incubation.

4. To develop and refine the understanding of the factors responsible for the formation of spherulites from the debranched starch in aqueous solution.

5. To characterize the crystal structure, morphology, physical properties and enzyme digestibility of spherulite.

1.3 Research hypotheses

The debranched starch with high proportion of extra long chain may slow starch digestibility and give a significant RSIII yield in which the relative long chains involve in double helices and provide a high thermal stability. Recrystallized polycrystalline aggregates with A-type crystalline structure are more compact morphology and more resistant to enzymatic digestion than that of B-type crystalline structure. Differences in chain length distribution, concentration and temperatures can change the nucleation processes, crystal growth mechanism and kinetics of development of starch crystallites during debranching and incubation. Completely debranched starch with containing a high proportion of extra long chains is essential for the formation of spherulites. Difference in chain length distribution of debranched starch and crystallization conditions (cooling rate) led to different spherulitic morphologies, probably related to different self-assembly mechanism. Furthermore, the resulting spherulites are resistant to enzymatic digestion and exhibit controlled enzyme digestibility.

1.4 Scope of the study

1.4.1 Preparation and characterization of debranched starch from rice starch from four Thai rice varieties. Debranched starches were obtained by debranching using isomylase at 50 °C for 24 h. The molecular structure of debranched starches was characterized in degree of hydrolysis, beta-amylolysis limit, the chain length distribution using high-performance size-exclusion chromatography coupled to multiangle laser light scattering and differential refractive index detection (HPSEC-MALLS-DRI) and high-performance anion exchange chromatography with pulsed amperometric detector system (HPAEC-PAD).

1.4.2 The effects of chain length distribution, concentration and crystallization temperature on crystallization behavior were studied in relation to resistant starch formation. The effects of each factor and the combined factors on RS formation were investigated using statistic analysis. Subsequent hydrothermal treatments, annealing and heat moisture treatment (HMT), were used to improve the resistant starch quantity and quality. The resistant starch content and its properties were compared to that untreated sample. Differential scanning calorimetric (DSC), Wide Angle X-ray diffraction (WAXD), Scanning electron microscopy (SEM) and will be utilized to describe the crystalline and microstructure of resistant starch.

1.4.3 Isothermal crystallization behavior during debranching and incubation was studied by an in-situ synchrotron radiation wide-angle x-ray scattering (WAXS). The Avrami model was used to study the kinetics of crystallization.

1.4.4 Spherulitic crystallization from completely debranched starch in concentrated aqueous solution was investigated. The effect of chain length distribution and cooling rate on the formation and characteristics of spherulites was

examined. The formation of spherulite was assessed using optical light microscopy. DSC, SEM, XRD, synchrotron SAXS and AFM techniques will be utilized to describe the micro- and nanostructure of spherulites. The resistant starch content and alpha-amylolytic hydrolysis was also analyzed to provide a basis for future investigation of the end-use application. In addition, the morphology and crystalline structure of resulting spherulites was studied in relation to enzyme digestibility.

1.5 Expected results

Results from this research will lead to develop a fundamental, quantitative understanding of the crystallization behavior of both aggregation and spherulitic crystallization of different molecular structures on the micro- and nanostructure, as a biologically-inspired material with applications in the food and pharmaceutical industries. Regarding fundamental knowledge, it will contribute a better understanding of the fine structure of the A- and B-allomorph in crystalline starch and will lead to more understanding of spherulite formation in polymers.

1.6 References

Aarathi, A., Urooj, A., and Puttaraj, S. (2003). In vitro starch digestibility and nutritionally important starch fractions in cereals and their mixtures. **Starch-Stärke.** 55(2): 94-99.

Akerberg, A., Liljeberg, H., and Bjorck, I. (1998). Effects of amylose/amylopectin ratio and baking conditions on resistant starch formation and glycaemic indices. **Journal of Cereal Science.** 28(1): 71-80.

Bhosale, R. G. and Ziegler, G. R. (2010). Preparation of spherulites from amylose–

palmitic acid complexes. **Carbohydrate Polymers.** 80(1): 53-64.

Birkett, A. M., Cui, X., Shi, Y-C., and Thatcher, M. G. (2006). Resistant starch prepared by isoamylase debranching of low amylose starch. **CA Patent No. 2,428,514.**

Brennan, C. S. (2005). Dietary fibre, glycaemic response, and diabetes. **Molecular Nutrition and Food Research.** 49(6): 560-570.

Buléon, A. and Colonna, P. (2007). Physicochemical Behaviour of Starch in Food Applications **The Chemical Physics of Food** (pp. 20-67): Blackwell Science Ltd.

Buléon, A., Colonna, P., Planchot, V., and Ball, S. (1998). Starch granules: structure and biosynthesis. **International Journal of Biological Macromolecules.** 23(2): 85-112.

Buléon, A., Véronèse, G., and Putaux, J. (2007). Self-Association and Crystallization of Amylose. **Australian Journal of Chemistry.** 60(10): 706-718.

Byars, J. A., Fanta, G. F., and Felker, F. C. (2003). The effect of cooling conditions on jet-cooked normal corn starch dispersions. **Carbohydrate Polymers.** 54(3): 321-326.

Cai, L. and Shi, Y-C. (2010). Structure and digestibility of crystalline short-chain amylose from debranched waxy wheat, waxy maize, and waxy potato starches. **Carbohydrate Polymers.** 79(4): 1117-1123.

Cai, L. and Shi, Y-C. (2013). Self-Assembly of Short Linear Chains to A- and B-Type Starch Spherulites and Their Enzymatic Digestibility. **Journal of Agricultural and Food Chemistry.** 61(45): 10787-10797.

Cai, L. and Shi, Y-C. (2014). Preparation, structure, and digestibility of crystalline A- and B-type aggregates from debranched waxy starches. **Carbohydrate Polymers.** 105(0): 341-350.

Cai, L., Shi, Y-C., Rong, L., and Hsiao, B. S. (2010). Debranching and crystallization of waxy maize starch in relation to enzyme digestibility. **Carbohydrate Polymers.** 81(2): 385-393.

Conde-Petit, B., Handschin, S., Heinemann, C., and Escher, F. (2007). Self-Assembly of Starch Spherulites as Induced by Inclusion Complexation with Small Ligands. In E. Dickinson and M. E. Leser (eds.). **Food colloids: Self-assembly and material science** (pp 117-126). Cambridge, RSC publishing.

Creek, J. A., Ziegler, G. R., and Runt, J. (2006). Amylose crystallization from concentrated aqueous solution. **Biomacromolecules.** 7(3): 761-770.

Davies, T., Miller, D. C., and Procter, A. A. (1980). Inclusion complexes of free fatty acids with amylose. **Starch-Stärke.** 32(5): 149-158.

Dongowski, G., Jacobasch, G., and Schmiedl, D. (2005). Structural stability and prebiotic properties of resistant starch type 3 increase bile acid turnover and lower secondary bile acid formation. **Journal of Agricultural and Food Chemistry.** 53(23): 9257-9267.

Eerlingen, R., Deceuninck, M., and Delcour, J. (1993). Enzyme-resistant starch. II. Influence of amylose chain length on resistant starch formation. **Cereal Chemistry.** 70(3): 345-350.

Ellis, R. P., et al. (1998). Starch production and industrial use. **Journal of the Science of Food and Agriculture.** 77(3): 289-311.

Fanta, G. F., Felker, F. C., and Shogren, R. L. (2002). Formation of crystalline aggregates in slowly-cooled starch solutions prepared by steam jet cooking. **Carbohydrate Polymers.** 48(2): 161-170.

Fanta, G. F., Felker, F. C., Shogren, R. L., and Salch, J. H. (2006). Effect of fatty acid

structure on the morphology of spherulites formed from jet cooked mixtures of fatty acids and defatted cornstarch. **Carbohydrate Polymers.** 66(1): 60-70.

Fanta, G. F., Felker, F. C., Shogren, R. L., and Salch, J. H. (2008). Preparation of spherulites from jet cooked mixtures of high amylose starch and fatty acids. Effect of preparative conditions on spherulite morphology and yield. **Carbohydrate Polymers.** 71(2): 253-262.

Fuentes-Zaragoza, E., Riquelme-Navarrete, M. J., Sánchez-Zapata, E., and Pérez-Álvarez, J. A. (2010). Resistant starch as functional ingredient: A review. **Food Research International.** 43(4): 931-942.

Haralampu, S. G. (2000). Resistant starch–a review of the physical properties and biological impact of RS3. **Carbohydrate Polymers.** 41(3): 285-292.

Heinemann, C., Escher, F., and Conde-Petit, B. (2002). Structural features of starch-lactone inclusion complexes in aqueous potato starch dispersions: the role of amylose and amylopectin. **Carbohydrate Polymers.** 51(2): 159-168.

Heinemann, C., Escher, F., and Conde-Petit, B. (2003). Structural features of starch-lactone inclusion complexes in aqueous potato starch dispersions: the role of amylose and amylopectin. **Carbohydrate Polymers.** 51(2): 159-168.

Hoover, R. (2001). Composition, molecular structure, and physicochemical properties of tuber and root starches: a review. **Carbohydrate Polymers.** 45(3): 253-267.

Le Corre, D., Bras, J., and Dufresne, A. (2010). Starch nanoparticles: A review. **Biomacromolecules.** 11(5): 1139-1153.

Lehmann, U., Jacobasch, G., and Schmiedl, D. (2002). Characterization of resistant starch type III from banana (Musa acuminata). **Journal of Agricultural and Food Chemistry.** 50(18): 5236-5240.

Lynch, D. R., et al. (2007). Glycemic index - A review and implications for the potato industry. **American Journal of Potato Research.** 84(2): 179-190.

Ma, U. V. L., Floros, J. D., and Ziegler, G. R. (2011). Effect of starch fractions on spherulite formation and microstructure. **Carbohydrate Polymers.** 83(4): 1757-1765.

Miles, M. J., Morris, V. J., and Ring, S. G. (1985). Gelation of amylose. **Carbohydrate Research.** 135: 257-269.

Nordmark, T. S. and Ziegler, G. R. (2002a). Spherulitic crystallization of gelatinized maize starch and its fractions. **Carbohydrate Polymers.** 49(4): 439-448.

Nordmark, T. S. and Ziegler, G. R. (2002b). Structural features of non-granular spherulitic maize starch. **Carbohydrate Research.** 337(16): 1467-1475.

Ozturk, S., Koksel, H., Kahraman, K., and Ng, P. K. (2009). Effect of debranching and heat treatments on formation and functional properties of resistant starch from high-amylose corn starches. **European Food Research and Technology.** 229(1): 115-125.

Parada, J. and Aguilera, J. M. (2009). In vitro Digestibility and Glycemic Response of Potato Starch is Related to Granule Size and Degree of Gelatinization. **Journal of Food Science.** 74(1): E34-E38.

Schmiedl, D., Bäuerlein, M., Bengs, H., and Jacobasch, G. (2000). Production of heat-stable, butyrogenic resistant starch. **Carbohydrate Polymers.** 43(2): 183-193.

Shamai, K., Bianco-Peled, H., and Shimoni, E. (2003). Polymorphism of resistant starch type III. **Carbohydrate Polymers.** 54(3): 363-369.

Shogren, R. L., Fanta, G. F., and Felker, F. C. (2006). X-ray diffraction study of crystal transformations in spherulitic amylose/lipid complexes from jet-cooked

starch. **Carbohydrate Polymers.** 64(3): 444-451.

Sievert, D. and Wursch, P. (1993). Thermal Behavior of Potato Amylose and Enzyme-Resistant Starch from Maize. **Cereal Chemistry.** 70(3): 333-338.

Singh, J., Kaur, L., and McCarthy, O. J. (2007). Factors influencing the physico-chemical, morphological, thermal and rheological properties of some chemically modified starches for food applications-A review. **Food Hydrocolloids.** 21(1): 1-22.

Singh, J., Lelane, C., Stewart, R. B., and Singh, H. (2010). Formation of starch spherulites: Role of amylose content and thermal events. **Food Chemistry.** 121(4): 980-989.

Topping, D. L. and Clifton, P. M. (2001). Short-chain fatty acids and human colonic function: roles of resistant starch and nonstarch polysaccharides. **Physiological reviews.** 81(3): 1031-1064.

Wisker, E. (2000). Physiological effects of resistant starch Part 2: Effect in the colon, and conclusion. **Ernahrungs-Umschau.** 47(2): 49-52.

Yin, Y. L., et al. (2004). Nutritional and health functions of carbohydrate for pigs. **Journal of Animal and Feed Sciences.** 13(4): 523-538.

Ziegler, G. R., Creek, J. A., and Runt, J. (2005). Spherulitic crystallization in starch as a model for starch granule initiation. **Biomacromolecules.** 6(3): 1547-1554.

Ziegler, G. R., Nordmark, T. S., and Woodling, S. E. (2003). Spherulitic crystallization of starch: influence of botanical origin and extent of thermal treatment. **Food Hydrocolloids.** 17(4): 487-494.

CHAPTER II

LITERATURE REVIEWS

2.1 Starch

Starch is the predominant carbohydrate reserve in many plants. Starch is biosynthesized as semicrystalline granule. The variation in granule size, shape, size distribution, association as individual (simple) or granule cluster (compound) as composition are depends strongly on the botanical origin (Buléon, Colonna, Planchot and Ball, 1998; Tester, Karkalas and Qi, 2004). Starch granules are composed of two types of α-glucan, amylose and amylopectin, which represent approximately 98-99% of the dry weight. Starches of different origins have different amylose and amylopectin ratios which differ significantly in many physical properties i.e. gelatinization, solubility, pasting and textural characteristic of starch and also enzyme digestibility. In addition, the ratio of amylose to amylopectin in starch varies considerably depending on the origin, plant species, variety within plants, plants organs, age of organ, and growth conditions. This results in various crystalline organization of starch in the granules and henceforth different sensitivities of starch to enzymatic hydrolysis.

2.1.1 Amylose

Amylose is essentially linear, consist of α-(1,4)-linked D-glucopyranosyl units (Fig 2.1) and many amylose molecules have a few α-(1,6)-linkages branches, about 0.1% to 0.5% (Ball et al., 1996; Whistler and BeMiller, 1997). The level of

amylose and its molecular weight varies with the botanical source of the starch and it affected by the climatic and soil conditions during grain development (Morrison, Milligan and Azudin, 1984; Yano, Okuno, Kawakami, Satoh and Omura, 1985). There are many different procedures available to measure amylose content. A number of techniques based on iodine binding capacity, including colorimetric (Juliano et al., 1981), potentiometric (Bates, French and Rundle, 1943) or amperometric titration techniques (Larson, Gilles and Jenness, 1953) have been used for determining amylose content more often due to its simplicity and long history of usage in the food industry. However, these methods require a reliable pure amylose from different sources to construct a calibration curve; thus the selection of an amylose standard curve is usually problematic (McGrance, Cornell and Rix, 1998). Moreover, iodine also binds to long amylopectin chains and intermediate size polymers, albeit with a much lower affinity, which would affect the accuracy of the results (Himmelsbach, Barton, McClung and Champagne, 2001). Therefore, results from these methods could either be lower or higher than the actual value, and the value obtained should be termed apparent amylose (AAC) or amylose equivalent (AE) (Eliasson, 2004). Another method, an amylose determination method measuring enthalpy formed with a specific complex between amylose and lipo-substances using differential scanning calorimetry (DSC) has also been developed (Mestres, Matencio, Pons, Yajid and Fliedel, 1996), this method also requires a standard curve. Alternative technique, the concanavalin-A precipitation (Megazyme amylose/amylopectin kit) has been used in popularity. This method employs a procedure based on the specific precipitation of amylopectin by concanavalin-A lectin. However, it is a relatively long and complicated procedure. Currently, the more precise and efficient method for determining the amylose content

is still in dispute. Based on amylose content, rice is generally classified into four groups as follows: waxy (0-2 % amylose), very low amylose (2 – 12 %), low amylose (12 – 20 %), intermediate amylose (20-25 %) and high amylose (25-33 %) (Mitchell, 2009).

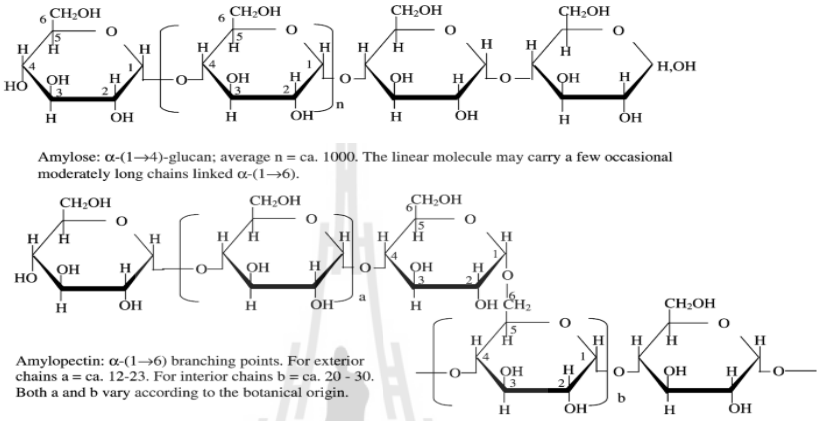

Figure 2.1 The molecular structure of amylose and amylopectin (Reproduced from (Tester et al., 2004).

Amylose can be easily characterized by size-exclusion chromatography coupled online to multi-angle laser light scattering (SEC–MALLS). It has a molecular weight of approximately 1×10^5 to 1×10^6 g/mol, a degree of polymerization by number (DP_n) of 324-4920 with about 9–20 branch points equivalent to 3–11 chains per molecule and average chain length (CL) of 200-700 (Tester et al., 2004). Rice starch amyloses have DP_n value of 920-1,110 with 2-5 branch chain per molecule and CL of 250-370 (Tester et al., 2004). The branched amylose molecule has been suggested to have a structure intermediate between that of linear amylose and amylopectin, frequently referred to as intermediate material (Takeda, Tomooka and Hizukuri, 1993).

Amylose is located in the granule as bundles between amylopectin clusters and or randomly dispersed. They could be located either the amorphous or crystalline regions of the amylopectin clusters (Eliasson, 2004). In starch granules, the amylose chain displays a natural twist in a helical conformation with six anhydroglucose units per turn. The inside of the helix is lipophilic where there are only hydrogen atoms. On the outside, there are hydrophilic hydroxyl groups (Zobel, 1988). The ability of amylose to form complexes with guess molecule provides an application for separating amylose from amylopectin by selective precipitation (Schoch, 1942) or determining amylose content as mention previously or an application as new starch based product for drug (Putseys et al., 2009) or flavor encapsulation (Conde-Petit, Escher and Nuessli, 2006; Heinemann, Escher and Conde-Petit, 2003; Jouquand, Ducruet and Le Bail, 2006) and texture reformation (Putseys, Lamberts and Delcour, 2010; Jin Peng Wang et al., 2013).

2.1.2 Amylopectin

Amylopectin, consisting of α-1,4-linked D-glucopyranosyl chains, is highly branched (5% to 6%) with α-1,6-bonds (Figure 2.1) (Buléon et al., 1998). Reported weight average molar masses (M_w), radii of gyration (R_G), and hydrodynamic radii (ν_G) values are 10^6-10^8 g.mol^{-1}, 163-229 and 0.37-0.49, respectively (Rolland-Sabaté, Colonna, Mendez-Montealvo and Planchot, 2007). The DP_n value ranged from of 4,700 to 12,800, CL values of 17 to 24, and β-amylolysis limits of 55% to 60% (Tester et al., 2004). Takeda et al (2003) reported that the DP_n of amylopectins from starches of different botanical origins is in the range of 9,600 to 15,900. Moreover, they revealed the presence of large (DP 13,400 to 26,500), medium (DP 4,400 to 8,400), and small (DP 700 to 1,200) species. In common with amylose,

the molecular size, shape, structure and polydispersity of the molecule varies with botanical origin. In rice starch, rice amylopectins have a DP_n of 8,200 to 12,800, CL of 19 to 23, β-amylolysis limits between 49% and 59% (Takeda, Hizukuri and Juliano, 1987; Wang et al., 2010), average external chain lengths (ECL) of 11.3 to 15.8, and average internal chain lengths (ICL) of 3.2 to 5.7 (Lu, Chen and Lii, 1997).

For description of the unit chain composition of amylopectin, the chains are grouped into with three categories (Figure 2.2a): A-chains, the outer chains are short chains not carrying other chains, B-chains, the inner chains are short chains carrying other chains through α-1,6-linkage and C-chain, the single inner chain per molecule carrying other chains and contain the reducing terminal residue (Buléon, Colonna, Planchot, and Ball, 1998). In rice starch, single clusters consist of approximately 10–23 chains, each with a length of 6–36 glucosyl residues (Bertoft and Koch, 2000). The following composition was proposed for waxy rice amylopectin: A (CL 13), B1 (CL22), B2 (CL 42), B3 (CL 69), and B4 (CL 101) (Hizukuri, 1986). Enevoldsen and Juliano (1998) reported that waxy and amylopectin of low amylose rice have similar molar ratios of A to B-chains (1.1 to 1.5) (Enevoldsen and Juliano, 1988). In a recent investigation, Bertoft, Piyachomkwan, Chatakanonda and Sriroth (2008) analyzed the internal unit chain distribution in amylopectins from a range of different plants. The internal chains, which all are B-chains, were divided into short (BS) and long chains (BL). Both categories possessed typically two subgroups: BS-chains were divided into very short "fingerprint" B_{fp}-chains with a degree of polymerization (DP) 3–7, and a major group, BS_{major}, with DP ~8–25; the exact range depending on the origin of starch. BL-chains were divided into B2-chains (DP ~26–50) and B3-chains (DP > 50), which apparently corresponded to

the respective groups found in the whole, original amylopectins (Bertoft, Koch and Åman, 2012). The molecular structure of amylopectin can be studied at different structural levels, such as domains, clusters and building blocks. Interconnecting more than one cluster forms domains. Clusters are defined as groups of chains separated by

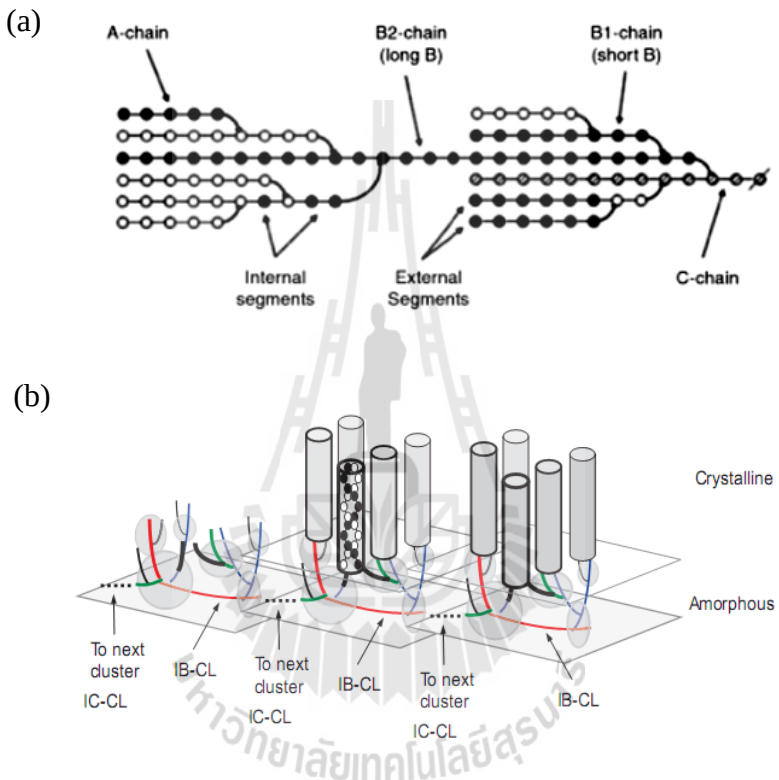

Figure 2.2 (a) Basic labelling of chains in amylopectin adapted from Bertoft, Koch and Åman, 2012. Circles denote glucosyl residues, horisontal lines (1–4) and bent arrows (1–6) linkages. The reducing-end residue is to the right. (b) A schematic representation of clusters of amylopectin that build up the semi-crystalline and amorphous lamellae (reproduced from Pérez and Bertoft, 2010). The building blocks (highlighted by circles) are attached to a backbone forming a network of chains in the amorphous lamella; Gray colour cylinders represent double-helices in the crystalline lamella; IB-CL = inter-block chain length; IC-CL = inter-cluster chain length.

internal chain segments with less than nine glucosyl residues (Bertoft, 2007b). Building blocks are tightly branched areas where the average internal chain length between branches is only 2-3 glucose residues. The DP of building blocks varies largely from 5 to 40 and was grouped into types 2–7 with a corresponding estimated number of chains from 2 to 7 (Bertoft et al., 2000). According to two-directional the backbone cluster model proposed by Bertoft et al., (2012) the backbone, which is highly branched, builds up the amorphous lamellae of the starch granules. The branches of clusters in the amorphous lamellae form building blocks. According to the backbone model the chains inside the clusters are interconnected by short chains and clusters are interconnected by long B-chains (indicated by IC-CL). A hypothetical model of the building block structure of amylopectin cluster is shown in Figure 2.2b (Pérez and Bertoft, 2010).

2.1.3 Granular structure of native starch

Native starch granules display a hierarchical structural periodicity (Figure 2.3). When observed by light and electron microscopy, starch granules have a characteristic layered structure. The core is surrounded by concentric semicrystalline growth rings of decreasing width towards the periphery, alternating with amorphous growth rings of more uniform thickness (Wang and Copeland, 2013). The semi-crystalline growth rings are composed mainly of crystalline amylopectin interspersed with amylose molecules, whereas the amorphous growth rings are composed mainly of extended chains of amylopectin interconnecting the crystalline regions and interspersed amylose molecules with a repeat distance of 9 to 11 nm (Cameron and Donald, 1992). The crystalline regions of the lamellae are mainly formed by double helices of amylopectin side chains packed laterally into a crystalline lattice, whereas

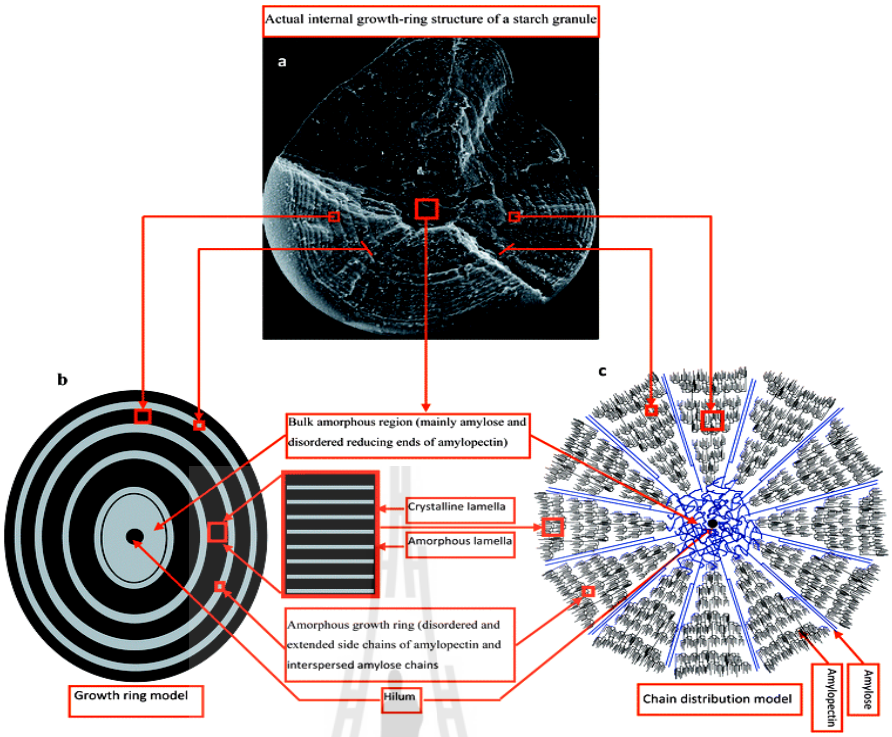

Figure 2.3 Model of starch granule organization (Reproduced from Wang and Copeland, 2013). The panels show an SEM image of a pea starch granule after 2 days of acid hydrolysis (a) and representations of a starch granule according to the growth ring model (b) and the chain distribution model (c).

amorphous regions contain amylose and the amylopectin branching points. Amylopectin clusters may contain amylose chains, which are amylose molecules that pass through both the crystalline and amorphous layers. It is proposed that these amylose tie molecules are in a straightened conformation in crystalline regions and in a disordered conformation in amorphous regions (Kozlov, Blennow, Krivandin and Yuryev, 2007; Matveev et al., 1998). Although different levels of organization within the granule are broadly understood, there are still uncertainties for instance at the level of organization between growth rings and lamellar. At least two models have been proposed to describe arrangements; these are Oostergetel's model of superhelices

(Oostergetel and van Bruggen, 1993) and the theory of blocklets (Gallant, Bouchet and Baldwin, 1997; Peng, Zhongdong and Kennedy, 2007).

The crystalline amylopectin clusters are responsible for a further level of organization, i.e. the arrangement of the starch polymers into two different crystal structures, which are A- and B-type polymorphic structures (Fig. 2.4) (Gallant et al., 1997). A-polymorphs are found in cereal starches, while B-polymorphs are found in tuber starches and in high-amylose cereal starches (Imberty, Buléon, Tran and Péerez, 1991). The A-polymorph crystallizes in an orthogonal unit cell with slightly distorted hexagonal packing and 4 water molecules per unit cell, whereas the B-polymorph crystallizes in a hexagonal unit cell with more open hexagonal packing and 36 water molecules per unit cell (Zobel, 1988). The C-polymorphic structure is a mixture of A and B unit cells. Molecular modeling has shown that the organized molecular structure of glucans with α-(1-4) linkages, having the lowest energy, is based on double helices, regardless of the polymorphic type (Imberty, Chanzy, Pérez, Buléon and Tran, 1988).

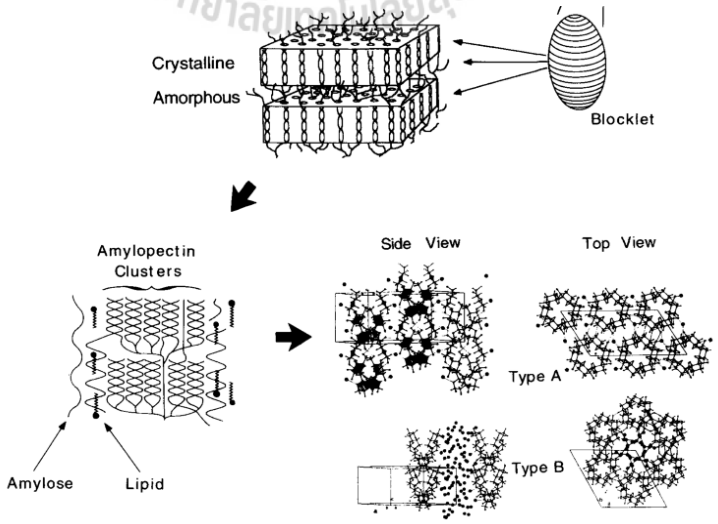

Figure 2.4 Organization of amylopectin chain into crystal structures (Reproduced from Gallant et al., 1997).

The ability to view the lamellar semicrystalline structure only in hydrated starch and not in dry starch led to the definition of a 'side-chain liquid-crystalline polymer' (SCLCP) model for starch (Waigh, Gidley, Komanshek and Donald, 2000). The framework approach of the SCLCP has been used to study the structure and physical properties of starch. There are three components necessary i.e. mesogens (the rigid units of double helices of the amylopectin side chains), flexible spacers (amorphous units) and a flexible backbone. In this model, side chains of amylopectin are considered to behave as a liquid-crystalline polymer (Daniels and Donald, 2004; Waigh, Gidley, et al., 2000; Waigh, Kato, et al., 2000). In the presence of water, plasticization of amylopectin branch points, which act as flexible spacers, allows the double helices to be decoupled from the polymer backbone and aligned into lamellar register, resulting in a transition from the nematic (no long-range order of position, but there is a preferred direction) to smectic (aligned with ordered) phase (Figure 2.5). In the absence of water, the branch points become less flexible, pulling the double helices out of register and leading to the development of a nematic phase, in which the long range correlation between the layers is lost.

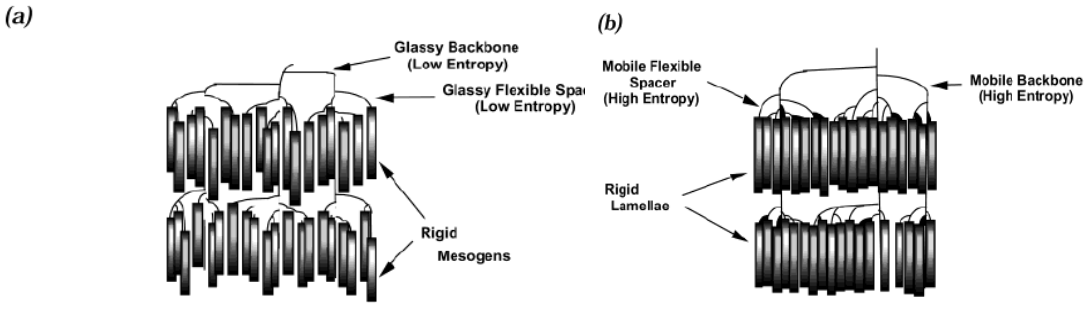

Figure 2.5 Lamellar structure of smectic side-chain liquid-crystalline polymer, including a schematic diagram of flexible spacer and rigid mesogen units (a) out of register and (b) in register (Reproduced from Daniels and Donald, 2004).

2.2 Disassociation of starch during gelatinization

The starch granules are disrupted by heating in the present of enough water, commonly known as gelatinization. During starch gelatinization process, the molecular order of the granule is gradually and irreversibly destroyed. It is manifested by irreversible changes in properties, including granular swelling, melting of starch crystallites, loss of birefringence, and starch solubilization. The endothermic phenomenon is most commonly observed using differential scanning calorimetry. The gelatinization temperature is the characteristic of the starch type and depends on the starch source and its amylose content.

Starch gelatinization process is more complex than a simple granular order-to-disorder transition. Several gelatinization mechanisms have been proposed in order to interpret observed changes during heating starch granules in excess water. According to Jenkins and Donald (1998), water first enters the amorphous growth rings, causing these regions to swell. After a significant amount of water enters the amorphous regions, a large amount of swelling occurs, providing sufficient stress through connectivity of molecules from the amorphous growth ring to the semi-crystalline lamellae, resulting in the disruption of starch crystallites, as evidenced by the loss of crystallinity (Jenkins and Donald, 1998).

Based on data from DSC and XRD analyses, the SCLCP model can be applied to explain various starch gelatinization behaviours (Waigh, Kato, et al., 2000). For instance, in the case of starch hydration, the addition of water brings about the self-assembly of the amylopectin helices in the lamellae to form a crystalline smectic hexagonal phase, causing the appearance of the smectic periodicity, whereas the amorphous backbone and spacers are in a plasticized liquid phase with the appearance

of the B-type inter-helix spacing. Consequently, during gelatinization, at low water contents (<5%), a single DSC endoderm is observed due to the glassy nematic helix-coil transition. Intermediate water contents (5-40%) result in two endotherms. The first is due to the rearrangement of dislocations of constituent amylopectin helices, leading to a smectic-nematic transition. The second is the helix-coil transition as the amylopectin helices unwind in an irreversible transition. In excess water (>40%), the lamellae break up and helix-coil transition occurs at the same point, as free unassociated helices are unstable.

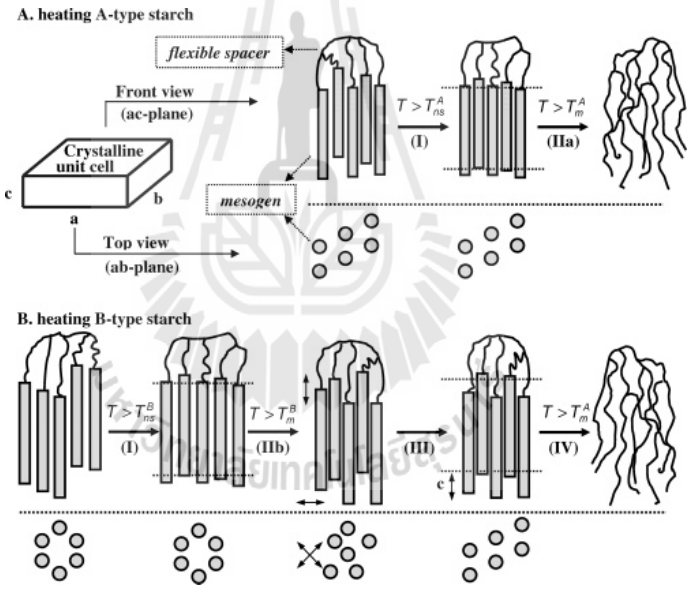

Figure 2.6 Schematic diagram of changes during the gelatinization of A-type (A) and B-type (B) starch at low level of water content (Reproduced from Vermeylen et al., 2006).

Vermeylen et al. (2006) proposed the model for starch gelatinization at low level of moisture using SCLCP approach. They presented a schematic view on the gelatinization process of A-type and B-type starches as shown in Figure 2.6. In this

model, temperatures above ambient temperature promote a secondary transformation from the nematic to the smectic phase. For A-type starch, the lamellar structure is disturbed when the temperature exceed the melting temperature of liquid crystal, the helix-coil transition of amylopectin helices unwind in an irreversible transition (Waigh, Gidley, et al., 2000). For B-type starch, the limited transition of B-type into A-type occurred during gelatinization. The sequence of gelatinization follows as (i) melting of B-type crystals, (ii) recrystallization into A-type crystallites, and (iii) melting of A-type crystallites. Therefore, the gelatinization of starch is an inter-play between self-assembly and the breakdown of structure during heating.

Gelatinization normally occurs between 50-75 °C. Dissolution of crystalline starch is dependent on crystal thickness and type. The predicted disssolution temperature of crystalline strucuture of amylose in water ranges from 57 to 147 °C for low to high molecular weight amylose (Moates, Noel, Parker and Ring, 1997). Creek et al. (2006) explained the phenomenon of amylose dissolution at high temperature as shown in Figure 2.7. The double-helical crystallites melt on heating at temperature about 70 °C, and the fixed network entanglements are thermally dissociated by temperature at 130 °C to form a liquid crystalline phase (probably nematic phase) comprising relatively flexible chains with some regions of rigid helical conformation. These regions are stabilized by near neighbours. Upon heating, both the number and length of these regions decrease, and the system become isotropic at a temperature between 160 and 180 °C in which the characteristic temperature at the liquid crystalline phase became isotropic is called the ‘clearing temperature’. The remaining starch-starch hydrogen bond was replaced by starch-water hydrogen bond above this temperature. They stated further that the ability of starch to recrystallize partially was

lost at these high temperatures in a transition involving the breakage intramolecular hydrogen bonds. Furthermore, amylose loosed its rigid, helical nature and became more flexible above 170 °C when rapidly quenched from this temperature, where the kinetic of chain folding may favour over helix formation, as flexible chains could be folded into lamella crystalline.

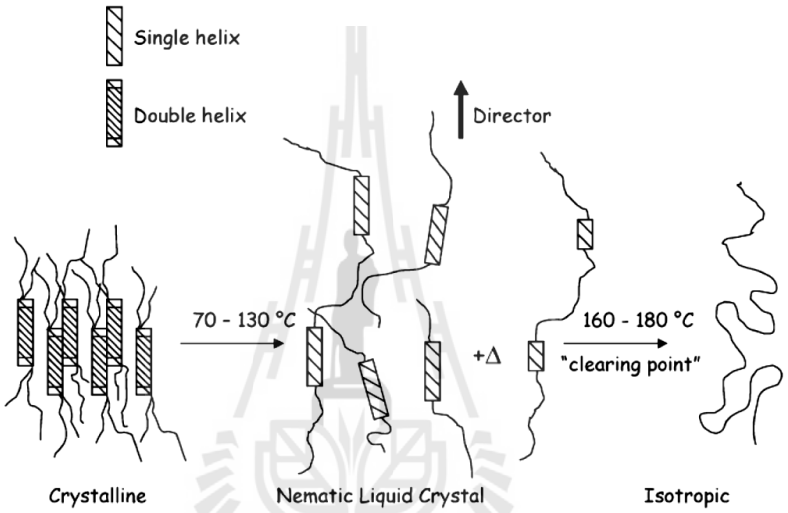

Figure 2.7 Schematic of proposed transitions on heating crystalline amylose in excess water (Reproduced from Creek, Ziegler and Runt, 2006).

2.3 Starch crystallization

2.3.1 Starch crystallization behavior

Starch crystallization, which follows starch gelatinization, is a non-equilibrium process as well known as retrogradation. Retrogradation results from the reassociation and recrystallization of the linear regions of the polymers to form insoluble crystallites containing short linear segments of α-(1→4)-linked glucose units (Gidley et al., 1995). Retrogradation may take to form from several hours to several days in the case of high-amylose starch and high-amylopectin starches,

respectively. During the retrogradation process, the two polysaccharides, amylose and amylopectin play different roles. Retrogradation is a thermoreversible gelation-via-crystallization process. Gidiey and Bulpin (1989) showed that short chain lengths and low concentrations favored precipitation of amylose, whereas for long chain lengths, extensive cross-linking occurred, which would lead to gelation. Gidley (1989) proposed that the cross-linking mechanism was through double helical junction zones; then, if the length of a junction zone was significantly shorter than the total chain length, a single chain could take part in several separated junction zones to form a cross-linked network (Gidley and Bulpin, 1989). However, if the junction zone length was not significantly shorter than the total chain length, chain alignment would dominate, and if lateral aggregation followed, precipitation would eventually be the result.

As opposed to amylose crystallization, amylopectin was crystallized due to its branched structure. Once the helices had formed, they were still connected to the main polymer chain through α-(1→6) branch points and, on aggregating to form crystals (Goodfellow and Wilson, 1990; Klucinec and Thompson (1999). It was believed that, as with amylose retrogradation, there were two distinct stages involved in amylopectin retrogradation (Goodfellow and Wilson, 1990). Additionally, Eliasson er al. (1987) found that the length of the linkage formed by the all (α1→6) branch point was very similar to the van der Waals distance formed between double helices. The resulting partially crystalline structure can best be conceptualized using the "Fringed micelle" model, used by Levine and Slade (1988), in which they adapted from partially crystalline synthetic polymer science. The model shows that amorphous starch regions surround the starch crystals; the former part of the system contains the

water that acts as a plasticizer. Within the “Fringed micelle” model, it is possible for one polymer chain to have numerous helical and random coil regions situated in various crystallite and amorphous regions respectively. Another approach that is often used to describe retrograded starch is the chain-folded lamellae model, where the theory to describe their crystallization kinetics was developed for synthetic polymers by Lauritzen and Hoffman (1973). In chain-folded lamellae polymers, the crystalline regions are made up of lamellae, where the chains are placed in adjacent positions and perpendicular to the surface of the lamellae, and they then fold back on themselves.

2.3.2 Factors affecting starch crystallization base on temperature and moisture content aspect

Crystallization of starch can be considered as crystallization in partially crystalline polymer system in which this phenomenon is governed by glass transition temperature (T_g) and melting temperature (T_m) of crystal. In general, crystallization consists of three steps: 1) formation of critical nuclei by initiation of order chain segments intramolecularly (nucleation), 2) growth of the crystal from nuclei by intermolecular aggregation of ordered segments (propagation) and 3) crystal perfection or continuous slow growth (maturation) (Roos, 1995). Nucleation is typically classified as primary or secondary nucleation. The presence or absence of crystals of the crystallizing compound in the system prior to nucleation defines whether primary or secondary nucleation occurs. Primary nucleation occurs in the systems that do not contain crystal of crystallizing compound prior nucleation whereas secondary crystallization requires the presence of crystal of the crystallizing compound (Eliasson, 2004). Rate of nucleation and crystal growth are affected by temperature, as shown in Figure 2.8. The overall crystallization rate mainly depends

on the nucleation and propagation rate. Below the T_g, nucleation is unlikely to occur due to the extremely high viscosity of the system (Marsh and Blanshard, 1988), making molecular mobility difficult. A temperature near the T_g favors nucleation rate whereas a higher temperature up to the T_m favors propagation rate. The maturation is dependent on temperature similar to that of propagation rate. The net result of both nucleation and growth on the rate of crystallization is that it has a bell-shaped dependency on temperature, where the maximum occurs approximately halfway between T_g and T_m (1/2 T_g+T_m). For B-type starch gels containing more than 27% water content have T_g of about -5 °C, and T_m of amylose is about 150 °C; therefore crystallization of amylose can occur between these temperature limit (Eerlingen, Crombez and Delcour, 1993).

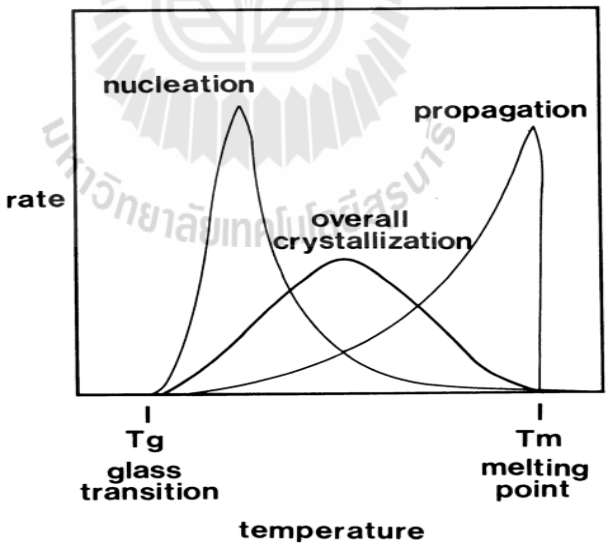

Figure 2.8 Temperature dependence of the nucleation, propagation and overall crystallization rates according to partially crystalline polymer system (Reproduced from Eerlingen et al., 1993).

Moisture content is an important parameter for determining the rate of crystallization. Water, being a relatively small molecule, can act as an effective plasticizer for starchy materials, as shown by several researchers (Orford er al., 1989; Kalichevsky and Blansharcl. 1993; Farhat et al, 2000) and reviewed by Levine and Slade (1988). By adding water to a system, its T_g and T_m will decrease. However, whether an increase in the moisture content of the system will result in an increased rate of crystallization, it depends on where precisely the sample is located on the bell-shaped curve of crystallization rate versus temperature, as shown in Figure 2.9. The assumption is made that a sample was obtained that was located on the solid black curve. If the sample was located to the left of the maximum crystallization rate, then adding a small amount of plasticizer to that system would enhance the crystallization rate, whereas if the sample had been located to the right of the maximum, the addition of plasticizer would lead to a depression of the crystallization rate. Therefore, it is not possible, without knowing the storage temperature relative to T_g and T_m of a sample, to draw a conclusion as to what the effect of added plasticizer would be on the rate of crystallization.

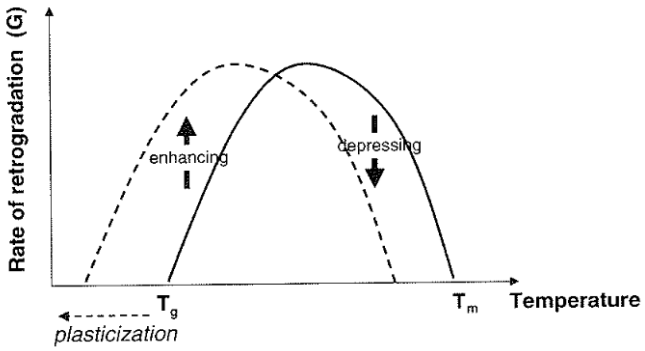

Figure 2.9 Effect of plasticizer on crystallization kinetics of partial crystalline polymer (Reproduced from Farhat et al., 2000).

It is a well known fact that the crystalline structure of the retrograded material is not the same as that found in the parent native starch. Starch can crystallized into various morphologies i.e. aggregates, precipitates, gels, crystals, etc. and polymorphic types (A, B and V-type), depending on factors such as molecular weight, concentration and temperature. At higher storage temperature and lower moisture content conditions, the A-type starch crystal would form preferentially. In contrast, at low temperature and high moisture content conditions, the B-type crystal polymorph would be favor (Buléon, Véronèse and Putaux, 2007). Shamai, Bianco-Peled and Shimoni (2003) and Zabar, Shimoni, and Bianco-Peled (2008) demonstrated that the retrogradation at low temperature (40ºC) leads to the formation of B-type structure. On the other hand, the crystallization at high temperature (95ºC) yields a mixture which contains A-type and V-type structure.

2.3.3 Split crystallization during debranching

Starch can be crystallized during enzymatic debranching by split crystallization (Pohu et al., 2004). The B-type crystalline structure was observed after 12 h of debranching maltodextrin at high concentration (25% w/v). Then, the gradual transition from B-type to A-type crystalline structure was observed between 12 h and 48 h of incubation time. Pohu et al. (2004) reported that the shift from B-type to A-type crystalline was not a result of a polymorphic transition from the precipitated B-type structure into A-type structure, as observed for starchy samples in specific conditions of temperature, pressure and hydration as shown for raw starch (Nishiyama, Putaux, Montesanti, Hazemann and Rochas, 2010) or B-type lintners (Gérard**,** Colonna**,** Buléon and Planchot, 2002). It was attributed to a split crystallization phenomena that involves, in the first stage, the aggregation of the

longer linear or branched chains into B-type networks, followed by the precipitation of shorter linear chains into aggregates of A-type crystalline. Cai, Shi, Rong and Hsiao (2010) also demonstrated the crystallization of debranched waxy maize starch during debranching at high concentration. Morphology of resulting product was appeared similar to debranched maltodextrins, consisting of wormlike objects with 5-10 nm observed at the first hour of debranching and after 4 h of debranching, the aggregate particles were evident. Cai et al. (2010) proposed the three steps of crystallization during debranching, including (1) association of starch chains into double helixes and forming clustering, wormlike structure, (2) rearrangement of semi-crystalline unit into nano-particle and (3) growth of particles into large aggregates.

2.3.4 Spherulitic crystallization of starch

Spherulites are normally found in melt-crystallized synthetic polymers (Bassett, 2003; Magill, 2001). It has also been observed in self-association with biological macromolecule of natural polymers such as cellulose (Kobayashi et al., 2000), chitin and chitosan (Murray and Neville, 1998), bovine insulin (Krebs, Bromley, Rogers and Donald, 2005), DNA (Stanley, Hong and Strey, 2005), amylose (Creek et al., 2006) and starch (Nordmark and Ziegler, 2002). Spherulites are radially symmetric, semicrystalline entity and thereby exhibit a characteristic “Maltese cross” when they are viewed between crossed polarize using light microscopy. The change in polarizability is explained as the change of reflective index (n) which the birefringence of the spherulite is defined as $\Delta n = n_{//} - n_{\perp}$, where $n_{//}$ is the refractive index parallel to the chain axis and $n_{\perp}$ is the refractive index perpendicular to it (Murayama, 2002). The sign of the birefringence can be characterized as positive or negative based on the color-combination caused by the sensitive tint plate (Figure 2.10). This phenomenon

can imply the inner information of the orientation for the molecular chain (optical ellipsoid) in the spherulites i.e. the radial and tangential orientation (Figure 2.11).

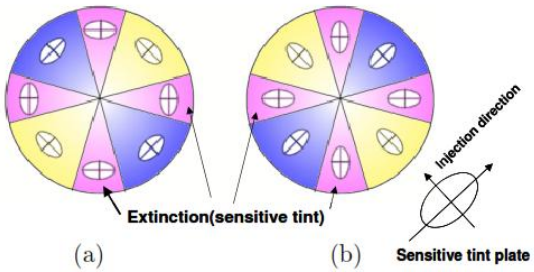

Figure 2.10 Optical sign of the spherulite using a sensitive tint plate; (a) negative spherulite and (b) positive spherulite (Reproduced from Murayama, 2002).

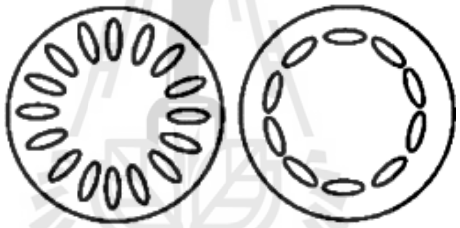

(a) (b)

Figure 2.11 Possible two arrangements of optical ellipsoids within a spherulite (a) spherically symmetric array with the major axis of ellipsoid parallel to the radius vector (radial orientation corresponding to the positive spherulites) and (b) spherically symmetric array with the major axis of ellipsoid perpendicular to the radius vector (tangential orientation corresponding to the negative spherulites) (Reproduced from Yoshioka, Fujimura, Manabe, Yokota and Tsuji, 2007).

Starch spherulites have typically been obtained by three cases: 1) as induced by amylose inclusion complexation with small ligand 2) by precipitating

through solvent treatment of low molecular weight amylose solution (DP10-20) 3) by crystallizing after super-heat treatment of amylose and native starch at high concentration. Spherulitic crystallization in all cases will be discussed below.

For the first case, spherulitic crystallization can be occurred by the formation of helical amylose inclusion complex in the presence of suitable ligands that induced the helix formation of amylose (Conde-Petit, Handschin, Heinemann and Escher, 2006). In cereal starches, endogenous lipid may promote the spherulite formation. The addition of lipid to starch dispersion lead to a precipitation of amylose in the form of spherulites (Fanta et al., 2002, 2005, 2006, 2008; Byars et al., 2003) and Bhosale and Ziegler (2009). This spherulite is formed when amylose dispersion is heated over 140 °C in the presence of lipid, followed by slow cooling. It was reported that the spherulites was formed with difference in morphologies, i.e. spherical/loped shaped and torus/disc shape and difference in polymorphic type (V_6 or V_7-type). The spherulite characteristics varied depending on the starch concentration, fatty acid used, and the pH of the dispersion, the cooling rate, heating temperature and whether the dispersion was stirred during cooling. The spherical/lobed type was generally larger than torus/disc type. The smaller sized spherulites were disc or torus shape, which exhibited V_{6I}-type WAXS pattern whereas the larger particles were more spherical and lobed appearance and exhibited V_7-type or mixed V_{6I} and V_7-type pattern (Fanta et al., 2006; Fanta et al., 2008; Bhosale and Ziegler, 2009). Beside monoacyl lipids, other ligands suitable for inducing the formation of starch spherulites are terpene and lactone (Conde-Petit, Escher, et al., 2006).

For the second case, starch spherulites produced by crystallizing limit dextrins from acid-hydrolyzed potato starch DP 15-22 (Helbert, Chanzy, Planchot,

Buléon and Colonna, 1993; Ring, Miles, Morris, Turner and Colonna, 1987; Williamson et al., 1992). B-type spherulites were obtained by direct cooling of the aqueous solution, whereas A-type spherulites were crystallized by ethanolic precipitation. Their size ranged from 5 to 15 μm but the morphology was very different depending on the crystalline type. A-type spherulites consisted of a radial assembly of thin elongated single crystals, while B-type spherulites were spherical with a smoother surface and tangential organization of amylose chain. These spherulites were used to a model system to study enzymatic hydrolysis of starch crystallites, giving their well-defined morphology and their low susceptibility to hydrolysis (Planchot, Colonna and Buléon, 1997).

The third case of spherulite was formed when aqueous starch dispersion was heated above 170 ºC, followed by rapid cooling. In this case, an elevated temperature was necessary for spherulite formation. It is hypothesized that between 160°C and 180°C, the amylose liquid crystals transition into random coils and the dispersion becomes isotropic as describe previously (starch gelatinization). In addition to inducing the helix to coil transition and removing nuclei for non-spherulitic crystallization (Ziegler, Nordmark, and Woodling, 2003; Creek, Ziegler, and Runt, 2006), superheating an aqueous starch dispersion could resulted in the degradation of the amylopectin into short, linear, intermediate material with fewer branch points per molecule than unmodified amylopectin and therefore more spherulite formation material in solution (Nordmark and Ziegler, 2002b; Vesterinen, Suortti, Autio, 2001). Creek el al. (2006) proposed that spherulitic crystallization of amylose could be considered as a competition between phase separation and gelation (Doublier and Choplin, 1989; Guenet, 1996). Based on polymer solutions, the relation of starch

concentration, temperature and cooling rate concerning phase separation and crystallisation is schematically presented in a phase diagramm (Figure 2.12) by Ziegler el al. (2005). The cooling rate demixing curve (crd-curve) indicates the conditions where liquid-liquid demixing can occur. When, for example, amylose solution was rapidly cooled, liquid-liquid phase separation into a polymer-rich and a polymer-poor phase will occur prior to crystallization. Under these conditions it is hypothesized that spherulites may be formed in the polymer-rich phase. Otherwise, crystallization continues with existing nuclei such as remnants of crystalline phases and gelation is favored.

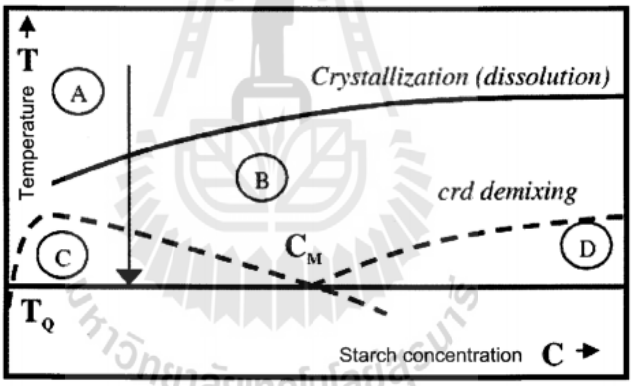

Figure 2.12 Schematic phase diagram showing the relation between starch concentration (C) and the temperature (T) starch dispersion. Phase A is a single phase of homogeneous solution. Phase B is a gel phase. Phase C is a liquid-liquid phase separation into a phase of low starch concentration and a phase with concentration C_M. Phase D contains the pure solid and demixed phase of concentration. T_Q is the final system temperature. The cooling-rate-dependent demixing curve (crd-demixing) is indicated by the dashed line (adapted from Ziegler et al., 2005).

This spherulitic morphology closely resembled that of native starch granule in early stage of development. This spherulitic crystallization was proposed as model for starch granule initiation *in vivo* (Ziegler, Creek and Runt, 2005). This type of spherulitic assembly presented a B-type crystalline, which corresponds to a double-helical arrangement of starch in the crystal. The spherulites were mainly composed of amylose or lightly branched material and their crystallization was preceded by a phase separation process. The formation of spherulite was influenced by several factors such as amylose concentration (Lay ma, Ziegler and Floros, 2009, 2011), starch source (Ziegler et al., 2003), cooling rate and quench temperature (Ziegler, Creek and Runt, 2005; Creek et al., 2006). Well-developed starch spherulites were found to be easily formed in mung bean starch, potato starch, acid modified maize starch and high amylomiaze starch, respectively (Ziegler et al., 2003). Creek et al., 2006 concluded that the formation of spherulite was favored by linear material whereas a highly branch molecule of amylopectin can hinder phase separation and crystallization into spherulites. Ma el al. (2011) also demonstrated that a higher ratio of amylose to amylopectin resulted in the formation of large amount of spherulites and better developed spherulites. Starch spherulites were developed from a sheaf-like precursor, and have an internal radial organization and blocklet structure similar to some synthetic spherulites (Ma, Floros and Ziegler, 2011). In addition, spherulitic crystallization is also affected by other factors such as degree of branching, chain length, and chain length distribution. The size and morphology of spherulite can be controlled by amylose concentration, chain length and cooling rate condition.

Starch spherulites offer unique functionality, particularly as a food ingredient. Starch spherulites form a spreadable, gel-like paste when suspended. This

paste exhibits more effective gelling properties than maltodextrin, which is currently used as a starch-based fat substitute (Steeneken and Woortman, 2008). In addition, starch spherulites could be used to encapsulate flavors. Starch spherulites are partially resistant to enzymatic digestion, due in part to the arrangement of the crystalline unit cell. Starch spherulites typically have what is called a B-type arrangement (Nordmark and Ziegler, 2002a). Starches with a B-type unit cell are more resistant to enzymatic digestion than starches with other unit cell configurations (Annison and Topping, 1994). For this aspect, it implied that they can act as a soluble fiber to deliver probiotics to the colon. Clearly, a low-calorie fat substitute that could be flavored and used to promote gastrointestinal health is worth pursuing on a large scale production.

2.4 Impact of crystallization in relation to enzymatic digestibility of starch

2.4.1 Nutritional classification of starch

The susceptibility of starch to enzymatic digestion is of considerable importance to human digestion and health. Starch digestibility may be assessed by in vitro or in vivo methods, which are complementary rather than alternatives. From a nutritional point of view, starch can be classified into three different fractions based on its in vitro digestibility by amylases, namely rapidly digested starch (RDS, digested enzymatically within 20 min), slowly digested starch (SDS, digested between 20 and 120 min) and resistant starch (RS, starch undigested by enzymes after 120 min) (Berry, 1986; Englyst et al., 1992). It was found that RS are not digested by enzymes, they are fermented in the intestine, the fermentation of which results in the production of short chain fatty acids (e.g. Goni et al., 2000) that are believed to be

beneficial to health and decrease the risk of colonic cancer (Vanmunster and Nagengast, 1993). There are five types of resistant starches: RS1 is physically inaccessible starch, such as that in partially milled grains, seeds, and legumes; RS2 is starch granules which cannot be digested by amylases until gelatinized. RS2 are found, for example, in green banana, uncooked potatoes, peas, and high amylose starch; RS3 is retrograded starch; RS4 is a chemically modified starch; and RS5 is amylose-lipid complex (Englyst et al., 1992, Eerlingen and Delcour 1995; Yue and Waring 1998; Champ et al. 1999; Sajilata et al. 2006).

2.4.2 Resistant starch type 3

Among the resistant starches RS3 has particular interesting due to its resistance against thermal processing resulting in preserving nutritional functionality after cooking processes. RS3 is retrograded starch and is inaccessible because of crystalline structure. RS3 contains mainly retrograded amylose; however amylopectin crystallization can significantly increase the amount of resistant starch (Eerlingen and Delcour, 1995; Sievert, Czuchajowska and Pomeranz, 1991; Lehmann, Jacobasch, and Schmiedl, 2002). RS are important as they can yield foods with greater nutritional quality. Hence, attempting to produce starches with slow-digesting properties and high RS content is an important objective for the food industry.

RS3 can be prepared by heat treatment, enzyme treatment, combined heat treatment and enzyme treatment, and chemical treatment. Technically, it is possible to increase the RS3 content in foods by modifying the process conditions such as pH, heating temperature and time, number of heating and cooling cycles, freezing, and drying (Eerlingen and Delcour 1995; Thompson 2000; Shamai et al. 2003). Many factors, however, influence the formation of RS3 including: inherent

properties of starch (crystallinity, granular structure, amylose-amylopectin ratio, amylose chain length, etc.), heat and moisture, interaction of starch with other components (protein, dietary fiber, iron, sugar, etc.), processing conditions (baking, autoclaving, extrusion cooking, etc.), thermal processing, and miscellaneous treatments (Eerlingen and Delcour 1995; Cairns et al. 1996). A number of commercially available RS preparations would make it possible for a wide range of application with nutraceutical implications (i.e. drug encapsulation) (Sajilata et al. 2006).

The formation of RS3 after retrogradation is due to a greater interaction between starch components (amylose and amylopectin) upon cooling or dehydration (Eerlingen and Delcour, 1995; Haralampu, 2000). The length of chains influences a RS type III formation significantly. The RS3 was found to contain short and linear chains of thermally stable glucans of about 10-100 chain lengths, substantial double helix content and moderate crystallinity (mostly B-type) (Eerlingen, Deceuninck and Delcour, 1993; Gidley et al, 1995; Shamai, Shimoni and Bianco-Peled, 2004). Debranching of high amylopectin starch produces short linear chains with a relatively narrow molecular weight distribution, which cloud crystallize into RS products with a high degree of crystallinity (Shi, Birkett and Thatcher, 2006; Cai and Shi, 2010). The chain length (CL) distribution of debranched amylopectin is relevant to its crystalline polymorphs (Hizukuri, 1985). In general, the amylopectin of A-type polymorphic starches have shorter average chain lengths and larger proportions of short chains, whereas B-type polymorphic starch have longer average chain lengths and higher proportions of long chains. The amylopectin of the C-type starch have intermediate average branch chain lengths and larger proportions of both short and long chains

(Hanashiro, Abe, Hizukuri, 1996; Jane et al., 1999). Therefore, the CL distributions of debranched starches from A-,B- and C- type starches affects the level and formation of resistant starch (Shu et al., 2007). Cai and Shi (2010) reported the effect of CL distribution of amylopectin after debranching contributing towards RS3. They stated that debranched waxy potato starch is the preferred starting material to produce product with high resistant starch content. It was due to debranched waxy potato starch had a higher average CL than that of debranched waxy wheat and waxy maize starches, which resulted in a higher yield of crystallized product with stronger crystalline structure, higher peak melting temperature, and higher RS content. However, there is only one report of CL distribution of amylopectin after debranching contributing towards RS3 and this aspect is need to further investigate. There is still a need for information on the relationship of amylopectin structure after debranching and resistant starch content.

There are many different researches which are studied on the structural features of recrystallized starches in terms of morphological and polymorphism in relation to enzyme digestibility. Pohu, Planchot, Putaux, Colonna and Buléon (2004) investigated the crystallization of debranched maltodextrin and found that a loose B-type network containing linear and branched chain of high MW was formed during an initial stage of debranching, whereas the aggregates of A-type crystalline consisting of short linear chains were produced during a late stage of debranching. The resulting product appeared as a thick, dense precipitate. Shamai et al. (2003, 2004) reported that the crystallization condition affected polymorph structure of RS3 in high amylose corn starch, wheat starch and corn flour. It was found that the crystallization at low temperature led to B-polymorph, whereas a high crystallization temperature led to a

mixture of A and V polymorph. They also found that the polymorphic type of RS influenced enzymatic susceptibility differently from that of native starch (Zabar, Shimoni and Bianco-Peled, 2008). However, the detailed structure of the RS3 product was difficult to define because of its complexity.

Cai et al (2010) reported that the longer chains aggregate with loose B-type network and poorly crystalline were rather susceptibility to enzyme hydrolysis by α-amylase. The resistance to amylase was attributed to the particularly dense and compact morphology, the accessibility of double helices to α-enzyme being strongly reduced by aggregation of A-type crystalline (Cai, Shi, Rong and Hsiao, 2010). In general, B-type crystalline structure is known to be more resistant to enzymatic hydrolysis than A-type substrate for native starches, especially potato starch, but these differences may be the result of surface area because potato starch granule are very big and therefore the surface per volume is smaller. Spherulite with A or B crystalline structures product from potato amylose were also shown to differ in their resistance to enzyme hydrolysis. The A-polymorph was found to be more susceptible to hydrolysis than B-polymorph (Gerard, Planchot, Buléon and Colonna, 2001). Scanning electron microscopy (SEM) investigation has shown that the A-type spherulites possess an uneven surface which allows the enzyme to break down spherulites into smaller fragments and, hence, increase the surface area available for hydrolysis (Williamson et al, 1992). For a resistant starch (RS) product with A-type crystalline structure, the enzyme digestibility of this product was contrary with native starch and spherulite. It is remarkable that the resistance on enzyme hydrolysis is not depending on polymorphic type, it depends on structural morphology of product. The overall morphology of solid substrates has direct impact on diffusion and absorption of

enzyme, which are the limiting factors in such a reaction (Planchot, Colonna and Buléon, 1997). The morphology of this debranched product was dense aggregate with more rigid and smooth surface, therefore, the high cohesion of precipitates resulting in a reduced accessibility of double helices to enzyme.

Pohu et al. (2004b) investigated the ultrastructure of the A-type RS product using TEM and comparison to model A-type amylose crystal with similar diffraction pattern. They used two model substrates, waxy maize starch nanocrytals obtained by acid hydrolysis and A-type amylose crystal prepared from a low degree of polymerization (DP) amylose, to explain the origin of the limited α-amylolysis of the RS product. They proposed the schematic model of RS aggregate, developing by epitaxial growth of element crystalline A-type platelets. The mechanism involved in α-amylolysis hydrolysis takes place on the side of the double helices instead of at their ends present at the surface of lamellar crystals. Double helices are too big to enter the catalytic site of amylases, all the more so when involved in a crystalline structure. As the proper catalytic action needs the first disentanglement of the double helix strands, it could be realized during the adsorption stage. Consequently, the resistance of the RS product to α-amylolysis was attributed to the high cohesion of precipitate resulting in a limited accessibility of amylose double helices to enzymes.

The lamellar nanostructure was observed for high amylose starch that crystallized at low temperature (Shamai, Shimoni, and Bianco-Peled, 2004). It showed a shoulder at s = 0.05 nm^{-1} in small angle X-ray scattering (SAXS) profile, which corresponds to Bragg periodic distance of about 20 nm. Shamai, Shimoni, and Bianco-Peled, 2004 and Zabar, Shimoni, and Bianco-Peled (2008) applied the "modified lamellar model" (Cameron and Donald, 1992; Wenig and Bramer, 1978) to

fit the scattering data to characterize the nanostructure of resistant starch and they found that the “modified lamellar model” gave a good fit to patterns form native high amylose corn starch (HACS) and samples obtained at low temperature. This model was previously used to analyze scattering patterns from native starches. The model describes randomly oriented finite domains, made up of alternating layers of crystalline and amorphous material, each layer being of effective infinite extent (Wenig and Bramer, 1978). The calculation of the scattering pattern of the lamellar model is facilitated by the fact that each stack shows electron density variations in one direction only. The structural parameters of which obtained by fitting to the theoretical model, indicating that the crystallinity of lamellar phase in recrystallized sample is much lower than the crystallinity appeared in the native HACS. Their crystal has a long-range periodicity of D = 14.8 nm, much larger than periodicity D observed in native HACS. The long-rang periodicity D was also slightly increased after apply autoclaving-cooling cycles, is about 15-20 nm.

2.4.3 Enzyme susceptibility of starch spherulites

Amylolysis of amylose spherulites, both A- and B-type, was studied by Williamson et al. (1992) and Planchot et al. (1997) using spherulites formed from 20 DP and 15 DP lintnerized potato starch, respectively. Both reports agreed that A-type spherulites were more susceptible to amylolysis than B-type spherulites. After hydrolysis, no spherulitic structure was observed by optical microscopy and SEM for A-type spherulites, whereas no clear difference was seen for B-type spherulites. Planchot et al. (1997) proposed that the susceptibility of spherulites depended on a combination of parameters including crystalline type, morphology, crystal defects and interrelations of the crystals of amylose spherulites. Williamson et al. (1992) also

suggested that susceptibility of A-type spherulites was related to crystalline type and weak inner cohesion among crystals. Leloup et al. (1991) used untreated B-type spherulites and acid treated spherulites to study the adsorption of α-amylase and hydrolysis kinetics. The authors suggested that enzyme was binding to the dangling chains or hair structure on the untreated spherulite surface. No adsorption and no hydrolysis were detected on the acid treated spherulites with smooth surface. The kinetic study showed that adsorption precedes catalysis. These researchers also observed the hydrolysis rate continuously decreased with time which possibly due to strong effect of the hydrolysis products that reduce enzyme-substrate adsorption and hydrolysis (Leloup et al. 1991). Therefore, the adsorption/binding of enzyme onto the spherulite surface and diffusion/penetration of enzyme into spherulitic substrate could be the primary limiting parameters of hydrolysis reaction of starch spherulites.

2.5 Hydrothermal treatment for improvement of resistant starch

Hydrothermal treatment induces changes in the physicochemical properties of starch without destroying the granule structure. Hydrothermal treatments which are commonly used in modifying the physicochemical properties and enhance the RS content are annealing and heat–moisture treatment (HMT), autoclave cooling and temperature cycling. Annealing and HMT are techniques that modify starch structure without destroying its granular form. They modify the physicochemical properties of starches by improving crystalline perfection and by facilitating interactions between glucan chains (Hoover, 2010). Annealing is referred to as treatment of starch in excess water (>65%) or at intermediate moisture (40-55% w/w) for a certain time period at a temperature above the T_g but below the onset temperature of gelatinization

(T_o) (Hoover, 2010; Jacobs, Mischenko, Koch, Eerlingen, Delcour and Reynaers, 1998; Jayakody and Hoover, 2008; Tester and Debon, 2000). Heat moisture treatment (HMT) of starches is defined as a physical modification that involves treatment of starch granules at low moisture levels (<35% moisture w/w) over a certain time period (15 min-16 h) and at temperature (80-130°C) above (Tg) but below the melting temperature (T_m) (Hoover, 2010; Kulp and Lorenz, 1981; Sair, 1967; Stute, 1992). Jacobs et al. reported that annealed starch showed resistance to enzyme digestion and that heat-moisture treated starch exhibited increased enzymatic susceptibility owing to reduced relative crystallinity. HMT has been shown to influence morphology, X-ray diffraction pattern, crystallinity, granule swelling, amylose leaching, gelatinization parameters, viscosity, retrogradation and susceptibility towards acid and α amylase hydrolysis of the starch granule (Chung, Liu and Hoover, 2010; Gunaratne and Hoover, 2002; Hoover, 2010; Hoover and Manuel, 1996; Hoover and Vasanthan, 1994; Stute, 1992; Varatharajan et al., 2011; Varatharajan, Hoover, Liu and Seetharaman, 2010). However, the type and extent of change depends on the botanical origin (e.g. cereal, tuber, root or legume), starch composition (e.g., amylose amylopectin ratio and lipid content) and treatment conditions (temperature, moisture and duration of heating) (Hoover, 2010; Zavareze and Dias, 2011).

Perry and Donald (2000) and Waigh, Jenkins, and Donald (1996) have proposed that double helices in unhydrated form of starch are intact, but are not arranged regularly side by side, which is referred to as nematic state. During annealing, molecules in the amorphous regions of the granule hydrate and increase the mobility of amorphous area, and cause a limited but reversible swelling of the granule. This dynamic nature allows for flexibility in the crystalline domains with

limited side by side movements of the double helices (Perry and Donald, 2000) resulting in the formation of asmectic type structure. This process leads to an increase in the melting temperature of polymers and a narrowing of their calorimetric peaks due to the formation of more perfect crystals (Kiseleva, Genkina, Tester, Wasserman, Popov and Yuryev, 2004). However, previous investigations on effects of hydrothermal treatment on structural and physicochemical properties of starch have focused on native starches and few studies have been conducted on recrystallized starch.

2.6 References

Ball, S., et al. (1996). From Glycogen to Amylopectin: A Model for the Biogenesis of the Plant Starch Granule. **Cell.** 86(3): 349-352.

Bassett, D. C. (2003). Polymer Spherulites: A Modern Assessment. **Journal of Macromolecular Science, Part B.** 42(2): 227-256.

Bates, F. L., French, D., and Rundle, R. (1943). Amylose and amylopectin content of starches determined by their iodine complex formation1. **Journal of the American Chemical Society.** 65(2): 142-148.

Bertoft, E. and Koch, K. (2000). Composition of chains in waxy-rice starch and its structural units. **Carbohydrate Polymers.** 41(2): 121-132.

Bertoft, E., Koch, K., and Åman, P. (2012). Building block organisation of clusters in amylopectin from different structural types. **International Journal of Biological Macromolecules.** 50(5): 1212-1223.

Bertoft, E., Piyachomkwan, K., Chatakanonda, P., and Sriroth, K. (2008). Internal unit chain composition in amylopectins. **Carbohydrate Polymers.** 74(3): 527-

543.

Buléon, A., Colonna, P., Planchot, V., and Ball, S. (1998). Starch granules: structure and biosynthesis. **International Journal of Biological Macromolecules.** 23(2): 85-112.

Cai, L., Shi, Y.C., Rong, L., and Hsiao, B. S. (2010). Debranching and crystallization of waxy maize starch in relation to enzyme digestibility. **Carbohydrate Polymers.** 81(2): 385-393.

Cameron, R. and Donald, A. (1992). A small-angle X-ray scattering study of the annealing and gelatinization of starch. **Polymer.** 33(12): 2628-2635.

Conde-Petit, B., Escher, F., and Nuessli, J. (2006). Structural features of starch-flavor complexation in food model systems. **Trends in Food Science & Technology.** 17(5): 227-235.

Conde-Petit, B., Handschin, S., Heinemann, C., and Escher, F. (2007). Self-Assembly of Starch Spherulites as Induced by Inclusion Complexation with Small Ligands. In E. Dickinson and M. E. Leser (eds.). **Food colloids: Self-assembly and material science** (pp 117-126). Cambridge, RSC publishing.

Creek, J. A., Ziegler, G. R., and Runt, J. (2006). Amylose crystallization from concentrated aqueous solution. **Biomacromolecules.** 7(3): 761-770.

Daniels, D. and Donald, A. (2004). Soft material characterization of the lamellar properties of starch: Smectic side-chain liquid-crystalline polymeric approach. **Macromolecules.** 37(4): 1312-1318.

Eerlingen, R., Crombez, M., and Delcour, J. (1993). Enzyme-Resistant Starch. 1. Quantitative and Qualitative Influence of Incubation-Time and Temperature of

Autoclaved Starch on Resistant Starch Formation. **Cereal Chemistry.** 70(3): 339-344.

Eliasson, A-C. (2004). **Starch in food: Structure, function and applications.** CRC Press.

Enevoldsen, B. and Juliano, B. (1988). Ratio of A chains to B chains in rice amylopectins. **Cereal Chemistry.** 65: 424-427.

Gallant, D. J., Bouchet, B., and Baldwin, P. M. (1997). Microscopy of starch: evidence of a new level of granule organization. **Carbohydrate Polymers.** 32(3): 177-191.

Heinemann, C., Escher, F., and Conde-Petit, B. (2003). Structural features of starch–lactone inclusion complexes in aqueous potato starch dispersions: the role of amylose and amylopectin. **Carbohydrate Polymers.** 51(2): 159-168.

Helbert, W., Chanzy, H., Planchot, V., Buléon, A., and Colonna, P. (1993). Morphological and structural features of amylose spherocrystals of A-type. **International Journal of Biological Macromolecules.** 15(3): 183-187.

Himmelsbach, D., Barton, F., McClung, A., and Champagne, E. (2001). Protein and apparent amylose contents of milled rice by NIR-FT/Raman spectroscopy. **Cereal Chemistry.** 78(4): 488-492.

Hizukuri, S. (1986). Polymodal distribution of the chain lengths of amylopectins, and its significance. **Carbohydrate Research.** 147(2): 342-347.

Imberty, A., Buléon, A., Tran, V., and Péerez, S. (1991). Recent advances in knowledge of starch structure. **Starch-Stärke.** 43(10): 375-384.

Imberty, A., Chanzy, H., Pérez, S., Buléon, A., and Tran, V. (1988). The double-helical nature of the crystalline part of A-starch. **Journal of Molecular Biology.** 201(2): 365-378.

Jenkins, P. J. and Donald, A. M. (1998). Gelatinisation of starch: a combined SAXS/WAXS/DSC and SANS study. **Carbohydrate Research.** 308(1): 133-147.

Jouquand, C., Ducruet, V., and Le Bail, P. (2006). Formation of amylose complexes with C6-aroma compounds in starch dispersions and its impact on retention. **Food Chemistry.** 96(3): 461-470.

Juliano, B., et al. (1981). International cooperative testing on the amylose content of milled rice. **Starch-Stärke.** 33(5): 157-162.

Kobayashi, S., et al. (2000). Formation and Structure of Artificial Cellulose Spherulites via Enzymatic Polymerization. **Biomacromolecules.** 1(2): 168-173.

Kozlov, S. S., Blennow, A., Krivandin, A. V., and Yuryev, V. P. (2007). Structural and thermodynamic properties of starches extracted from GBSS and GWD suppressed potato lines. **International Journal of Biological Macromolecules.** 40(5): 449-460.

Krebs, M. R. H., Bromley, E. H. C., Rogers, S. S., and Donald, A. M. (2005). The Mechanism of Amyloid Spherulite Formation by Bovine Insulin. **Biophysical Journal.** 88(3): 2013-2021.

Larson, B. L., Gilles, K. A., and Jenness, R. (1953). Amperometric method for determining sorption of iodine by starch. **Analytical Chemistry.** 25(5): 802-804.

Lu, S., Chen, L-N., and Lii, C.Y. (1997). Correlations Between the Fine Structure, Physicochemical Properties, and Retrogradation of Amylopectins from Taiwan Rice Varieties. **Cereal Chemistry.** 74(1): 34-39.

Ma, U. V. L., Floros, J. D., and Ziegler, G. R. (2011). Effect of starch fractions on spherulite formation and microstructure. **Carbohydrate Polymers.** 83(4): 1757-1765.

Magill, J. H. (2001). Review Spherulites: A personal perspective. **Journal of Materials Science.** 36(13): 3143-3164.

Matveev, Y. I., et al. (1998). Estimation of Contributions of Hydration and Glass Transition to Heat Capacity Changes During Melting of Native Starches in Excess Wate. **Starch-Stärke.** 50(4): 141-147.

McGrance, S. J., Cornell, H. J., and Rix, C. J. (1998). A simple and rapid colorimetric method for the determination of amylose in starch products. **Starch-Stärke.** 50(4): 158-163.

Mestres, C., Matencio, F., Pons, B., Yajid, M., and Fliedel, G. (1996). A Rapid Method for the Determination of Amylose Content by Using Differential Scanning Calorimetry. **Starch-Stärke.** 48(1): 2-6.

Mitchell, C. R. (2009). Rice Starches: Production and Properties. In J. N. BeMiller and R. L. Whistler (eds.). **Starch: chemistry and technology** (pp. 569-578). Academic Press.

Moates, G. K., Noel, T. R., Parker, R., and Ring, S. G. (1997). The effect of chain length and solvent interactions on the dissolution of the B-type crystalline polymorph of amylose in water. **Carbohydrate Research.** 298(4): 327-333.

Morrison, W. R., Milligan, T. P., and Azudin, M. N. (1984). A relationship between the amylose and lipid contents of starches from diploid cereals. **Journal of Cereal Science.** 2(4): 257-271.

Murayama, E. (2002). Optical properties of ringed spherulites. **Polymer Preprints Japan.** 51: 460-462.

Murray, S. B. and Neville, A. C. (1998). The role of pH, temperature and nucleation in the formation of cholesteric liquid crystal spherulites from chitin and chitosan. **International Journal of Biological Macromolecules.** 22(2): 137-144.

Nordmark, T. S. and Ziegler, G. R. (2002). Structural features of non-granular spherulitic maize starch. **Carbohydrate Research.** 337(16): 1467-1475.

Oostergetel, G. T. and Van Bruggen, E. F. (1993). The crystalline domains in potato starch granules are arranged in a helical fashion. **Carbohydrate Polymers.** 21(1): 7-12.

Peng, L., Zhongdong, L., and Kennedy, J. F. (2007). The study of starch nano-unit chains in the gelatinization process. **Carbohydrate Polymers.** 68(2): 360-366.

Pérez, S. and Bertoft, E. (2010). The molecular structures of starch components and their contribution to the architecture of starch granules: A comprehensive review. **Starch-Stärke.** 62(8): 389-420.

Planchot, V., Colonna, P., and Buléon, A. (1997). Enzymatic hydrolysis of α-glucan crystallites. **Carbohydrate Research.** 298(4): 319-326.

Putseys, J., Lamberts, L., and Delcour, J. (2010). Amylose-inclusion complexes: Formation, identity and physico-chemical properties. **Journal of Cereal Science.** 51(3): 238-247.

Putseys, J. A., et al. (2009). Functionality of short chain amylose-lipid complexes in starch-water systems and their impact on in vitro starch degradation. **Journal of agricultural and food chemistry.** 58(3): 1939-1945.

Ring, S., Miles, M., Morris, V., Turner, R., and Colonna, P. (1987). Spherulitic crystallization of short chain amylose. **International Journal of Biological Macromolecules.** 9(3): 158-160.

Rolland-Sabaté, A., Colonna, P., Mendez-Montealvo, M. G., and Planchot, V. (2007). Branching features of amylopectins and glycogen determined by asymmetrical flow field flow fractionation coupled with multiangle laser light scattering. **Biomacromolecules.** 8(8): 2520-2532.

Schoch, T. J. (1942). Fractionation of starch by selective precipitation with butanol. **Journal of the American Chemical Society.** 64(12): 2957-2961.

Stanley, C. B., Hong, H., and Strey, H. H. (2005). DNA Cholesteric Pitch as a Function of Density and Ionic Strength. **Biophysical Journal.** 89(4): 2552-2557.

Takeda, Y., Hizukuri, S., and Juliano, B. O. (1987). Structures of rice amylopectins with low and high affinities for iodine. **Carbohydrate Research.** 168(1): 79-88.

Takeda, Y., Tomooka, S., and Hizukuri, S. (1993). Structures of branched and linear molecules of rice amylose. **Carbohydrate Research.** 246(1): 267-272.

Tester, R. F., Karkalas, J., and Qi, X. (2004). Starch-composition, fine structure and architecture. **Journal of Cereal Science.** 39(2): 151-165.

Waigh, T. A., Gidley, M. J., Komanshek, B. U., and Donald, A. M. (2000). The phase transformations in starch during gelatinisation: a liquid crystalline approach. **Carbohydrate Research.** 328(2): 165-176.

Waigh, T. A., et al. (2000). Side-Chain Liquid-Crystalline Model for Starch. **Starch-Stärke.** 52(12): 450-460.

Wang, J. P., et al. (2013). Emulsifiers and thickeners on extrusion-cooked instant rice product. **Journal of food science and technology.** 50(4): 655-666.

Wang, L., et al. (2010). Physicochemical properties and structure of starches from Chinese rice cultivars. **Food Hydrocolloids.** 24(2-3): 208-216.

Wang, S. and Copeland, L. (2013). Molecular disassembly of starch granules during gelatinization and its effect on starch digestibility: a review. **Food and Function.** 4(11): 1564-1580.

Whistler, R. L. and BeMiller, J. N. (1997). **Carbohydrate chemistry for food scientists.** Eagan press.

Williamson, G., et al. (1992). Hydrolysis of A-and B-type crystalline polymorphs of starch by α-amylase, β-amylase and glucoamylase. **Carbohydrate Polymers.** 18(3): 179-187.

Yano, M., Okuno, K., Kawakami, J., Satoh, H., and Omura, T. (1985). High amylose mutants of rice, *Oryza sativa* L. **Theoretical and Applied Genetics.** 69(3): 253-257.

Yoshioka, T., Fujimura, T., Manabe, N., Yokota, Y., and Tsuji, M. (2007). Morphological study on three kinds of two-dimensional spherulites of poly(butylene terephthalate) (PBT). **Polymer.** 48(19): 5780-5787.

Zobel, H. (1988). Molecules to granules: a comprehensive starch review. **Starch-Stärke.** 40(2): 44-50.

CHAPER III

EFFECT OF CRYSTALLIZATION CONDITIONS AND HYDROTHERMAL TREATMENTS ON RESISTANT STARCH FORMATION

3.1 Abstract

This study investigated the effects of recrystallization conditions and hydrothermal treatments on the resistant starch content and crystal, thermal and morphological from debranched rice starches with different chain length distributions. Rice starches were debranched at 10 and 21% solid concentrations, incubated at 25 °C or 50 °C, and further subjected to annealing or heat moisture treatment (HMT). The 10% solids of debranched starches with higher proportion of extra-long chains (ELC) had a higher RS content when incubated at 25 °C but they were not different for 21% solids. The crystallization at 25 °C favored the formation of the B-type structure, whereas crystallization at 50 °C led to the A-type structure with a higher melting temperature (100-120 °C) and a higher RS content (52%). All incubated samples showed an increase in RS content after subsequent hydrothermal treatments. The sample incubated at a high temperature contained the highest RS content (74.5%) after HMT with larger/perfect crystallites. These results suggested that the RS formation could be manipulated by crystallization conditions and improved by hydrothermal treatments which are dependent on the initial crystalline perfection.

Keywords: Resistant starch, Recrystallization, Annealing, Heat moisture treatment

3.2 Introduction

Starch is predominantly digested in the small intestine by digestive enzymes. A portion of starch known as resistant starch (RS) resists enzymatic hydrolysis in the small intestine and it is fermented by the colonic microflora. Consequently, RS provides many benefits to human health. RS reduces the glycemic and insulin responses and reduces the risk for developing type II diabetes, obesity, and cardiovascular disease. RS also reduces calorie content of foods and enhances lipid oxidation, which reduce body fat and impact body composition. In addition, the fermentation of RS in the colon promotes a healthy colon and reduces the risk of colon cancer. RS is classified into five types. The RS1 is the physically inaccessible starch; RS2 is native granular starch; RS3 is the retrograded amylose; RS4 is chemically modified starch and RS5 is amylose-lipid complex starch. The RS3 is of particular interest because of its thermal stability and remains after normal cooking (Kim et al., 2010). The production of RS3 usually involves gelatinization/dispersion and retrogradation/reassociation of starch. RS3 is mainly composed of retrograded amylose. The content and chain length of amylose is the major factor governing the formation of RS3 (Eerlingen and Delcour, 1995; Haralampu, 2000; Sajilata, Singhal and Kulkarni, 2006). Eerlingen, Deceuninck and Delcour (1993) found that RS content was higher with increasing amylose DP up to 100 but the chain length of RS is independent of the chain length of amylose which ranged from DP19-26 (Eerlingen, Deceuninck and Delcour, 1993). Chain lengths with DP10-35 are optimal not only for a high proportion of crystallinity, but also a high output of heat stable

butyrogenic RS (Kettlitz, Coppin, Roper and Bornet, 2000; Schmiedl, Bäuerlein, Bengs and Jacobasch, 2000). Enzymatic debranching of waxy starches could produce two major distributions of chain length DP 6-19 and 20-67. The crystallization of these chains could be attributed to the dense crystalline structure with more resistance to enzyme digestion (Cai, Shi, Rong and Hsiao, 2010). Rice starch amylopectin chains within a single cluster have an average chain length of 10-15, whereas chains extending into several clusters have an average chain length of 40-44 (Vandeputte and Delcour, 2004). Therefore, debranching of rice starch could release linear chains in which unit chains could be sufficient long available for double helix formation with expectation of high RS content.

The formation of RS can be considered as crystallization, which consists of three mechanisms of nucleation, propagation and maturation. The overall crystallization depends mainly on the nucleation and propagation which is dependent upon the temperature (Eerlingen, Crombez and Delcour, 1993). Therefore, the retrogradation conditions had an influence on the orientation and ordering of starch and thus affecting the formation of RS and its characteristics (Miao, Jiang and Zhang, 2009; Mutungi, Onyango, Jaros, Henle and Rohm, 2009; Mutungi, Rost, Onyango, Jaros and Rohm, 2009). For most studies, the common RS yields B-type semicrystalline aggregates, which are different in RS content and its thermal properties depending on starch sources, chain length of amylose chains, concentrations and temperatures during storage. Pohu, Putaux, Planchot, Colonna and Buléon (2004) reported that the RS produced by debranching and crystallization of maltodextrin at high concentration (25%w/v) formed the A-type crystal aggregates with limiting enzyme accessibility to double helix. Cai, Shi, Rong and Hsiao (2010)

also demonstrated that the A-type semicrystalline aggregates contained high levels of RS with thermal stability.

Hydrothermal treatments have been used to improve the level RS (Kim et al., 2010; Mutungi, Rost, et al., 2009; Ozturk, Koksel, Kahraman and Ng, 2009). Heat moisture treatment (HMT) and annealing (ANN) are two types of hydrothermal treatments that are applied to modify starch digestibility. Both treatments involve incubation of starch granules at specified moisture conditions and temperature above glass transition temperature (Tm) but below the gelatinization temperature (T_m) (Jacobs and Delcour, 1998). The formation of RS after hydrothermal treatment is due to increased interaction between starch components. However, the amount of RS varies largely, depending on starch sources. If RS formation is related to enhancement of ordering and packing of semicrystalline material, HMT and ANN should enhance the amount and thermal stability of RS. Previous investigations on effect of hydrothermal treatment on structural and physicochemical properties of starch focused on native starch but few studies have been conducted on retrograded starch.

A higher yield and high thermal stability of RS is required for a wide range of applications. Most research on RS has focused on starches from wheat, maize, potatoes, peas, waxy maize and amylomaize. A limited report is available on RS formation of starches derived from crops indigenous to the tropical regions, including rice starch. Thus, the purpose of the present study was (1) to investigate the combined effects of polymer chain length, solid concentration and incubation temperature on RS formation and their physicochemical properties from four different debranched rice starches and (2) to increase the yield and thermal properties of resulting products by hydrothermal treatment. According to the assumption that RS is crystalline starch, the

treatments of ANN and HMT may be promising strategies to reach this goal by optimizing processing conditions.

3.3 Materials and methods

3.3.1 Materials

Rice starch from four Thai rice varieties: waxy rice (RD6, 0% amylose), low-amylose rice (Phitsanulok1, PS1, 12.6% amylose), intermediate-amylose rice (Phitsanulok2, PS2, 26.0% amylose) and high-amylose rice cultivars (Chainat1, CN1, 29.6% amylose) was obtained from Udonthani, Phitsanulok and Chainat Rice Research Center under Bureau of Rice Research and Development (BRRD, Thailand). Rice starches were extracted using sodium chloride, ethanol and sodium hydroxide solution as described by (Ju, Hettiarachchy and Rath, 2001). Isoamylase (EC 3.2.1.68) and RS assay kit (K-RSTAR: lot 111105-1) were purchased from Megazyme International Ireland Limited, Ireland. Isoamylase had an activity of 1.2×10^3 isoamylase activity units (IAU)/mL at 50 ºC and pH 4.5.

3.3.2 Resistant starch preparation

3.3.2.1 Debranching and incubation

Starches (15 g, dry basis, db) were mixed with sodium acetate buffer (0.05 M, pH 4.5) to obtain 10 and 21% (w/w) solid concentrations. Their slurries were gelatinized in shaking water bath using a multi-step process: heating at 60 °C for 10 min, 85 °C for 20 min and at 99 °C for 1 h. The pastes were cooled to 50 °C, and isoamylase (5 IAU/ g of dry starch) was added and maintained at 50 °C for 24 h with glass bead shaking. After 24 h of debranching, samples (40 and 20 mL for 10 and 21% solid, respectively) were taken and freeze-dried for molecular analysis

(detailed in appendix A). The remaining samples were incubated at either low temperature (LT, 25 ℃ for 3 days) or high temperature (HT, 50 ℃ for 6 days). The LT-incubated samples were air dried overnight at room temperature (25 ± 2 ℃), while the HT-incubated samples were dried at 50 ℃ overnight until the moisture content was about 14-15%. The resulting dried-incubated samples were ground and sieved through a 120 mesh screen.

3.3.2.2 Annealing

The dried-incubated samples (1 g, db) were mixed with 2.33 mL of distilled water in tightly-closed tubes and subjected to nitrogen bubble for 10 min to remove dissolved oxygen and prevent oxidation during the high temperature treatment. Annealing was performed at 15 and 7 °C below the main peak temperature (T_p) for 16 h in a hot air oven. After 16 h of annealing, the samples were filtered through a glass filtering crucible (PYREX G4) and dried at 40 ℃ overnight until the moisture reduced to 14-15%, ground and sieved through a 120 mesh screen. Each experiment was done in duplicate.

3.3.2.3 Heat-moisture treatment

The dried-incubated samples (1 g, db) were weighed into tightly-closed tubes and then the moisture content is adjusted to obtain 30% by mixing with 0.43 mL of distilled water. The oxygen in the air space was removed by purging the air space with nitrogen for 5 min. The tubes were placed in hot air oven at 130 ℃ for 2 and 4 h. Finally, the HMT samples were oven dried at 40 ℃ until the moisture reduced to 14-15%, ground and sieved through a 120 mesh screen.

3.3.3 Resistant starch content determination

The resistant starch (RS) was analyzed according to the official methods

AOAC method 2002.02. (McCleary and Monaghan, 2002). The dried samples (100 mg) were mixed with 4 mL of enzyme mixture of pancreatic α-amylase (10 mg/mL) and amyloglucosidase (3U/mL) and then incubated at 37 °C for 16 h with agitation. After incubation, unhydrolyzed starches were collected by ethanol precipitation and centrifugation. The pellets were treated with 2 mL of 2M KOH to solubilize the RS. The RS solution was adjusted to pH 4.75 with 8 mL of 1.2 M acetate buffer (pH 3.8) and then amyloglucosidase (3300 U/mL) were added and incubated at 50 °C for 30 min. The samples were centrifuged at 3000× g for 10 min. The liberated glucose of supernatant was measured by reacting with GOPOD reagent at 50 °C for 20 min, and then the absorbance was measured at 510 nm against a reagent blank. The RS contents were calculated from liberated glucose content multiplied by 0.9.

3.3.4 Differential scanning calorimetry (DSC)

DSC measurement was conducted using DSC Q100 (TA Instruments Inc, Eschborn, Germany) calibrated with indium. Duplicate samples (9 mg) were weighed into hermetic aluminium pans, and 40 μL of DI water was added. The pans were hermitically sealed and allowed to equilibrate overnight at ambient temperature. DSC runs were performed from 10 to 200 °C at a heating rate of 3 °C/min. A 40 μL quantity of water was used as the reference to counterbalance. The data was analyzed using Universal Analysis 2000 V4.4 software (TA Instruments–Waters LLC).

3.3.5 Wide Angle X-ray diffraction (WAXD)

WAXD was performed after water content adjustment by water phase sorption for 10 days in desiccators under partial vacuum at 90% of relative humidity. Approximately 20 mg the dried samples were then sealed between two tape foils to prevent any significant change in water content during measurement. Diffraction

diagrams were recorded on an BRUKER^{TM} (Karlsruhe, Germany) D8 Discover diffractometer with Cu $K\alpha_1$ radiation (λ = 1.5405 Å). The diffracted beam was collected with a two-dimensional GADDS detector and recording time was 600 sec. The distance from the sample to detector was 100 mm. The samples were examined over the angular range of 3 to 40° (2θ) with a step size of 0.01 and a sampling interval of 10 s. X-ray spectra data were visualized and normalized using KaleidaGraph software. Spectra were then baseline corrected and peaks assigned and integrated using Origin Pro 8 (OriginLab Corporation, Northampton, USA). Pearson VII function was used to fit the individual crystalline peaks corresponding A, B and V-type allomorph reflections (Lopez-Rubio, Flanagan, Gilbert and Gidley, 2008), whereas Gaussian function was used to fit an amorphous peak at 2θ = 19°. The relative crystallinity and composites were calculated according to Frost et al (Frost, Kaminski, Kirwan, Lascaris and Shanks, 2009), based on the existence of two phases in the material. The relative crystallinity was calculated by dividing the crystalline area by the total area under the diffractogram, whereas the percentage proportions of individual allomorphs were calculated as the total area under the allomorph specific peaks divided by total crystalline area. The lateral crystal size was established from peak half width of 100 reflection (2θ ~5.6°), using the Scherre equation: $D_{hkl} = k\lambda/\beta \cos\theta$, where D_{hkl} is the average length of the diffraction domains normal to the family plane (*hkl*), *k* is a constant as 0.9 for cellulose, λ is wavelength used and β is the peak half width (Cairns, Bogracheva, Ring, Hedley and Morris, 1997).

3.3.6 Scanning electron microscopy (SEM)

A thin layer of sample was placed on aluminum stubs with conductive carbon tape and sputter coated with gold-palladium by using a JEOL JFC-1100 Fine

Coater Ion Sputter coater (Tokyo, Japan). The sample was observed using a JEOL JSM-5800LV scanning electron microscope (Tokyo, Japan) operating at an accelerating voltage of 20 kV.

3.3.7 Statistical analysis

All of the experiments were conducted in duplicate. Analysis of variance (ANOVA) was performed using SPSS version 15.0 for Windows evaluation version software (SPSS Institute Inc., Cary, NC, USA). Comparison of mean was executed using Duncan's tests.

3.4. Results and discussions

3.4.1 Molecular weight distribution of debranched starch

The MW distribution of the debranched starch from four Thai rice varieties; waxy rice (RD6), low amylose rice (PS1), intermediate-amylose rice and high-amylose rice (CN1) starches, as determined by HPSEC-MALLS-DRI, are shown in Figure 3.1. A bimodal distribution of low MW and high MW was observed for DBRD6, whereas a trimodal distribution of low, high and very high MW was observed for DBPS1, DBPS2 and DBCN1. These results were consistent with those obtained from gel permeation chromatography (Koroteeva et al., 2007). The first major peak corresponds to amylopectin short unit chains with a number-average degree of polymerization (DP_n) of 19-23, followed by the second peak of amylopectin long chains with DP_n 63-72. The minor third peaks with DP_n 623-775 that were observed for DBPS1, DBPS2 and DBCN1, which corresponded to amylose and super-long chains of amylopectin (Koroteeva et al., 2007). Table 3.1 summarizes the molecular weight distribution of four debranched starches. Thus, the first molecular

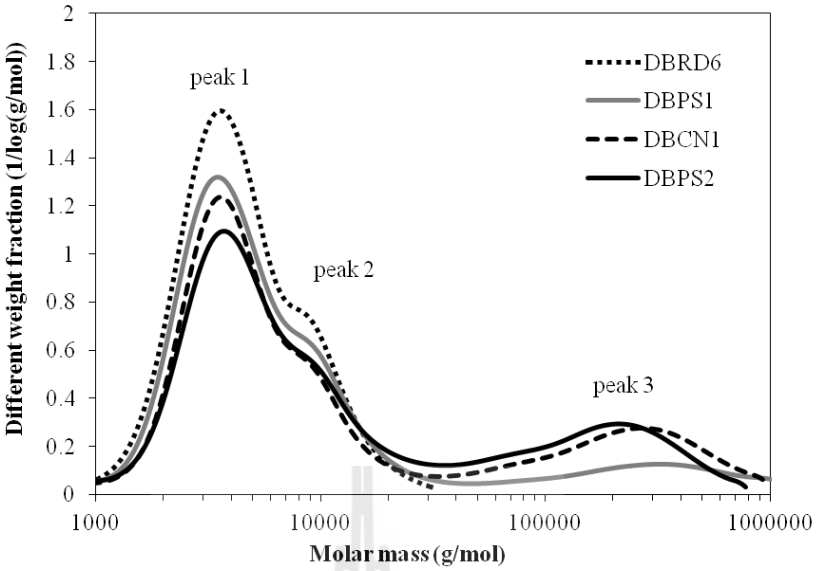

Figure 3.1 Molecular weight distributions of debranched rice starches.

Table 3.1 Molecular weight of debranched rice starches.

parameter	DBRD6		DBPS1			DBPS2			DBCN1		
	LC	SC	ELC	LC	SC	ELC	LC	SC	ELC	LC	SC
Mass fraction (%)	22	78	15	20	65	28	18	54	27	17	56
DP_{max}	55	19	1450	59	20	993	65	22	1417	66	23
DP_w	73	23	1811	83	23	1157	99	26	1504	104	26
DP_n	63	19	687	72	20	623	73	23	775	64	21
P	1.2	1.2	2.4	1.2	1.2	2.1	1.2	1.2	2.3	1.2	1.2

DP_{max}, the maximum degree of polymerization; DP_w, the weight-average degree of polymerization, DP_n, the number-average degree of polymerization; P, polydispersity index

weight distribution with DP_n 19-23, the second with DP_n 63-72, and the third with DP_n 623-775 would designated as “short chains (SC)”, “long chains (LC)”, and “extra long chains (ELC)”, respectively, in this study. Thus, DBCN1 and DBPS2 possessed a greater amount of ECL than DBPS1 and DBRD6 respectively. However,

the ECL of DBPS1 had a higher DP_n compared with those ECL of DBCN1 and DBPS2, reflecting the longer chain length of ECL of DBPS1 than DBCN1 and DBPS2 respectively. However, those LC and SC of four different debranched starches had similar molecular characteristics, as showing the same polydispersity (P) of LC and SC and had a similar ratio of mass fraction of LC to SC (3.0-3.5).

Appendix A demonstrated that all debranched rice starches hydrolyzed at 10% solid were completely debranched in which the β–amylolysis was found to be in the range of 97.2–99.5%. To confirm that those four debranched starches were completely debranched, the freeze-dried whole debranched starch samples were further debranched by isoamylase. Slightly change in MW distribution was observed (see Appendix A), indicating that the most chain of debranched starches were linear. Nevertheless, the debranched starch of PS1 hydrolyzed at 21% solid was not fully debranching, as reflected by the β–amylolysis limit value (79.7%). It was suggested that the branched molecules still present in 21%DBPS1 debranched sample.

3.4.2 Recrystallization condition dependence on product structure development

3.4.2.1 RS content

Chain length distribution has a very significant impact on the resistant content, as is shown in Table 3.2. After debranching, an increased in RS content is correlated with the proportion of ELC. The DBPS2 and DBCN1 with a greater ELC proportion gave a higher RS content than those of DBPS1 and DBRD6 in all cases (P<0.05). This result suggested that the released ELC were more preferentially crystallized than those of LC and SC. It is well established that the crystallization of long chains likewise amylose gives rise lamellar structure by chain folding, while short chains were aggregated in solution forming a micelle (Eerlingen

et al., 1993). This result suggested that the formation of lamellar structure was responsible for more resist to enzymatic digestion than a micelle. When comparing each step of productions (i.e. after debranching, following by incubation at LT (25 °C) and further drying), the RS content of all debranched starches was increased after LT incubation, as expected, due to the fact that the incubation at low temperature would promoted nucleation and enhanced RS formation (Shi and Gao, 2011). The RS content of retrograded-debranched starch was slightly increased after drying process, indicating the air-drying process had a little effect on the RS formation.

Table 3.2 RS content of 10% and 21% solid concentration of debranched rice starches as determined after each step of production.

Sample	debranching	LT Incubation	LT+Air drying
10%DBRD6 (0:22:78)[a]	0.9 ± 0.7^{a}	17.4 ± 1.5^{a}	27.1 ± 0.2^{a}
10%DBPS1 (15:20:65)	11.8 ± 0.5^{b}	28.0 ± 1.8^{b}	30.2 ± 0.4^{a}
10%DBCN1 (27:17:56)	22.2 ± 1.1^{c}	36.5 ± 1.6^{c}	36.4 ± 0.2^{b}
10%DBPS2 (28:18:54)	28.0 ± 2.4^{d}	36.1 ± 1.9^{c}	39.2 ± 0.6^{c}
21%DBRD6 (0:22:78)	3.2 ± 1.4^{a}	25.9 ± 0.3^{b}	27.9 ± 0.1^{a}
21%DBPS1 (15:20:65)	14.3 ± 1.5^{b}	24.5 ± 2.6^{b}	27.7 ± 0.4^{a}

[a] The number in parentheses is the mass fraction of ELC:LC:SC.

Mean values with different letters within each column are significantly different ($P<0.05$).

In order to obtain RS product with high yield, the starch solid concentration was an important factor, as reported in the literature for optimization of RS production (Mutungi et al., 2009); (Shi, Cui, Birkett and Thatcher, 2005); (Haynes et al., 2003); (Mutungi, Rost, et al., 2009). High starch concentration are preferred

because it facilitates drying and recovery of the product (Shi et al., 2005). In this study, the highest solid concentration that was suitable for debranching was 21% for starch containing low-amylose (PS1). However, the starches containing high amylose (i.e. PS2 and CN1) were not suitable for debranching at a high solid concentration due to the fact that a high strength gel from higher amylose content would limit enzyme diffusion and accessibility to substrate, leading to low level of hydrolysis and eventually RS formation. Nevertheless, the RS content in the final product of 21%DBRD6 and 21%DBPS1 was lower than that of 10%DBCN1 and 10%DBPS2. This indicated that the formation of RS is strongly influenced by chain length. During LT incubation, the long chains place themselves parallel and form hydrogen bridges, leading to realignment and lateral packing of chain, hence, more stable and rigid aggregate (Jayakody and Hoover, 2008a).

Table 3.3 RS content of dried-incubated samples at different recrystallization condition.

Sample	**solid concentration**	**Incubation temperature**	
	(% db. w/v)	**LT (25 °C)**	**HT (50 °C)**
DBRD6	10	27.1 ± 0.2^{a}	33.3 ± 1.6^{b}
(0:22:78)[a]	21	27.9 ± 0.1^{a}	55.4 ± 4.9^{d}
DBPS	10	30.2 ± 0.4^{ab}	32.8 ± 1.5^{b}
(15:20:65)	21	27.7 ± 0.0^{a}	49.0 ± 0.7^{c}

[a] The number in parentheses is the mass fraction of ELC:LC:SC.
Mean values with different letters are significantly different (P<0.05).

The combined effects of chain length distributions, solid concentration and incubation temperature on RS content are discussed here. Table 3.3 shows the RS content of the dried-incubated samples from DBRD6 and DBPS1 that

were debranched and incubated at different solid concentrations and incubation temperatures. Statistical analysis revealed that the type of debranched starch, DBRD6 and DBPS1, did not affect the RS content, while solid concentration and incubation temperatures showed an effect on the RS formation (P<0.05). No difference in RS content between DBRD6 and DBPS1 might suggest that that resistant starch fraction was composed mostly of recrystallized SC and LC or the ELC did not influence on the RS formation under this experiment condition. This observation might be rationalized in that the SC and LC had more mobility that was preferable to reassociate in crystallization and have dimensions critical for incorporation in the crystal structure. In addition, the amount of the ELC in DBPS1 was not sufficient to impair the diffusion of molecules for nuclei crystallization.

Under LT condition, all four samples from the 10% and 21% solid concentration of DBRD6 and DBPS1 were not statistically significant different in the RS content, indicating the solid concentration was not responsible for RS formation under this experiment condition. The RS content of all four LT-incubation samples yield was about 27-30 g/ 100g as similar to the reported by Shi and Gao for debranched waxy rice starch (Shi et al., 2011). On the contrary, under HT condition, a higher solid concentration raised the RS content significantly. In addition, the HT incubation yielded the RS content higher than that of their counterpart incubated at LT condition. This observation can be explained in terms of recrystallization kinetics which depends on temperature and plasticization effect. This phenomenon was governed by glass transition temperature (T_g) and melting temperature (T_m) of the crystals. In general, nucleation is favored at temperatures far below the T_m, but above T_g, while propagation is favored under conditions far above T_g but well below T_m

(Eerlingen, Crombez, et al., 1993). The high amount of water or plasticizer in the system, its T_g will decrease and favored the nuclei formation at temperature close to T_g but far below T_m. A lot of nuclei were formed but the growth of the formed nuclei was limited. Consequently, low solid concentration yielded lower amount of RS due to excess plasticizer that led to weak intra helical linkage between double helix. On the other hand, with high solid concentration, the rate of diffusion was increased, subsequently enhancing lateral association and double helix formation which enabled rapid attainment of critical nuclei size at far above T_g. The double helix formation were able to arrive to the site of nucleation with a fast rate to promote growth of the nucleus (more nucleation, more propagation), resulting in a maximum yield of RS. Consequently, nucleation and propagation, which are both liquid-state event requiring orientation mobility of linear molecules were suitable at 50 °C and a high solid concentration of 21% provided a sufficient plasticization effect. In addition, crystallization of debranched starches in this study took place between T_g (-5 °C for B-type starch gel) (Eerlingen et al., 1995) and T_m of the crystals (ca. 90 °C). The temperature of 50 °C used in this study might closer to temperature (T_{max}) of maximum crystallization rate where T_{max} = 1/2 (T_g+T_m), promoting either nucleation or propagation; thus, a maximum yield of RS would be expected. Therefore, if recrystallization conditions are manipulated where crystallization is favored, and if the system contains a high concentration of linear chains sufficiently available for double helix formation, and if the incubation temperature promotes the growth of crystals, the high levels of strongly resistant starch could be obtained.

The RS content of 21% DBPS1 at HT condition was significantly lower than that of 21% DBRD6 which was attributed to incomplete debranching, as

reflected in β-amylolysis value of 79.7% (Appendix A). It could be due to the branched chains of 21%DBRD6 impede the packing of double helices to form crystalline structure, leading to the formation of less dense structures and more susceptible to enzymatic action. In this study, the best condition to obtain the highest RS content of 55% was debranching of RD6 at 21% solid concentration, followed by incubation at 50 °C. This RS content was comparable to the report on Hylon V and Hylon VII which are most preferred material for producing RS-containing food ingredient, treated with autoclaving-storing cycle after debranching, yielded 41-58% RS content with the same analysis method (Ozturk, Koksel and Ng, 2009; Ozturk, Koksel, Kahraman, et al., 2009). However, less step and uncomplicated conditions for RS preparation were used in this study and that be important for obtaining RS with a larger scale.

3.4.2.2 Crystalline structure

The X-ray diffraction pattern, their corresponding crystalline type and crystallinity of debranched starches and dried-incubated samples are presented in Figure 3.2, Table 3.4 and Table 3.5. The 10% DBRD6 and 21%DBRD6 displayed an amorphous pattern (Figure 3.2A), referring the crystallization of short and long chains did not occur during debranching and coincide with a very low RS content of DBRD6. The other debranched starches with the exception of 21%DBPS1 showed a mixture of B- and V_h-polymorph with a typical peak at 2θ = 5.6°, 14.8°, 16.9°, 21.9° and 23.7° for B-polymorph. The additional peak at 2θ = 19.8° implied the presence of small regions of V- type amylose-lipid complexes. The 21%DBPS1 showed a mixture of A- and V- polymorph with strong reflection at 2θ = 15.1°, 16.9°, 17.8° and 23.2° for A-polymorph and an additional peak at 2θ = 19.8° for V-polymorph. The presence

of crystalline polymorph during debranching implied that the crystallization of the polymer chains occurred over sufficiently long linear and concentration under a high temperature. The formation of B- and V-polymorphs was attributed to a high proportion of ECL, whereas the formation of A-polymorph could be a result of the co-crystallization of SC and LC during debranching at sufficiently high concentrations. The B-type packing is usually observed in debranched starches containing long chains after debranching step (Mutungi, Onyango, et al., 2009; Mutungi, Rost, et al., 2009). Similar observation of a conspicuous A-type packing pattern has been reported in debranched maltodextrins after 24 h of debranching due to the spilt crystallization of short chains into dense aggregated crystal (Pohu, Planchot, Putaux, Colonna and Buléon, 2004). The 10% debranched starches with B-type crystalline packing had a similar percentage of crystallinity (38-44%), whereas A-type crystalline packing from the 21%DBPS1 had a high crystallinity (Table 3.4).

The X-ray diffraction patterns from the different incubated samples (Figure 3.2B and 3.2C) indicated that two different polymorphs were indeed formed due to the different crystallization temperature. Generally, high temperature, high concentration and short chains are well known to favor A-type crystallization, whereas low temperature, low concentration and longer chains promote B-type crystallite packing (Cai et al., 2010; A Pohu et al., 2004; Pohu, Putaux, Planchot, Colonna and Buléon, 2004; Shamai, Bianco-Peled and Shimoni, 2003). For this study, all of the LT-incubated samples exhibited strong reflection at 2θ = 5.6°, 13.9°, 14.9°, 16.9°, 21.9° and 23.7° with auxiliary peaks at 2θ = 10.0° and 11.2° and 25.8° (Figure 3.2B) which was a typical B-type polymorph. Furthermore, the reflection at 2θ = 17.8° implied the presence of small regions of A-type packing and its reflection

intensity was also higher than that of debranched starch counterparts. The presence of such A-type packing was probably due to an initial recrystallization during debranching and then partial crystallization during subsequent slowly cool down to room temperature. The reflection pattern of all LT-incubated samples thus ascribed to the C_B crystalline type, based on relative content of the real A- and B-allomorphs (Table 3.5). In addition, most of the incubated samples with the exceptional of 10%DBRD6-LT and 21%DBRD6-LT exhibited the V_h-polymorph, as recognized by a typical peak at 2θ = 12.9° and 19.8°. Instead, the 10%DBRD6-LT and 21%DBRD6-LT appeared the weak reflection at 2θ = 19.2° which was attributed to the ordered single amylose helices (Lopez-Rubio et al., 2008) and coincided with the absence of the amylose fraction in waxy starch. This result suggested that the low temperature incubation led to the formation of B-polymorph and also enabled stabilization of a significantly higher amount of single helical chains into entities capable of diffracting X-rays. These incubated samples exhibited a higher crystallinity than debranched starch counterparts. An increase in crystallinity is consistent with development of crystalline domain that are sufficient large and regularly arranged to diffract X-rays. In addition, the lateral crystal size calculated from the (100) reflection at 2θ = 5.6° in the diffractogram (Figure 3.2B) was increased with decreasing average chain length (Table 3.5). This is consistent with a strong ability of short chains to reorganize into large crystal.

In contrast, the HT-incubated samples showed a distinctive A-type crystalline patterns as characterized by distinguished doublet at 2θ = 16.9° and 17.8° and singlet at 2θ = 14.8° and 23.2° (Figure 3.2C). Besides the A-type profile, an additional peak appearing at 2θ = 5.6° for the 21%DBRD6-HT and the 21%DBPS1-

HT indicated the presence of small region of B-type packing which was probably the result of the existed B-type network from aggregation of longer chains or branched chain at 24 h of debranching (Pohu et al., 2004). The reflection patterns of the 21%DBRD6-HT and the 21%DBPS1-HT thus denoted a C_A-type packing with the B-type coexisting 2% of total crystallinity. Furthermore, another observation is that the 21%DBRD6-HT and the 21%DBPS1-HT patterns gave a better resolution of the peaks at $2\theta = 14.8°$, 16.9° and 17.8° as compared to the 10% DBRD6-HT or the 10% DBPS1-HT patterns, indicating that high temperature and higher concentration would facilitate the formation of more perfected A-type crystallites. The 21%DBRD6-HT and the 21%DBPS1-HT exhibited a higher RS content as well as higher crystallinity. The development of A-type crystalline packing and the resistance on enzymatic digestion can be explained as induced by both temperature and dehydration effect.

The relative crystallinity of the incubated samples is shown in Table 3.4. The difference in the crystallinity can be related to difference in crystal size, amount of crystalline regions, orientation of the double helices within crystalline domain, and extent of interaction between double helices (Mutungi et al., 2009). However, the relative crystallinity of all incubated samples was not strictly correlated with the RS content as well as the type of polymorphic formed. Although the incubated samples with mainly A-type structure are more resistant to enzyme digestion than those of B-type structure, the co-existed A-type and V-type crystal seems

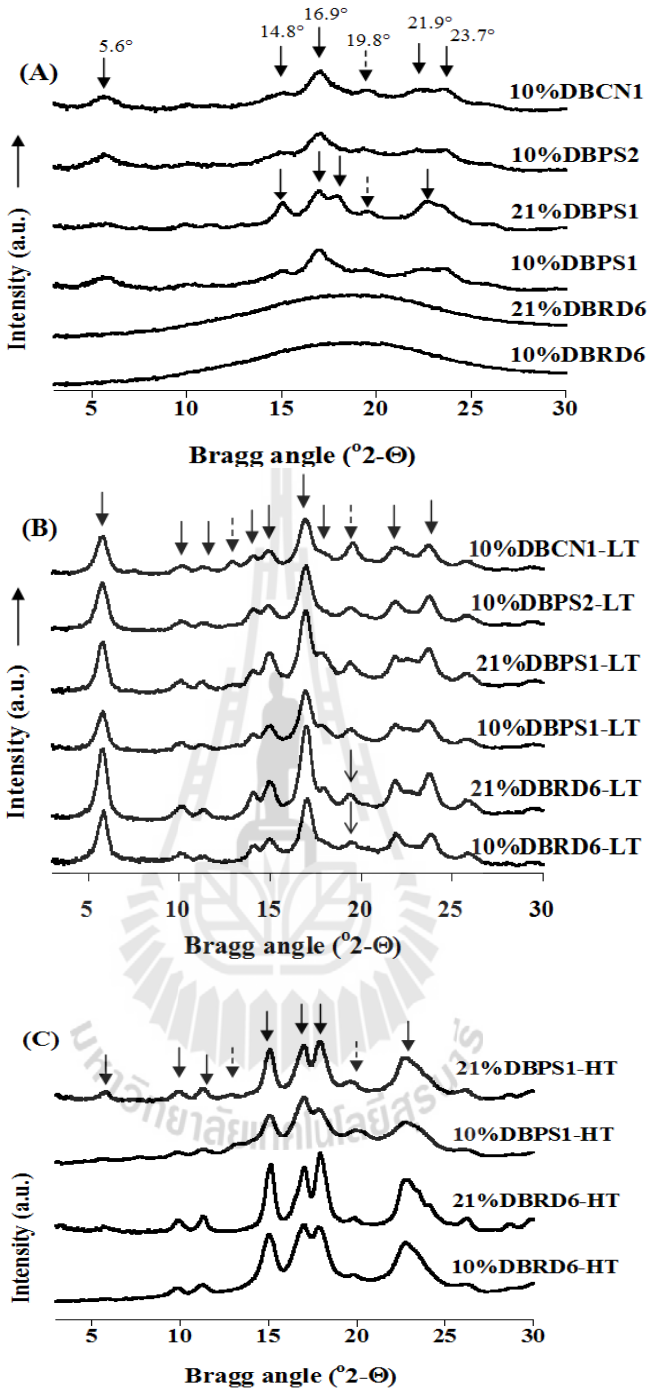

Figure 3.2 WAXD patterns of (A) the 10% or 21% debranched starches with four different varieties (RD6, PS1, PS2 and CN1), (B) incubated samples obtained from 10% or 21% debranched starches that were incubated at low temperature (LT) and (C) incubated samples obtained from 10% or 21% debranched starches that were incubated at high temperature (HT).

Table 3.4 Crystal types and crystallinity of debranched starches.

sample	Crystal types	Crystallinity (%)
10%DBRD6	amorphous	0
10%DBPS1	B + V_h	40.6
10%DBPS2	B + V_h	38.2
10%DBCN1	B + V_h	44.1
21%DBRD6	amorphous	0
21%DBPS1	A+V_h	54.6

Table 3.5 Crystal types, crystallinity and lateral crystal size of the incubated samples.

sample	Crystal types	Crystallinity (%)	Lateral crystal size (nm)	A type	B type
10%DBRD6-LT	C_B	60.3	12.23	1	99
10%DBPS1-LT	C_B + V_h	67.5	11.39	9	91
10%DBPS2-LT	C_B + V_h	67.0	10.64	1	99
10%DBCN1-LT	C_B + V_h	61.2	10.84	5	95
21%DBRD6-LT	C_B	73.1	12.29	7	93
21%DBPS1-LT	C_B + V_h	69.1	12.35	12	88
10%DBRD6-HT	A	68.4	-	100	0
10%DBPS1-HT	A + V_h	57.0	-	100	0
21%DBRD6-HT	C_A	81.0	-	98	2
21%DBPS1-HT	C_A + V_h	70.9	-	98	2

to have no significant influence on the RS content. The results suggested that the content of RS was not depends on the crystalline type and crystallinity. Other factors such as morphology, crystal defects, crystal size, and the orientation of the crystallites should be considered for their ability to resist the enzyme digestibility.

3.4.2.3 Thermal properties

The thermal properties of incubated sample are shown in Figure 3.3 and the transition parameters are summarized in Table 3.6. The 10%DBRD6-LT and 21%DBRD6-LT exhibited with a single broad endothermic peak ranging from 55 to 100 °C with the main endothermic peaks (T_{p1}) of 77 and 84 °C for 10% and 21%, respectively. In contrast, the 10%DBPS1-LT, 21%DBPS1-LT, 10%DBPS2-LT and 10%DBCN1-LT containing ELC fraction exhibited two major transition endotherms ranging from 50 to 120 °C with the first endothermic peak (T_{p1}) of 84 to 88 °C and the second endothermic peak (T_{p2}) at 106 to 107 °C. The single endothermic indicates the crystalline homogeneity, whereas endothermic multiplicity and broad were directly opposite, indicating crystalline inhomogeneity relevant to varying molecular stabilities of crystallites. These melting endotherm were depending on crystal size and chain length involved in crystallites (Buléon, Véronèse and Putaux, 2007; Moates, Noel, Parker and Ring, 1997). The broad endothermic peak might be due to the broad chain length distribution in debranched starches. Furthermore, the lower of enthalpy (ΔH) of both 10%DBRD6-LT and 21%DBRD6-LT indicated lower double helical order than those of other debranched starches probably involve to aggregation of short chain amylose to micelle that less stable double helix conformation than lamella packing of long amylose (Eerlingen, Deceuninck, et al., 1993). Thus, the endotherm at T_{p1} is probably, in part, micelle structure by aggregation of SC and LC which associated into weak crystal, lack of critical dimension necessary for involve into stable RS (Gidley et al., 1995) whereas the endotherm at T_{p2} is probably lamellar structure by chain folding of ELC and/or amylose-lipid complex, which is heat stable RS fraction (Karkalas, Ma, Morrison and Pethrick, 1995). A decrease in melting

temperature from 84 °C to 77 °C was observed for the 21%DBRD6-LT as compared with low solid concentration (10%DBRD6-LT) as well as the backwards shift of T_{p1} from 88 to 84 °C in the 21%DBPS1-LT. It suggested that high concentration favored a high nucleation rate, subsequently leading to a higher crystallization rate, resulting in smaller crystal dimensions upon incubated at LT condition.

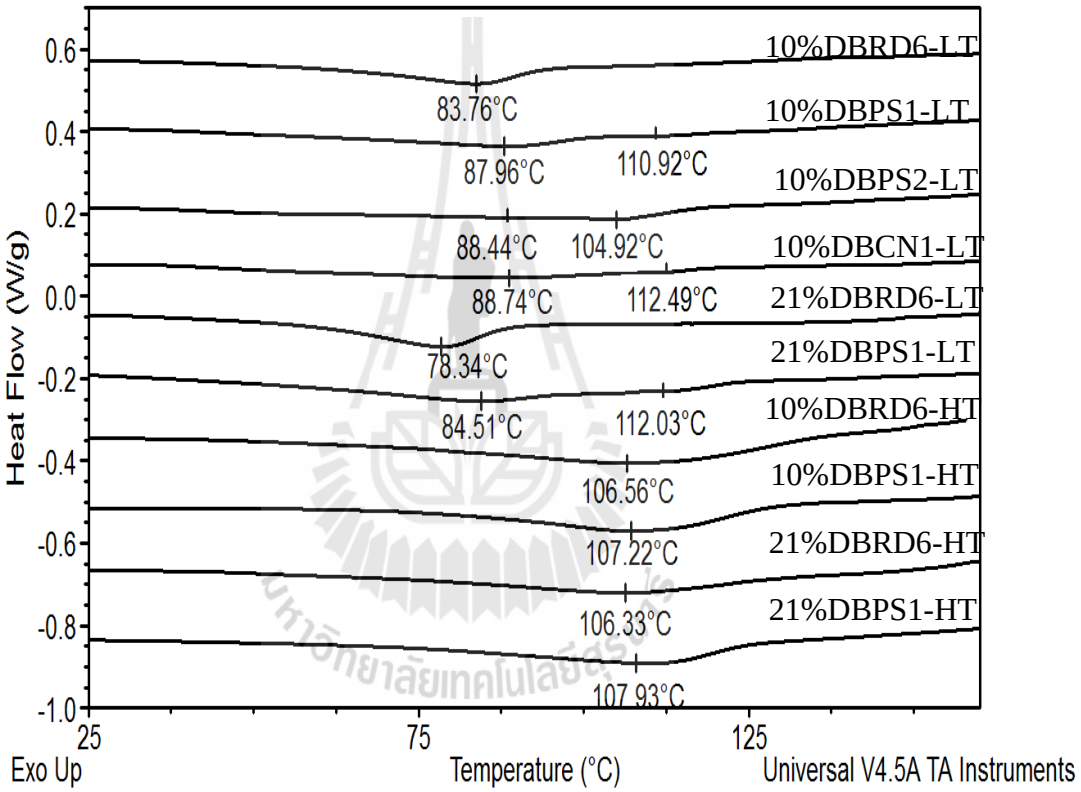

Figure 3.3 DSC thermograms of the incubated samples obtained from the 10% or 21% debranched starches with four different varieties (RD6, PS1, PS2 and CN1) that were incubated at low temperature (LT) or high temperature (HT).

Under HT incubation, a very broad unique endotherm that ranged from 59 to 135 °C with T_p of 107 °C was observed for all four debranched starches (10%DBRD6-HT, 21%DBRD6-HT, 10%DBPS1-HT and 21%DBPS1-HT), revealing the formation of crystalline with numerous of large crystal and dense ordered structure upon this HT incubation due to higher propagation at high temperature (Eerlingen, Crombez, et al., 1993). Although all samples incubated at HT showed the similar melting temperature, the 21%DBRD6-HT samples displays a higher ΔH value than other samples and consistent with the higher RS content. Furthermore, it was found that the Δ*H* value was positively correlated with RS content (R^2 = 0.81, P<0.05). The Δ*H* can be explained in terms of ordering and stabilization of double helical structure though hydrogen bond and other intermolecular forces (Mutungi, Rost, et al., 2009). Accordingly, it can be concluded that the high temperature crystallization favored A-type crystallites with large crystal size and more ordering/perfection. It resulted in less susceptible to enzyme hydrolysis.

Table 3.6 Thermal transition of the incubated samples.

sample	T_o (°C)	T_{p1} (°C)	T_{p2} (°C)	ΔT (°C)	ΔH (J/g)
10%DBRD6-LT	58.8	83.5	-	40.6	27.3
10%DBPS1-LT	51.7	88.1	112.1	71.4	34.5
10%DBPS2-LT	43.6	88.8	104.8	74.4	33.5
10%DBCN1-LT	46.1	87.1	112.1	72.5	29.9
21%DBRD6-LT	55.5	77.4	100.8	59.3	32.2
21%DBPS1-LT	47.1	84.1	107.9	79.3	34.5
10%DBRD6-HT	74.3	107.6	-	59.9	48.7
10%DBPS1-HT	64.1	106.6	-	64.4	36.8
21%DBRD6-HT	63.9	107.9	-	69.4	50.1
21%DBPS1-HT	58.9	107.8	-	67.7	40.3

The ratio of sample (dry basis) and water was 1:4.

3.4.2.4 Microstructure

The microstructure of the incubated samples was observed by SEM, as shown in Figure 3.4. It is interesting that the 10%DBRD6-LT and the 21%DBRD6-LT showed aggregates of micrometer-size spherical particles, suggesting the short chain and long chain could precipitate as B-type polycrystalline spherical morphologies (Figure 3.4A and 3.4B) with an exceptionally high crystallinity (Table 3.5). In addition, these particles seem to be aggregated together into large particles, which commonly occurred during air-drying process. For the other samples, the aggregates showed an irregular particle shape with different surface topography as commonly found in RS (Cai et al., 2010; Mutungi, Rost, et al., 2009). The surface topography of 10%DBPS1-LT and the 21%DBPS1-LT contained a fluffy structure characterized by small crystalline bodies that are loose adhered to each other (Figure 3.4C and 3.4D). On the other hand, the surface feature of 10%DBRD6-HT and 10%DBPS1-HT exhibits larger crystalline bodies, more laterally and closely packed (Figure 3.4E and 3.4G) compare to LT-samples. On the contrary, the surface of 21%DBRD6-HT and 21%DBPS1-HT possess a smooth plate-like appearance with more dense and thick structure (Figure 3.4F and 3.4H). These SEM observations support the conclusion that the incubation at high temperature and high solid concentration induce crystalline order and perfection by favoring the growth of large and dense crystals. The results obvious that aggregation and surface structure are very important factor that impact enzyme susceptibility of RS.

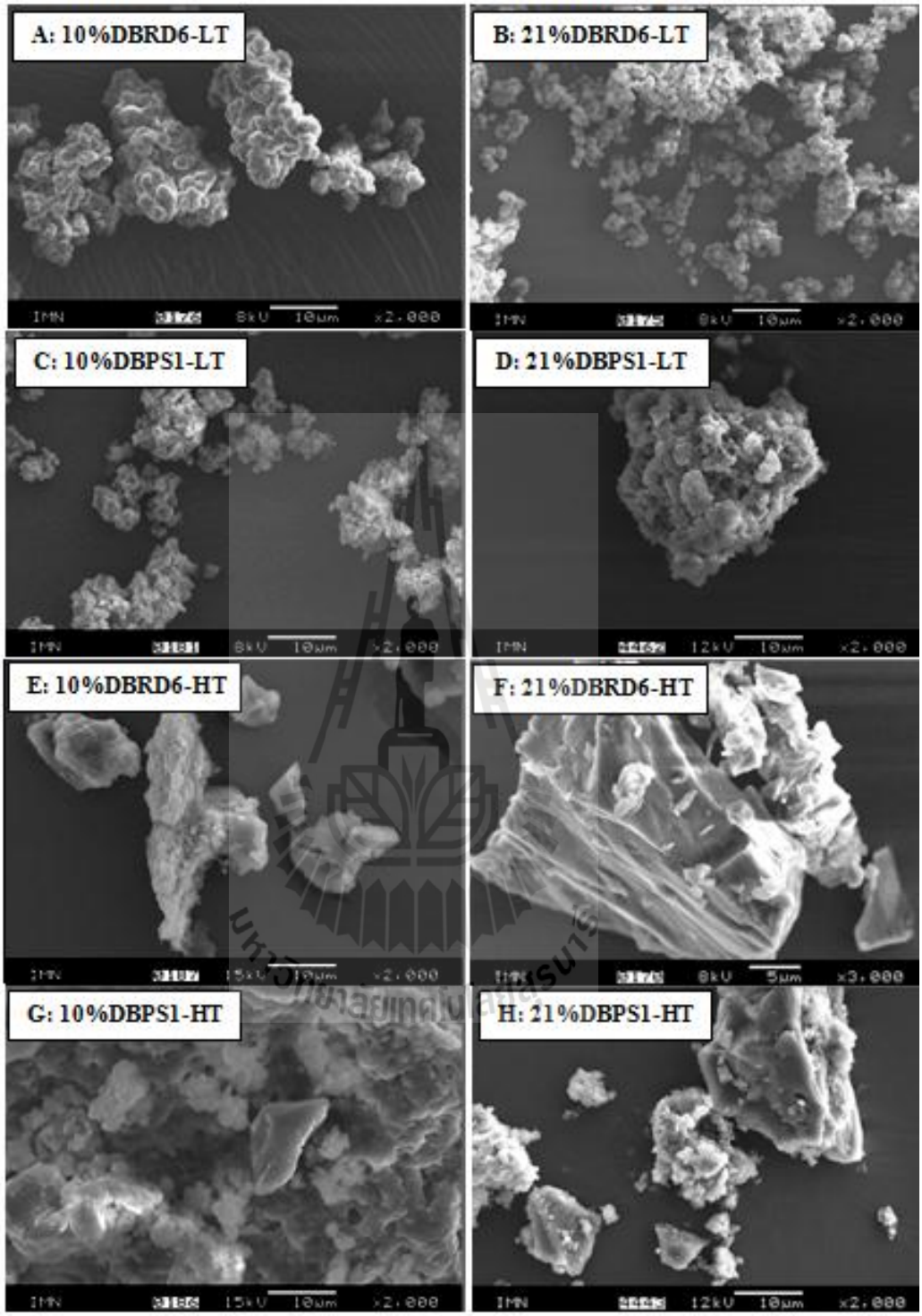

Figure 3.4 SEM images of the incubated samples obtained from the 10% or 21% debranched starches with four different varieties (RD6, PS1, PS2 and CN1) that were incubated at low temperature (LT) or high temperature (HT). Scale bar marked on image.

3.4.3 Effect of hydrothermal treatment on formation and structural characteristics of resistant starch

3.4.3.1 Effect of hydrothermal treatment on resistant starch content

The hydrothermal treatment was expected to improve the RS content. The RS contents of all incubated samples undergoing annealing and heat moisture treatment (HMT) are presented Table 3.7. As compared to the results in Table 3.3, annealing and HMT had an influence on RS content of all incubated samples, depending on the hydrothermal conditions (temperatures and times). For overall result, the hydrothermal treatment, either annealing or HMT increased the RS content of all samples, except for the 21%DBRD6-LT after HMT for 2 h. The level of RS improvement after the hydrothermal treatment was influenced by initial RS content. The low initial RS content groups with 27-33% RS content, i.e. all LT-incubated samples, 10%DBRD6-HT and 10%DBPS1-HT, yielded approximately a 1.5-2 times RS increment when they underwent hydrothermal treatments. The high initial RS content groups with 49-55% RS content of 21%DBRD6-HT and 21%DBPS1-HT were observed to similar or slightly increase in the RS content approximately 1.2-1.3 times. An increase in enzymatic resistance due to subsequent annealing and HMT can be attributed to enhancing interaction and the aggregation of helical structure by strong intermolecular forces forming a dense and compact supra-molecular structure which is unable to fit into the active site of α-amylase and one that has a reduced number of enzyme absorption sites on starch crystallites (Leloup, Colonna and Ring, 1991). Moreover, higher activation energies have to provide enough energy to disentanglement of the structure during the enzyme adsorption stage (Segel, 1993).

Table 3.7 RS content of hydrothermal treatment samples.

sample	Annealing		HMT	
	$T<T_m$ 15 °C	**$T<T_m$ 7 °C**	**2 h**	**4 h**
10% DBRD6-LT	42.9 ± 3.2^{a}	32.5 ± 1.0^{a}	47.4 ± 0.3^{c}	42.4 ± 0.7^{a}
21% DBRD6-LT	44.0 ± 0.9^{a}	37.9 ± 0.3^{ab}	47.5 ± 0.0^{a}	49.6 ± 1.5^{b}
10% DBPS1-LT	49.3 ± 0.8^{bc}	41.8 ± 2.5^{ab}	47.6 ± 0.0^{c}	39.1 ± 2.4^{a}
21% DBPS1 -LT	43.1 ± 1.4^{a}	38.6 ± 2.1^{ab}	24.7 ± 3.2^{b}	41.4 ± 0.7^{a}
10% DBRD6-HT	52.2 ± 1.9^{c}	67.5 ± 1.3^{d}	70.5 ± 0.7^{d}	60.1 ± 1.0^{c}
21% DBRD6-HT	64.1 ± 1.6^{d}	74.5 ± 2.5^{e}	70.0 ± 0.1^{d}	56.9 ± 0.7^{c}
10% DBPS1 -HT	47.6 ± 2.3^{bc}	54.2 ± 1.8^{c}	60.0 ± 0.8^{d}	45.3 ± 2.5^{ab}
21% DBPS 1-HT	51.8 ± 1.2^{b}	58.3 ± 4.6^{c}	48.1 ± 0.4^{c}	56.7 ± 1.8^{c}

Mean values with different letters within each column are significantly different ($P<0.05$)

Figure 3.5 shows that the 10%DBRD6, 21%DBRD6, 10%DBPS1 and 21%DBPS1 incubated at HT followed by either annealing or HMT tended to yield more RS than those of their counterpart incubated at LT ($P<0.001$). Under LT incubation, annealing at T_m-15 °C tended to yield more RS content than annealing at T_m-7 °C for all incubated samples, while HMT for 2 h increased the RS content of the 10%DBRD6-LT and 10%DBPS1-LT but decreased the RS content of 21% DBRD6-LT and 21%DBPS1-LT. However, effect of the nature of debranched starch and solid concentration after annealing and HMT showed no difference in RS content ($P<0.05$), reflecting that the presence of extra long chains as amylose did not promote the structural reordering and chain interaction between short and long chains. Under incubation at HT, the opposite effect was observed for annealing in that an increase in RS content was more pronounced at T_m-7 °C. HMT for 2 h increased RS content than HMT for 4 h. A decline of RS content occurred when heating exceeded 4

h probably due to the disruption of weak double helices in the crystalline and amorphous regions, resulting in formation of weak zone susceptible to hydrolysis (Hoover and Vasanthan, 1994). The highest yield of 68-75% RS content was obtained for 10% DBRD6-HT and 21%DBRD6-HT followed by annealing at T_m-7 °C or HMT at 130 °C for 2 h (Figure 3.5). A similar increase in the RS contents to about 80% was reported on debranched banana and cassava starch after HMT (Lehmann, Jacobasch and Schmiedl, 2002)·(Mutungi, Rost, et al., 2009). However, the report of RS content in the literature cannot be compared due to the determination technique used. Regard to public information, this is the highest RS type III content obtained by annealing or HMT measured by AOAC method 2002.02. This knowledge can be used to produce a product of high RS content by combination of HT incubation and subsequent hydrothermal treatment either annealing or HMT process.

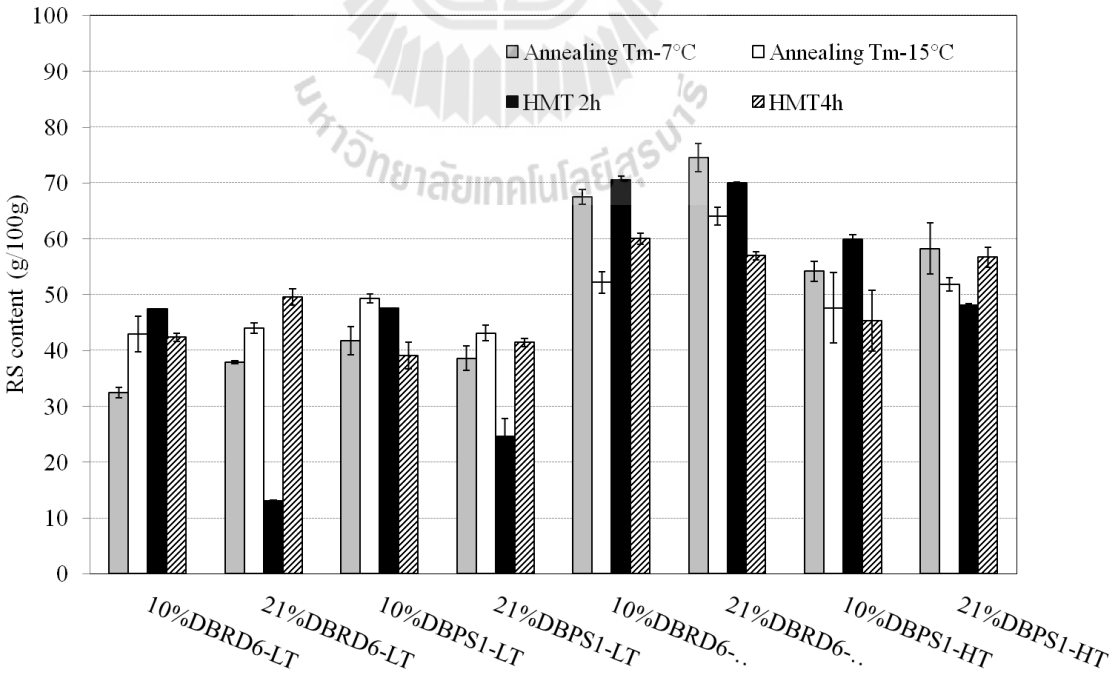

Figure 3.5 Effect of hydrothermal treatment on RS content of incubated samples formed from DBRD6 and DBPS1.

3.4.3.2 Effect of hydrothermal treatment on crystalline structure

Figure 3.6 and Figure 3.7 show the XRD patterns of the incubated samples that were treated with annealing or HMT. It was generally found that an annealing does not impact on starch polymorphic forms, however its effect was more pronounced in the B-type starches than A-type starches (L. Jayakody and R. Hoover, 2008). For LT-incubated samples with C_B-polymorph, no obvious change in the crystalline packing type was observed upon annealing. However, the reflection at 2θ = 17.8° representing co-existed A-crystallites revealed weakness after annealing. This might be suggested that the water molecules were hydrated into the central channel of A-type double helices and changed the orientation of the double helical from the monoclinic into hexagonal packing with 36 water molecules per unit cell. Similar result of a transformation from A-type toward B-like pattern has been reported for native starch by pressure treatment in a water suspension (Katopo, Song and Jane, 2002). Therefore, an improvement of such crystalline structure as a consequence of annealing in B-type starch was due to the decrease of crystalline defect, which involved the changes of imperfect crystalline region and subsequent new crystallization and/or re-crystallization of double helices into more perfect crystalline structure. In the case of HT-incubated samples with C_A or A-polymorph, annealing shows no effect on polymorphic type of all samples but shows an increased in the intensity of the reflection at 2θ = 12.9° and 19.8° for the DBPS1-HT, indicated that new amylose–lipid complexes were formed upon annealing.

For HMT, the change in polymorphic form was observed similar to native starch. For native starch, XRD patterns of cereal starches (A-type) indicate that their chain packing remains unchanged after HTM treatment, except for the

development of V-type structures. In contrast, the B-pattern of tuber starches or C-pattern of cassava starch shifts toward an A-pattern, as readily recognized by the loss of the characteristic d-spacing at 15.8 Å (Biliaderis, 2009). Likewise, the results show that the XRD pattern of the 10%DBRD6-LT, 21%DBRD6-LT, 10%DBPS1-LT and 21%DBPS1-LT were converted from the B or C_B-type into A-type structure, whereas A-type XRD patterns of the 10%DBRD6-HT, 21%DBRD6-HT, 10%DBPS1-HT and 21%DBPS1-HT remained unchanged after HMT. These structural alterations caused by HTM treatments indicate a closer packing of the double helices, i.e. there is a shift from the less stable polymorphs B (with hexagonal packing of double helices and about 36 water molecules inside every cell) into the more stable monoclinic A-structure (with about six water molecules inside the helices) (Genkina, Wasserman and Yuryev, 2004; Gunaratne and Hoover, 2002; Hoover et al., 1994; Vermeylen, Goderis and Delcour, 2006). In this context, a molecular model for the solid-state transition of B- to A-starch, involving the progressive removal of inter-helical water and a unidirectional slipping of the chain duplexes, has been reported by (Pérez, Imberty, Scaringe, French and Brady, 1990). Although, the A-type pattern remained unchanged upon HMT, the doublet at 2θ = 16.9° and 17.8° was stronger and sharper, reflecting a more compact structure of the packing of double helices after heating at high temperature (Le Bail, Bizot and Buléon, 1993; Vermeylen et al., 2006). Furthermore, an increase in individual reflection was very obvious in the 10%DBRD6-HT and 10%DBPS1-HT, implying that crystalline enhancement involves orientation modifications on the surface of crystallite rather than the internal rearrangement (Mutungi, Rost, et al., 2009). Beside B-type polymorphic transition and enhancement of ordering of double helices into more compact structure, the

development of V-type amylose-lipid complex was also observed, as recognized by the higher intensity of the reflection at 2θ = 12.9° and 19.8°.

From the results of WAXD analysis, it can be suggested that the pre-existing crystallites of the incubated samples may be modified by annealing or heat-moisture treatment, which may influence the enzyme digestibility. The results suggested that the increase in RS content upon annealing was likely due to enhanced interactions between starch chains that were formed but not disrupted during annealing, whereas HMT might increase the mobility of double helices, resulting in a disruption of some of the hydrogen bonds linking adjacent double helices. For both hydrothermal treatment resulted in an increase in crystalline perfection, the formation of large/ or more perfect crystallite and the new formation of amylose-lipid complex.

In addition, the B-type annealed samples or A-type HMT samples arising from polymorphic transition had a similar RS content (Table 3.7), such as B-polymorph of annealed of 10%DBRD6 and A-polymorph of HMT of 10%DBRD6 yield RS content of 42-47%. This result suggested that the content of RS was not dependent on the crystal type. Although, the increase in crystallinity coincided with higher amount of RS after HMT, overall crystallinity of both HMT and annealing was not correlated with the RS content (Figure 3.8). Quantitative difference in crystallinity can be implied to the differences in crystal size, amount of crystalline regions and orientation of double helices within the crystalline domains and extent of interaction between double helices or interplay of these factors. Furthermore, the total crystallinity involves to alternating layers of crystalline structures, chain folding and lattice dislocation arising from the polydisperse of debranched starch which in turn have an impact on the enzyme susceptibility of the

RS (Creek, Ziegler and Runt, 2006; Anne Pohu et al., 2004).

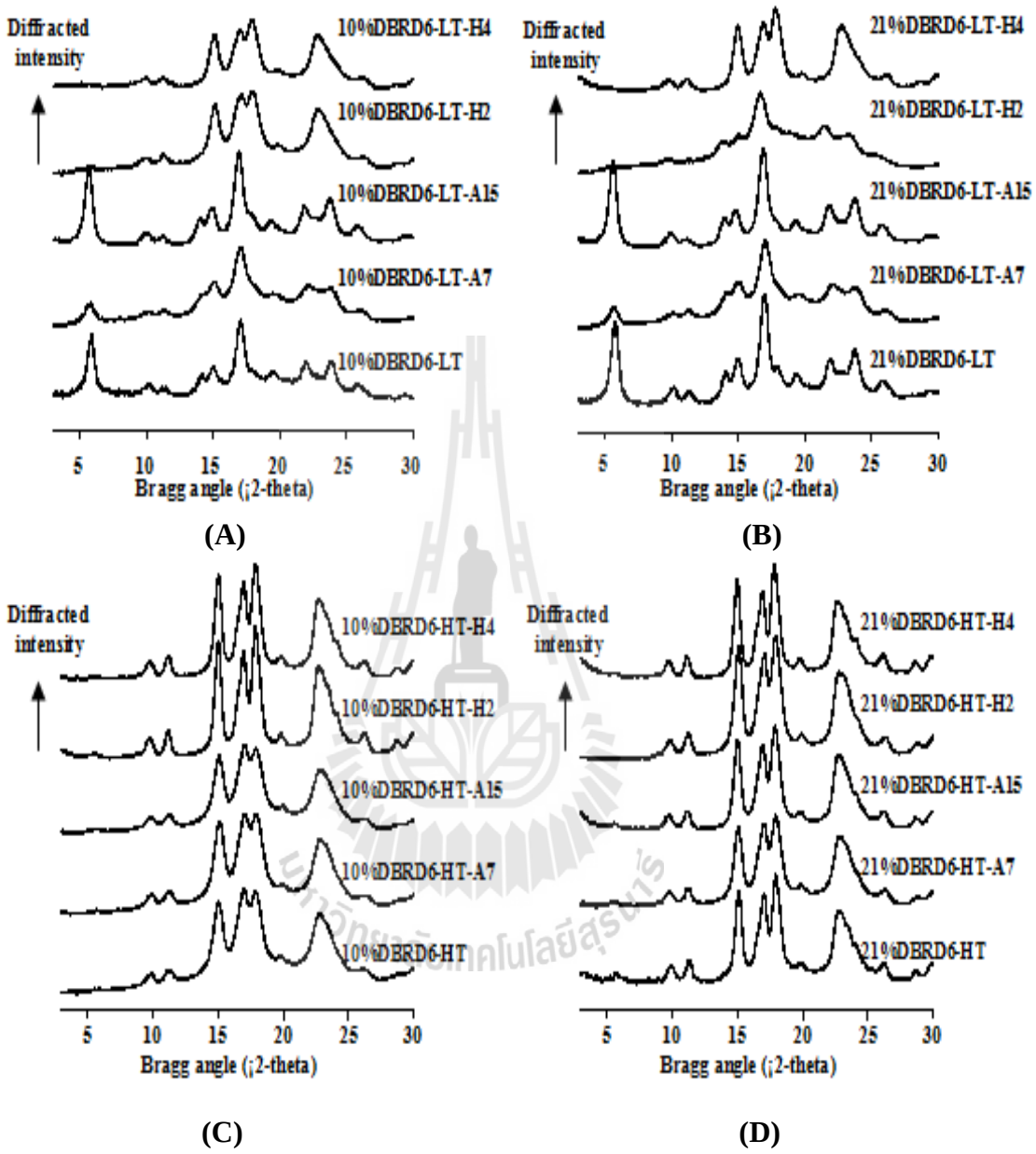

Figure 3.6 WAXD patterns of the annealed- and HMT-treated samples obtained from (A) 10%DBRD6-LT, (B) 21%DBRD6-LT, (C) 10%DBRD6-HT (D) 21%DBRD6-HT. A7 and A15 represent an annealing at 7 and 15 °C below the melting temperature of each incubated sample respectively. H2 and H4 represent heat moisture treatment for 2 and 4 h at 130 °C respectively.

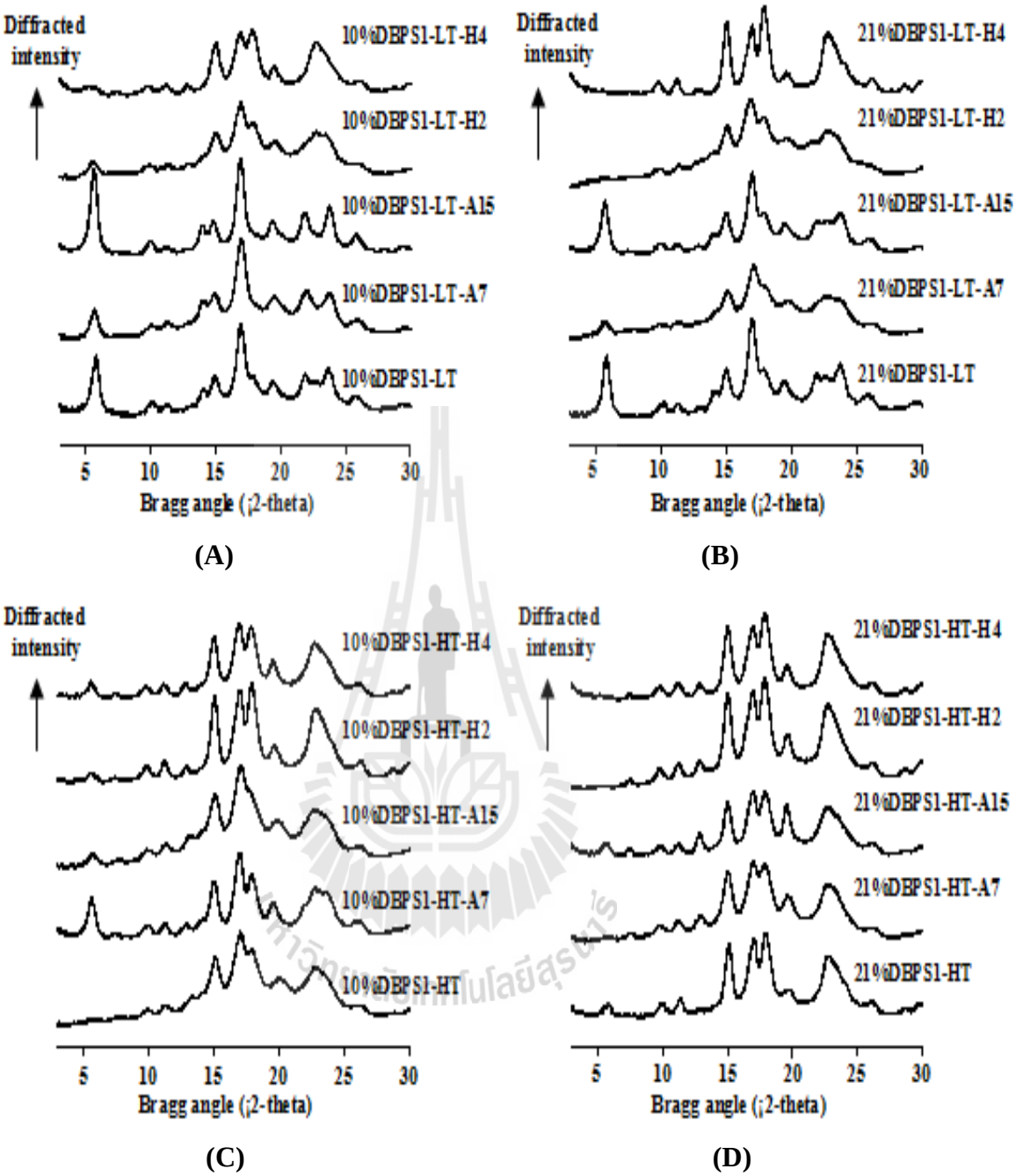

Figure 3.7 WAXD patterns of the annealed- and HMT-treated samples obtained from (A) 10%DBPS1-LT, (B) 21%DBPS1-LT, (C) 10%DBPS1-HT (D) 21%DBPS1-HT. A7 and A15 represent an annealing at 7 and 15 °C below the melting temperature of each incubated sample respectively. H2 and H4 represent heat moisture treatment for 2 and 4 h at 130 °C respectively.

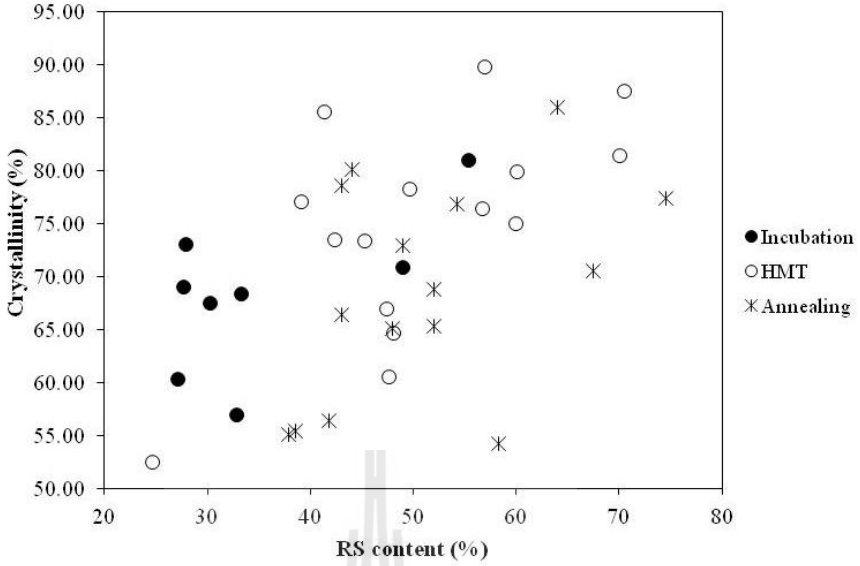

Figure 3.8 RS content as a function of crystallinity

3.4.3.3 Effect of hydrothermal treatment on thermal properties

Figure 3.9 shows DSC endotherm of annealed and HMT samples selected from the treatment yielding higher RS content and the corresponding transition parameters are displayed in Figure 3.10. For every annealed sample, the narrower transition peaks and a significant shift of T_o and T_p to higher temperature were observed upon annealing, which was attributed to more ordered and perfection of pre-existing crystallites (L Jayakody and R Hoover, 2008; Tester and Debon, 2000). The annealed samples of the 10%DBPS1-LT and 21%DBPS1-LT had higher T_o and T_p when compared to the corresponding annealed samples of the 10%DBRD6-LT and 21%DBRD6-LT (Figure 3.10). It suggested that the interactions between short, long and extra long chains are more pronounced upon annealing which was attributed to their amylose content, longer average chain length of long chains and lower proportion of short chains. Furthermore, after annealing, the T_{p2} disappeared for the 10%DBPS1-LT and the T_{p2} was decreased for the 21%DBPS1-LT (Figure 3.10).

These changes could imply the realignment and reordering of extra long chain segment. In addition, annealing resulted in decreased ΔH for all samples. A decrease in ΔH could be attributed to the loss of its helical conformation or the disruption of weakly associated double helices present in either the crystalline or non crystalline region (Gunaratne et al., 2002). The decline in ΔH values was also coincident with the disappearance of A-type pre-existing. This coherence might be hypothesized that the A-type pre-existing crystallites might be loosely associated and hence prone to disruption and reorganization when the temperature of annealing is closer to T_o of crystallites. In the case of DBPS1, a decrease in ΔH might relate to a decrease in endotherm peak at T_{p2}. It might be postulated that the disruption of extra long chains that did not fully crystallized but rather existed as loose amorphous matrices caged within crystalline part of the short and long chains, in which water could be absorbed into this amorphous region and in turn facilitated the hydration and dissociation of double helical conformation (Tester et al., 2000). The effect of annealing can thus be described as the facilitation of molecular mobility within the amorphous region accompanied by the disruption of weak crystallites allowing the chain interaction within the amorphous and crystalline domain, the formation of double helices, crystalline perfection and completion of crystallization of more stable crystalline structure.

Obviously, HMT caused a shift of the endotherm to higher temperature of all LT-incubated samples, whereas the endothermic range of all HT-incubated sample remain in the same range (Figure 3.9), suggesting that HMT was more pronounced in the LT- incubated sample with B-type structure than that of the HT-incubated sample with A-type crystalline structure. It is interesting to notice that a

greater increase in T_o and T_p of the 10%DBRD6-LT, 21%DBRD6-LT, 10%DBPS1-LT and 21%DBPS1-LT was consistent with the change of crystalline type (B or C_B to A-type), in which the packing of double helices within the A-type polymorphic structure was much more densely and closely packed than the B-type (Buléon et al., 2007). However, the change of B to A-type crystalline structure did not significantly improve the enzyme resistance. It seems that the crystal types are not key factors that control the enzyme digestibility. Furthermore, HMT caused a significant decrease in ΔH of all samples, suggesting the disruption of double helices in crystalline region by HMT (Jacobs et al., 1998). Therefore, it can be postulated that the HMT had an effect on recrystallized glucans by change in packing arrangement of double helices in crystallites from B- to A-type crystallinity, transformation of amorphous into helices, disruption of crystallites and formation of crystalline amylose-lipid complexes.

HMT or annealing did not significantly affected T_p value of the HT-incubated samples with A-type crystalline structure (Figure 3.10) and their melting region remained relatively unchanged after annealing or HMT (Figure 3.9). It could be assumed that crystalline organization of these samples with A-type crystalline structure was already highly perfect. Therefore, HMT or annealing products could not make any more perfect. This observation may imply the minimal internal relocation of the glucans probably because of more dense packing of double helices of initial samples which did not facilitate the absorption of water and restricts the molecular mobility. In addition, a higher enhancement of the RS content after hydrothermal treatment was observed in the DBRD6 than in the DBPS1. DSC also supported that the enthalpy of hydrothermal treated debranched RD6 was higher and it consistent with the better resolution and higher crystallinity in XRD. This suggested

that essentially short chains would allow the potential mobility of the chains to be realigned and form more highly ordered structure.

From overall results, annealing and HMT resulted in a higher T_o, T_p and relative crystallinity but the lower ΔH value. A decrease in melting enthalpy of the samples reflects the loss of double helices within both the amorphous and crystalline region (Gunaratne et al., 2002). An increase in melting temperature and relative crystallinity of the samples indicate the crystallite growth or perfection of already existing crystallites, change in orientation of starch crystallites, crystallites perfection, formation of new crystallites (Jacobs et al., 1998; L Jayakody et al., 2008).

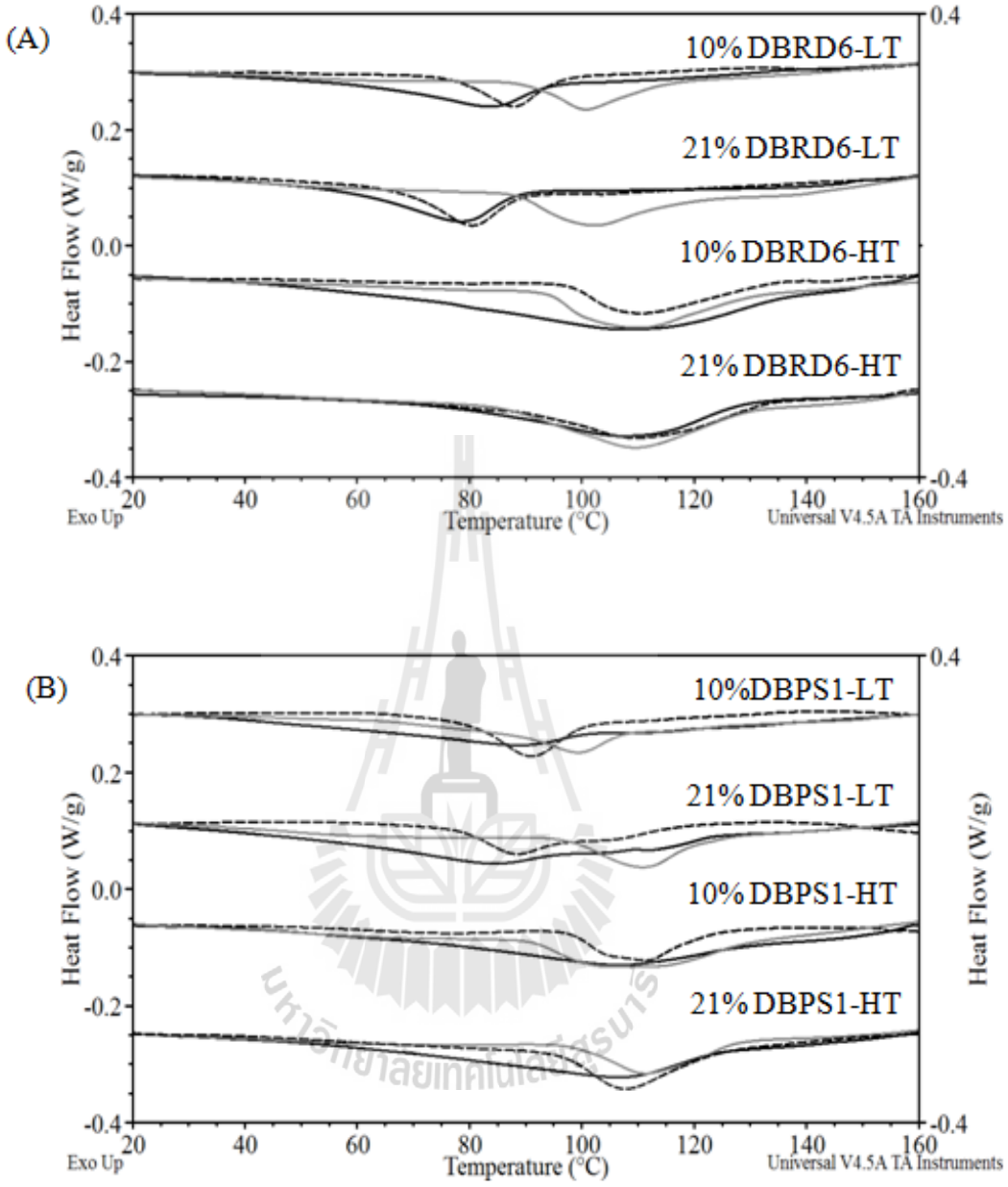

Figure 3.9 DSC thermograms of the annealed- and HMT-treated samples obtained from (A) 10% and 21%DBRD6 incubated at low temperature (LT) and high temperature (HT) and (B) 10% and 21%DBPS1 incubated at low temperature (LT) and high temperature (HT). Black solid lines represent the incubated samples, dot lines represent the annealed-treated samples and gray solid lines represent the HMT-treated samples.

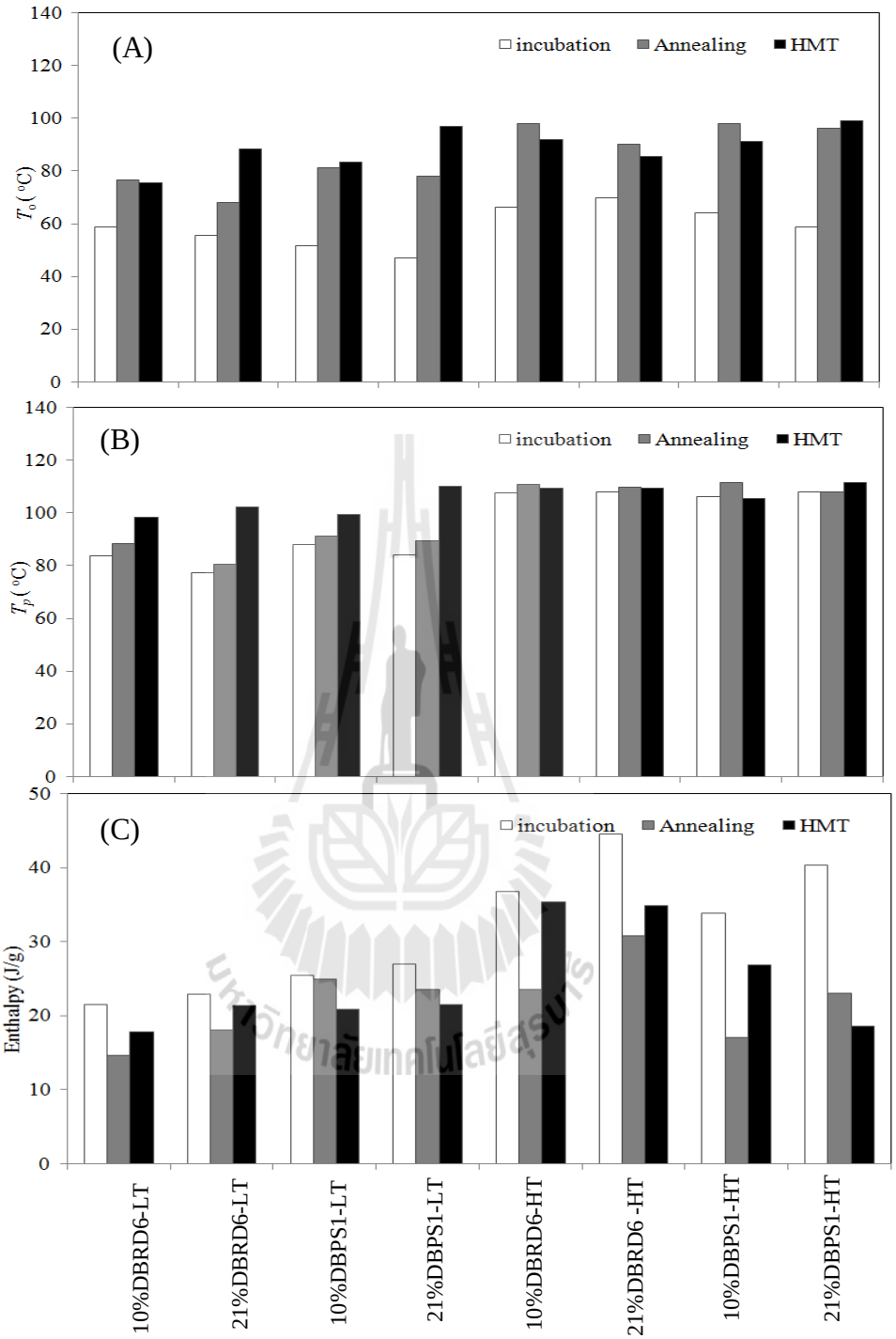

Figure 3.10 Onset temperature (A), peak temperature (B) and enthalpy (C) of the incubated samples, the annealed- and HMT-treated samples obtained from 10% and 21%DBRD6 and 10% and 21%DBPS1 that were incubated at low temperature (LT) and high temperature (HT).

3.4.3.4 Effect of hydrothermal treatment on microstructure

SEM images of the annealed and HMT treated samples are given in Figure 3.11. The effect of hydrothermal on microstructure was studied in the B-type spherical polycrystalline of 10%DBRD6-LT and 21%DBRD6-LT and B-type irregular polycrystalline of 10%DBPS1-LT. The 10%DBRD6-LT and 21%DBRD6-LT still retained their spherical morphology after annealing or HMT. However, surface topography of B-type annealed samples of 10%DBRD6-LT-A15 (Figure 3.11A) and 21%DBRD6-LT-A15 (Figure 3.11C) appeared rough surface as well as the crystalline bodies are larger, more aggregate and closely packed. On the contrary, A-type HMT samples of 10%DBRD6-LT-H2 (Figure 3.11B) and 21%DBRD6-LT-H2 (Figure 3.11D) exhibited smooth surface with larger crystalline bodies and more close adhering when compared to annealed sample and their particle surface seem to be fused together due to the melt of amorphous and imperfect crystalline region during HMT. Although it is noticed that the A-type crystallites had smoother surface than their B-type counterparts, the enzyme digestibility of two difference polymorphs was not different. It is possible that crystallite size and the extent of perfection, length of chain in crystalline domain and the behavior of non crystalline regions may have strong influence on the melting and digestibility (Mutungi, Rost, et al., 2009). For 10%DBPS1-LT comprising fluffy structure (Figure 3.11E and 3.11F), the surface profile in which crystalline bodies were more laterally ordered and closely packed and possessed surface porosity in annealed sample (Figure 3.11E), however, more closely packed and merged particle were observed in HMT treated sample (Figure 3.11F). These SEM observations can be suggested that the aggregation and surface morphology

are very important factor besides crystallinity, and interplay of these factors have an impact on the thermal stability and enzyme susceptibility of RS.

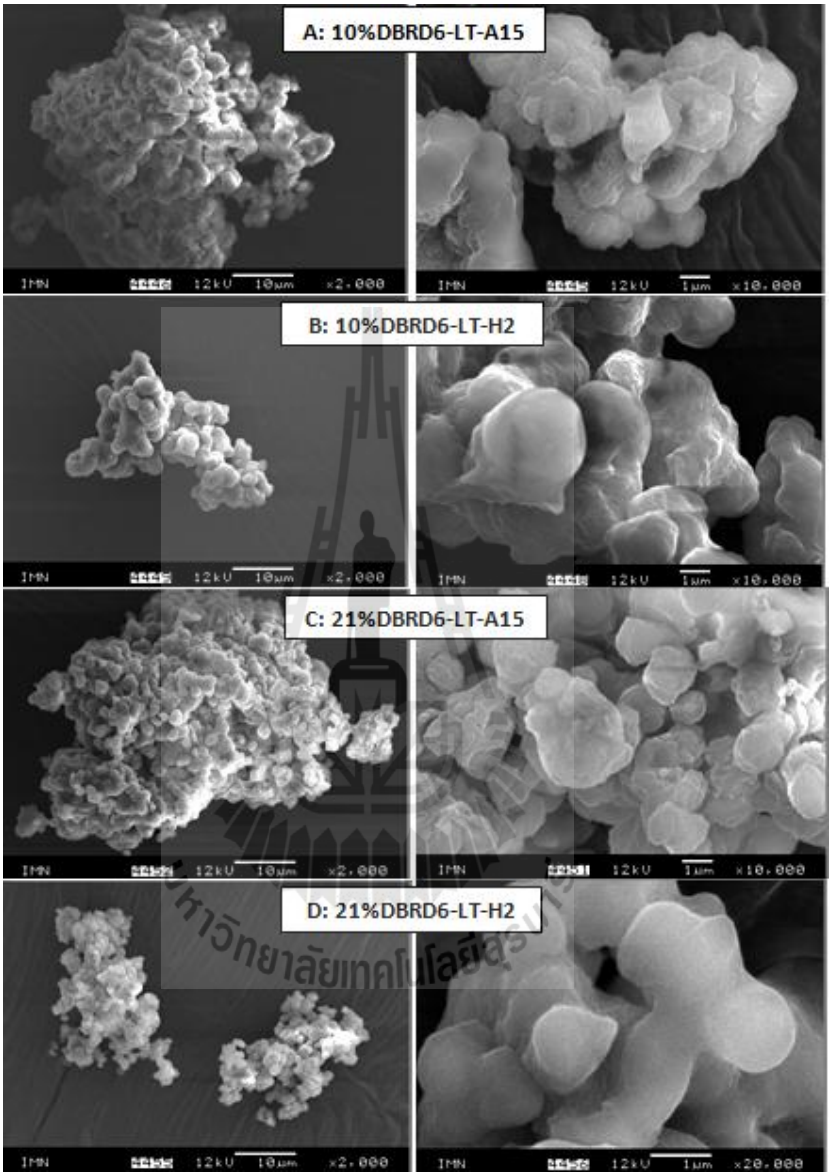

Figure 3.11 SEM images of the annealed treated sample and HMT-treated sample obtained from the 10% and 21%DBRD6 and 10% and 21%DBPS1 that were incubated at low temperature (LT) and high temperature (HT). A15 represents an annealing for 16 h at 15 °C below the melting temperature of each incubated sample. H2 represents heat moisture treatment at 130 °C for 2 h. Scale bar marked on image.

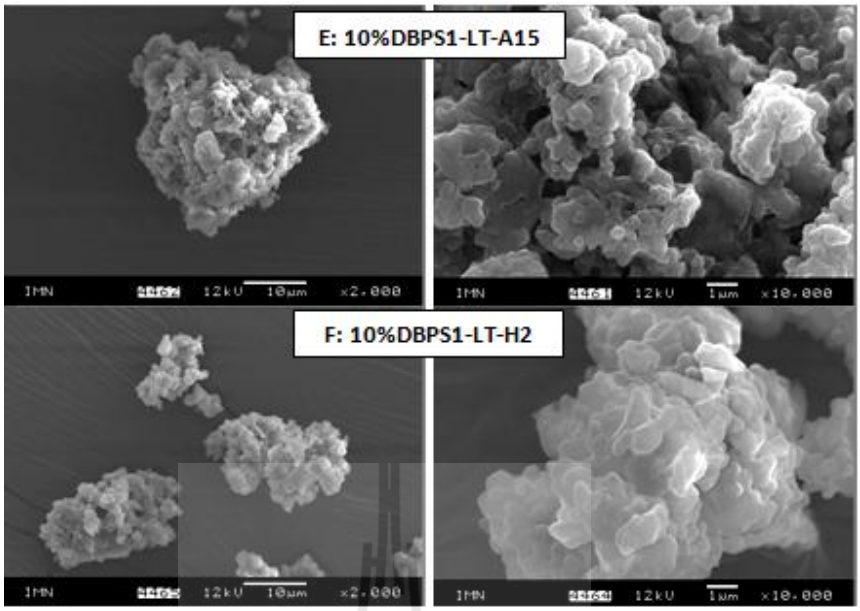

Figure 3.11 SEM images of the annealed treated sample and HMT-treated sample obtained from the 10% and 21%DBRD6 and 10% and 21%DBPS1 that were incubated at low temperature (LT) and high temperature (HT). A15 represents an annealing for 16 h at 15 °C below the melting temperature of each incubated sample. H2 represents heat moisture treatment at 130 °C for 2 h. Scale bar marked on image (*continued*)

3.5 Conclusions

This study demonstrated that the formation of resistant starch was affected by many structural factors. The RS yield of debranched starch was strongly influenced by different chain length distributions and applying the treatment conditions (temperature, solid concentration and hydrothermal treatment). The highest yield of thermo-stable RS could be obtained when crystallization occurs with a high concentration of sufficiently long linear chains for double helix formation and crystallization under high temperature (more nucleation and more propagation). The

resistant starch consisted of double helices ordered in a three-dimensional structure of the A- or the B-type, depending on the incubation temperatures, concentrations and chain lengths. Hydrothermal treatments, both annealing and HMT, interfered on the disruption of imperfect co-existed crystallites, enhanced the growth of pre-exist crystallites and induced the formation of new crystallites and change orientation of crystallites, thus improving the perfection of the crystallites which enhanced RS formation. The initial imperfectness of the packing of the double helices within crystallites were extremely important factors contributing to further perfection of crystallites and the improvement of the melting temperature, which contributed to RS enhancement on resistance against thermal process. In addition, aggregation and surface morphology were very important factors which in turn had an impact on enzyme susceptibility of RS. This knowledge could be used to produce a range of product with varying degree of resistance to enzyme digestion and thermal stability based on the crystallization conditions.

3.6 References

Biliaderis, C. (2009). Structural transitions and related physical properties of starch. **Starch: Chemistry and technology.** 293-372.

Buléon, A., Véronèse, G., and Putaux, J. (2007). Self-Association and Crystallization of Amylose. **Australian Journal of Chemistry.** 60(10): 706-718.

Cai, L., Shi, Y-C., Rong, L., and Hsiao, B. S. (2010). Debranching and crystallization of waxy maize starch in relation to enzyme digestibility. **Carbohydrate Polymers.** 81(2): 385-393.

Cairns, P., Bogracheva, T. Y., Ring, S., Hedley, C., and Morris, V. (1997). Determination

of the polymorphic composition of smooth pea starch. **Carbohydrate Polymers.** 32(3): 275-282.

Creek, J. A., Ziegler, G. R., and Runt, J. (2006). Amylose crystallization from concentrated aqueous solution. **Biomacromolecules.** 7(3): 761-770.

Eerlingen, R., Crombez, M., and Delcour, J. (1993). Enzyme-Resistant Starch. 1. Quantitative and Qualitative Influence of Incubation-Time and Temperature of Autoclaved Starch on Resistant Starch Formation. **Cereal Chemistry.** 70(3): 339-344.

Eerlingen, R., Deceuninck, M., and Delcour, J. (1993). Enzyme-Resistant Starch. II. Influence of Amylose Chain Length on Resistant Starch Formation. **Cereal Chemistry.** 70(3): 345-350.

Eerlingen, R. and Delcour, J. (1995). Formation, analysis, structure and properties of type III enzyme resistant starch. **Journal of Cereal Science.** 22(2): 129-138.

Frost, K., Kaminski, D., Kirwan, G., Lascaris, E., and Shanks, R. (2009). Crystallinity and structure of starch using wide angle X-ray scattering. **Carbohydrate Polymers.** 78(3): 543-548.

Genkina, N. K., Wasserman, L. A., and Yuryev, V. P. (2004). Annealing of starches from potato tubers grown at different environmental temperatures. Effect of heating duration. **Carbohydrate Polymers.** 56(3): 367-370.

Gidley, M., et al. (1995). Molecular order and structure in enzyme-resistant retrograded starch. **Carbohydrate Polymers.** 28(1): 23-31.

Gunaratne, A. and Hoover, R. (2002). Effect of heat–moisture treatment on the structure and physicochemical properties of tuber and root starches. **Carbohydrate Polymers.** 49(4): 425-437.

Haralampu, S. (2000). Resistant starch-a review of the physical properties and biological impact of RS3. **Carbohydrate Polymers.** 41(3): 285-292.

Haynes, L., et al. (2003). Enzyme-resistant starch for reduced-calorie flour replacer: **US patent No. 6,352,733.**

Hoover, R. and Vasanthan, T. (1994). Effect of heat-moisture treatment on the structure and physicochemical properties of cereal, legume, and tuber starches. **Carbohydrate Research.** 252: 33-53.

Jacobs, H. and Delcour, J. A. (1998). Hydrothermal modifications of granular starch, with retention of the granular structure: A review. **Journal of Agricultural and Food Chemistry.** 46(8): 2895-2905.

Jayakody, L. and Hoover, R. (2008). Effect of annealing on the molecular structure and physicochemical properties of starches from different botanical origins–A review. **Carbohydrate Polymers.** 74(3): 691-703.

Jayakody, L. and Hoover, R. (2008). Effect of annealing on the molecular structure and physicochemical properties of starches from different botanical origins – A review. **Carbohydrate Polymers.** 74(3): 691-703.

Ju, Z., Hettiarachchy, N., and Rath, N. (2001). Extraction, denaturation and hydrophobic properties of rice flour proteins. **Journal of Food Science.** 66(2): 229-232.

Karkalas, J., Ma, S., Morrison, W. R., and Pethrick, R. A. (1995). Some factors determining the thermal properties of amylose inclusion complexes with fatty acids. **Carbohydrate Research.** 268(2): 233-247.

Kettlitz, B. W., Coppin, J. V. J.-M., Roper, H. W. W., and Bornet, F. (2000). Highly fermentable resistant starch. **EP Patent No. 0,846,704.**

Kim, N. H., et al. (2010). Combined effect of autoclaving-cooling and cross-linking

treatments of normal corn starch on the resistant starch formation and physicochemical properties. **Starch-Stärke.** 62(7): 358-363.

Koroteeva, D. A., et al. (2007). Structural and thermodynamic properties of rice starches with different genetic background: Part 1. Differentiation of amylopectin and amylose defects. **International Journal of Biological Macromolecules.** 41(4): 391-403.

Le Bail, P., Bizot, H., and Buléon, A. (1993). 'B'to 'A'type phase transition in short amylose chains. **Carbohydrate Polymers.** 21(2): 99-104.

Lehmann, U., Jacobasch, G., and Schmiedl, D. (2002). Characterization of resistant starch type III from banana (Musa acuminata). **Journal of Agricultural and Food Chemistry.** 50(18): 5236-5240.

Leloup, V., Colonna, P., and Ring, S. G. (1991). α-Amylase adsorption on starch crystallites. **Biotechnology and Bioengineering.** 38(2): 127-134.

Lopez-Rubio, A., Flanagan, B. M., Gilbert, E. P., and Gidley, M. J. (2008). A novel approach for calculating starch crystallinity and its correlation with double helix content: A combined XRD and NMR study. **Biopolymers.** 89(9): 761-768.

McCleary, B. V. and Monaghan, D. A. (2002). Measurement of resistant starch. **Journal of AOAC International.** 85(3): 665-675.

Miao, M., Jiang, B., and Zhang, T. (2009). Effect of pullulanase debranching and recrystallization on structure and digestibility of waxy maize starch. **Carbohydrate Polymers.** 76(2): 214-221.

Moates, G. K., Noel, T. R., Parker, R., and Ring, S. G. (1997). The effect of chain length and solvent interactions on the dissolution of the B-type crystalline polymorph of amylose in water. **Carbohydrate Research.** 298(4): 327-333.

Mutungi, C., Onyango, C., Jaros, D., Henle, T., and Rohm, H. (2009). Determination of optimum conditions for enzymatic debranching of cassava starch and synthesis of resistant starch type III using central composite rotatable design. **Starch-Stärke.** 61(7): 367-376.

Mutungi, C., Rost, F., Onyango, C., Jaros, D., and Rohm, H. (2009). Crystallinity, thermal and morphological characteristics of resistant starch type III produced by hydrothermal treatment of debranched cassava starch. **Starch-Stärke.** 61(11): 634-645.

Ozturk, S., Koksel, H., Kahraman, K., and Ng, P. K. (2009). Effect of debranching and heat treatments on formation and functional properties of resistant starch from high-amylose corn starches. **European Food Research and Technology.** 229(1): 115-125.

Ozturk, S., Koksel, H., and Ng, P. K. (2009). Characterization of resistant starch samples prepared from two high-amylose maize starches through debranching and heat treatments. **Cereal chemistry.** 86(5): 503-510.

Pérez, S., Imberty, A., Scaringe, R., French, A., and Brady, J. (1990). **Computer modeling of carbohydrate molecules.** Paper presented at the ACS Symposium Series.

Pohu, A., Planchot, V., Putaux, J., Colonna, P., and Buléon, A. (2004). Split crystallization during debranching of maltodextrins at high concentration by isoamylase. **Biomacromolecules.** 5(5): 1792-1798.

Pohu, A., Putaux, J.-L., Planchot, V., Colonna, P., and Buléon, A. (2004). Origin of the limited α-amylolysis of debranched maltodextrins crystallized in the A form: A TEM study on model substrates. **Biomacromolecules.** 5(1): 119-125.

Sajilata, M., Singhal, R. S., and Kulkarni, P. R. (2006). Resistant starch–a review. **Comprehensive Reviews in Food Science and Food Safety.** 5(1): 1-17.

Schmiedl, D., Bäuerlein, M., Bengs, H., and Jacobasch, G. (2000). Production of heat-stable, butyrogenic resistant starch. **Carbohydrate Polymers.** 43(2): 183-193.

Segel, I. H. (1993). **Enzyme kinetics**: Wiley New York.

Shamai, K., Bianco-Peled, H., and Shimoni, E. (2003). Polymorphism of resistant starch type III. **Carbohydrate Polymers.** 54(3): 363-369.

Shi, M-M. and Gao, Q-Y. (2011). Physicochemical properties, structure and in vitro digestion of resistant starch from waxy rice starch. **Carbohydrate Polymers.** 84(3): 1151-1157.

Shi, Y-C., Cui, X., Birkett, A. M., and Thatcher, M. G. (2005). Slowly digestible starch product. **US Patent No. 0,117,265.**

Tester, R. F. and Debon, S. J. (2000). Annealing of starch-a review. **International Journal of Biological Macromolecules.** 27(1): 1-12.

Tm, T. (1993). Enzyme-resistant starch. I. Quantitative and qualitative influence of incubation time and temperature of autoclaved starch on resistant starch formation. **Cereal Chemistry.** 70(3): 339-344.

Vandeputte, G. and Delcour, J. (2004). From sucrose to starch granule to starch physical behaviour: a focus on rice starch. **Carbohydrate Polymers.** 58(3): 245-266.

Vermeylen, R., Goderis, B., and Delcour, J. A. (2006). An X-ray study of hydrothermally treated potato starch. **Carbohydrate Polymers.** 64(2): 364-375.

CHAPER IV

CRYSTALLIZATION BEHAVIOR OF DEBRANCHED RICE STARCHES IN AQUEOUS SOLUTION: TIME-RESOLVED SYNCHROTRON RADIATION WIDE-ANGLE X-RAY SCATTERING STUDY

4.1 Abstract

Crystallization behavior kinetics during enzymatic debranching and incubation of rice starches were studied using time-resolved synchrotron radiation wide-angle x-ray scattering (WAXS). Crystalline structure of debranched rice starches gel are two-phase systems, composed of crystalline domains and regions containing amorphous polymer chains and water. As revealed by Synchrotron WAXS, a shoulder at 2θ of 4.3° interpreted as the long-range order structure of the gel network. A change in the intensity ratio of the shoulder expressed phase change behavior from amorphous gel to crystalline phase. Crystallization kinetics was quantified using the Avrami model. Two-stage crystallization was observed during debranching and incubation. Crystallization during debranching was favored by extra-long chains and the mode of crystallization was rod-like growth from sporadic nuclei, whereas crystallization during incubation was favored by short chains with a preferential growth into rod-like or disk-like geometry when crystallization at low or high temperature respectively.

Keywords: Crystallization behavior, Kinetic, Avrami equation, Synchrotron WAXS

4.2 Introduction

Understanding the starch structure and function relationship is of fundamental importance in starch technological applications. Starch is composed of two component, amylose and amylopectin. The molecular structure of amylose is essentially linear with a few relatively long branches. In contrast, the molecular structure of amylopectin is highly branched via 1, 6-α linkages (Wang, Bogracheva and Hedley, 1998; Zobel, 1988). Since natural starch generally has a granular structure, it needs to be modified before it can be used as food or industrial materials. Starch debranching technique has been applied to disrupt starch granules, producing the linear starch chains with low molecular weight. Debranched starch products have been used in various nutritional and pharmaceutical applications that function as slow digestible starch (SDS) (Shin et al., 2004), resistant starch (RS) (González-Soto, Mora-Escobedo, Hernández-Sánchez, Sanchez-Rivera and Bello-Pérez, 2007; Thompson, 2000), opacifying agents and fat replacer (Chiu, 1992; Chiu and Henley, 1993) and tabletting excipient for controlled release (Arends-Scholte et al., 2000; Wai-Chiu and Kasica, 1992).

The properties of debranched starches are dependent on amylose content and chain length distribution of starting starch, degree of debranching, type of debranching enzyme used and crystallization conditions, which, in turn, affect the physical, functionality, nutritional value and technological properties (Chiu, 1990; Leong, Karim and Norziah, 2007; Mutungi, Passauer, Onyango, Jaros and Rohm, 2012). During debranching, the long chains and short chains have the tendency to form double helices that will further aggregate into crystallites (Pohu, Planchot, Putaux, Colonna and Buléon, 2004). Three crystal structures (A, B, C) has been

found, depending on concentration and temperature (Cai and Shi, 2014; Cai, Shi, Rong and Hsiao, 2010; Pohu et al., 2004; Shamai, Bianco-Peled and Shimoni, 2003). Differences in the prebiotic properties from different preparations indicated that the crystalline structure and morphological variations could be used to delineate the physiological capabilities of crystallized starch (Cai and Shi, 2014).

Most research has disclosed the influence of starch structure on crystallization kinetic parameters in native starch system. But a comprehensive study on the relationship between debranched starch structure and crystallization kinetic during debranching and incubation has not been reported yet, it is therefore important to know how the combination of parameters (i.e., chain distribution, concentration and temperature) affects the crystallization behavior and kinetics of the debranched starches. Avrami's theory has often been employed for kinetic study of the starch crystallization during isothermal incubation (Doona, Feeherry and Baik, 2006; Jagannath, Nanjappa, Das Gupta and Arya, 2001; Yao, Zhang and Ding, 2002). In this chapter, the parameters in the Avrami equation were used to descript the crystallization behaviors and kinetics of debranched starch either during debranching or during incubation.

Wide-angle X-ray scattering (WAXS) has been used for studies on change in long range ordering and crystallization behavior of starch in the dry state (Cai, Shi, et al., 2010; Pohu et al., 2004; van Soest, Tournois, de Wit and Vliegenthart, 1995). Up to now, no information is available concerning the crystallization in the inhomoginities in the crystalline gel. This study will point out crystalline structure occurring in the domains with higher electron density to gain understanding of the intramolecular order and intermolecular structure of the debranched chains during

debranching and incubation. This study also employed WAXS to kinetically monitor the crystallization process of debranched rice starches and investigate the effect of crystallization conditions (chain distribution, concentration and temperature) on crystallization behaviors and to correlate these factors with Avrami parameters describing the crystallization kinetics of debranched starches during both debranching and incubation.

4.3 Materials and Methods

4.3.1 Materials

Rice starch from four Thai rice varieties: waxy rice (RD6, 0% amylose), low-amylose rice (Phitsanulok1, PS1, 12.6% amylose), intermediate-amylose rice (Phitsanulok2, PS2, 26.0% amylose) and high-amylose rice cultivars (Chainat1, CN1, 29.6% amylose) was obtained from Udonthani, Phitsanulok and Chainat Rice Research Center under Bureau of Rice Research and Development (BRRD, Thailand). Rice starches were extracted using sodium chloride, ethanol and sodium hydroxide solution as described by (Ju, Hettiarachchy and Rath, 2001). Isoamylase (EC 3.2.1.68) was purchased from Megazyme International Ireland Limited, Ireland, having an activity of 1.2×10^3 isoamylase activity unit (IAU)/ml. One IAU is defined as the amount of isoamylase that liberates 1 μmol of glucose in 1 min under the condition at 50 ºC, pH 4.5 of the isoamylase activity.

4.3.2 Sample preparation

The gelatinized samples were prepared by suspending 10% (w/v) or 21% (w/v) of starch in 25 mL sodium acetate buffer (0.05M, pH 4.5). Then, the suspensions were submitted to heat in shaking water bath over multi-step process: 60

°C for 10 min, 85 °C for 20 min and finally at 99 °C for 1 h. The gelatinized samples were then allowed to cool down to 50 °C before carrying out the debranching reaction. The isoamylase enzyme (5 IAU/ g of dry starch) was added to homogenized sample and the reaction was maintained at 50 °C for 24 h with glass bead shaking. During this time interval, the samples were taken from the reaction mixture and the samples solutions were loaded into the sample cell with thin flat aluminium windows and then inserted into a sample-holder in a vertical orientation (Figure 1). The scattering patterns were immediately examined using Synchrotron WAXS.

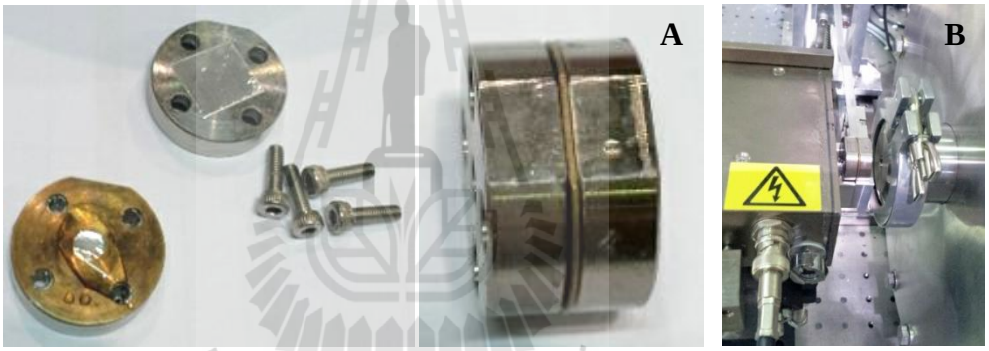

Figure 4.1 Sample cell and sample holder: (A) sample cell (B) sample holder.

After 24 h of debranching reaction, the samples were loaded into the sample cell with thin flat aluminium windows. The sample cells were sealed with paraffin film and aluminium sealing tape to prevent the water loss and then stored at either 25 °C for 3 days or 50 °C for 5 days in an incubator. The crystallization conditions at 25 °C or 50 °C were named as ‘‘LT’’ or ‘‘HT’’ respectively. During this time interval, the samples were inserted into a sample-holder and the scattering patterns were then examined using Synchrotron WAXS. No weight changes were observed for the sample before and after heating, indicating that no moisture lost during the

experiment. The buffer containing 5 IAU isoamylase was also loaded into the sample cell in order to subtract background properly.

For powder sample, the samples were dehydrated after 3 days or 5 days of incubation. The incubated samples with LT were air dried overnight at room temperature (25±3 °C), while the HT- incubated samples were dried overnight at 50 °C in a hot air oven until the moisture content was about 14-15%. The dried-incubated samples were ground and sieved through a 120 mesh screen. The powder samples were analyzed the crystalline structure using WAXS.

4.3.3 Synchrotron radiation experiments

Experiments were carried out at the BL1.3W: SAXS (Small/Wide Angle X-ray Scattering), Synchrotron Light Research Institute (SLRI), Nakhon Ratchasima, Thailand. The details of the beamline setup at the BL1.3W beamline have been reported elsewhere (Soontaranon and Rugmai, 2012). The 8 keV synchrotron X-ray beam monochormatized by a doulble multilayer monochromator was used, the beam beam size at the sample position was 1×0.2 mm^2 and a flux density was above 10^{10} photons/sec/μm^2. The scattering patterns were recorded with a MAR-CCD (SX165) detector. The explosion time for each data collection was 60 sec. The sample-to-detector distance was determined to be 139.33 mm by Titanium dioxide standard.

4.3.4 Data processing

The program called SAXSIT (Small Angle X-ray Scattering Image Tool) developed in-house using Matlab was used for data reduction and collection. After the data acquisition, the obtained two-dimensional (2D) images were integrated into one-dimensional (1D) scattering curves by means of the SAXSIT program. The sample scattering pattern were normalized to the photodiode value (intensity of the

transmitted beam) and exposure time and corrected by subtraction of a dark current. The sample scattering pattern was calculated from:

$$\tilde{I}_{sam} = \frac{(\bar{I}_{sam} - \bar{I}_{dark})}{T_{sam}.\, i_{sam,IC}} \quad (1)$$

Where,

$\bar{I}_{sam} = \frac{I_{sam}}{t_{sam}}$ = sample pattern divided by sample exposure time t_{sam},

$\bar{I}_{dark} = \frac{I_{dark}}{t_{dark}}$ = dark current pattern divided by accumulated time t_{dark},

$T_{sam} = \frac{i_{sam,PD}/i_{sam,IC}}{i_{cell,PD}/i_{cell,IC}}$ = sample transmission

$i_{sam,PD}$ is beam intensity (measured by a photodiode at the beamstop), integrated over the measurement period of the sample and $i_{cell,PD}$ is that for the empty sample cell

$i_{sam,IC}$ and $i_{cell,IC}$ are x-ray intensity, measured by the ion chamber, integrated over the period of the measurements of sample and the empty sample cell, respectively.

The sample scattering pattern was aligned and then the pattern was calculated along a radial path starting from the specified origin from 250 to 290 deg with step size of 0.5 deg/step. The intensity values are obtained from each pixel lied in the path. The number of points which the intensity is obtained is approximately the number of pixels in that path. The radial distance from the origin to a point on the detector plane is converted into the scattering angle (θ). The scattering angle is given by

$$2\theta = \tan D^{-1} \left(\frac{D}{L}\right) \quad (2)$$

where *D* is the distance from the origin to the point on the detector plane, calculated using the pixel size and *L* is the sample-detector distance.

4.4. Results and discussions

4.4.1 Structure of the incubated-debranched starch in an aqueous solution

Figure 4.2 shows the WAXS patterns of the solvent, waxy rice starch gel, incubated-debranched samples in aqueous solution and in powder samples considered in this study. From figure 4.2A, it is observed that the WAXS pattern of the solvent (a) displayed two broader scattering shoulders at 2θ = 5.2° and 27.4°. Appearance of broad WAXS shoulder of a sodium acetate buffer solution was similar to binary ethanol-water solution that has been considered as living transient three-dimensional labile networks of hydrogen bonds (Diat et al., 2013). The existence of this network, with enhanced electronic density due to more oxygen atoms and less CH_3 groups which is the origin of the broad peak observed in WAXS. The shoulder at 2θ = 27.4° = q = 1.92 Å might arise from intramolecular interactions, such as O–H (0.99 Å) within acetate and water molecules and C–O (1.44 Å) bonds and non-bonding O···H(CH_3) (2.07 Å) within acetate one (Takamuku, Saisho, Nozawa and Yamaguchi, 2005). The WAXS pattern of waxy rice starch gel (Figure 4.2Ab) was identical with that observed from the solvent (Figure 4.2Aa), displaying the scattering shoulder at 2θ = 4.3° and 26.9°. No broadening of the amorphous peak as observed in gelatinized sample powder is detected (Figure 4.2Bb). In this study the shoulder at 2θ = 26.9° = q = 1.88 Å was equivalent to the distance of 3.35 Å (q = 2Π/D). This distance was correspond to the interatomic distance of O···O hydrogen bonds betweeen water molecule (Takamuku et al., 2005). In addition, it was correspond to the distance between oxygen atom and water molecule, which is long to form the hydrogen bond. (Popov et al., 2009; Takahashi, Kumano and Nishikawa, 2004). For

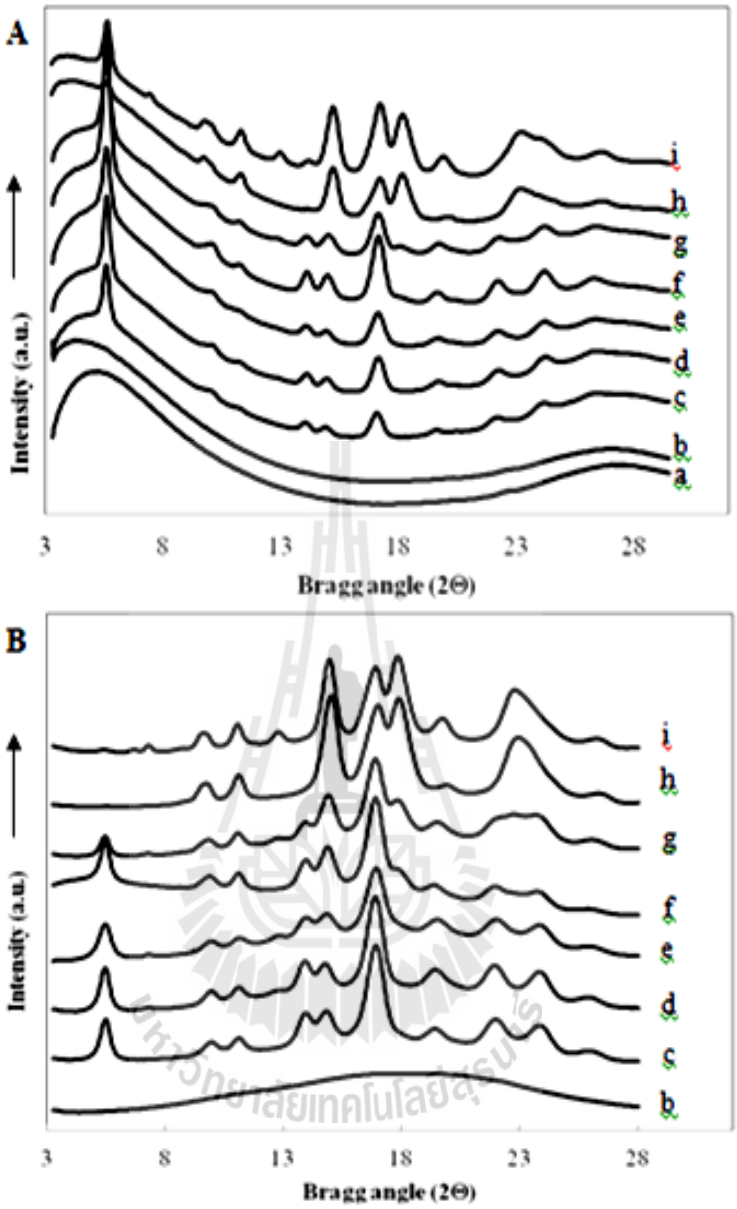

Figure 4.2 WAXS patterns of (A) samples in aqueous suspension and (B) powder samples: (a) diluents buffer, (b) 10% waxy rice starch gel, (c) 10%DBRD6-LT, (d) 10%DBPS1-LT, (e) 10%DBCN1-LT, (f) 21%DBRD6-LT, (g) 21%DBPS1-LT, (h) 21%DBRD6-HT and (i) 21%DBPS1-LT.

the shoulder at $2\theta = 4.3°$ of amorphous gel as equivalent to the distance of 20.6 Å, it cannot assign this shoulder to specific conformations. The position of this shoulder

was found to be lower than the long-range ordering of free buffer/water. Therefore, it can be referred to the long-range ordering of buffer/water to surrounding starch molecules which existed in three forms as bound water, loosely bound water, and free water (Zhong and Sun, 2005). This may suggested that the long-range ordered structure formed in the gel. The microstructure of starch gel is generally a three-dimensional gel network, making up from cross-linking of amylose and amylopectin with its surrounding free water molecules and a large number of intermolecular hydrogen bonds (Chaudhary and Adhikari, 2010). It could be concluded that this waxy rice starch gel is a single phase system containing amorphous polymer chains and rich in water. For incubated-samples in aqueous suspension (Figure 4.2Ac-i), it is observed that their WAXS patterns exhibited a lower resolution of the scattering peaks than those of powder samples (Figure 4.2Bc-i), which attributed to the water scattering effect. Although, the scattering pattern of the samples in aqueous suspension were not identical with those patterns of powder samples, the scattering angles and intensities relations of identified peaks were in agreement with those in the scattering peaks of powder samples. The correspondence of all scattering peaks demonstrated that the crystalline domains in the samples in aqueous suspension had the same unit cell as the powder samples in an A- or B-conformation. The 10%DBRD6-LT (c), 10%DBPS1-LT (d), 10%DBCN1-LT (e) consequently display a typical of B-type pattern, while the 21%DBRD6-LT (f) and 21%DBPS1-LT (g) show C_B- and C_B+V-type pattern respectively. The 21%DBRD6-HT (h) and 21%DBPS1-HT (i) show A-type and C_A+V crystal structures respectively. In addition, a peak at 2θ = 17.8° was more predominant in powder samples as compared to samples in aqueous suspension, suggesting that A-type crystal was developed during drying. This

study confirms the previous report (Chapter 3) in that the formation of B-type crystallinity was favored by low concentration and low temperature and was independent from chain length distribution, while A-type crystallization was favored by high concentration, high temperature and low DP.

As compared with powder samples, the peak haft width for 100 reflections (2θ = 5.6°) of samples in aqueous suspension was narrower, thus the crystal size (based on the Scherre equation: $D_{hkl} = k\lambda/\beta \cos\theta$) was larger than those of the powder samples. It could be suggested that the large and perfect crystal was formed during incubation in aqueous suspension. The shape of scattering backgrounds of incubated-debranched samples in aqueous solution are identical with starch gel and the position of scattering peaks coincide with the peaks of the A or B-type crystal structure corresponding to crystalline phase (Lopez-Rubio, Flanagan, Gilbert and Gidley, 2008). Consequently, the structure of the incubated-debranched samples solutions are two-phase systems, compose of crystalline domain with large and perfect crystal and regions containing amorphous polymer chains and water.

4.4.2 Phase behavior and aggregation of rice starches during debranching and incubation

The change in WAXS intensity was observed with the incubation time (Figure 4.3). With increasing time, a higher long range ordering was developed from the gel. It was also observed that the intensity of shoulder at 2θ = 4.3° had a tendency to decrease over time (inserted in Figure 4.3), which resulted in a lower of background at initial Bragg angle (2θ 3° to 16°). A decrease in this intensity suggested that there is a reduction in the electron density differences between the different structures. Change of intensities shoulders are due to change in specific

chain conformations of long-range ordering of double helices, involving amylose aggregation, amylose gelation and crystallization (Gidley, 1989; van Soest et al., 1995). These could be related to a change in phase behavior from gel-like state to a more crystalline state during debranching and storage. Previous studies have shown that the amylose chain can reorganize or self-associate over long periods, allowing amylose-amylose interaction in the present of water, which results in water being pushed out of the matrix and creating the crystalline amylose (Chaudhary et al., 2010). Gidley and Bulpin (1989) reported that phase behavior and aggregation of amylose dependence on the amylose chain length and concentration. It has been found that precipitation (and not gelation) occurred for chain lengths of DP < 110, whereas gelation occurred for amylose DP > 250 at concentrations of >1.0%. In this study, during long term incubation, the DBRD6 samples containing essentially SC were found to precipitate at all concentrations and incubation temperatures, whereas the DBPS1 and DBCN1 containing ECL samples were found to form hard gels on LT incubation and soft gels on HT incubation. Consequently, the change in intensity shoulder could be sensitive to such morphological development. The change in phase behavior could be expressed by using the ratio of the WAXS intensity at $2\theta = 4.3°$ of the final time and each different time (I_{final} (4.3°)/I_t (4.3°)), where I_{final} represents the intensity of fully crystallized samples after storage for $t = \infty$ and I_t represents the intensity of amorphous gel of each starch for t min. The WAXS intensity ratio was taken and plotted against time as displayed in Figure 4.4. It can be seen that the WAXS intensity ratio of the DBRD6 samples (Figure 4.4A) did not change over the debranching time scale from 0 to 24 h, sugeesting no aggregation and crystallization of amylopectin or branched molecules took place during debranching. After completely

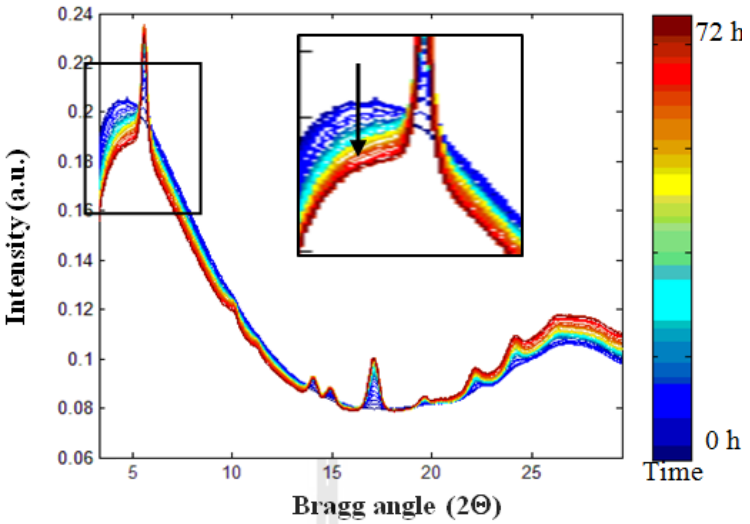

Figure 4.3 Experimental WAXS patterns change in a 10% debranched waxy rice during incubation at 25 °C (10%DBRD6-LT) from 0 to 72 h where blue and red colors are the time at 0 and 72 h, respectively.

debranching of DBRD6, the polydisperse linear chain having a wide range of LC (*DP* 62) and SC (*DP* 19) were obtained. The DBRD6 samples were found to form fine precipitates upon incubation at LT and HT condition (see Appendix B). The change in intensity ratio was observed during subsequent incubation, in which this the ratio was increased with the incubation time.

It can be seen that a phase change on aggregation behavior of debranched starch with the high number of short chains depends primarily on concentration and temperature. The phase change occurs faster at high concentration and low temperature (21%DBRD6-LT), whereas the high concentration and high temperature condition (21%DBRD6-HT) has gradually changed to more aggregate and eventually precipitate after 64 h. The WAXS intensity ratios of debranched starches containing ELC fraction (Figure 4.4B), i.e. DBPS1 and DBCN1, were found to be

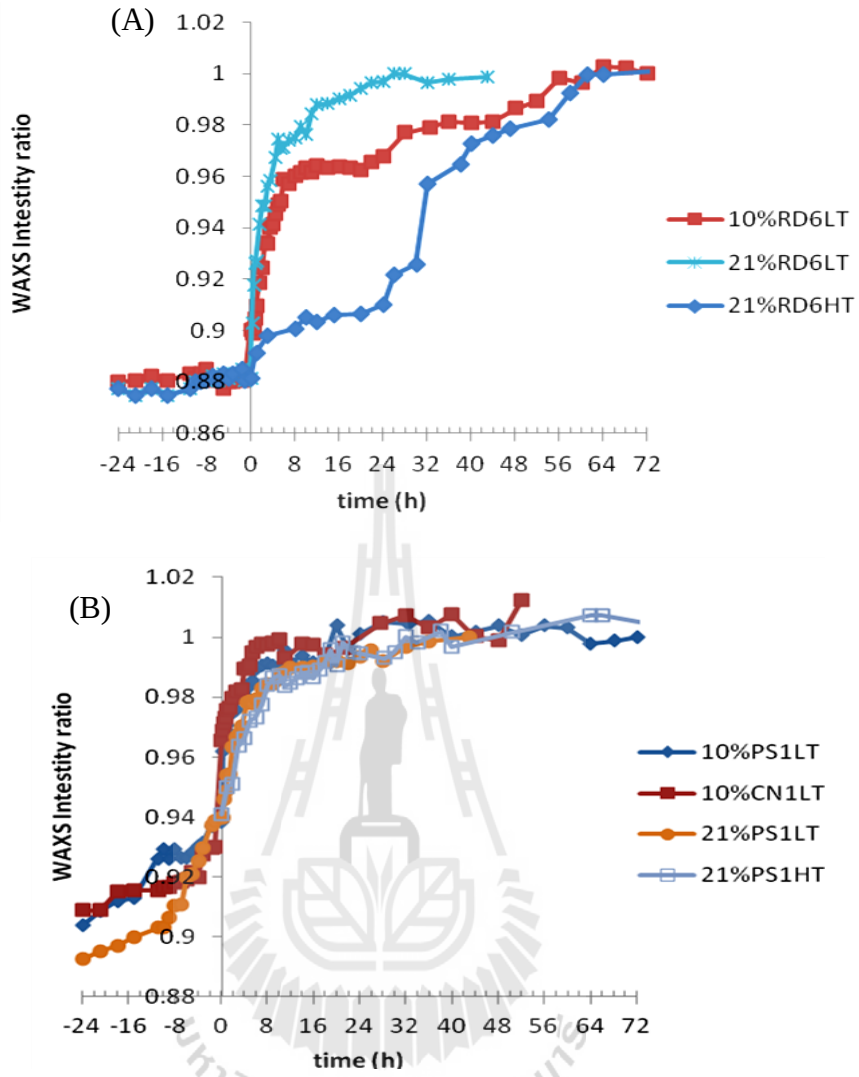

Figure 4.4 Change in WAXS intensity ratio of I_{final}/I_t at 2θ = 4.3° of (A) 10% and 21%DBRD6 and (B) 10% or 21%DBPS1 and DBCN1 during debranching (from -24 to 0 h) and incubation at 25 °C (LT) or 50 °C (LT) for 72 h.

gradually increased during 24 h of debranching, then a rapid change occurs within 6 h of incubation with independent of temperature and concentration, the ratio was found to gradually increase for all samples from 6 to 72 h. This could suggest that a multi-stage process occurs during debranching and incubation. Gidley (1989) studied the

effect of chain length and concentration on gelation and retrogradation of amylose. The gelation can occur for DP > 250 amd is favored by longer chain lengths, high concentrations and faster cooling rates, whereas the precipitation is favored by shorter chain lengths (DP<100), lower concentrations and slower cooling rates. Therefore, during debranching, the aggregation and gelation were dominated by the formation of doubles helices of ELC fraction (DP 844-1054) which result in the formation of a macromolecular network, eventually resulting in gelation. The subsequent crystallization was indued by aggregation of these helices (Gidley, 1989). When completely linear chains of LC (DP 70) and SC (DP 20) were released, the precipitation together with gelation was favored, both cross-linking and chain alignment can occur lead to increased nucleation rates (Gidley and Bulpin, 1989), therefore, a rapid phase change occurs at initial incubation time. After longer incubation time (over 8 h), a slightly increase in an intensity ratio indicated a further helices aggregation and crystallization. The phase behavior at this stage was found to be dependent primarily on concentration. A WAXS intensity ratio of low concentration samples (10%DBCN1-LT and 10%DBPS1-LT) showed slightly higher than that of high concentration samples (21%DBPS1-HT and 21%DBPS1-LT), where a volume fraction of solution was greater for the low concentration samples. This was in agreement with precipitation behavior which was favored for particularly shorter chains and lower concentration, resulting in more syneresis occurred for 10%DBCN1-LT and 10%DBPS1-LT during the time span of WAXS measurement.

4.4.3 WAXS data evaluation and crystallinity determination

As mentioned earlier, the structure of the incubated-debranched samples in aqueous suspension are two-phase systems, composing of crystalline domain and

regions containing amorphous polymer chains and water. Based on the two-phase concept of starch polymer, it is assumed that relatively perfect crystalline domains (crystallites) are interspersed with amorphous regions. Therefore, a appropriate method for approaching the crystalline structure of starch from aqueous solution should be calculated by weight subtraction of the solvent scattering placing in amorphous region (Reuther et al., 1984). The scattering of crystalline phase was estimated according by

$$I(2\theta) = I_{sam}(2\theta) - (1\text{-}w)\, I_{solv}(2\theta) \qquad (3)$$

where $I_{sam}(2\theta)$ = scattering intensity of sample measured at each time

$I_{solv}(2\theta)$ = scattering intensity of solvent

w = volume concentration

2θ = scattering angle

However, the phase behavior changed over the time during crystallization as previously mentioned, causing water loss and changes in water volume during incubation period. Here, we, therefore, reformulate the approach to calculate WAXS data by explicitly taking into account the sources of experimental data variability. For this purpose, the measured scattering intensity difference is written as:

$$I(2\theta) = \alpha\, I_{sam}(2\theta) - (1\text{-}w)\, I_{solv}(2\theta) \qquad (4)$$

where the variable sample rescaling factor $\alpha \approx 1$ ($I_{final\ (4.3^{\circ})}$/ $I_{sam\ (4.3^{\circ})}$) accounts for the concentration uncertainty at which the phase change from amorphous gel into solid crystalline phase.

In Figure 4.5, an example of derived WAXS patterns of the 10%DBRD6LT sample as calculated by Eq. (4) displays a change in WAXS patterns during incubation from 0 to 72 h.

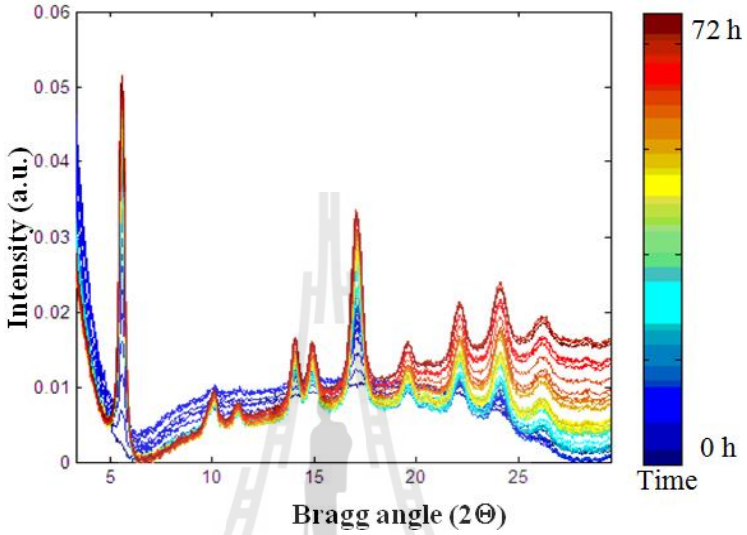

Figure 4.5 Derived WAXS patterns of 10%DBRD6-LT experimented at different incubation time where blue and red colors are the time at 0 and 72 h, respectively.

The result in figure 4.5 shows that there is the uncertainty in the measurements of transmitted intensities probably due to the solvent scattering effect of the supernatant water, resulting in a shift of the baseline. Consequently, all of the WAXS patterns were adjusted the baseline slope by baseline correction. The baselines of each WAXS data was determined by fitting the baseline of data at a specific reflection 2θ at 3.5–8° with a quadratic polynomial equation and a specific reflection 2θ at 8–30° with linear equation. Then, the scattering data of sample was subtracted with the coherent intensity of baseline. The WAXS pattern results are shown in Figure 4.6.

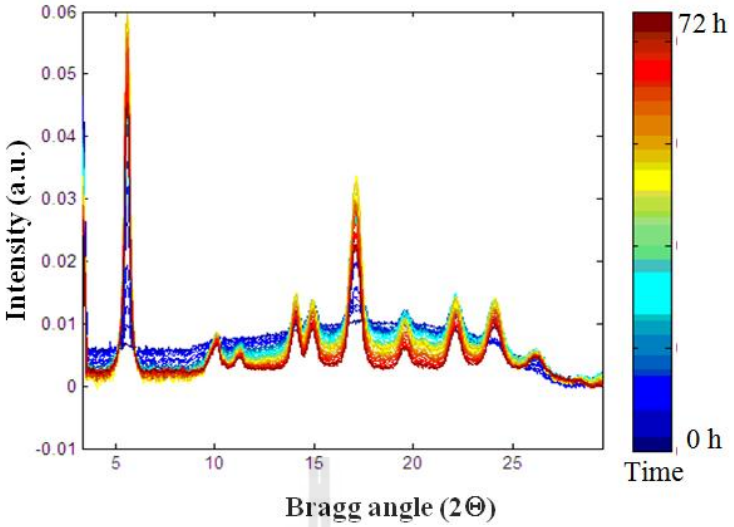

Figure 4.6 The WAXS patterns of the 10%DBRD6-LT experimented at different incubation time where blue and red colors are the time at 0 and 72 h, respectively

Starch crystallinity has normally been calculated considering the granule as a two phase system and, thus, dividing the area under the crystalline peaks by the total area under the diffractogram was conducted (Frost, Kaminski, Kirwan, Lascaris and Shanks, 2009; Lopez-Rubio, Flanagan, Gilbert and Gidley, 2008). Relative crystallinity was calculated using Eq. (5)

$$\text{Relative crystallinity} = \frac{\text{crystalline area}}{(\text{crystalline} + \text{amorphous})\ \text{area}} \quad (5)$$

The baseline of WAXS patterns from Figure 4.7 were adjusted to zero in the range of 2θ = 3–8° and 8–30°, then all patterns were normalized to give an area under the pattern equal to 100 (Figure 4.7A), the amorphous was modeled and then the peak is superimposed on an amorphous background (Figure 4.7B). In this study, the sample

at time 0 min is 100% amorphous. If both scattering intensity of amorphous sample I_a(b) and that of the coherent intensity sample I(b) are given, then the degree of crystallinity (%X_c) can be expressed as:

$$\% X_c = \left(\left(\int_{b1}^{b2} I(b)\mathrm{d}b - \int_{b1}^{b2} I_a(b)\mathrm{d}b \right) \Big/ \int_{b1}^{b2} I(b) \right) \times 100 \qquad (6)$$

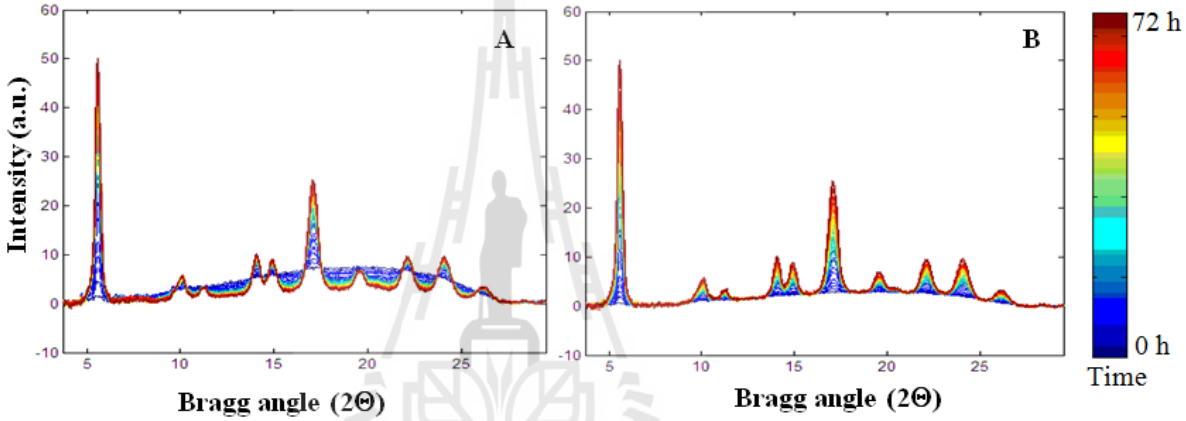

Figure 4.7 WAXS data processing of the 10%DBRD6-LT.

4.4.4 Crystallization behavior of rice starches during debranching and incubation

All WAXS data of RD6, PS1 and CN1 rice starches were evaluated to examine the crystallization (crystallinity changes) during debranching and incubation at high and low temperature over 5-day period (Figure 4.8, 4.9, 4.10). For The 10% and 21% waxy rice starch, there were no crystallization during debranching (data not shown), exhibiting an amorphous pattern after debranching (Figure 4.8A and 4.8B). The amorphous phase of the gel permits the further crystallization into the B-type crystal structure for incubation at LT, which is independent on the concentration

(Figure 4.8A and 4.8B), whereas the A-type crystal structure was progressively developed in the time course of gel under HT-incubation (Figure 4.8C). In Figure 4.9A and 4.9B, there were a typical V-type polymorph of amylose-lipid complexes contributed in the amorphous system of the gelatinized 10%PS1 and 10%CN1, as identified by the peaks at 2θ = 7.5°, 12.9° and 19.9°. These amylose-lipid complexes could be naturally present in starch or formed upon gelatinization (Putseys, Lamberts and Delcour, 2010). It can be seen that such V-crystals were not developed during debranching, while new crystallites with B-type structure (as indicated by the peak at 2θ = 5.6° and 16.9°) gradually developed during debranching and grown to the crystalline B-form during incubation at LT. The peaks development during debranching of the 10%CN1 was faster than that of the 10%PS1, which was attributed to a higher amount of ELC fraction. Interestingly, the peaks at 2θ = 7.5°, 12.9° correspond to V-type structure was reduced and disappeared over longer incubation time, while stronger and broaden peak at 2θ = 19.9° was observed. V_h-amylose is single, left-handed helices complexes with native-lipid of starch, has mostly been described as an orthorhombic structure with unit cell dimensions depending on the ligand type, position of the ligand, temperature of complexation and hydration (Ambigaipalan, Hoover, Donner and Liu, 2014; Putseys et al., 2010). Therefore, this discrepancy might result from lattice distortions in crystalline domains of V-form amylose-lipid complex in specific condition of temperature. In Figure 4.10A and 4.10B, as the 21% gelatinized PS1 sample, the gradual transition from B to A-type was observed during debranching. The shift from a global B-type to A-type crystallinity has been observed during debranching of maltodextrins at high concentration, which was attributed to a split crystallization with a preferential B-type

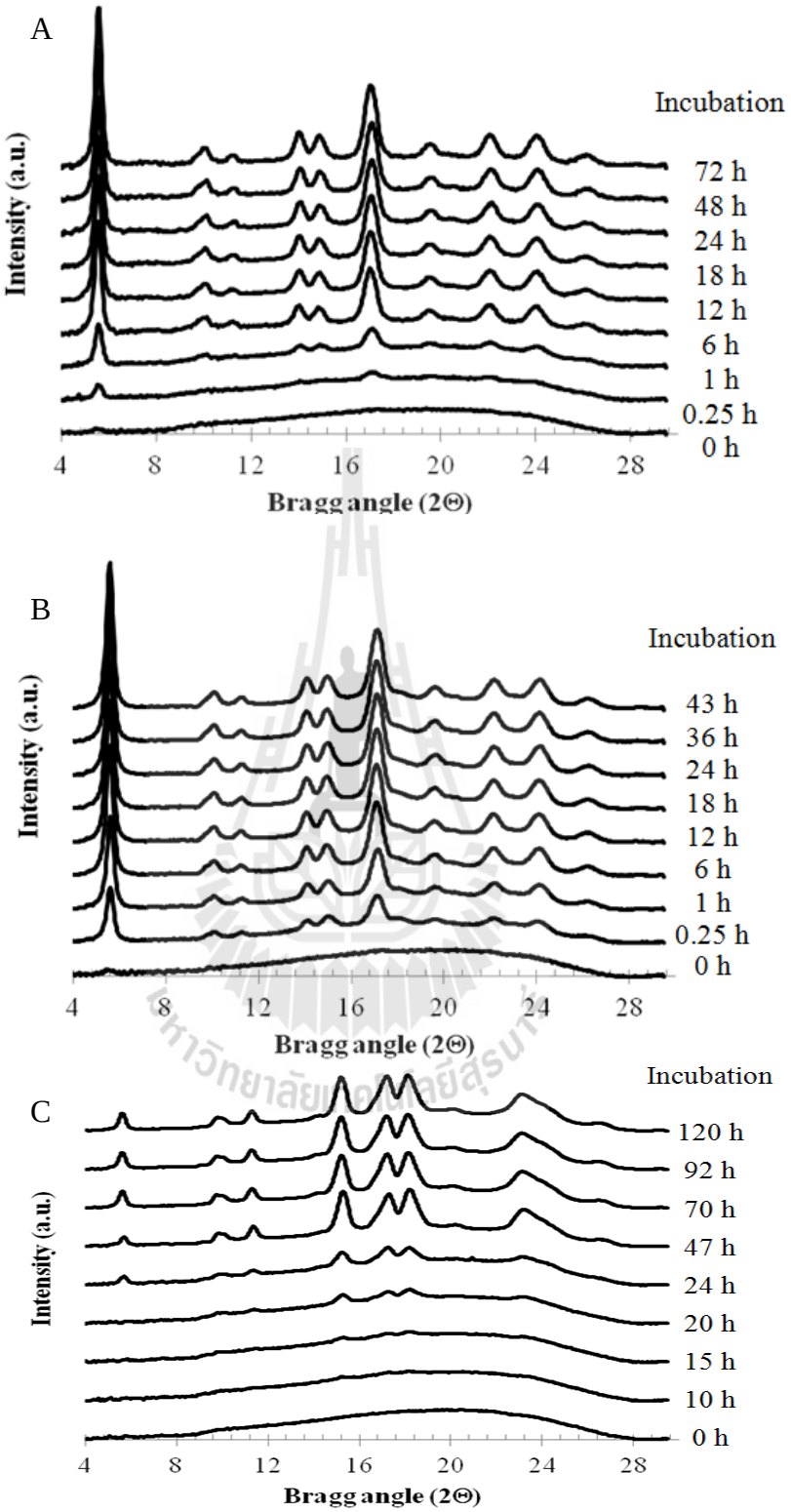

Figure 4.8 WAXS patterns relative to the samples of (A) 10%DBRD6-LT, (B) 21%DBRD6-LT and (C) 21%DBRD6-HT that debranched and then incubated at 25 or 50 °C at different times.

crystallization during the first 12 h, followed by A-type crystallization between 12 to 48 h of debranching (Pohu et al., 2004). With continuing incubation at HT (Figure 4.10B), the peaks corresponding to a characteristic A-type crystal (2θ = 14.8°, 16.9°, 17.8° and 23.2°) became progressively stronger, while the peak at 2θ = 5.6° of B-type was relatively constant during incubation period. In contrast, with an incubation at LT (Figure 4.10A), all peaks corresponding to the B-type crystal gradually developed and were further dominant over its incubation time. This suggested that the dominant B-type structure is favored by low temperature. By comparison of WAXS pattern of the 21%DBRD6-HT and 21%DBPS10-HT (Figure 4.8C and 4.10B), it can be noted that the dominant of A-type structure was observed for the 21%DBRD6-HT more than the 21%DBPS1-HT which was consistent with a higher proportion of SC containing in the DBRD6. Our results agree with the general finding in that high concentration, high temperature and short chains favored A-type crystallization while B-type crystallites were formed in the opposite conditions (Buléon, Véronèse and Putaux, 2007; Cai and Shi, 2010; Cai et al., 2014; Miao, Jiang and Zhang, 2009). In overall results, a narrower of the peaks and the shift to high intensity of all samples were observed with increasing storage time, suggesting the growth and development of crystallites into larger and more perfect crystal.

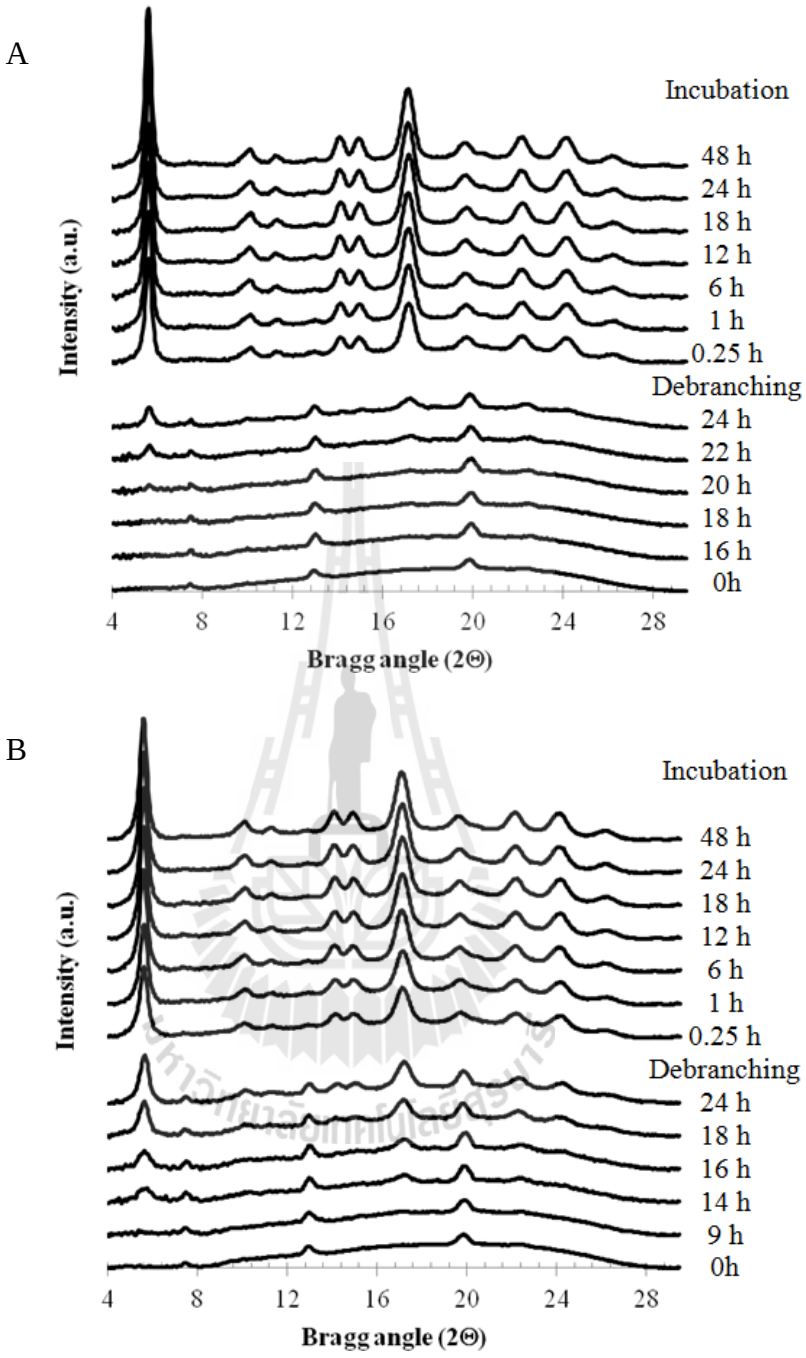

Figure 4.9 WAXS patterns relative to the samples of (A) 10%DBPS1-LT (B) 10%DBCN1-LT that debranched and then incubated at 25 °C at different times.

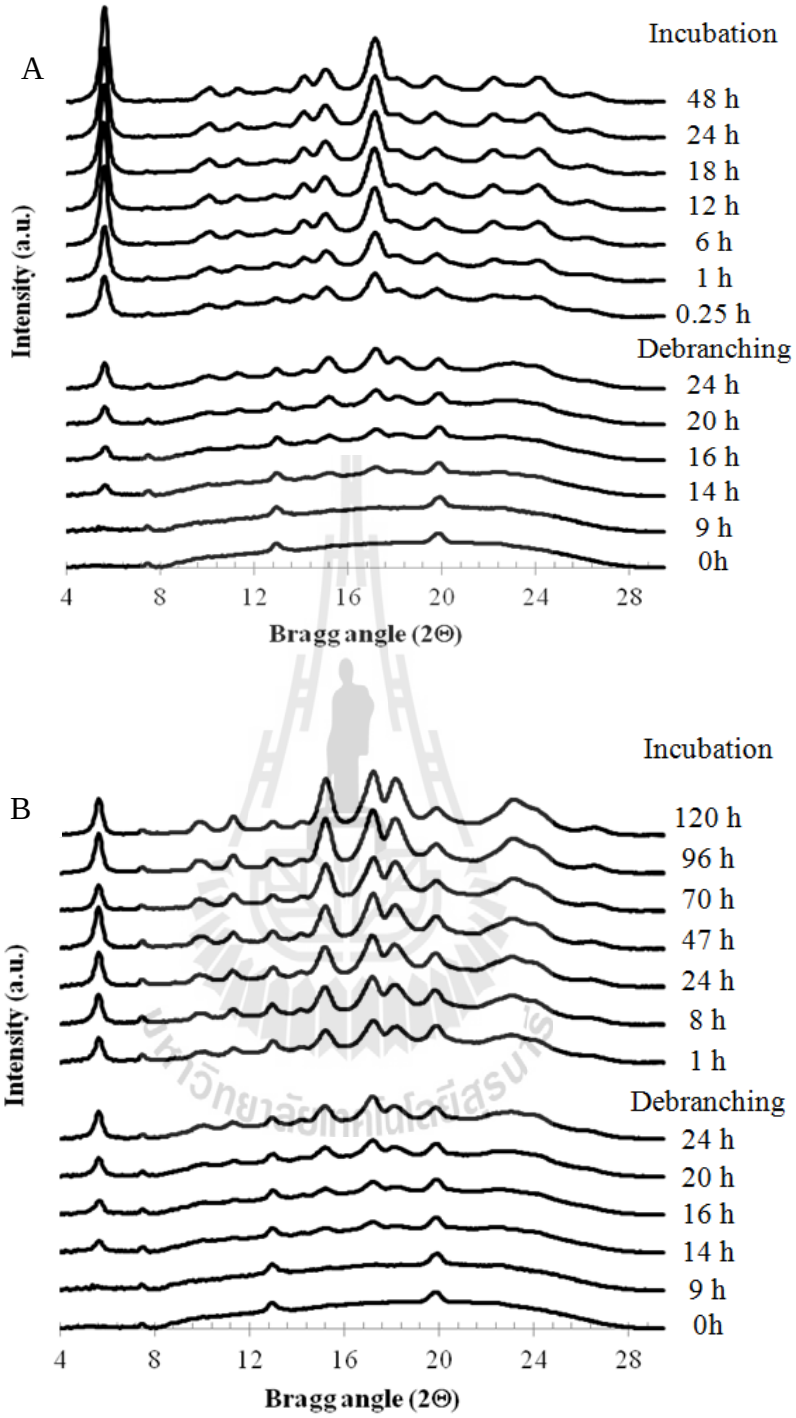

Figure 4.10 WAXS patterns relative to the samples of (A) 21%DBPS1-HT and (B) 21%DBPS1-HT that debranched and then incubated at 25 or 50 °C at different times.

4.4.5 Modeling the crystallization kinetics

The change in long-range ordering occurring over debranching time and incubation, expressed in terms of crystallinity, is shown in Figure 4.11 and Figure 4.12. As previously stated, the 10% and 21% gel of RD6 samples did not crystallize during debranching due to the lacking of ECLs fraction. Figure 4.11A illustrates crystallinity change in 10%DBRD6 and 21%DBRD6 during incubation at LT and HT. The crystallinity was rapidly increased after incubation at LT; a plateau was reached after ~20 h for 21%DBRD6 and after ~50 h for 10%DBRD6. For the incubation at HT, the change in crystallinity was observed after 10 h and was increased dramatically after 56 h with a high crystallinity of ~80%. The difference in the crystallization kinetic can clearly be seen from the normalized plots (Figure 4.11B), where, at the same LT, the crystallization of 21%DBRD6 was slightly faster than 10%DBRD6, while the 21%DBRD6 incubated at HT showed the slowest kinetic.

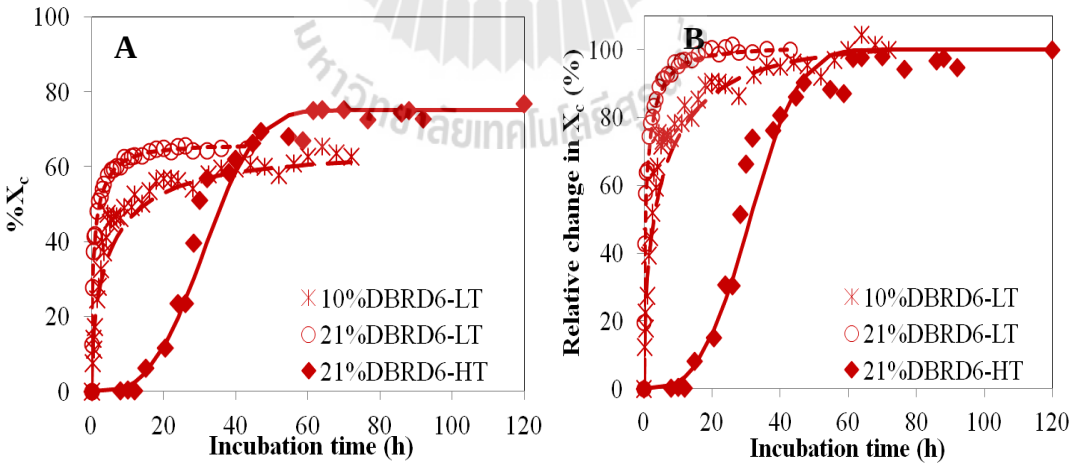

Figure 4.11 (A) Crystallization in incubated DBRD6 starch during incubation at LT or HT, monitored through the crystallinity as calculated using Eq. 6 (line was calculated using Eq. 7) and (B) the relative change in crystallinity upon storage (from panel A).

Figure 4.12 shows the change in crystallinity as a function of time of DBPS1 and DBCN1 with different concentration during debranching and incubation. Three different phases were observed: an initial low of crystallinity (3-6%) occurred during the first 9 h of debranching, then the crystallinity was increased significantly at the last stage of debranching and initial incubation stage, and a final was maintained constant thereafter for all samples. An increase in crystallinity during debranching could be related to the chain length distribution of starch as shown in an inserted figure (Figure 4.12A). The 10%CN1with higher ELC fraction had a higher crystallization rate than those of DBPS1 with low ELC fraction. Although the number of ELC was in the order 21%PS1>10%CN1>10PS1%, the change in crystallinity degree of the 21%PS1after16 h was lower than that of the 10%CN1. The lower crystallinity degree of the 21%PS1 might be due to the fact that LC and SC were slowly released and cannot be completely released after debranching, in which the β-amylolysis estimated to be 80% after debranching. An increase in crystallinity during incubation can clearly be seen from Figure 4.12B. The result shows that the crystallinity was rapidly increased and increased in the same rate for all LT-samples, reaching crystallinity after ~20 h of incubation. The incubation at HT resulted in the slowest crystallization.

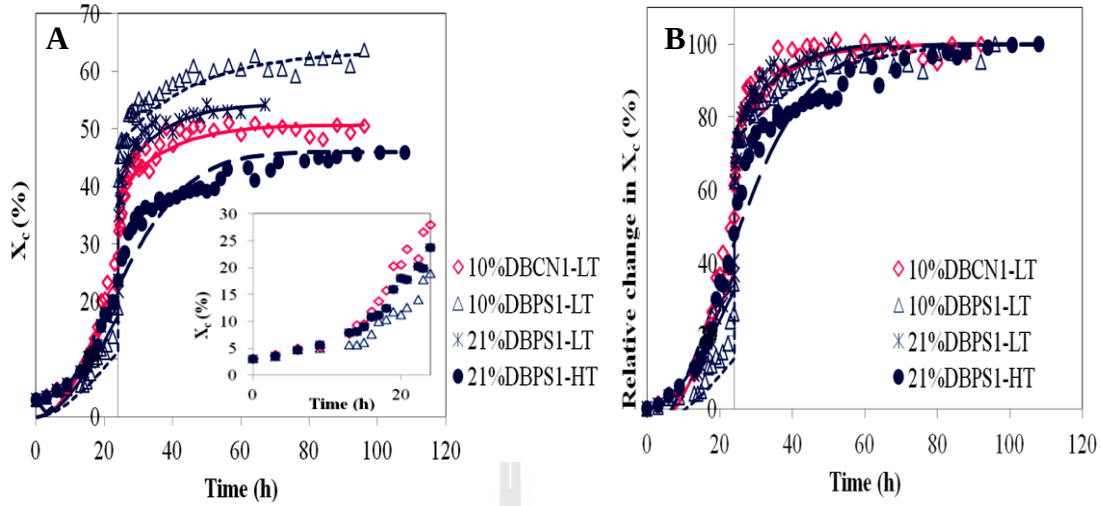

Figure 4.12 (A) Crystallization in DBPS1 and DBCN1 starch during debranching from 0 to 24 h and subsequent incubation at LT or HT from 24 to 120 h, monitored through the crystallinity as calculated using Eq. 6 (line was calculated using Eq. 7) and (B) the relative change in crystallinity upon debranching and storage (from panel A).

The crystallization results were analyzed using the Avrami equation, in which the crystalline phase change against time can be written as follows:

$$\mathrm{X}(t) = \frac{X_{ct} - X_{c0}}{X_{c\infty} - X_{c0}} = 1 - exp^{(-kt^n)} \qquad (7)$$

The parameters in Eq (7) are usually determined by taking the double logarithm and expressing in the form:

$$\log(-\ln(1 - \mathrm{X}(t)) = n\ log\ t + \log k \qquad (8)$$

where X(t) is defined as the normalized crystallinity at time *t*, X_{ct} is the crystallinity at time *t*, X_{c0} is the crystallinity at time 0, $X_{c\infty}$ is the maximum crystallinity at the end of incubation period, *k* is rate constant of crystallization (time^{-1}) and *n* is the Avrami exponent, respectively.

The Avrami exponent (*n*) is related to the mode of crystallization (McIver, Axford, Colwell and Elton, 1968). Avrami exponent of 1 as representing rod-like growth from instantaneous nuclei, 2 as rod-like growth from sporadic nuclei, 3 as disc-like growth from instantaneous or sporadic nuclei, and 4 as spherulitic growth from instantaneous or sporadic nuclei. The mode of crystal growth is self-evident: three dimensional (spheres), two dimensional (discs) and one dimensional (rods) are defined by the number of faces of the crystal upon which more molecules may condense (Stauffer, 1990).

Figure 4.13 displayed the Avrami plot of log(–ln 1–X(t)) against log *t*. The intercept is the logarithm of the rate constant, and the slope of the plot equals *n*. The Avrami exponent (*n*) and the rate constants (*k*) are listed in Table 4.1. For the DBRD6, without crystallization during debranching, the avrami plot is a straight line and its slope is constant (Figure 4.13A-4.13C), suggesting a single-stage of crystallization behavior. In contrast, the avrami plot of the DBPS1 and DBCN1 showed two different straight lines (Figure 4.13D-4.13G), indicating two-stages of crystallization behavior during debranching and incubation. The n_1 values of DBPS1 and DBCN1 crystallization during debranching were 1.7-1.9 (Table 4.1) which closed to 2, indicating that crystallization growth during debranching was one-dimensional, corresponding rod-like growth from sporadic nuclei (Mua and Jackson, 1998; Stauffer, 1990). The k_1 values were 8.5×10^{-4} for 10%DBPS1 (15% ELC) and 11.6×10^{-4} for 10%DBCN1 (27% ELC) which showed positive correlation with the proportion of ELC (DP_n>600), confirming that ECL were crystallized during debranching. During incubation at LT, the n_2 values were changed to be 0.87-1.15 for 10%DBPS1-LT, 21%DBPS1-LT and 10%DBCN1-LT. The *n* values of 10%DBRD6-LT and

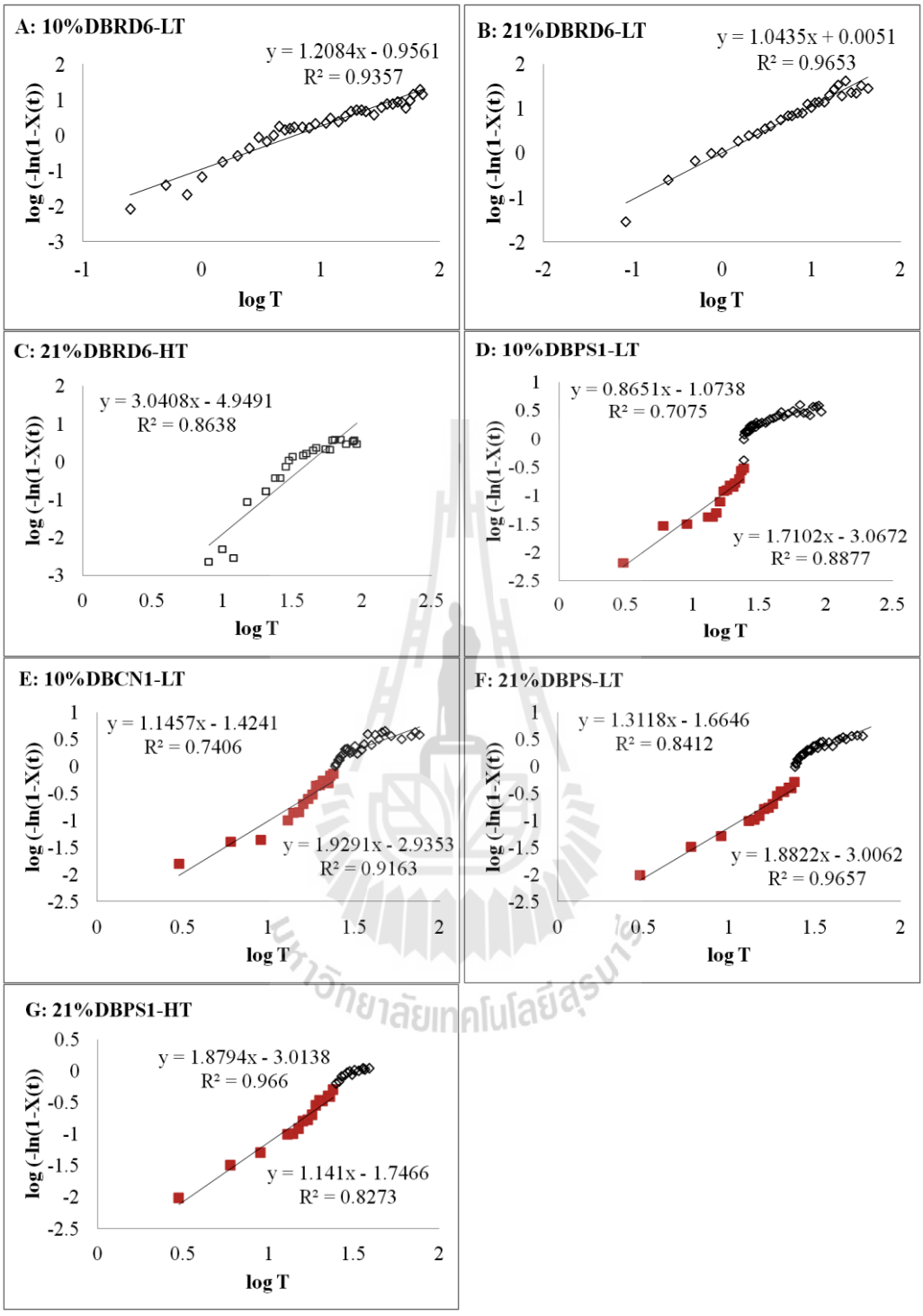

Figure 4.13 Avrami plot for (A) 10%DBRD6-LT, (B) 21%DBRD6-LT, (C) 21%DBRD6-HT, (D) 10%DBPS1-LT, (E) 10%DBCN1-LT, (F) 21%DBPS1-LT and (G) 21%DBPS1-HT during debranching at 50 °C (■) and incubation at 25 or 50 °C (□).

21%DBRD6-LT were also found in range 1.04-1.20. This indicated that crystallization of chains during incubation at LT was one-dimensional crystal growth and has instantaneous nucleation, followed by rod-like growth of crystal (Mua and Jackson, 1998). The k_2 values were correlated with the amount of SC where a higher SC content corresponds to a higher crystallization rate constant (k) (Table 4.1). In addition, the k_2 values of second stage kinetics (during incubation) was higher than the corresponding k_1 value of early-stage kinetics (during debranching). It should be noted that crystallization of starch with a higher proportion of ELC fractions and longer average chain lengths revealed significantly greater n_1 values and smaller k_1 values. Values for n_2 and k_2 showed an influence from the amount of short chain. Gidley and Bulpin (1989) reported that a minimum chain length of DP10 is required for the formation of double helices. Since SC (DP_n 20) constitute the major portion of debranched chain, it is considered that a high amount of SC facilitates the formation of double helices and thus results in a higher crystallization rate. This result suggests that the SC play an important role in crystallization at low temperature, which may be related to crystallite forming by affecting either number of nuclei or the orientation of double helices in the crystalline displaying A or B-type X-ray diffraction pattern. The n value for 21%DBRD6-HT was 3.04 and the k value was 1.1×10^{-5}, indicating that crystallization at HT occurred very slow and had a disc-like growth from instantaneous nuclei. This finding suggested that the mechanism by which crystallization is initiated and proceeds depends on chain length distribution and temperature.

It could be concluded that crystallization behavior of debranched starch is depended on chain length distribution and temperature used. Crystallization of

debranched waxy starch revealed one dimensional or two dimensional crystal growths when crystallization at low or high temperature respectively. On the other hand, crystallization of debranched starch from starch containing amylose showed two-stages of crystallization. First stage, nucleation occurs sporadically due to random molecular motion of amylose (ELC) allows the formation of a crystal nucleus during debranching at 50 °C, followed by rod-like growth from sporadic nuclei. Second stage, nucleation of new nuclei is subsequent instantaneous when cooled to 25 °C due to the existence of critical nuclei after debranching, followed by rod-like growth from instantaneous nuclei during incubation.

The haft-time ($t_{1/2}$) of crystallization was calculated as follows (Jagannath et al., 2001):

$$\log(t_{1/2}) = \frac{\log(\ln 2) - \log k}{n} \qquad (9)$$

The haft-time of crystallization depends on temperature and concentration. The value of $t_{1/2}$ was found to be highest for 21%DBRD6-HT and lowest for 21%DBRD6-LT (Table 4.1). In addition, the $t_{1/2}$ depends on chain length distribution. The value of $t_{1/2}$ was lower in 10%DBRD6-LT, followed by 10%DBPS1-LT and 10%DBCN1-LT.

It has been reported that starch crystallization occurs with two kinetically distinct processes, in a first stage, rapid gelation of amylose though the formation of double helical chains, followed by helix-helix aggregation and slow recrystallization of amylopectin chain (Miles, Morris, Orford and Ring, 1985; van Soest et al., 1995). This study can imply that debranched starch crystallization takes

place by two kinetically mechanisms: (1), rapid time-independent crystallization of amylose and (2), slow time-dependent crystallization of linear short chains. It can be assumed that the presence of pre-exits crystallites could accelerate the nucleation rate due to heterogeneous nucleation but the growth rate is decreased due to retarded mobility of SC and LC. Therefore, the resulting crystallinity appears to be lower in the DBCN1 and DBPS1 than that of the DBRD6 (Table 4.2). This result was in agreement with Cheetham and Tao (1998) in that the crystallinity decreased with increasing amylose/amylopectin ratio (Cheetham and Tao, 1998). Crystallinity of powder samples compared to that of samples in aqueous suspension are shown in Table 4.2

Table 4.1 Crystallization kinetics and structural parameters of rice starches during debranching and incubation

Sample	Avrami parameters[a]						$t_{1/2}$[d]	Amount of chain (g/ 100 mL of sample)[e]		
	n_1[b]	k_1[c]	r_1^2	n_2[b]	k_2[c]	r_2^2	(h)	ELC	LC	SC
10%DBRD6-LT	-	-	-	1.208	0.110	0.936	4.56	0	2.20	7.80
21%DBRD6-LT	-	-	-	1.044	1.012	0.965	0.70	0	4.62	16.38
10%DBPS1-LT	1.710	8.5×10^{-4}	0.888	0.865	0.084	0.708	11.40	1.50	2.00	6.50
10%DBCN1-LT	1.929	11.6×10^{-4}	0.916	1.146	0.038	0.741	12.70	2.70	1.70	5.60
21%DBRPS1-LT	1.882	9.8×10^{-4}	0.966	1.312	0.022	0.841	14.04	3.15	4.20	13.65
21%DBRD6-HT	-	-	-	3.041	1.1×10^{-5}	0.864	31.13	0	4.62	16.38
21%DBPS1-HT	1.879	9.7×10^{-4}	0.966	1.141	0.019	0.873	24.61	3.15	4.20	13.65

[a] See Equation (8) for calculations.

[b] Avrami parameter related to crystallite growth mode of chain during debranching, n_1, and during incubation at LT and HT, n_2.

[c] Avrami parameter described the crystallization rate constant of chain during debranching, k_1, and during incubation at LT and HT, k_2.

[d] See Equation (9) for calculations.

[e] The amount of chain fraction in g/100 mL of sample.

Table 4.2 Crystallinity of powder samples and samples in aqueous suspension

Sample	Crystallinity[a] (%)	Crystallinity[b] (%) (experimental values)			Crystallinity[c] (%) (fitted values)	
		X_{Ci}	X_{Cd}	$X_{C\infty}$	X_{Cd}'	$X_{C\infty}'$
10%RD6LT	60.3	0	0	62.7	0	63.7
10%PS1LT	67.5	3.06	18.9	63.8	18.6	61.4
10%CN1LT	61.2	3.09	27.1	50.6	16.2	49.8
21%RD6LT	73.1	0	0	64.8	0	65.5
21%PS1LT	69.1	3.33	23.7	54.2	18.4	52.8
21%RD6HT	81.0	0	0	76.9	0	76.9
21%PS1HT	70.9	3.33	20.4	55.4	15.8	47.2

[a] Crystallinity in powder samples as analysis using in-house WAXS

[b] Crystallinity of samples in aqueous suspension as analysis using synchotron WAXS and the $\%X_c$ was calculated using Eq. (5): X_{Ci} is initial crystallinity at time 0 min; X_{Cd} is crystallinity of debranched starch at time 24h; $X_{C\infty}$ is crystallinity of incubated-debranched starch at final time.

[c] Crystallinity of samples in aqueous solution as analysis using synchotron WAXS and the $\%X_c$ was calculated using Eq. (7) (Avrami equation): X_{Cd}' is crystallinity of debranched starch at time 24h; $X_{C\infty}'$ is crystallinity of incubated-debranched starch at final time.

4.5 Conclusions

The starch gel was single phase system containing amorphous polymer chains and rich in water. The crystalline domains were developed and embedded in a polymer solution which was ordered chain segment, during crystallization. A change in long range ordering of bound water in gel is related to phase changes from gel to crystalline state, which depended on chain length distribution, gel concentration, debranching and incubation temperature. Waxy rice starch could not crystallize during debranching while normal rice starch crystallized into a B-form or A-form, depending on the gel concentration. The formation of double helical structure during subsequent incubation was dependent on the pre-exits crystallites of debranched starch. With regard to crystallization kinetics, the values of the kinetic exponent *n* suggested a rod-like growth from sporadic of ELC during debranching. Incubation at low temperature promoted crystallization of LC and SC that crystallites underwent rod-like growth from instantaneous nuclei, while incubation at high temperature led to crystal growth in mode of disc-like growth from instantaneous nuclei. Debranched starch crystallization took place by two kinetically mechanisms: rapid time-independent crystallization of ELC and slow time-dependent crystallization of linear short chains. Slow time-dependent crystallization led to low crystallinity when the samples were stored at the low temperature. In addition, the slowest crystallization kinetics upon high temperature incubation led to the slowest growing of crystal which resulted in a development of A-type with high crystallinity. The fundamental information on the crystallization of debranched rice starch of this study provided the possibility for future investigations of the effects of crystallization at various

conditions on debranched starch and the application process in pharmaceutical and nutraceutical products.

4.6 References

Ambigaipalan, P., Hoover, R., Donner, E., and Liu, Q. (2014). Starch chain interactions within the amorphous and crystalline domains of pulse starches during heat-moisture treatment at different temperatures and their impact on physicochemical properties. **Food Chemistry.** 143: 175-184.

Arends-Scholte, A. W., et al. (2000). Starch products as tabletting excipient, method for preparing same, and method for making tablets. **US Patent No. 6,010,717.**

Buléon, A., Véronèse, G., and Putaux, J. (2007). Self-Association and Crystallization of Amylose. **Australian Journal of Chemistry.** 60(10): 706-718.

Cai, L. and Shi, Y-C. (2010). Structure and digestibility of crystalline short-chain amylose from debranched waxy wheat, waxy maize, and waxy potato starches. **Carbohydrate Polymers.** 79(4): 1117-1123.

Cai, L. and Shi, Y-C. (2014). Preparation, structure, and digestibility of crystalline A- and B-type aggregates from debranched waxy starches. **Carbohydrate Polymers.** 105(0): 341-350.

Cai, L., Shi, Y-C., Rong, L., and Hsiao, B. S. (2010). Debranching and crystallization of waxy maize starch in relation to enzyme digestibility. **Carbohydrate Polymers.** 81(2): 385-393.

Chaudhary, D. S. and Adhikari, B. P. (2010). Understanding polymeric amylose retrogradation in presence of additives. **Journal of Applied Polymer Science.** 115(5): 2703-2709.

Cheetham, N. W. and Tao, L. (1998). Variation in crystalline type with amylose content in maize starch granules: an X-ray powder diffraction study. **Carbohydrate Polymers.** 36(4): 277-284.

Chiu, C-W. (1990). Partially debranched starches and enzymatic process for preparing the starches. **US Patent No. 4,971,723.**

Chiu, C-W. (1992). Partially debranched starch clouds. **EP Patent No. 0,553,368.**

Chiu, C-W. and Henley, M. (1993). Foods opacified with debranched starch. **EP Patent No. 0,616,778.**

Diat, O., et al. (2013). Octanol-rich and water-rich domains in dynamic equilibrium in the pre-ouzo region of ternary systems containing a hydrotrope. **Journal of Applied Crystallography.** 46(6): 1665-1669.

Doona, C. J., Feeherry, F. E., and Baik, M-Y. (2006). Water dynamics and retrogradation of ultrahigh pressurized wheat starch. **Journal of Agricultural and Food Chemistry.** 54(18): 6719-6724.

Frost, K., Kaminski, D., Kirwan, G., Lascaris, E., and Shanks, R. (2009). Crystallinity and structure of starch using wide angle X-ray scattering. **Carbohydrate Polymers.** 78(3): 543-548.

Gidley, M. J. (1989). Molecular mechanisms underlying amylose aggregation and gelation. **Macromolecules.** 22(1): 351-358.

Gidley, M. J. and Bulpin, P. V. (1989). Aggregation of amylose in aqueous systems: the effect of chain length on phase behavior and aggregation kinetics. **Macromolecules.** 22(1): 341-346.

González-Soto, R., Mora-Escobedo, R., Hernández-Sánchez, H., Sanchez-Rivera, M., and Bello-Pérez, L. (2007). The influence of time and storage temperature on

resistant starch formation from autoclaved debranched banana starch. **Food Research International.** 40(2): 304-310.

Jagannath, J., Nanjappa, C., Das Gupta, D., and Arya, S. (2001). Crystallization kinetics of precooked potato starch under different drying conditions (methods). **Food Chemistry.** 75(3): 281-286.

Ju, Z., Hettiarachchy, N., and Rath, N. (2001). Extraction, denaturation and hydrophobic properties of rice flour proteins. **Journal of Food Science.** 66(2): 229-232.

Leong, Y. H., Karim, A. A., and Norziah, M. H. (2007). Effect of pullulanase debranching of sago (Metroxylon sagu) starch at subgelatinization temperature on the yield of resistant starch. **Starch-Stärke.** 59(1): 21-32.

Lopez-Rubio, A., Flanagan, B. M., Gilbert, E. P., and Gidley, M. J. (2008). A novel approach for calculating starch crystallinity and its correlation with double helix content: A combined XRD and NMR study. **Biopolymers.** 89(9): 761-768.

McIver, R. G., Axford, D., Colwell, K., and Elton, G. (1968). Kinetic study of the retrogradation of gelatinised starch. **Journal of the Science of Food and Agriculture.** 19(10): 560-563.

Miao, M., Jiang, B., and Zhang, T. (2009). Effect of pullulanase debranching and recrystallization on structure and digestibility of waxy maize starch. **Carbohydrate Polymers.** 76(2): 214-221.

Miles, M. J., Morris, V. J., Orford, P. D., and Ring, S. G. (1985). The roles of amylose and amylopectin in the gelation and retrogradation of starch. **Carbohydrate Research.** 135(2): 271-281.

Mua, J. P. and Jackson, D. S. (1998). Retrogradation and gel textural attributes of corn starch amylose and amylopectin fractions. **Journal of Cereal Science.** 27(2): 157-166.

Mutungi, C., Passauer, L., Onyango, C., Jaros, D., and Rohm, H. (2012). Debranched cassava starch crystallinity determination by Raman spectroscopy: Correlation of features in Raman spectra with X-ray diffraction and ^{13}C CP/MAS NMR spectroscopy. **Carbohydrate Polymers.** 87(1): 598-606.

Pohu, A., Planchot, V., Putaux, J., Colonna, P., and Buléon, A. (2004). Split crystallization during debranching of maltodextrins at high concentration by isoamylase. **Biomacromolecules.** 5(5): 1792-1798.

Popov, D., et al. (2009). Crystal structure of A-amylose: A revisit from synchrotron microdiffraction analysis of single crystals. **Macromolecules.** 42(4): 1167-1174.

Putseys, J., Lamberts, L., and Delcour, J. (2010). Amylose-inclusion complexes: Formation, identity and physico-chemical properties. **Journal of Cereal Science.** 51(3): 238-247.

Reuther, F., et al. (1984). Molecular gelation mechanism of maltodextrins investigated by wide-angle X-ray scattering. **Colloid and Polymer Science.** 262(8): 643-647.

Shamai, K., Bianco-Peled, H., and Shimoni, E. (2003). Polymorphism of resistant starch type III. **Carbohydrate Polymers.** 54(3): 363-369.

Shin, S. I., et al. (2004). Slowly digestible starch from debranched waxy sorghum starch: preparation and properties. **Cereal Chemistry.** 81(3): 404-408.

Soontaranon, S. and Rugmai, S. (2012). Small angle X-ray scattering at Siam photon

laboratory. **Chinese Journal of Physics.** 50(2): 204-210.

Stauffer, C. E. (1990). **Functional additives for bakery foods.** Springer Science and Business Media.

Takahashi, Y., Kumano, T., and Nishikawa, S. (2004). Crystal structure of B-amylose. **Macromolecules.** 37(18): 6827-6832.

Takamuku, T., Saisho, K., Nozawa, S., and Yamaguchi, T. (2005). X-ray diffraction studies on methanol-water, ethanol-water, and 2-propanol-water mixtures at low temperatures. **Journal of Molecular Liquids.** 119(1): 133-146.

Thompson, D. B. (2000). Strategies for the manufacture of resistant starch. **Trends in Food Science and Technology.** 11(7): 245-253.

van Soest, J. J., Tournois, H., de Wit, D., and Vliegenthart, J. F. (1995). Short-range structure in (partially) crystalline potato starch determined with attenuated total reflectance Fourier-transform IR spectroscopy. **Carbohydrate Research.** 279: 201-214.

Wai-Chiu, C. and Kasica, J. J. (1992). Enzymatically debranched starches as tablet excipients. **EP Patent No. 0,499,648**.

Wang, T. L., Bogracheva, T. Y., and Hedley, C. L. (1998). Starch: as simple as A, B, C? **Journal of Experimental Botany.** 49(320): 481-502.

Yao, Y., Zhang, J., and Ding, X. (2002). Structure-retrogradation relationship of rice starch in purified starches and cooked rice grains: a statistical investigation. **Journal of Agricultural and Food Chemistry.** 50(25): 7420-7425.

Zhong, Z. and Sun, X. S. (2005). Thermal characterization and phase behavior of cornstarch studied by differential scanning calorimetry. **Journal of Food Engineering.** 69(4): 453-459.

Zobel, H. (1988). Molecules to granules: a comprehensive starch review. **Starch-Stärke.** 40(2): 44-50.

CHAPER V

SPHERULITIC CRYSTALLIZAION OF DEBRANCHED STARCH IN CONCENTRATED AQUEOUS SOLUTION AND ITS EFFECT ON ENZYME DIGESTIBILITY

5.1 Abstract

Starches and amylose display spherulitic morphologies after heating and rapid quenching, but these phenomena have never been reported in debranched starch. Debranched starches were heated to 170 °C and then cooled to 10 °C using a differential scanning calorimetry (DSC), in order to form spherulitic morphologies. More numerous, well-formed spherulites (~8 μm in diameter) with positive birefringence and sintered-like morphology were formed in the DBCN1 and DBPS2 starches, which contained long linear chains. Negative spherulites with spherical and smooth surface were formed in the DBRD6 which contained essentially linear short chains. All spherulites showed a B-type crystalline structure with similar melting temperature (85±2 °C) and melting enthalpy (30±0.9 J/g). However, the DBRD6 spherulites showed a higher resistant starch content (55%) than that of the DBPS1, DBPS2 and DBCN1 (23%, 19% and 18% RS, respectively). This higher enzyme resistance was attributed to their tangential organization and their smoother and denser surface as observed by SEM and AFM. The influence of morphology features of spherulites is discussed in relation to their resistance to enzymatic hydrolysis.

Keywords: Spherulitic crystallization, debranched starch, enzyme digestibility

5.2 Introduction

Spherulites are normally found in melt-crystallized synthetic polymers (Bassett, 2003; Magill, 2001). The characteristics of spherulite are spherical semicrystalline entities and contain amorphous material between highly ordered lamellae, exhibit a distinctive black and white extinction crosses; classical named is "Maltese Cross", when viewed under polarized light microscopy. The sign of the birefringence can be characterized as positive or negative based on the comparison of the indices, which is defined as the difference between the radial and tangential reflective index (Murayama, 2002). This phenomenon can imply the inner information of the orientation for the molecular chain in the spherulites.

The spherulitic crystallization for starch-based spherulites can be generated by amylose inclusion complexation in the presence of suitable ligands i.e. butanol (Schoch, 1942), terpenes, lactones (Heinemann, Escher and Conde-Petit, 2003) and fatty acids that induce the helix formation of amylose (Fanta, Felker, Shogren and Salch, 2006). In cereal starches, the native lipid present in the starch granule formed complexes with the amylose fraction and formed in spherocrystals (Davies, Miller and Procter, 1980; Nordmark and Ziegler, 2002b). This crystallization process was termed high temperature retrogradation because a high process temperature and high storage temperature were required for their formation (Davies et al., 1980). However, a lack of lipid in native starch or only amylose fraction could also form spherulites (Creek, Ziegler and Runt, 2006; Nordmark and Ziegler, 2002a). The spherulitic crystallization of native starches was obtained when aqueous starch dispersions were heated to 160-

180 ℃, which was termed “clearing temperature” (Creek et al., 2006), followed by rapid cooling (Fanta, Felker and Shogren, 2002; Ziegler, Nordmark and Woodling, 2003). These spherulites were mainly composed of amylose and lightly branched starch polymers, and their crystallization was preceded by liquid-liquid phase separation prior to polymer association (Creek et al., 2006). The spherulites were found to be B-type crystallinity and radially oriented structure, which was consistent with the core and region of native granules (Creek et al., 2006; Ziegler, Creek and Runt, 2005). The overall morphology and crystalline structure of the spherulites are dependent on the starch sources, amylose content, and crystallization conditions such as concentration of starting materials, cooling rate and crystallization temperature (Conde-Petit, Handschin, Heinemann and Escher, 2006; Creek et al., 2006; Nordmark et al., 2002a; Singh, Lelane, Stewart and Singh). (Ziegler et al., 2003)(2003) and (Singh, Lelane, Stewart and Singh, 2010) found that the formation of spherulite formation depended on the starch source. They demonstrated that spherulite formation was easily formed in high amylose starch and acid modified starch. Similarly, (Ma, Floros and Ziegler, 2011) reported that a higher ratio of amylose to amylopectin resulted in a formation of well-developed spherulites.

An alternative spherulitic precipitation was found in concentrated solutions of short-chain amylose in which their crystallization conditions resulted in a different morphological features of spherulites (Helbert, Chanzy, Planchot, Buléon and Colonna, 1993; Ring, Miles, Morris, Turner and Colonna, 1987). B-type spherocrystals was obtained by direct cooling of the aqueous solutions whereas A-type spherocrystals were formed by ethanolic precipitation (Helbert et al., 1993; Ring et al., 1987). A-type spherocrystals showed a radial organization, confirming that the

positive birefringence was observed in these spherulites while B-type spherocrystals exhibited spherical shape with smooth surface and a tangential organization. These spherocrystal were used as model systems to study the enzymatic hydrolysis of starch crystallites (Planchot, Colonna and Buléon, 1997; Williamson et al., 1992) . It was remarked that the susceptibility to hydrolysis of spherulites related to crystalline type, morphology, crystal defect and inner cohesion among crystals of amylose.

Although spherulite formation favored by association of linear materials, the self-assembly of polydisperse linear chains into spherulites never been reported. The multi-scale organization of spherulites and its effect on digestibility has not been studied. It would be an idea for novel biomaterial with controlled properties for delivery system. A particular interest of this study is focused on the investigation of spherulite formation in comparison between different debranched starches with different chain lenght distribution. The objective of this study was to investigate the effect of molecular weight distribution on spherulites formation, their morphological features and consequence on their enzymatic digestibility.

5.3 Materials and Methods

5.3.1 Materials

Rice starch from four Thai rice varieties: waxy rice (RD6, 0% amylose), low-amylose rice (Phitsanulok1, PS1, 12.6% amylose), intermediate-amylose rice (Phitsanulok2, PS2, 26.0% amylose) and high-amylose rice cultivars (Chainat1, CN1, 29.6% amylose) was obtained from Udonthani, Phitsanulok and Chainat Rice Research Center under Bureau of Rice Research and Development (BRRD, Thailand). Debranched starches were obtained from debranching of 10% starch gel as described

in previous chapters (chapter III and Appendix A). The chain length distribution and degree of polymerization has been reported in Chapter III.

5.3.2 Starch spherulites preparation

The freeze-dried debranched starches (15 mg) were weighted in high-volume (60 μL) stainless steel differential scanning calorimetry (DSC) pans (TA Instruments, New Castle, DE) and the millipore water was added to obtain a 30% (w/w) dispersion. The pans were hermitically sealed and stored overnight at room temperature to ensure moisture equilibration. Sample pans were heated from 25 ℃ to 170 ℃ at the rate of 5 ℃/min and then immediately cooled down to 10 ℃ at cooling rates of 10 or 25 ℃/min in a TA Q100 DSC (TA Instruments, New Castle, DE). The samples were held overnight at room temperature before analyzing by DSC, or the pans were opened and the samples were taken for further analysis. The samples were carefully collected from pan with a laboratory spatula and dried at room temperature. The DSC was calibrated with indium, and a 35 μL of the millipore water in DSC pan was used as a reference during all heating and cooling procedures. Re-scans were performed from 10 to 200 ℃ at heating rate 3 ℃/min. The Thermal Advantage Universal Analysis software (TA Instruments, New Castle, DE) was used to calculate transition temperature (℃) and enthalpy (J/g). Experiments were conducted at least in duplicate.

5.3.3 Optical and polarized optical microscopy

After opening the pans, the samples were immediately removed using a spatula and then dispersed in a drop of Millipore water on a microscopy slide, and a cover slip was place on the top of the slide. The sample was observed using an

Olympus BX51 microscope (Zeiss, Germany) equipped with polarizing filter and 530 nm compensating filter. The photographs were recorded using a digital camera.

The particle sizes of spherulites were analyzed by mathematical morphology. The sample particles were stained with iodine/potassium iodine solution. Each sample was scanned and captured over twenty different regions under 100 x magnifications. Color images were converted into monochromatic images with grey levels ranging from 0 to 255 using ImageJ software (ImageJ, http://rsbweb.nih.gov/ij/). Grey level histograms of all slices were examined altogether. A grey level threshold of 100 was visually chosen to extract the slices from the background. A granulometry analysis based on mathematical morphology permitted to determine the size distribution of spherulites with their mean value and standard deviation. The granulometry analysis consisted of morphological openings of increasing size, which was comparable to an image sieving (Soille, 2003). The Gaussian distribution was used to estimate the particle size distribution of spherulites.

5.3.4 Scanning electron microscopy (SEM)

The dried-spherulite samples were gently pressed using a spatula to separate the aggregates that formed during drying. A thin layer of sample was placed on aluminum stubs with conductive carbon tape and sputter coated with gold-palladium by using a JEOL JFC-1100 Fine Coater Ion Sputter coater (Tokyo, Japan). The sample was observed using a JEOL JSM-5800LV scanning electron microscope (Tokyo, Japan) operating at an accelerating voltage of 20 kV.

5.3.5 Wide angle X-ray diffraction (WAXD)

X-ray diffraction was performed after water content adjustment by water phase sorption for 10 days in desiccators under partial vacuum at 90% of relative

humidity. Approximately 20 mg dried spherulite samples were sealed between two tape foils to prevent any significant change in water content during measurement. Diffraction diagrams were recorded on a BRUKER^{TM} (Karlsruhe, Germany) D8 Discover diffractometer with Cu Ka_1 radiation (λ = 1.5405 Å) at 40 kV and 40 mA. The diffracted beam was collected with a two-dimensional GADDS detector and recording time was 600 sec. The distance from the sample to detector was 100 mm. The samples were examined over the angular range of 3 to 40° (2θ) with a step size of 0.01 and a sampling interval of 10 s. X-ray spectra data were visualized and normalized using KaleidaGraph software. Spectra were then baseline corrected and peaks assigned and integrated using Origin Pro 8 (OriginLab Corporation, Northampton, USA). Pearson VII function was used to fit the individual crystalline peaks corresponding A, B and V-type allomorph reflections (Lopez-Rubio, Flanagan, Gilbert and Gidley, 2008), whereas Gaussian function was used to fit an amorphous peak at $2\theta = 19°$. The relative crystallinity were calculated according to Frost et al (Frost, Kaminski, Kirwan, Lascaris and Shanks, 2009), based on the existence of two phases in the material. The relative crystallinity was calculated by dividing the crystalline area by the total area under the diffractogram. The lateral crystal size was established from peak half width of 100 reflection ($2\theta \sim 5.6°$), using the Scherrer equation: $D_{hkl} = k\lambda/\beta \cos\theta$, where D_{hkl} is the average length of the diffraction domains normal to the family plane (*hkl*), *k* is a constant as 0.9 for cellulose, λ is wavelength used and β is the peak half width (Cairns, Bogracheva, Ring, Hedley and Morris, 1997).

5.3.6 Synchrotron Small Angle X-ray Scattering (SAXS)

Experiments were carried out on the BL1.3W: SAXS (Small/Wide Angle X-ray Scattering), Synchrotron Light Research Institute (SLRI), Nakhon

Ratchasima, Thailand. The details of the experimental setup have been reported elsewhere (Soontaranon and Rugmai, 2012). The sample-to-detector distance was determined to be 1512.18 mm by silver behnate ($AgC_{22}H_{43}O_2$) standard. Dried samples were hydrated with DI water to obtain 50% moisture. The hydrated samples were loaded into the sample cell with thin flat aluminium windows. An 8 keV synchrotron X-ray beam, monochromatized by a double multilayer monochromator, was used andthe SAXS profiles were recorded with a MAR-CCD (SX165) detector. The exposure time for each data collection was 30 seconds. The program called SAXSIT, developed in-house using Matlab was used for data reduction and analysis. The SAXS data were collected in the scattering vector range of $0.017 \leq q \leq 0.200$ ($Å^{-1}$) ($q = 4\Pi \sin \theta/\lambda$). All SAXS patterns was subtracted with empty cell to eliminate the background scattering originating from the sample holder and possible other sources. The position of SAXS peak (q_{max}) was determined by the graphical method and the Bragg distance was calculated with Wolf–Bragg equation (Vladimir P. Yuryev et al., 2004). Desmeared SAXS curves under the range of $0.023 \leq q \leq 0.919$ ($Å^{-1}$) were also analyzed according to the paracrystalline one-dimensional lamellar stack model as described elsewhere (Roldan, 1966; Vladimir P. Yuryev et al., 2004).

From paracrystalline diffraction theory (Roldan, 1966), It was assumed that a cross-section of all crystalline lamellae has the same single step function for the electron density profile of width *L*, and that paracrystalline lattice distortions arise from a variation of the thickness of the amorphous layers separating crystalline lamellae. The SAXS intensity was assumed to be the sum of the paracrystalline diffraction and the additional scattering component. The equation parameters are

calculated by group contributions of paracrystalline, power law, Ornstein-Zernike and Broad peak:

$$I(q) = C * \left\{ I_0 \exp(-\sigma_{in}^2 q^2)\ \overline{|F(q,L)|^2} S(q) + aq^{-x} + \frac{b}{1+q^2\xi^2} + \frac{I_{0b}}{1+(|q-q_0|\xi_0)^m} \right\} + \text{k} \quad (1)$$

In this expression, the exponential $\exp(-\sigma_{in}^2 q^2)$ comes from the smoothing of crystalline-amorphous interface.

and $\overline{|F(q,L)|^2}$ is the averaged crystalline form factor,

$$\overline{|F(q,L)|^2} = \frac{1}{\sqrt{2\pi}\sigma_L} \int_{-\infty}^{\infty} |F(q,x)|^2 \exp\left(-\frac{(x-L)^2}{2\sigma_L^2}\right) dy \quad (2)$$

and $F(q,L)$ is the lamellar form factor for a single crystalline lamella of thickness L,

$$F(q,L) = \frac{\sin\left(\frac{qL}{2}\right)}{qL/2} \quad (3)$$

and $S(q)$ is the interference function (lattice factor),

$$S(q) = \frac{1 - |G(q)|^2}{1 - 2|G(q)|\cos(q\alpha) + |G(q)|^2} \quad (4)$$

where $G(q)$ is the Fourier transform of the period size distribution function

$$G(q) = \mathcal{F}[H(y)]$$

with the Gaussian period size distribution function

$$H(y) = \frac{1}{\sqrt{2\pi}\sigma_a} \exp\left(-\frac{(y-\alpha)^2}{2\sigma_a^2}\right)$$

The paracrystalline structure parameter L, α and σ for the crystalline lamellar of spherulites were determined. Average repeat distance α corresponded to thickness for the alternating crystalline and amorphous lamellae, σ is its mean square deviation, and L_{crl} corresponded to crystalline lamella thickness.

5.3.7 Atomic force microscopy (AFM)

AFM images were acquired either in air using a Park Scientific Instrument Autoprobe CP (Sunnyvale, CA) or in liquid using a Bruker Instruments Bioscope (Santa Barbara, CA). The AFM images were recorded in the tapping mode using conventional pyramidal silicon nitride cantilevers obtained from Digital Instruments (Santa Barbara, CA). All tapping mode images (both amplitude and topography images) were acquired at the lowest possible stable scanning force (less than 10 nN) with a line scan frequency of 1 Hz.

5.3.8 Resistant starch content determination

The official methods (AOAC method 2002.02, AACC Method 32-40) for in vitro RS determination was used (McCleary and Monaghan, 2002). Approximately 25 mg of dried-spherulite sample was mixed with 1 mL of enzyme mixture solution (10 mg/mL pancreatic α-amylase and 3U/mL amyloglucosidase in 0.1 M, pH 6 sodium malate buffer containing 0.3 g/L $CaCl_2$ and 0.2 g/L NaN_3). The sample was incubated at 37°C for 16 h with constant shaking at 200 strokes/min. After 16 of digestion, unhydrolyzed starch was collected by ethanol precipitation and centrifugation at 1500g for 10min (repeated 3 times). The pellet was resuspended in 2 mL of 2 M potassium hydroxide with stirring for 20 min in an ice/water-bath. The solubilized sample was adjusted to pH 4.75 by added 8 mL of 1.2 M, pH 3.8 sodium acetate buffer. Immediately, a 0.1 mL aliquot of amyloglucosidase (3300 U/mL) was added and incubated at 50°C for 30 min with constant agitation to liberated glucose. The contents of the tubes were quantitatively transferred to 25 mL volumetric flask. The liberated glucose was measured by reacted with 3 mL of GOPOD reagent (glucose oxidase >12,000 U/L, peroxidase >650 U/L, 4-aminoantipyrine 0.4 mM) at

50°C for 20 min, and then the absorbance was read at 510 nm against a reagent blank and compared to the glucose standard supplied with the kit.

5.3.9 Enzyme digestibility of spherulites

After opening the pans, the spherulite samples (30 mg, 30% w/w db) were digested in 1 ml of sodium maleate buffer (0.1 M, pH 6.0) containing 10 mg/ml of pancreatic α-amylase (3 Ceralpha Units/mg, K-RSTAR, Megazyme International Ireland, Ireland) and 3 U/mL of amyloglucosidase (3300 Units/mL, K-RSTAR, Megazyme International Ireland, Ireland). Enzyme solution was freshly prepared and centrifuged to remove solid at 1,500×*g* for 5 min prior to each digestion. The mixed solution was incubated at 37 °C for 0, 2, 4, 6, 8, 10, 12 and 16 h. After each interval time, 100 μL of aliquot was taken, and 100 μL of 95% ethanol was added to inactivate the enzyme and centrifuged at 1500×*g* for 10 min. Then, the supernatants were collected. An aliquot of the supernatant were analyzed for soluble carbohydrate concentration using the sulphuric acid-orcinol colorimetric method (Planchot, Colonna and Saulnier, 1997). The degree of hydrolysis was expressed as the amount of glucose which is released per 100 mg of dry starch. The pellet was observed for the change in morphology as a function of hydrolysis time using an optical and polarized light microscopy.

5.4 Results and Discussion

5.4.1 Spherulitic crystallization in debranched starch

On the cooling of the DBCN1, DBPS2 and DBPS1, the broad exothermic peak with a T_c around 65-68 °C was observed (Figure 5.1A). The crystallization enthalpy (ΔH_c) of the DBCN1, DBPS2 and DBPS1 were 3.4, 3.6, and

2.1 J/g, respectively. These enthalpies were correlated well with the ELC proportion of debranched starches (mass fraction of ELC was 27, 28 and 15% for the DBCN1, DBPS2, and DBPS1, respectively). Therefore, the exothermic peak was attributed to spherulitic crystallization of amylose. This result was in agreement with the result of (Creek et al., 2006) and the double-helical network of amylose are usually developed at low temperature (70°C) (Bayer & Baltá Calleja, 2005). However, the ΔH_c of DBCN1 (3.44 J/g) was a low value compared to melting enthalpy (ΔH_m) of subsequent reheating (Figure 5.1B). Furthermore, the ΔH_c values were about 6–11% of ΔH_m of spherulites (ΔH_m of spherulites was 29.9, 33.5 and 34.5 J/g in the DBCN1, DBPS2 and DBPS1 spherulites, respectively) or equivalent to about 35–40% of ELC fraction. It indicated that amylose ELC were partially crystallized during cooling. No exothermic peak was observed for the DBRD6 (Figure 5.1A), which was consistent with no ELC fraction. Nevertheless, the DBRD6 showed a single exotherm and single endotherm during subsequence heating (Figure 5.1B). The appearance of exotherm with T_c around 25 °C could be due to the crystallization of some parts of SC and LC, whereas the endothermic peak at T_m 89 °C reflects to melting of their crystallites. It should be noted that the spherulitic crystallization behavior of debranched starches depended on chain length distribution. For debranched waxy starch containing essential short chains, the SC and LC were crystallized at low temperature (25 °C). For debranched starches with ELC fraction (normal rice starches), the ELC was partial crystallization during cooling at a temperature of 65 °C, followed by crystallization of SC and LC at low temperature. The spherulitic crystallization of debranched starches containing ELC, LC and SC was similar to spherulitic growth PES/PEO blend with non-isothermal crystallization which was crystallized separately

at different temperatures and the process was termed ‘step-crystallization’ (He and Liu, 2007).

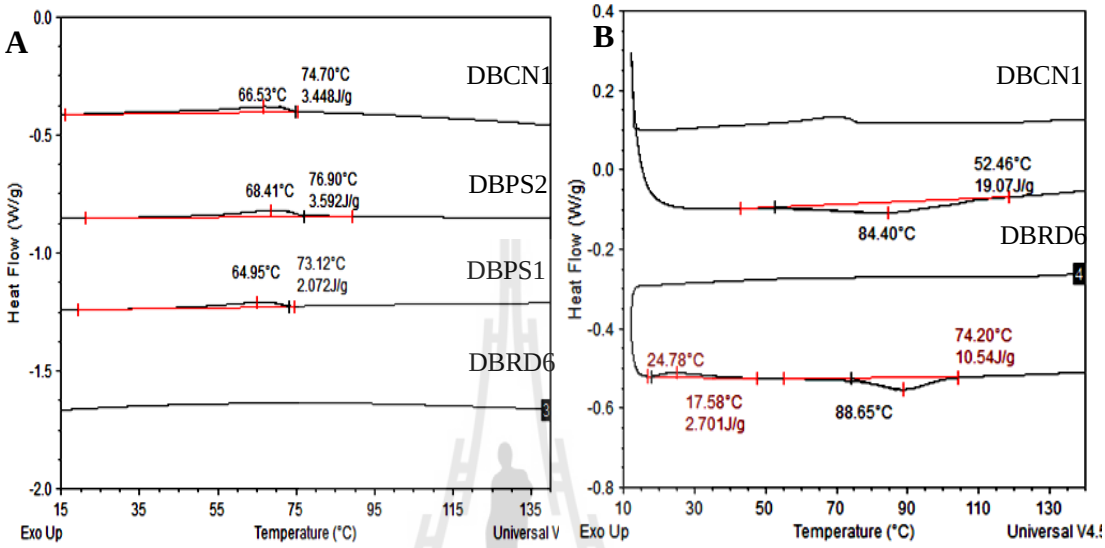

Figure 5.1 DSC cooling (A) and cooling and subsequent reheating (B) curves of debranched starches. Debranched starches were cooled from 170°C to 10 °C at rate of 10 °C.min^{-1} and reheated to 200 °C at rate of 3 °C.min^{-1}.

5.4.2 Spherulitic morphology by optical microscopy

Figure 5.2 showed the optical micrograph of recrystallized debranched starches at cooling rate 10 °C.min^{-1}. Recrystallized DBCN1 and DBPS2 appeared as micron-sized spherical particles (Figure 5.2Aa and 5.2Ba) and homogeneous size distribution with an average diameter of 8 μm (Figure 5.3A and 5.3B). All particles of DBCN1 and DBPS2 exhibited strong birefringence and Maltese cross under cross polarizers (Figure 5.2Ab and Figure 5.2Bb), indicating spherulitic organization with homogeneous orientation. Starch spherulites with strong birefringence was previously observed in mung bean starch spherulites (Ziegler et al., 2005) and amylose

spherulites (Creek et al., 2006). Under crossed polarize with the compensator inserted, the DBCN1 and DBPS2 particles exhibited positive birefringence (a blue color in their upper-right and lower-left quadrants and yellow in the other two, Figure 5.2Ac and 5.2Bc), implying that the direction of the main chain axes were parallel to the radius of the spherulite (Murayama, 2002; Yoshioka, Fujimura, Manabe, Yokota and Tsuji, 2007). Our result was in agreement with previous literatures (Creek et al., 2006; Ma et al., 2011; Singh et al., 2010; Ziegler et al., 2005) in that amylose is favored the formation of well-formed spherulites. It was probably that the ELC stabilized the radial organization of spherulites. Therefore, it seems that the presence of ELC is necessary for the formation of well-formed spherulites, for example by being involved in different crystalline lamellae and, thus, stabilizing the overall architecture. Radial chain organization is not the typical chain organization within a spherulite of synthetic polymers (Wang, Chen, Cheng, Liao and Wang, 2002); however, radial alignment of polymer chains within crystalline component has been previously reported for amylose spherulites prepared from ethanol solutions (Helbert et al., 1993) and Hylon VII spherulites by heating and cooling step using DSC instrument (Nordmark et al., 2002b). The morphology of recrystallized DBPS1 shows an aggregated particles and smaller spherical particles with a size of 6 μm (Figure 5.2Ca and 5.3C). It displayed an irregular birefringence without Maltese cross which is typical for the spherulites under cross polarizer (Figure 5.2Cb-c). This result is consistent with previous report in which the formation of spherulite was favored in starches with a high percentage of linear molecules (Ziegler et al., 2003). For the latter sample, the recrystallized DBRD6 show an aggregated particles and large spherical particles (average size of 15 μm) with and large size distribution (Figure 5.2Da and 5.3D). The resulting birefringence is

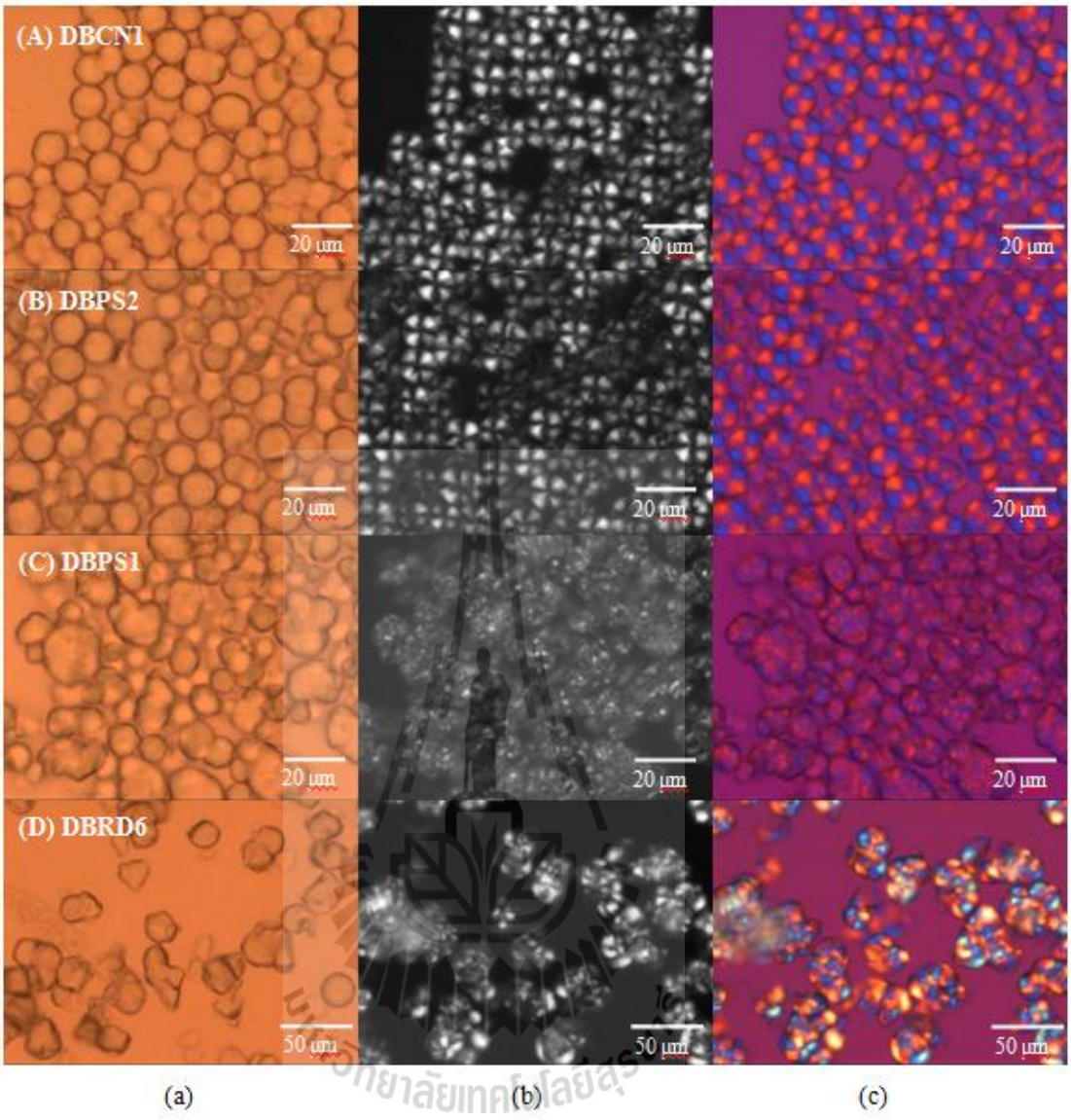

Figure 5.2 Optical micrographs showing image of the particles crystallized from the debranched starches of (A) DBCN1, (B) DBPS2, (C) DBPS1and (D) DBRD6; (a) under brightfield (b) under cross polarizers (c) under cross polarizers with a compensator inserted. All samples were prepared by heating to 170 °C and follow by cooling from 170 °C to 10°C at rate of 10 °C.min^{-1}.

much more difficult to interpret but it appears to be negative birefringence rather than positive birefringence (Figure 5.2Db-c). The observation of negative birefringence has been reported in amylose spherulites which the main chains axis were oriented tangentially to the spherulite radius (Creek et al., 2006). A larger spherical particle of DBRD6 might be explained by considering the mobility contribution of molecule chain modifying the crystal growth rate. Short polymer chains had higher mobility than long molecules; thus, the crystallization process slowly resulted in linear chains gradually developed into large superstructure with fully extended chain crystals (Carvalho, Cormier, Lin and Dalnoki-Veress, 2012).

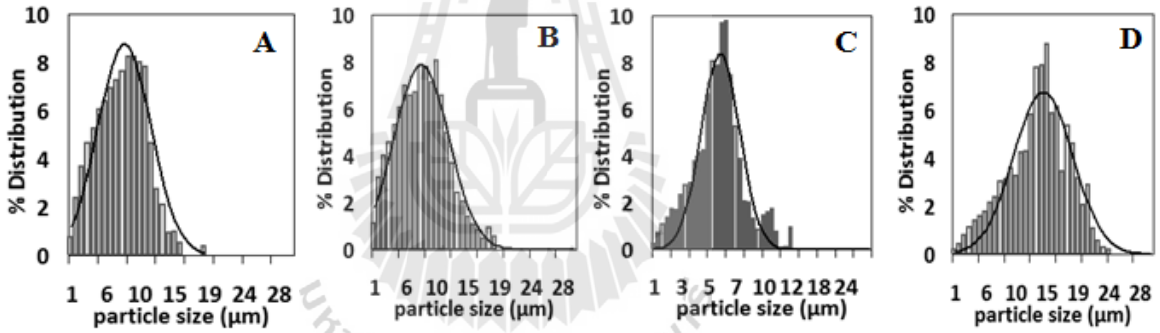

Figure 5.3 Particle size distribution of the particles crystallized from the debranched starches of (A) DBCN1, (B) DBPS2, (C) DBPS1and (D) DBRD6.

The influence of cooling rate on the formation of spherulitic morphology in DBCN1 and DBRD6 was studied in order to find the optimal cooling rate for the formation of well-formed spherulites. Cooling rate influencing spherulitic morphologies has previously reported and found that starch spherulite could be obtained over a wide range of cooling rate from 1 to 250 °C.min^{-1} and the spherulite size was highly dependent on cooling rate (Creek et al., 2006; Nordmark et al., 2002b;

Ziegler et al., 2005). The DBCN1 was observed to form spherulites at all cooling rates used in the present experiments (Figure 5.4). It was found that well-formed spherulites with strong positive birefringence and Maltese cross pattern were observed in the cooling rate of 10 °C.min^{-1}. The DBCN1 prepared at slow cooling rate (1 °C.min^{-1}) displayed some of branched morphology and some of starry night image (bright separated spots in very small spherulites) which resemble the nucleated crystalline structures found in mung been starch (Ziegler et al., 2005). Quenching the DBCN1 at cooling rate of 25 °C.min^{-1} resulted in the presence of spherulitic material with showed weak birefringences. It leads to the implication that it is due to the limited time for diffusion of amylose and stabilizing radial organization. For the DBRD6 prepared at a cooling rate of 1 °C.min^{-1}, apparently non-spherulitic material identical to gel-like structure was observed (Ziegler et al., 2005; Ziegler et al., 2003). For the DBRD6 prepared at cooling rate of 25 °C.min^{-1}, a large amount of spherulites resembles the negative-type birefringence but imperfect Maltese cross was observed (Figure 5.4 and 5.5). The well-defined spherulites of the DBRD6 (Figure 5.5 in zoom) displayed two different types of spherulites; usual-negative type and unusual-negative type. The images of usual-negative type (bottom) reflects a tangential orientation of the main chain axis, and in unusual-negative type (top), the main chains axes were tilted by 45° to the radial axis of spherulite (Murayama, 2002; Yoshioka et al., 2007).

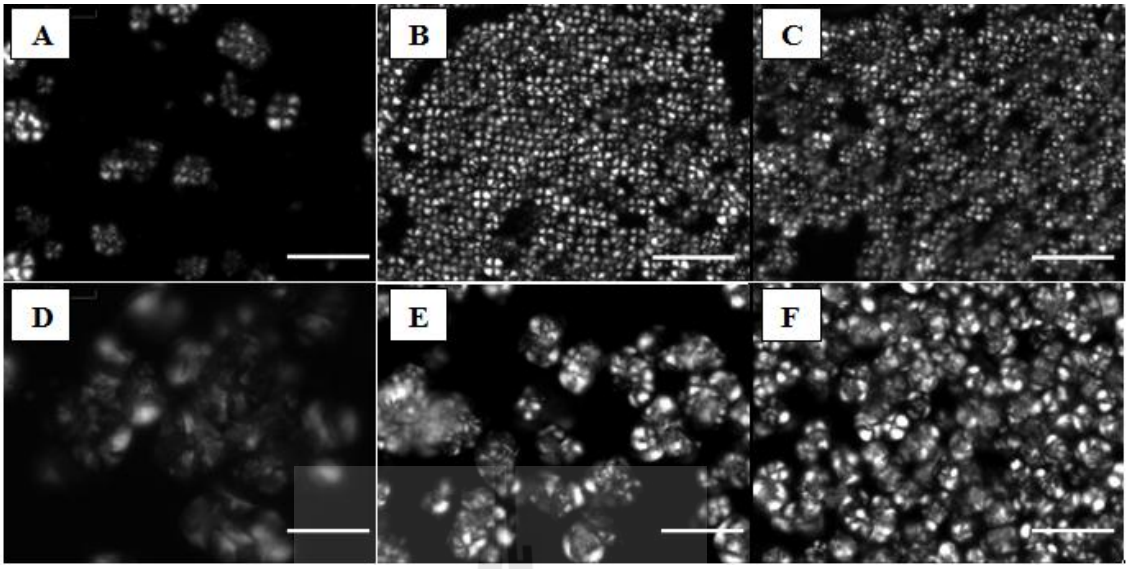

Figure 5.4 Optical micrographs showing representative spherulitic structures formed from (A-C) DBCN1 and (D-F) DBRD6 cooled from 170 °C to 10°C at differing cooling rates. Sample cooled at 1 °C.min^{-1} (A and D); 10 °C.min^{-1} (B and E); 25 °C.min^{-1} (C and F). All images acquired under crossed polarizers. All scale bars represent 50 μm.

The transformation of amorphous polymers to crystalline form after melting and fast quenching has been reported in the literature (Qi, Avalle, Saklatvala, & Craig, 2008). The cooling rates and the DSC pan conditions have been reported to affect the transformation of amorphous melts (Qi et al., 2008). During heating, the synthetic polymers form gels up to a certain temperature (T_m) and only spherulites are formed above T_m (Guenet, 1996). Crystal nucleation for spherulite growth may have occurred directly from the melt, producing probably single crystals in the melt matrix, though the rate of crystallization is extremely slow at that stage (Imai & Kaji, 2006).

It should be noted that the DBCN1 containing extra-long chain could form positive spherulites with well-organization. Nevertheless, our results indicated

that even lack of amylose component, the formation of negative spherulites can be developed from short and long chain molecules.

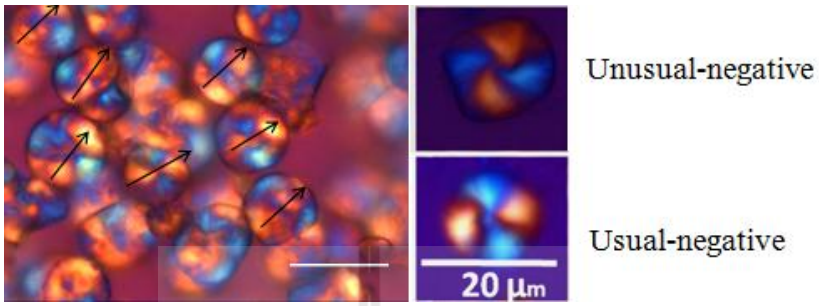

Figure 5.5 Spherulitic morphology of DBRD6 prepared at a cooling rate of 25 °C.min^{-1} and investigated by polarizing optical microscope. The arrows show that the first and third quadrants are yellow-orange and the others are blue-green which is the characteristic of negative spherulites (Yoshioka et al., 2007). The right side shows the representative of well-defined spherulites viewed under crossed polarizers with a compensator plate. All scale bars represent 20 μm.

5.4.3 Microstructure of spherulites by SEM and AFM

Well-formed spherulites prepared at optimal condition for each debranched starch was imaged by SEM and AFM, where the DBCN1, DBPS2 and DBPS1 spherulites were prepared at a cooling rate of 10 °C.min^{-1} and the DBRD6 spherulites were prepared at a cooling rate of 25 °C.min^{-1}. The SEM image of the DBCN1 and DBPS2 spherulites exhibited aggregates of spherical microparticles (Dia ~ 8 μm) with sintering-like morphology, had high porosity and large pore size ranging from 150 to 500 nm (Figure 5.6A and 5.6B). These spherulites appeared to be stick

together which could occur during drying due to adhesion forces existing at the surface among those

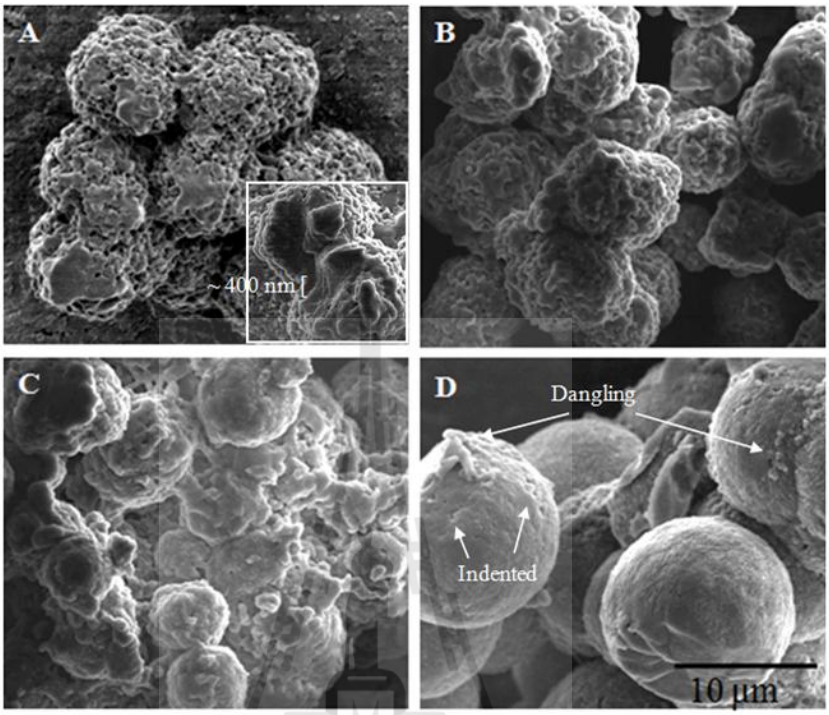

Figure 5.6 SEM image of spherulites prepared from different debranched starch of (A) DBCN1, (B) DBPS2, (C) DBPS1 and (D) DBRD6. DBCN1, DBPS2 and DBPS1 spherulites were prepared at a cooling rate of 10 °C.min^{-1}, whereas DBRD6 spherulites were prepared at a cooling rate of 25 °C.min^{-1}.

spherulite particles. Furthermore, it seems that the DBCN1 spherulites consisted of stacking of lamellar-like layers with an average thickness of 400 nm (Figure 5.6A). It is possible that crystalline lamella sheet consists of double helices oriented along the radial direction. The rough surface morphology of DBCN1 spherulites was similar to that of the spherulites from high amylose maize starch reported by (Singh et al., 2010), which resulted from the imperfect stacking of lamellae that occur due to repulsive forces from the portion of uncrystallized polymer chains and, therefore,

extending from the lamellar surface. The DBPS1 spherulites were irregular shape with various particle morphologies such as plate-like, aggregate, and etc. It was interesting that the morphology of DBRD6 spherulite was significantly different from those of other spherulites. It shown to consist of aggregates of large spherical microparticles (Dia ~14 μm) with a smooth and dense surface (Figure 5.6D). A small amount of indentation and non-spherulitic dangling particles was also observed on the surface of the DBRD6 spherulites.

The morphological difference was associated with differences in spherulitic crystallization phenomenon that initiated from a homogeneous or heterogeneous nucleation process (Hurle, 1994). It suggested that the difference in chain length distribution resulted in the formation of spherulitic crystals with very different morphologies, probably related to different self-assembly pathways. The DBCN1, DBPS2 and DBPS1 that crystallized undergone two-step crystallization process, could be classified as heterogeneous nucleation process. Rough surface morphology of the DBCN1and DBPS2 spherulites was similar to the spherulite from high amylose maize starch reported by (Singh et al., 2010), which resulted from the imperfect stacking of lamellae that occur due to repulsive forces from the portion of uncrystallized polymer chains and therefore extend from the lamellar surface. It was possible that the stacked lamellar morphology resulted in the formation of stacked lamella with alternating amorphous and crystalline layers that is often observed in synthetic polymer (Ashman and Booth, 1975). On the other hand, simultaneous crystallization of DBRD6 or as initiated by homogeneous nucleation process favored the formation of very symmetrical and spherical shapes spherulites.

The diameter sizes viewed under SEM images were well accordance with the size observed in Light microscope. This observation suggested that one particle is a single spherulite, having a single structure and morphology. Our result was different from spherulites prepared from high-amylose maize starches, in which the round spherulites observed under SEM consist of several smaller spherulitic particles (Singh et al., 2010).

The fine surface structure of two different spherulites, i.e. DBCN1 and DBRD6 spherulites was investigated using AFM. The AFM image of the DBCN1 spherulites showed a rough surface structure (Figure 5.7) as similar observed using SEM. When viewed at higher magnification, the surface of DBCN1 spherulites shows a shallow pore with an average height of 100-250 nm (Figure 5.8), which was attributed to stacking of lamella layers. Interestingly, the surface detail revealed lamellar-like structure under a higher magnification AFM image as shown in Figure 5.9. The lamellae were 7-9 nm thick, corresponding to 3.33 to 4.3 turns of six-fold helices or 20-25 DP amylose (Imberty and Perez, 1988). The length of corresponding chain was consistent with the length of SC fraction, which is the major mass fraction. Regarding the combination results of SEM and AFM, it might propose that a uniform layer of spherical microcrystalline consist largely of aggregates of SC fraction.

The AFM image of the DBRD6 spherulites confirms the structure described by SEM showing smoother and denser surface and had some of dangling material (Figure 5.10). At a higher magnification AFM image of the surface topography of the DBRD6 spherulites, it reveals different topographic patterns with different positions, indicating an inhomogeneous surface structure of the DBRD6 spherulites (Figure 5.11).

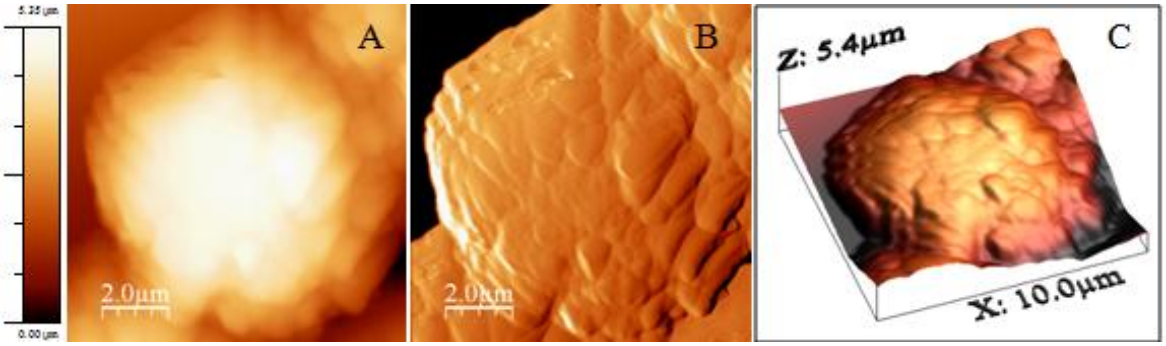

Figure 5.7 AFM topographic images showing a representative of DBCN1 spherulite. (A) height image (B) phase image and (C) the corresponding 3D images.

Figure 5.8 Higher magnification AFM topographic images of the representative of the DBCN1 spherulite. (A) height image (B) phase image and (C) the corresponding 3D images. These images were acquired from the top middle of the spherulite.

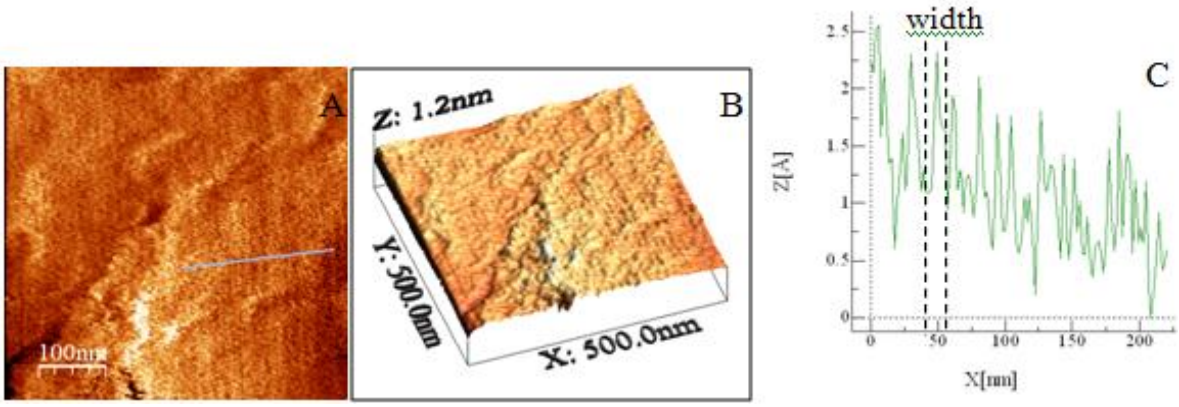

Figure 5.9 AFM topographic images of the representative of the DBCN1 spherulite. (A) height image (B) the corresponding 3D images and (C) line profile of the line on height image showing the width of surface lamellar of spherulite.

Figure 5.10 AFM topographic images showing representative of the DBRD6 spherulite. (A) height image (B) phase image and (C) the corresponding 3D images.

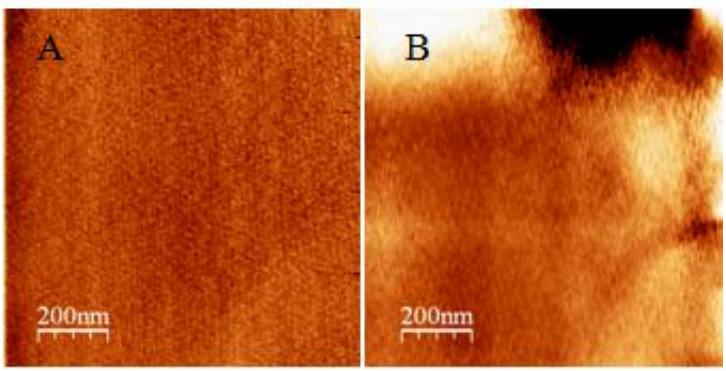

Figure 5.11 AFM topographic images of the DBRD6 spherulite at different positions.

5.4.4 Crystalline structure of spherulites by WAXD and synchrotron SAXS

Figure 5.12 shows the WAXD pattern of the DBCN1, DBPS2, DBPS1 and DBRD6 spehrulites. They displayed strong B-type X-ray diffraction diagram with an exceptionally high crystallinity (Table 5.1). This result indicated that spherulitic crystallization by heating at high temperature > 170 °C followed by rapid cooling to low temperature leads to a formation of B-type crystalline structure with crystallinity much higher than the granular form. Strong B-type crystallinity has been reported for short-chain amylose spherulites (Cai and Shi, 2013; Nishiyama, Putaux, Montesanti, Hazemann and Rochas, 2009; Ring et al., 1987).

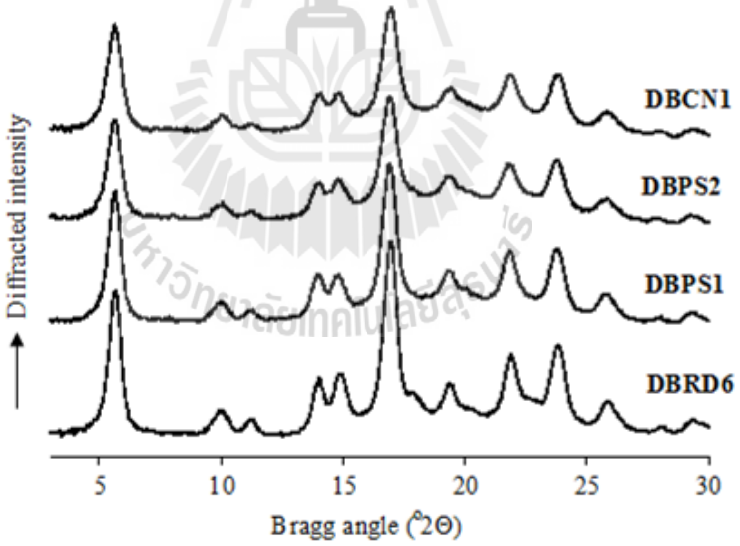

Figure 5.12 WAXS patterns of the spherulites prepared from different debranched starch: DBCN1, DBPS2, DBPS1 and DBRD6. The DBCN1, DBPS2 and DBPS1 spherulites were prepared at a cooling rate of 10 °C.min^{-1}, whereas the DBRD6 spherulites were prepared at a cooling rate of 25 °C.min^{-1}.

Table 5.1 Crystallinity, lateral crystal size and RS content of spherulites

Sample	%Crystallinity	Crystal size (100)	Crystal types
DBCN1 spherulites (27:17:56)	70.4	11.4	B
DBPS2 spherulites (28:18:54)	63.3	11.3	B
DBPS1 spherulites (15:20:65)	69.9	13.0	B
DBRD6 spherulites (0:22:78)	78.1	13.7	A+B

[a] The number in parentheses is the mass fraction of ELC:LC:SC.

In addition to B-type crystallinity, a small amount of A-type crystallinity (as evidenced by the shoulder at 2θ =17.8 and 22.4°) was observed for the DBRD6 spherulites. It is similar to amylose spherocrystals from crystallizing DP 20-40 synthetic amylose (Nishiyama et al., 2009). It is well known that the crystalline type of recrystallized starch depends on the chain length, the concentration and the crystallization temperature (Buléon, Véronèse and Putaux, 2007). Low temperature, low concentration and long chains favor the formation of B-type polymorph while high concentration, high temperature and short chains lead to A-type crystalline structure (Pohu, Planchot, Putaux, Colonna and Buléon, 2004; Zabar, Shimoni and Bianco-Peled, 2008). Therefore, the formation of B-polymorph spherulites could be favored by the temperature and concentration. A presence of co-existed A-type diffraction peak within the DBRD6 spherulites could result from essential short chains. In addition, the lateral crystal size (12.5±0.6 nm) (Table 5.1) drawn from the (100) reflection at 2θ around 5.6° in wide angle X-ray scattering spectra (Figure 5.12)

was increased with higher proportion of short chains. (Table 5.1).This is consistent with a strong ability of short chains to reorganize into large crystals.

Lamellar structure of the spherulites was observed by SAXS. The SAXS scattering curves of the spherulites samples showed a difference among three samples (Figure 5.13). The scattering pattern of the DBRD6 spherulites did not show any peak, indicating lack of periodic lamellar structure. On the other hand, the scattering curve of the DBCN1 and DBPS2 display a shoulder a shoulder at an q value of 0.4 nm^{-1} which corresponds to a periodical distance of ~15.7 nm. The appearance of shoulder reflect differences in electron density between crystalline and amorphous lamellae (Vladimir P. Yuryev et al., 2004), corresponding high defectiveness of crystalline lamellar causing by an accumulation of amylose tie-chains acting as defects and accumulation of amylose chains oriented transversely to the lamella stack within amorphous lamellae (Dasha A. Koroteeva et al., 2007; Noda et al., 2009). Therefore, the chain was plenty dangle outside crystalline lamellae and ELC oriented transversely within amorphous lamellae could be expected.

A better characterization of nanostructure of DBCN1 spherulite was gained by fitting the desmeared SAXS curve to “paracrystalline one dimensional lamella stack model” (Figure 5.14), which was previously used to analyze scattering patterns from native starch (Vladimir P. Yuryev et al., 2004). This model provides a good fit to the SAXS curve of hydrated DBCN1 spherulites. It represents the overall structure of DBCN1 spherulites, which contains the alternating layers of crystalline and amorphous regions resembling the semicrystalline growth rings of the starch granule. However, the overall structure of spherulites and native starch could be fundamentally different. In native starch, amylopectin molecules are oriented radially

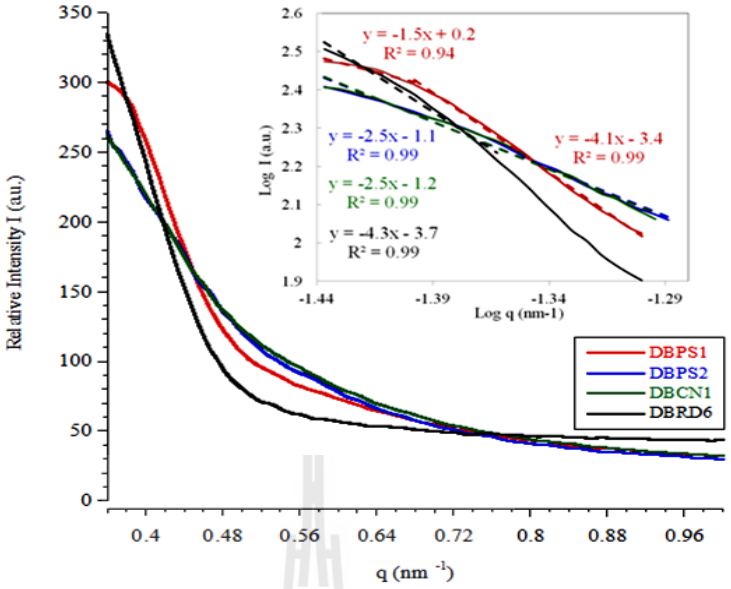

Figure 5.13 SAXS pattern of spherulites prepared from different debranched starch: DBCN1, DBPS2, DBPS1 and DBRD6. Inserted picture shows the fitting curves (dashed line) at $0.36<q<0.5$ nm^{-1} by the equation; $I \propto q^{\alpha}$, which represents fractal relationship.

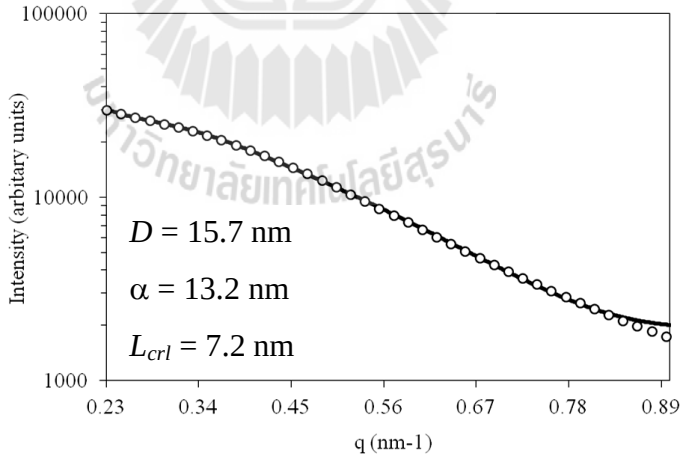

Figure 5.14 Desmeared SAXS curves of DBCN1 spherulites. Experimental data (dotted curve) and fit to the theoretical model (solid curve). Periodic Distance *(D)* was calculated from Wolf–Bragg's equation. Lamellar repeat distance (α) and thickness of crystalline lamellar (L_{crl}) was calculated from paracrystalline lamella stack model.

in the starch granule; the arrangement of amylopectin lead to the organization of alternating of the amorphous and crystalline regions (or domains) generating the concentric layers that contribute to the growth rings. On the other hand, the DBCN1 spherulite consisted of mainly of oriented linear chain from aggregation of SC and LC. Therefore, a typical crystallization pattern of linear polymers, i.e., laminated structures arranged in spherulites, could be expected. The analytical calculation of spherulite nanostructure could be based on an ideal lamella (Balta-Calleja and Vonk, 1989). From the fitting values, the DBCN1 spherulites had an average lamellar repeat distance (α) ~13.2 nm which is similar to that given by the Bragg distance, but included effects of random deviation of the period size. Additionally, the value of periodicity *D* for the DBCN1 spherulites was in accordance with the value of B-type retrograded starches from corn and HACS starches calculated using modified lamellar model (*D* of about 11-15 nm)(Shamai, Shimoni and Bianco-Peled, 2004; Zabar, Shimoni and Bianco-Peled, 2008). The thickness of crystalline lamellar was found to be L_{crl} = 7.2 nm corresponding to 3.4 turns of amylose chains of a double helix or equivalent to a length of DP 21 glucosyl residual. The chain length of crystalline lamellae was consistent with the chain length of SC which is a major component of debranched starch. Thus, the chains in the crystalline regions are certainly fractions of the total short chains. Amorphous lamellar were 6 nm thick and larger compared to the native starch, suggesting a high defectiveness in amorphous lamellae. According to the recently published data (Dasha A Koroteeva et al., 2007; Kozlov et al., 2007; Noda et al., 2009; V. P. Yuryev et al., 2004), the alteration in scattering intensity depends on the differences in the electron density between crystalline and amorphous lamellae. A decreased of electronic density between two phases reflected an

accumulation of defects both in crystalline and amorphous lamellae. In agreement with previous data, a defectiveness of spherulitic organization in the DBCN1 spherulite was probably due to an accumulation of dangling-chains and an accumulation of extra-long chains within amorphous lamellae.

According to Suzuki, Chiba and Yano (1997), the SAXS curves could be interpreted on the basis of fractals with the scattering power law: $I \propto q^{\alpha}$, where I is the scattering intensity and q is the scattering vector. The exponent α, which can take range from –1 to –4, relates to the fractal characteristics of the scattering objectives. For $-4 < \alpha < -3$, the scattering object is classified as a surface fractal. The surface fractal dimension $D_s = 6 + \alpha$. For $-3 < \alpha < -1$, the scattering source is classified as a mass fractal. The mass fractal dimension $D_m = -\alpha$.

The slop α of the straight line of DBCN1 and DBPS2 spherulites was -2.5 (inserted picture in Figure 5.13), suggesting that DBCN1 and DBPS2 spherulites were mass fractal and had self-similar structure in nature. These scattering reflected the inner structure of spherulites rather than surface structure. According to $D_m = -\alpha = 2.5$, it can be interpreted that the arrangement of mass is surface-like arrangement (Suzuki, Chiba and Yarno, 1997), which affirmed a lamellar structure within these spherulites. The α value of DBRD6 spherulite was −4, suggesting that this spherulite was surface fractal. The D_s was 2 when $\alpha = -4$, indicating that the surface of this spherulite was smooth (Suzuki et al., 1997). For DBPS1 spherulites, the α value was −1.5 and −4, suggesting a mixture of mass and surface fractal.

5.4.5 Thermal properties of spherulites by DSC

All spherulites displayed a very broad melting endotherm with a peak maximum (T_p) of 81.5-85.6 °C (Figure 5.15).). It suggests that the melting behavior

does not depend on the morphology and direction of chain within the spherulites. The endothermic transitions of all spherulites were occurred in the same range of 40 to 106 °C, suggesting that similar the chain lengths distribution within spherelulitic crystalites. The chain length affecting dissolution of the B-type crystalline was studied by Moates, Noel, Parker, & Ring (1997) and found that the dissolution temperature of amylose crystallites increased from 57 ℃ to 119 ℃ with increasing chain length from 12 to 55 glucose units. The chain lengths of all debranched starches in this study were in agreement with literature data (Moates, Noel, Parker, & Ring, 1997). It suggested that the spherulitic crystallites composed mainaly of aggregates from SC and LC. The endotherm of the DBRD6 spherulites was sharper than that of the DBCN1 spherulite which can reflects a greater structural homogeneity of the substrates for the DBCN1 and DBPS2 spherulites, while a broader of endotherm of DBCN1 and DBPS2 spherulites indicate crystalline inhomogeneity, which could arise from the disordered arrangements of the different size glucans creating crystalline defects of varying intensities within individual crystallites. (Mutungi et al., 2011). The lower onset tempeature in DBCN1 and DBPS2 spherulites may be attributed to the melting transition of gel-like material's crystalline junction zone formed from long chain amylose or ECL (Ziegler et al., 2005). This indicated that the aggregation of ECL may defect structure in crystalline phase, led to the stacked layer structure forming in such spherulites. Additionally, a slightly higher melting temperature was observed for the DBRD6 spherulites (86.0 ℃), which could be attributed to a larger crystal size as calculated by Debye–Scherrer equation.

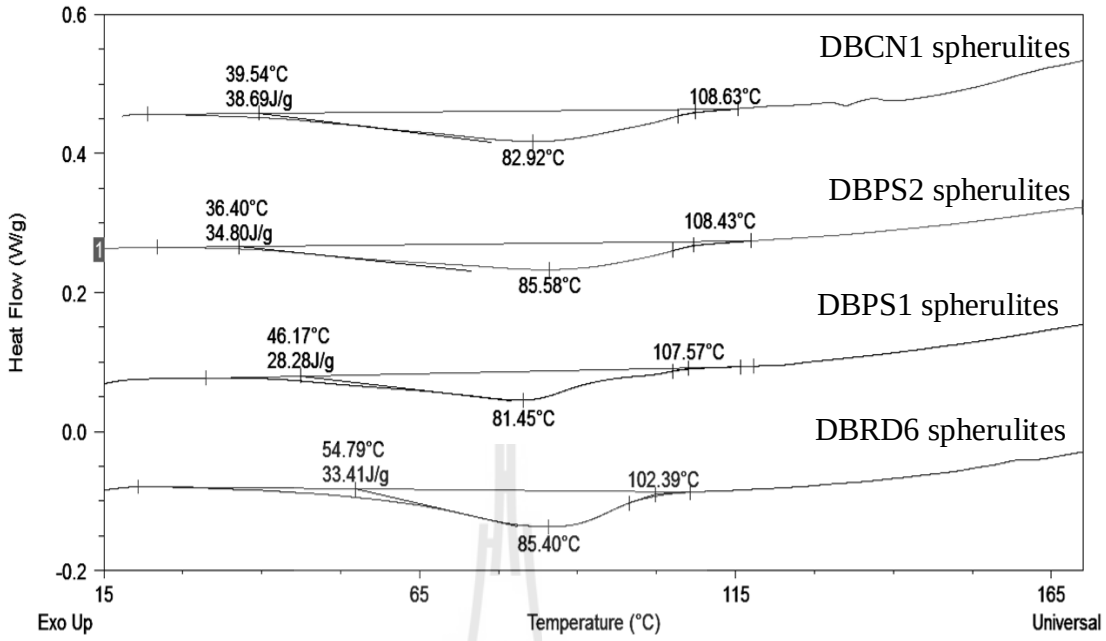

Figure 5.15 DSC melting curves of spherulites prepared from different debranched starch: DBCN1, DBPS2, DBPS1 and DBRD6.

The formation of spherulite from native starch and amylose after melting and fast quenching has been reported in the literature (Creek et al., 2006; Singh et al., 2010; Ziegler et al., 2005). The melting temperature was reported that it depended on cooling rate and starch source and concentration, which the dissolution temperature was observed in the range of 100-160 °C. The melting temperature observed in this study was lower than those of spherulites reported in literatures. However, melting temperatures of spherulites in this study were closed to B-type short-chain amylose spherulites, which has been prepared from the DP22 lintnerized starch (Ring et al., 1987) and debranched waxy maize starch (Cai et al., 2013), which were 70–90 °C in excess water conditions.

5.4.6 Enzyme susceptibility of spherulites

As shown in Table 5.2, the DBRD6 spherulites contain a very high resistant starch content (54.9%), whereas DBCN1, DBPS2 and DBPS1 spherulites contains a low RS content (18.3-22.7%). The high RS content in DBRD6 spherulites can be attributed to their large spherical size and smooth surface morphology. The DBCN1, DBPS2 and DBPS1 spherulites were less resistant, probably because there had rough surface and high porosity. The enzymatic digestibility might be related to the accessibility facilitating enzymatic attach of elementary units at the surface. In native starches, maize starch granules show the presence of pores on the granule surface that are attacked by the enzymes forming the interior channels, facilitating "inside-out" digestion from the inside to the surface of the granule (Fannon, Shull and BeMILLER, 1993; Zhang et al., 2014). On the contary, potato starch granules have smooth surfaces, lacking pores where dense surface structure limits the enzyme diffusion, and hence, the digestion takes place from the surface (exocorrosion) (Fannon, Hauber and BeMiller, 1992; Gallant, Bouchet, Buléon and Perez, 1992).

Table 5.2 RS content of spherulites

Sample	RS content (g/100g of sample)
DBCN1 spherulites	18.3 ± 0.2
DBPS2 spherulites	19.3 ± 2.2
DBPS1 spherulites	22.7 ± 3.4
DBRD6 spherulites	54.9 ± 1.0

Figure 5.16 shows the enzymatic hydrolysis profiles of these two different spherulites. The DBRD6 spherulites displayed lower digestibility than the

DBCN1 spherulites. The hydrolysis profile of the DBRD6 spherulite showed two distinct phases, whereas the hydrolysis pattern of the DBCN1 spherulite showed a linear digestive curve into three phases. In the case of the DBRD6 spherulite, the first phase was about 3 h long with a rate of 3.9%/h and a second phase was between 3 to 24 h at essentially a constant rate of 0.9%/h. For the DBCN1 spherulite, the first, second and third phases of hydrolysis were carried out from 0 to 1 h, 1 to 9 h, and 9 to 24 h with a rate of 13.5%/h, 1.8%/h and 0.3%/h, respectively. The final hydrolyzed fraction was 27.7% and 39.9% digestion for the DBRD6 and DBCN1 spherulites, respectively. It should be noted that the DBRD6 spherulites with a larger particle size, a smoother surface, and a tangentially-oriented chains were less susceptible to enzyme attack than the DBCN1 spherulites with a smaller size, a rougher surface, an imperfection of crystalline lamella and a radial organization of chains. The lower hydrolysis of the large particle in DBRD6 spherulites could be related to smaller surface to volume ratio, which may decrease the potential surface to be attached and hydrolysed by enzymes (Tester, Qi and Karkalas, 2006). In addition, rougher surface morphology observed in the DBCN1 spherulites which were higher the surface area facilitate more enzymatic digestion. According to (Veronique Planchot et al., 1997) and (Williamson et al., 1992), regardless of morphology and crystallinity, A-type spherocrystals with radial organization were more susceptible to amylolysis than those of B-type sherocrystals with tangential organization of amylose chains. It is possible that the tangential organization of the chains in spherulites was responsible for its resistance to enzymatic hydrolysis as compared to the radial organization of molecules in spherulites.

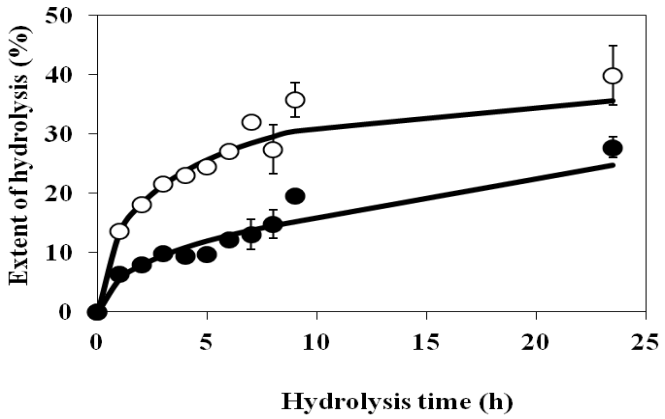

Figure 5.16 Time-resolved extent of enzymatic hydrolysis kinetics of particles crystallized from of the DBCN1 spherulites (o) and DBRD6 spherulites (•) samples

The digestion mechanism was also examined by viewing the residue left after enzyme hydrolysis under cross polarized light microscope (Figure 5.17). It was obvious that the breakdown of DBCN1 spherulites occurred more rapidly than for DBRD6 spherulites. The DBCN1 spherulites shows lower birefringence and some particles were fracture readily into small shatters along the spherulites radii after partial hydrolysis at 1 h (Figure 5.17) whereas the DBRD6 spherulites retain a large amount of visible spherical structure with strong negative birefringence (Figure 5.17). After 24h of hydrolysis in the DBCN1 spherulites, the initial spherical morphology and birefringence were completely lost and only a few fragments remained (Figure 5.17I), but the DBRD6 spherulites still exhibited particles with negative birefringence (Figure 5.17J). In agreement with Planchot, Colonna, Buléon and Gallant, 1997, a breakage of the DBCN1 spherulites into small shatters corresponded to a needle-like structures obtained from disruption of radial organization within the spherocrystal. The high susceptibility of the DBCN1 or radial spherulites could be associated with

the weak inner cohesion observed among individual crystals which facilitate enzyme to penetrate all direction to the spherulites center (Helbert et al., 1993). For the DBRD6 or tangential spherulites, the alignments of double helices in the crystalline regions was parallel to the surface of spherulite and were tightly packed at the periphery as reflected in a smoother surface (Figure 5.6), which could limits the adsorption capacity and diffusion of enzyme, a situation highly unfavorable for enzymatic digestion.

The hydrolysis curve indicates a first stage of rapid hydrolysis, corresponding to the degradation of the easier degradation fraction. The first stage of hydrolysis of the DBRD6 or spherulites could be related to hydrolysis of the non-spherulitic material, resulting in the residue left after 3 h digestion enriched in intact spherulites with strong birefringence and greater amount of perfect Maltese cross (Figure 5.17F). In the case of the DBCN1 spherulites, rapid hydrolysis at the first stage could be related to hydrolysis of the loose packed internal region (amorphous) of the spherulites, as showing discernible weak birefringence after partial hydrolysis. The rough surface of the DBCN1 spherulites might facilitate an enzymatic attachment of elementary units at the surface and penetration of amylase through surface pore (Fannon et al., 1992; Gallant et al., 1992). During the second stage, the hydrolysis rate was low. The DBRD6 spherulites were gradually hydrolyzed from the surface, where the hydrolysis of residuals appeared to be fused together due to an increased surface adhesion (Figure 5.17H and 5.17J). For the DBCN1 spherulites, the second and third stage appeared to be more extensive hydrolysis of the internal region of spherulites as a result of longer time hydrolysis, and spherulites were completely fragmented and disrupted (Figure 5.17E, 5.17G and 5.17I). Our results suggested a striking difference

on the enzymatic digestion of different spherulites. The digestion pattern of the DBRD6 spherulites was similar to B-type starches without pores, which was the side-by-side enzymatic hydrolysis pattern observed as “exo-pitting” because the enzyme begins digestion from the resistant surface; thereby the digestion proceeded in a constant slow digestion profile (Zhang, Ao and Hamaker, 2006). This is a reason that the DBRD6 or tangential spherulites with smooth surfaces are more resistant to digestion. On the other hand, the digestion pattern of DBCN1 spherulites with rough surface was almost similar to “inside-out” digestion pattern for A-type starches (Miao, Zhang, Mu and Jiang, 2011; Zhang et al., 2006). The inside-out enzymatic hydrolysis pattern is due to the presence of surface pores and interior channels, which are large enough for enzymes to enter into the starch granules. Miao et al (2011) demonstrated that starch hydrolysis began that the hydrolytic enzymes accessed to the interior of the granules via channels, and the surface pores and channels enlarge with concurrent hydrolysis from hilum region toward the outsides and eventually the granules were completely deformed and fragmented with a longer time hydrolysis. Fannon et al (1992) suggested that pores may be the site of initial enzyme attack in that these openings allow enzyme directly access to the center of granule interior. Enzymes can digest channels from selected points on the surface towards the center of the granule (endo-corrosion) by diffusion towards the surface of solid phase, adsorption, and finally catalytic reaction (Matsubara et al., 2004). This suggested that enzymatic hydrolysis of the DBCN1 or radial spherulites acted through endo-corrosion, which may be the cause of their higher digestibility. Our results suggested the relevance of particle size, surface morphology, crystal defects and chain organization for controlling the enzyme digestibility of spherulites.

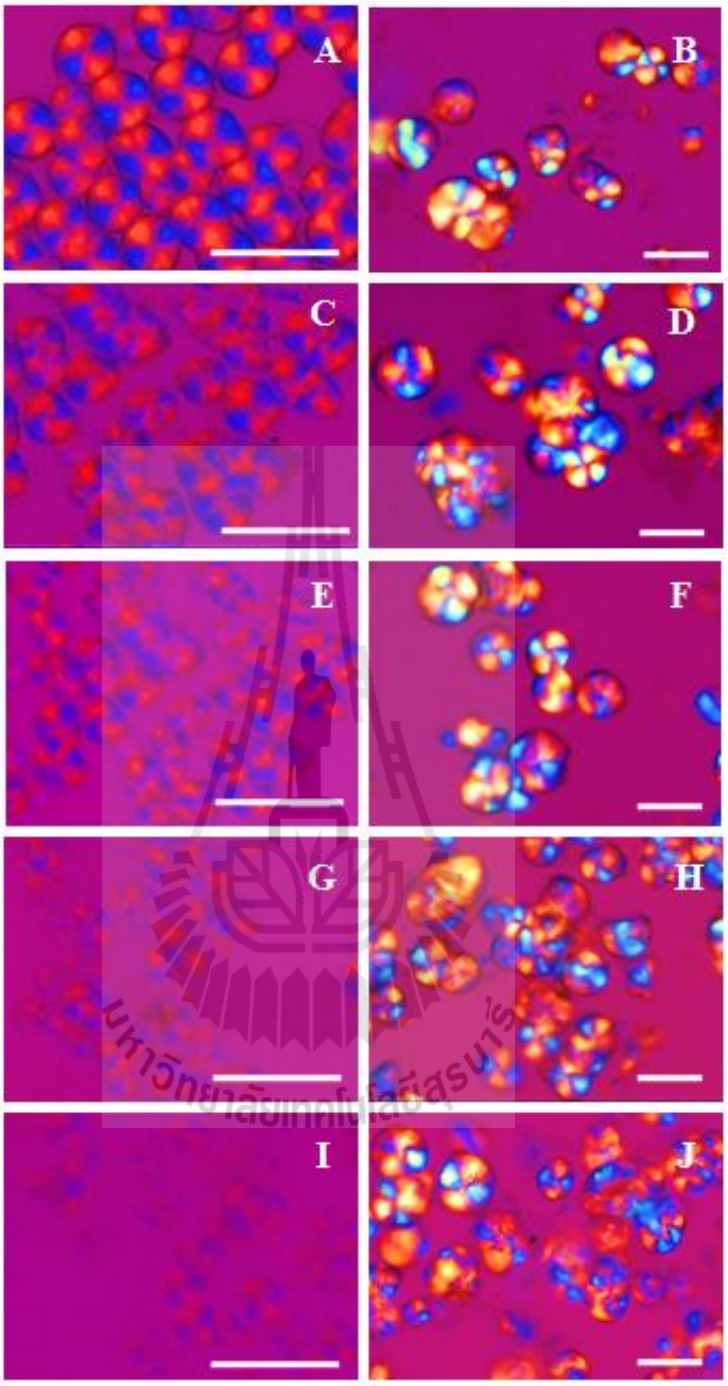

Figure 5.17 Polarized light micrographs of the hydrolyzed DBCN1 spherulites (A, C, E, G, I) and the hydrolyzed DBRD6 spherulites (B, D, F, H, J) at different digestion time: A and B, 0 h; C and D, 1 h; E and F, 3 h; H and G, 9 h; I and J, 24h. All scale bars represent 25 µm.

5.4.7 Proposed mechanism for the formation of spherulites in debranched starch aqueous solution

Spherulites generally develop from a single crystal precursor (nuclei) that were spread out in direction of growth and thus eventually became a spherical envelope (Abo el Maaty, Hosier and Bassett, 1998). It has been reported that spherulites are formed from high amylose starches, resulting from the folding of amorphous amylose to crystalline lamellae (Nordmark et al., 2002a). In our study, two different spherulites formation were obtained from crystallization of different chain length distribution.

The formation of radial spherulites was greatly affected by amylose chain length and distribution. The step-crystallization of DBCN1 suggested that the mechanism for the formation of radial spherulites might be the aggregation and stabilization of ECL amylose double helices. The ECL amylose might initiate the primary nucleation and growing in radial directions at high temperature, followed by secondary crystallization of LC and SC at low temperature which grew in the same direction (Figure 5.18). Based on the spherulitic morphology and growth rate, the radial spherulites should be fabricated from the long chain component. For the long chain system and large supercooling, the perfectly aligned and fully extended chain can form, if long chain molecules attach chain segments to the front via chain folding process to form well-defined nanoscale crystalline lamellae and develop into round spherulites (Carvalho et al., 2012). Therefore, ELC would be primary nucleated to form spherulites by the arrangement of crystalline lamellae which acted as the backbone chain of spherulites. This organization closely resembles that of the amorphous core and surrounding the hilum of granular starch (Wang, Blazek, Gilbert

and Copeland, 2012), which could be describe the organization of native starch granules in very early stages of development. According to the crystallization of Poly(ethylene succinate)/Poly(ethyl oxide) (PES/PEO) blend, PEO and PES crystallized separately with the same nucleus in the same spherulites under non-isothermal crystallization (He et al., 2007). The first component of polymer blend crystallizes while the other component is still in melting state. The melting component may be included in or rejected from the spherulite of the crystallized component (Keith and Padden, 1963). When the melt phase of second component was enfolded in the spherulites of the first component, the second component was crystallized inside the spherulites formed by the first component (He et al., 2007).

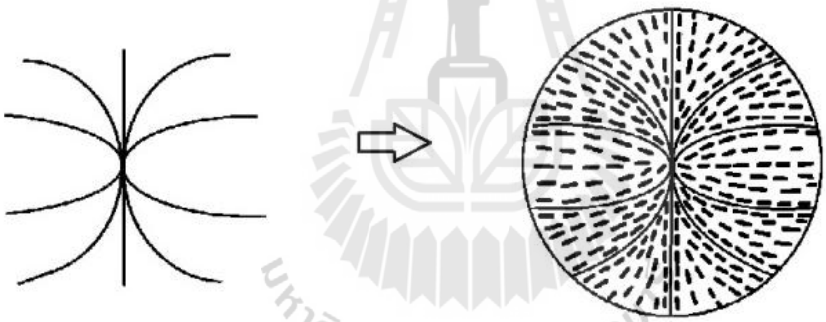

Figure 5.18 Schematic representation of the formation process of radial spherulite.

According to the crystallization into B-type crystalline in aqueous amylose solution (Jane and Robyt, 1984); (Eerlingen, Deceuninck and Delcour, 1993), here we used fringed micelles and chain folding (lamella) models to propose for molecular organization within the spherulites from debranched starches. Figure 5.19A shows a schematic model of the radial or positive spherulite of the DBCN1 spherulites that is composed of crystalline double helical regions, interspersed within amorphous regions containing dangling chains and some of extra-long chains. It could be

assumed that bundles of crystalline lamellae making up a positive spherulite were formed from chain-folded extra-long chains and fringed micelles from aggregation of shorter chains that were organized with many defects and, then growing or stacking in a radial direction from a central nucleus. For the second type of spherulite, a schematic model of tangential or negative spherulite is presented in Figure 5.19B. The negative spherulites obtained from DBRD6 are composed of aggregation of short chains in micelle structure that were arranged and grew in tangential direction. (Wang et al., 2002) observed the formation of spherulites with tangential lamellae from polystyrene. The mechanism leading to this type of spherulitic crystallization was described that several lamellar stacks are initiated and grew around a particular center. A spherical shape of lamellar-stack aggregates is apparently developed after impingement of neighboring lamellar stacks which leads to the noticable appearance of this type of spherulite. The growth of this spherulite is mainly determined by the formation of lamellar nuclei parallel to the existing lamellae at the outer surface of the spherulite.

However, to confirm that the crystalline material within spherulites has a radially oriented chain axis or tangentially oriented chain axis, additional experimentation is necessary.

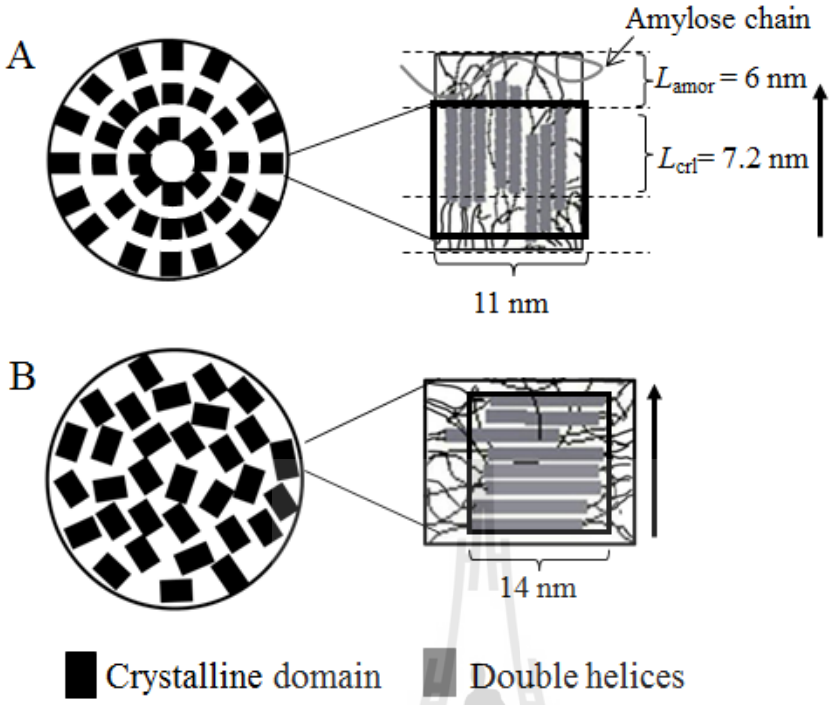

Figure 5.19 Schematic models of spherulite formation. (A) Schematic model of radial or positive spherulite of the DBCN1 spherulites. (B) Schematic model of tangential or negative spherulite of the DBRD6 spherulites. The arrows indicate the radial direction of the spherulite.

5.5 Conclusions

Ability to form spherulites and its features depended on the chain length distribution of debranched starch. Higher fraction of long linear chains promoted the formation of radial spherulites with small sphere and rough surface morphology with high porosity. In contrast, higher fraction of short linear chains led to the formation of large spherical particles with mixed morphology, dense and smooth surface and most chains were tangential orientation. The enzymatic digestibility depended on the morphological features and surface characteristics of material. The particularly dense and compact morphology of tangential-oriented spherulites limited the accessibility of

α-amylase, in contrast to rough and loose surface morphology of the radial-oriented spherulites, which in turn provided more susceptible to enzymatic hydrolysis. This knowledge could be used to produce starch-based novel biomaterials from starch spherulites with controlling enzymatic digestibility. Further research is needed to better understand the spherulite crystallization of each chain length fraction and the internal structure of debranched starch spherulites.

5.6 References

Abo el Maaty, M. I., Hosier, I. L., and Bassett, D. C. (1998). A Unified Context for Spherulitic Growth in Polymers. **Macromolecules.** 31(1): 153-157.

Ashman, P. C. and Booth, C. (1975). Crystallinity and fusion of ethylene oxide/propylene oxide block copolymers: 1. Type PE copolymers. **Polymer.** 16(12): 889-896.

Balta-Calleja, F. and Vonk, C. (1989). **X-ray scattering of synthetic polymers.** Elsevier Amsterdam.

Bassett, D. C. (2003). Polymer Spherulites: A Modern Assessment. **Journal of Macromolecular Science, Part B.** 42(2): 227-256.

Buléon, A., Véronèse, G., and Putaux, J. (2007). Self-Association and Crystallization of Amylose. **Australian Journal of Chemistry.** 60(10): 706-718.

Cai, L. and Shi, Y-C. (2013). Self-Assembly of Short Linear Chains to A- and B-Type Starch Spherulites and Their Enzymatic Digestibility. **Journal of Agricultural and Food Chemistry.** 61(45): 10787-10797.

Cairns, P., Bogracheva, T. Y., Ring, S., Hedley, C., and Morris, V. (1997). Determination of the polymorphic composition of smooth pea starch.

Carbohydrate Polymers. 32(3): 275-282.

Carvalho, J. L., Cormier, S. L., Lin, N., and Dalnoki-Veress, K. (2012). Crystal Growth Rate in a Blend of Long and Short Polymer Chains. **Macromolecules.** 45(3): 1688-1691.

Conde-Petit, B., Handschin, S., Heinemann, C., and Escher, F. (2007). Self-Assembly of Starch Spherulites as Induced by Inclusion Complexation with Small Ligands. In E. Dickinson and M. E. Leser (eds.). **Food colloids: Self-assembly and material science** (pp 117-126). Cambridge, RSC publishing.

Creek, J. A., Ziegler, G. R., and Runt, J. (2006). Amylose crystallization from concentrated aqueous solution. **Biomacromolecules.** 7(3): 761-770.

Davies, T., Miller, D. C., and Procter, A. A. (1980). Inclusion complexes of free fatty acids with amylose. **Starch-Stärke.** 32(5): 149-158.

Eerlingen, R., Deceuninck, M., and Delcour, J. (1993). Enzyme-Resistant Starch. II. Influence of Amylose Chain Length on Resistant Starch Formation. **Cereal Chemistry.** 70(3): 345-350.

Fannon, J. E., Hauber, R. J., and BeMiller, J. N. (1992). Surface pores of starch granules. **Cereal Chemistry.** 69(3): 284-288.

Fannon, J. E., Shull, J. M., and BeMiller, J. N. (1993). Interior channels of starch granules. **Cereal chemistry.** 70(5): 611-613.

Fanta, G. F., Felker, F. C., and Shogren, R. L. (2002). Formation of crystalline aggregates in slowly-cooled starch solutions prepared by steam jet cooking. **Carbohydrate Polymers.** 48(2): 161-170.

Fanta, G. F., Felker, F. C., Shogren, R. L., and Salch, J. H. (2006). Effect of fatty acid structure on the morphology of spherulites formed from jet cooked mixtures of

fatty acids and defatted cornstarch. **Carbohydrate Polymers.** 66(1): 60-70.

Frost, K., Kaminski, D., Kirwan, G., Lascaris, E., and Shanks, R. (2009). Crystallinity and structure of starch using wide angle X-ray scattering. **Carbohydrate Polymers.** 78(3): 543-548.

Gallant, D., Bouchet, B., Buléon, A., and Perez, S. (1992). Physical characteristics of starch granules and susceptibility to enzymatic degradation. **European Journal of Clinical Nutrition.** 46(Suppl. 2): S3-S16.

He, S. and Liu, J. (2007). Crystallization and Morphology Development of Binary Crystalline Poly(ethylene succinate)/Poly(ethylene oxide) (PES/PEO) Blend with Non-Isothermal Crystallization. **Polymer Journal.** 39(6): 537-542.

Heinemann, C., Escher, F., and Conde-Petit, B. (2003). Structural features of starch–lactone inclusion complexes in aqueous potato starch dispersions: the role of amylose and amylopectin. **Carbohydrate Polymers.** 51(2): 159-168.

Helbert, W., Chanzy, H., Planchot, V., Buléon, A., and Colonna, P. (1993). Morphological and structural features of amylose spherocrystals of A-type. **International Journal of Biological Macromolecules.** 15(3): 183-187.

Imberty, A. and Perez, S. (1988). A revisit to the three-dimensional structure of B-type starch. **Biopolymers.** 27(8): 1205-1221.

Jane, J-L. and Robyt, J. F. (1984). Structure studies of amylose-V complexes and retro-graded amylose by action of alpha amylases, and a new method for preparing amylodextrins. **Carbohydrate Research.** 132(1): 105-118.

Keith, H. and Padden, F. (1963). A phenomenological theory of spherulitic crystallization. **Journal of Applied Physics.** 34(8): 2409-2421.

Koroteeva, D. A., et al. (2007). Structural and thermodynamic properties of rice

starches with different genetic background: Part 2. Defectiveness of different supramolecular structures in starch granules. **International Journal of Biological Macromolecules.** 41(5): 534-547.

Koroteeva, D. A., et al. (2007). Structural and thermodynamic properties of rice starches with different genetic background: Part 1. Differentiation of amylopectin and amylose defects. **International Journal of Biological Macromolecules.** 41(4): 391-403.

Kozlov, S. S., et al. (2007). Structure of starches extracted from near-isogenic wheat lines - Part II. Molecular organization of amylopectin clusters. **Journal of Thermal Analysis and Calorimetry.** 87(2): 575-584.

Lopez-Rubio, A., Flanagan, B. M., Gilbert, E. P., and Gidley, M. J. (2008). A novel approach for calculating starch crystallinity and its correlation with double helix content: A combined XRD and NMR study. **Biopolymers.** 89(9): 761-768.

Ma, U. V. L., Floros, J. D., and Ziegler, G. R. (2011). Effect of starch fractions on spherulite formation and microstructure. **Carbohydrate Polymers.** 83(4): 1757-1765.

Magill, J. H. (2001). Review Spherulites: A personal perspective. **Journal of Materials Science.** 36(13): 3143-3164.

Matsubara, T., et al. (2004). Degradation of raw starch granules by alpha-amylase purified from culture of Aspergillus awamori KT-11. **Journal of biochemistry and molecular biology.** 37(4): 422-428.

McCleary, B. V. and Monaghan, D. A. (2002). Measurement of resistant starch. **Journal of AOAC international.** 85(3): 665-675.

Miao, M., Zhang, T., Mu, W., and Jiang, B. (2011). Structural characterizations of waxy maize starch residue following in vitro pancreatin and amyloglucosidase synergistic hydrolysis. **Food Hydrocolloids.** 25(2): 214-220.

Murayama, E. (2002). Optical properties of ringed spherulites. **Polymer Preprints Japan.** 51: 460-462.

Mutungi, C., et al. (2011). Long- and short-range structural changes of recrystallised cassava starch subjected to in vitro digestion. **Food Hydrocolloids.** 25(3): 477-485.

Nishiyama, Y., Putaux, J.-l., Montesanti, N., Hazemann, J-L., and Rochas, C. (2009). B→A allomorphic transition in native starch and amylose spherocrystals monitored by in situ synchrotron X-ray diffraction. **Biomacromolecules.** 11(1): 76-87.

Noda, T., et al. (2009). Origin of defects in assembled supramolecular structures of sweet potato starches with different amylopectin chain-length distribution. **Carbohydrate Polymers.** 76(3): 400-409.

Nordmark, T. S. and Ziegler, G. R. (2002a). Spherulitic crystallization of gelatinized maize starch and its fractions. **Carbohydrate Polymers.** 49(4): 439-448.

Nordmark, T. S. and Ziegler, G. R. (2002b). Structural features of non-granular spherulitic maize starch. **Carbohydrate Research.** 337(16): 1467-1475.

Planchot, V., Colonna, P., and Buléon, A. (1997). Enzymatic hydrolysis of α-glucan crystallites. **Carbohydrate research.** 298(4): 319-326.

Planchot, V., Colonna, P., Buléon, A., and Gallant, D. (1997). Amylolysis of Starch granules and alpha-glucanes crystallites. In P. J. Frazier, P. Richmond and A.

M. Donald (eds.), **Starch Structure and Functionality** (pp. 141-151). Royal Society of Chemistry.

Planchot, V., Colonna, P., and Saulnier, L. (1997). Dosage des glucides et des amylases. In B. Godon,W. Loisel (eds), **Guide Pratique d′ Analyses dans les Industries des Cereales** (pp 341-398). Paris, Lavoisier.

Pohu, A., Planchot, V., Putaux, J., Colonna, P., and Buléon, A. (2004). Split crystallization during debranching of maltodextrins at high concentration by isoamylase. **Biomacromolecules.** 5(5): 1792-1798.

Ring, S., Miles, M., Morris, V., Turner, R., and Colonna, P. (1987). Spherulitic crystallization of short chain amylose. **International Journal of Biological Macromolecules.** 9(3): 158-160.

Roldan, L. G. (1966). Diffraction of X-rays by chain molecules. **Journal of Polymer Science Part A-1: Polymer Chemistry.** 4(11): 2909-2909.

Schoch, T. J. (1942). Fractionation of starch by selective precipitation with butanol. **Journal of the American Chemical Society.** 64(12): 2957-2961.

Shamai, K., Shimoni, E., and Bianco-Peled, H. (2004). Small angle X-ray scattering of resistant starch type III. **Biomacromolecules.** 5(1): 219-223.

Singh, J., Lelane, C., Stewart, R. B., and Singh, H. Formation of starch spherulites: Role of amylose content and thermal events. **Food Chemistry.** 121(4): 980-989.

Singh, J., Lelane, C., Stewart, R. B., and Singh, H. (2010). Formation of starch spherulites: Role of amylose content and thermal events. **Food Chemistry.** 121(4): 980-989.

Soille, P. (2003). **Morphological image analysis: principles and applications.** New York, Springer-Verlag Inc.

Soontaranon, S. and Rugmai, S. (2012). Small angle X-ray scattering at Siam photon laboratory. **Chinese Journal of Physics.** 50(2): 204-210.

Suzuki, T., Chiba, A., and Yarno, T. (1997). Interpretation of small angle X-ray scattering from starch on the basis of fractals. **Carbohydrate Polymers.** 34(4): 357-363.

Tester, R. F., Qi, X., and Karkalas, J. (2006). Hydrolysis of native starches with amylases. **Animal Feed Science and Technology.** 130(1–2): 39-54.

Wang, C., Chen, C-C., Cheng, Y-W., Liao, W-P., and Wang, M-L. (2002). Simultaneous presence of positive and negative spherulites in syndiotactic polystyrene and its blends with atactic polystyrene. **Polymer.** 43(19): 5271-5279.

Wang, S., Blazek, J., Gilbert, E., and Copeland, L. (2012). New insights on the mechanism of acid degradation of pea starch. **Carbohydrate Polymers.** 87(3): 1941-1949.

Williamson, G., et al. (1992). Hydrolysis of A-and B-type crystalline polymorphs of starch by α-amylase, β-amylase and glucoamylase. **Carbohydrate Polymers.** 18(3): 179-187.

Yoshioka, T., Fujimura, T., Manabe, N., Yokota, Y., and Tsuji, M. (2007). Morphological study on three kinds of two-dimensional spherulites of poly(butylene terephthalate) (PBT). **Polymer.** 48(19): 5780-5787.

Yuryev, V. P., et al. (2004). Structural parameters of amylopectin clusters and semi-crystalline growth rings in wheat starches with different amylose content. **Carbohydrate Research.** 339(16): 2683-2691.

Yuryev, V. P., et al. (2004). Structural parameters of amylopectin clusters and semi-crystalline growth rings in wheat starches with different amylose content. **Carbohydrate Research.** 339(16): 2683-2691.

Zabar, S., Shimoni, E., and Bianco-Peled, H. (2008). Development of Nanostructure in Resistant Starch Type III during Thermal Treatments and Cycling. **Macromolecular Bioscience.** 8(2): 163-170.

Zabar, S., Shimoni, E., and Bianco-Peled, H. (2008). Development of nanostructure in resistant starch type III during thermal treatments and cycling. **Macromolecular Bioscience.** 8(2): 163-170.

Zhang, B., et al. (2014). Freeze Drying Changes the Structure and Digestibility of B-Polymorphic Starches. **Journal of Agricultural and Food Chemistry**.

Zhang, G., Ao, Z., and Hamaker, B. R. (2006). Slow Digestion Property of Native Cereal Starches. **Biomacromolecules.** 7(11): 3252-3258.

Ziegler, G. R., Creek, J. A., and Runt, J. (2005). Spherulitic crystallization in starch as a model for starch granule initiation. **Biomacromolecules.** 6(3): 1547-1554.

Ziegler, G. R., Nordmark, T. S., and Woodling, S. E. (2003). Spherulitic crystallization of starch: influence of botanical origin and extent of thermal treatment. **Food Hydrocolloids.** 17(4): 487-494.

CHAPTER VI

SUMMARY

The formation of resistant starch was affected by many structural factors. The RS yield of debranched starch was not influenced by different chain distributions of waxy rice and low-amylose rice starch, but it could be manipulated by applying treatment conditions (temperature, solid concentration and hydrothermal treatment). The highest thermo-stable RS can be obtained when crystallization occurs with a high concentration of essentially short chains and at a high temperature, resulting from a favored crystallization rate (more nucleation and more propagation). Hydrothermal treatments, both annealing and HMT, disrupted pre-exist crystallites, induced the formation of new crystallites and changed the orientation of crystallites, thus improving the perfection of the crystallites, which enhanced RS formation. The initial imperfection of the packing of double helices within crystallites were extremely important factors that contributed to further perfection of crystallites and the improvement of the melting temperature, consequently enhancing RS resistance against thermal processes. In addition, this knowledge can be applied to optimize RS-containing products with varying degrees of resistance to enzyme digestion based on the recrystallization conditions.

The starch gel was single phase system containing amorphous polymer chains and rich in water. The crystalline domains were developed and embedded in a polymer solution with disorder chain segment during crystallization. The domains obtain the

function of junction zone of starch chains. Change in long range ordering of bound water in gel was related to phase changes from gel to crystalline state, which was depend on chain distribution, gel concentration, debranching and incubation temperature. Waxy rice starch would not be crystallized during debranching while normal rice starch crystallized into B-form or A-form, depending on the gel concentration. The formation of double helical structure during subsequent incubation was, consequently, dependent of the pre-exits crystallites of debranched starch. By crystallization kinetics, the values of the kinetic exponent *n* suggest one-dimension growth in rod-like growth from sporadic for ELC occurred during debranching, while one-dimension growth in rod-like growth from instantaneous nuclei was found for LC and SC during storage at low temperature and two-dimension growth in disc-like growth from instantaneous nuclei were observed for LC and SC during storage at high temperature. Debranched starch crystallization took placed by two kinetically mechanism: rapid time-independence crystallization of ELC and slow time-dependent crystallization of linear short chains. Slow time-dependent crystallization led to low of crystallinity when the samples were stored at the low temperature. In addition, the slowest crystallization kinetics upon high temperature incubation led to the slowest growing of crystal which resulted in a development of A-type with high crystallinity. The fundamental information and insight on the crystallization of debranched rice starch that this study provided open the possibility for future investigations of the effects of crystallization at various conditions on debranched starch and the applications of debranched starch for preparation in pharmaceutical and nutraceutical products.

Spherulitic crystallization was greatly affected by the chain length distribution of debranched starches. Debranched starch containing extra-long chain as amylose could form the radial or positive spherulites with small spherical and rough surface morphology. However, lack of extra-long chains components resulted in the formation of tangential or negative spherulite with large spherical, dense and smooth surface morphology. Enzymatic digestibility depended on the morphological features and surface characteristics of material. The particularly dense and smooth surface morphology of tangential-oriented spherulites limited the accessibility to α-amylase, in contrast to a high porosity and rough surface morphology of the radial-oriented spherulites, which in turn provide more susceptible to enzymatic hydrolysis. This knowledge could be used to produce starch-based novel biomaterials from starch spherulites with controlling enzymatic digestibility. Further research is needed to better understand the spherulite crystallization of each chain length fraction and the internal structure of debranched starch spherulites.

APPENDIX

Appendix A

Preparation and structural characterization of debranched starches from four rice cultivars

A.1 Introduction

Starch consists mainly of two carbohydrates, amylose and amylopectin, that differ in molecular size and degree of branching. The molecular structure of amylose is essentially linear with a few relatively long branches (less than 1%). In contrast, amylopectin is highly branched macromolecule compose of linear glucan chains linked by 5–6% α(1, 6) bonds (Buléon, Colonna, Planchot and Ball, 1998). There is more amylopectin than amylose in normal starch granules. Chain length and branching characteristics are major parameters in determining functional and physical properties of amylopectin (Hoover, 2001). Since natural starch generally has a granular structure, most use of starch requires the disruption or modification of the starch granules through chemical, enzymatic and/or hydrothermal treatments (Buleon & Colonna, 2007; Singh, Kaur & McCarthy, 2007). Enzymatic debranching using pullulanase or isoamylase has been applied to produce linear starch chains, providing for more mobility of chains and ordered alignment; thus, the chains aggregate into perfectly crystalline structures (Cai, Shi, Rong and Hsiao, 2010; Ozturk, Koksel, Kahraman and Ng, 2009). The properties of debranched products are dependent on the chain length distribution, the degree of debranching and the debranching conditions. Through the use of debranching enzymes, followed by

size exclusion chromatography, chain length distribution of amylose and amylopectin can be obtained. In order to prepare the debranched starch, isoamylase was used in this study. The molecular structure including molecular weight and chain length distribution were analyzed using high-performance, size-exclusion chromatography (HPSEC) or high-performance, anion-exchange chromatography (HPAEC). Structural characteristics of debranched starch that prepared in high concentration were examined.

A.2 Materials and methods

A.2.1 Materials

Rice grain from four rice varieties: waxy rice (WxRD6) and normal rice starch, Phitsanulok1 (PS1), Phitsanulok2 (PS2) and Chainat1 (CN1) was obtained from Udonthani, Phitsanulok and Chainat Rice Research Center under Bureau of Rice Research and Development (BRRD, Thailand). Isoamylase from Pseudomonas amyloderamosa (glycogen 6-glucanohydrolase; EC3.2.1.68) with an activity of 1.2×10^3 isoamylase activity unit (IAU)/mL were purchased from Megazyme International Ireland Limited, Ireland. The enzyme activity was determined by incubation the enzyme with soluble waxy rice starch as a substrate at 50 ºC, pH 4.5, for 15 min and reducing sugar content was measured using the Nelson/Somogyi reducing sugar procedure (Somogyi, 1952). One IAU is defined as the amount of isoamylase that liberates 1 μmol of glucose in 1 min under the condition of the isoamylase activity.

A.2.2 Starch extraction

Rice grains were ground using wet milling process and air-dried using hot air oven at 50 °C for 6 h. Then, rice starches were extracted using sodium chloride,

ethanol and sodium hydroxide solution as described by Ju, Hettiarachchy and Rath (2001). The starches were extracted sequentially by agitation with 0.25% NaCl for 1h, 95% ethanol for 1 h and then 0.25% NaOH for 16 h. The resulting slurry was centrifuged using basket centrifuge and washed thoroughly by distilled water. This was followed by addition of distilled water to wash the pellets. This centrifugation step was repeated until the supernatant was almost colorless and their pH was neutral. The recovered starch was air-dried at 50 °C overnight and ground and sieved through a 120 mesh screen. Starches were stored in an air tight container under dry conditions.

A.2.3 determination of amylose content

Amylose contents were determined by three different ways: differential scanning calorimetry (DSC) (Ceballos et al., 2007, 2008), colorimetric method with iodine (Juliano, 1971) and determination of iodine binding capacity (IBC) (Pérez et al., 2011). The native starches were pretreated with dimethyl sulfoside as described by Rolland-Sabaté, Colonna, Potocki-Véronèse, Monsan, and Planchot (2004) before analysis. The granular starch (0.5 g) was first dissolved in 95% dimethyl sulfoside (DMSO) (20 mL) with magnetic stirring for 3 days at room temperature. The sample was then precipitated with cold 95% ethanol (200 mL) and stored overnight at 4 °C with agitation. The precipitate was separated by centrifugation at 9000 rpm for 20 min (3 times with 60 mL 95% ethalnol) and finally filtered over a glass filter (G4) and washed successively with acetone. The precipitate was air-dried under the hood to eliminate the solvents until the weight was stable and kept in air tight container with SORBSIL® CHAMELEON® Silica Gel (OKER-CHEMIE GMBH, *Silica Gel* Indicating Type, Germany).

A.2.3.1 Colorimetric amylose determination

Starch (100 mg db) or pure potato amylose (40 mg db) or pure potato amylopectin (40 mg db) were suspended in 1 mL 95% ethanol and then 9 mL of 1M NaOH was added to dispersed the sample and stirred with magnetic stirring until the sample solution was clear and free of lumps. The solution was made up volume to 100 mL in volumetric flask. An aliquot of 0.5 mL of solution was taken out and 9.2 mL of DI water was added, followed by 0.1 mL of 1 M acetic acid and then 0.2 mL of 0.2% iodine solution (2 g of potassium iodide and 0.2 g of iodine adjusted to 100 mL with DI water) were added. The solution was allowed to stand for 30 min min at ambient temperature prior to absorbance measurements at 620 nm. Standard curve was plotted for mixtures of pure amylose and amylopectin from potato starch. Amylose content was calculated from the standard curve.

Standard mixture of pure amylose and amylopectin

Standard mixture	**Content and concentration**					
Amylose (ml)	0	0.1	0.2	0.3	0.4	0.5
Amylopectin (ml)	0.5	0.4	0.3	0.2	0.1	0
%Amylose	0	20	40	60	80	100
%Amylose (g/100 g starch)	0	8	16	24	32	40

A.2.3.2 Amperometric amylose determination

Amylose content was measured using an amperometric titration method at 25 °C, using Mettler toledo DL53 titrator (Mettler-Toledo) with pure potato amylose as a reference standard for iodine biding capacity (IBC). Pretreated starch (25 mg) or pure potato amylose (5 mg) were solubilized in 5 mL of 1M potassium hydroxide (KOH) with magnetic stirring for 2 days at 4 °C. The resulting solution (1

mL) was transferred to sample container and 2 mL of 1 N HCl was added, followed by 1 mL of 0.4 N KI and then 15 mL of DI water. The sample container3 was maintained at 25 °C and the mixture was stirred at constant rate. An assembly carrying the electrode and the burette tip was then lowered into the solution. Under constant stirring, the mixture was then titrated continuously at 0.02 mL/second of 0.005 N KIO_3 for amylose containing starch or 0.0005 N KIO_3 for waxy starch until an amperometric potential of 10 μA or an added volume of 5 mL was reached. The titration was monitored by measuring the electric current with the use of dual-pin platinum electrodes (DM142). The titration curve shows a first linear part where iodine bind within the linear chains. When the polymer is saturated with iodine, an inflection point appears. Then, the second linear part corresponds to in the increase of free iodine within the solution. The total iodine bound up to the inflection point can be calculated by determining the intersection point of these two linear equations. The IBC represents the amount of iodine bound per 100 mg of polymer. The carbohydrate concentration was determined in an aliquot of staring solution by the sulphuric acid-orcinol colorimetric method (Planchot et al., 1996). The amylose content was calculated by the ratio of the IBC starch to that of the IBC reference amylose. An aliquot of final solution was taken to checked the wavelength at maximum absorption of amylose iodine complex (λ_{max}) using the spectrophotometer, recorded in the 450 to 750 nm.

A.2.3.3 Calorimetric amylose determination

Calorimetric determination of amylose content was performed using a TA Instrument DSC-Q100 (TA Instruments, DE, USA) equipped with intracooler. Pretrated starch (4 mg) or pure potato amylose (4 mg) was weighed in a

high pressure stainless steel pan (60 µL) and then 20 µL of 4% of L-a-lysophosphatidylcholine (LPC) was directly added and the pan was hermetically sealed. The sample pan and the reference pan (20 µL of DI water) were heated from 25 °C to 165 °C at a rate of 3 °C/min, held for 2 min at 165 °C and cooled to 25 °C at 10 °C/min, held for 2 min at 25 °C and reheated from 25 °C to 140 °C at 3 °C/ min, held for 2 min at 140 °C. The enthalpy of amylose-LPC complex fusion was of each sample were determined on the thermogram. The amylose content as a percentage was calculated using the equation below:

$$\%\text{amylose} = 100 \times \Delta H \text{ sample} / \Delta H \text{ amylose}$$

where ΔH sample: Enthalpy change of the amylose-LPC complex fusion in starch sample (J/g dry matter) and ΔH amylose: Enthalpy change of the amylose-LPC complex in pure potato amylose (J/g dry matter). The analysis was performed in duplicate, and the mean values were calculated.

A.2.4 Preparation of debranched starch in high concentration

Starches (15 g, dry basis, db) were mixed with sodium acetate buffer (0.05 M, pH 4.5) to obtain 10 and 21% (w/w) solid concentrations. Their slurries were gelatinized in shaking water bath using a multi-step process: heating at 60 °C for 10 min, 85 °C for 20 min and at 99 °C for 1 h. The pastes were cooled to 50 °C, and isoamylase (5 IAU/ g of dry starch) was added and maintained at 50 °C for 24 h with glass bead shaking. After 24 h of debranching, samples were taken off and the remaining suspension was freeze-dried for analysis. The freeze dried samples were ground and sieved through a 120 mesh screen.

A.2.5 Molecular analysis

Immediately after 24 h of debranching, debranched starch suspension (5 mL) was taken off and mixed with 3 mL of 95% DMSO and then heated at 90 °C for 15 min in order to inactivate enzyme and homogenize the sample. The homogenized solution was determined the reducing sugar (Somogyi, 1952) and total sugar (Dubois et al, 1956) to calculate degree of hydrolysis (DH). The residual debranched products were frozen with liquid nitrogen and liquid nitrogen frozen products were stored at -40 °C before freeze-drying. The freeze-dried debranched starches were analyzed beta-amylolysis limit according procedure (Mutungi, Rost, Onyango, Jaros and Rohm, 2009).

Molecular weight (MW) and chain length distribution of debranched starches were analyzed using high-performance size-exclusion chromatography coupled to multiangle laser light scattering and differential refractive index detection (HPSEC-MALLS-DRI) and high-performance anion exchange chromatography with pulsed amperometric detector system (HPAEC-PAD). The freeze-dried debranched starches (50 mg) were solubilized in 1 M KOH (500 μL) at 4 °C for 2 days under gentle magnetic stirring and subsequently diluted with 4.5 mL of deionized water (DI water). The resulting solution was neutralized by adding 5 mL of 0.1 M HCl and then filtered through a 0.2 and 0.45-μm filter prior to injection into HPAEC-PAD and HPSEC-MALLS-DRI, respectively. HPAEC-PAD and HPESC-MALLS-DRI profile were compared before and after debranching again by Isoamylase.

Isoamylase Debranching. The freeze-dried debranched samples (50 mg) were solubilized in 1M KOH (500μL) during 2 days at 4 °C under gentle magnetic stirring and subsequently diluted with 4.5 mL of DI water. Resulting solution were

neutralized by adding 5 mL of of 0.1 M HCl and then filtered through 5 μL Durapore^{TM} membranes (Millipore, Bedford, MA, USA). The filtrated solution (4 ml) were debranched by adding 60 μL of Sigma Isoamylase solution (EC 3.2.1.68, I5284) in 0.5 M NaOAc buffer pH 3.6 with containing 0.1% BSA and 0.02% NaN_3; and incubating 24 h at 40 °C in a water bath. The carbohydrate concentrations were also determined in an aliquot of staring and filtered solution by the sulphuric acid-orcinol colorimetric method (Planchot et al., 1996).

A.2.5.1 HPSEC-MALLS-DRI Analysis

The equipment was the same as previously described (Pohu, Planchot, Putaux, Colonna and Buleon, 2004). The SEC columns used were three HemaBio (1000, 100 and 40) (250 mm × 8 mm) from Sopares (Gentilly, France) coupled to a HemaBio guard column (Sopares, Gentilly, France). The precolumn and column were maintained at 40 °C using a Crococil temperature control system from Cluzeau (Bordeaux, France). The two-online detectors were a Dawn DSP-F MALLS instrument fitted with a K5 flow cell and a He-Ne laser (λ=658 nm) (Wyatt Technology Corporation, Santa Barbara, CA) and an ERC-7515A refractometer (Erma, Tokyo, Japan). Before the analysis, the mobile phase (Millipore water containing 0.1 N KOH) was carefully degassed and filtered through a Duropore GV (0.2 μm) membrane and eluted at a flow rate of 0.4 mL min^{-1}.

For data processing, the number and weight average molar masses ($\bar{M}_n = \sum c_i / \sum \frac{C_i}{M_i}$ and $\bar{M}_w = \sum c_i M_i / \sum c_i$ respectively) and the polydispersity index ($P = \bar{M}_w / \bar{M}_n$) were established using ASTRA software from Wyatt Technology Corporation, USA (version astra 6.1.1 for Windows). The quantities c_i

and M_i were obtained after processing the light scattering (LS) and DRI profiles. The refractive index increment *(dn/dc)* used for all the calculations was 0.146 mL g^{-1}. Normalization of photodiodes was obtained using a low molar mass pullulan standard (P20).

A.2.5.2 HPAEC-PAD Analysis

Chain length distribution was determined using HPAEC-PAD before and after isoamylase debranching. Sample were injected into a CarboPac PA-200 anion exchanger column (3 mm × 250 mm, P/N 062896) couple to a CarboPac PA-200 guard column (3 mm × 50 mm, P/N 062895). The acetate gradient system included three eluents: 150 mM NaOH (eluent A) and 150 mM NaOH containing 1 M NaOAc (eluent B). The flow rate was 0.5 min/mL. The eluent gradient was (i) 0-5 min with linear gradient from 10% to 12.5% eluent B and (ii) 5-10 min with a second linear gradient from 12.5% to 15% eluent B, (iii) 10-15 min with a third linear gradient from 15% to 17.5% eluent B, (iv) 15-20 min with a fourth linear gradient from 17.5% to 20% eluent B, (v) 20-30 min with a fifth linear gradient from 20% to 25% eluent B, (vi) 30-40 min with a sixth linear gradient from 25% to 30% eluent B, (vii) 40-50 min with a seventh linear gradient from 30% to 34% eluent B, (viii) 50-60 min with a linear gradient from 34% to 38% eluent B, (ix) 60-65 min with a linear gradient from 38% to 40% eluent B, (x) 65-80 min with 60% eluent A and 40% eluent B, and finally (xi) 80-85 min with a linear gradient from 40% to 10% eluent B and 85-115 min with 90% eluent A and 10% eluent B. As in HPAEC-PAD, response coefficients decreased with increasing DP, % area of long chain are not representative of the exact weight fraction of each DP.

A.3 Results and discussions

A.3.1 Amylose content

Altogether 4 rice varieties were used in this study and were grown at different locations in Thailand. These rice varieties were classified into three groups according to the amylose content: low, intermediate and high amylose content. Starch amylose contents ranged from 0% in waxy starch (RD6) to 30-34% high-amylose rice varieties (Chainat1, CN1), while amylose content of low-amylose rice varieties (Phitsanulok1, PS1) was 12-17% and 23-30% for intermediate-amylose rice varieties (Phitsanulok2, PS2). Amylose contents in rice starches were in agreement with those determined by (D. A. Koroteeva et al., 2007). The values obtained using DSC measurements were equivalent with the values obtained using IBC. The values of 30% amylose are the highest reported in the literature for rice starches (Ahmed, Maekawa, Tetlow, Maekawa and Tetlow, 2008; Dasha A. Koroteeva et al., 2007; Lawal et al.). λ_{max} values ranged from 534 nm (waxy rice, RD6) to 591-604 nm (rice starch containing amylose) (Table 1). λ_{max} values are influenced by the ratio of amylose to amylopectin.

Table A.1 Amylose content of different rice varieties

Amylose content*	**RD6**	**PS1**	**PS2**	**CN1**
Colorimetric amylose (%)	0	17.6 ± 0.3	23.2 ± 0.5	33.9 ± 1.6
Amperometric amylose (%)	0	12.6 ± 0.2	26.0 ± 0.3	29.6 ± 0.1
DSC amylose (%)	0	17.5 ± 0.2	30.3 ± 0.2	34.06 ± 0.6
λ_{max} (*n*m)	534	591	602	604

A.3.2 Degree of hydrolysis and beta-amylolysis limit of debranched starches

Table A.3.1 shows degree of hydrolysis and beta-amylolysis of debranched starches prepared at different starch concentrations. The degree of hydrolysis (DH) of debranched starches was in range 4.2-4.7 for debranching at 10% starch concentration and debranching at 21% of waxy starch concentration, these values were consistent with the number of branched linkages in amylopectin molecules, estimated to be 4-5% of total glycosidic linkages (Tester, Karkalas and Qi, 2004). However, the DH value was found to be 3.7% for debranching at 21% of PS1 starch concentration (21%DBPS1). The DH values were associated with β-amylolysis limit values. The β-amylolysis limit value is defined as the relative amount of maltose after hydolysis with β-amylase. β-Amylase hydrolyses every second α(1, 4) linkage from the non-reducing ends, thereby producing maltose, but it is blocked by α(1, 6) branch linkage. Thus, the β-amylolysis limits values of 97-99% having DH 4.2-5.0% were considered to be complete debranching, suggesting that whole debranched starches were linear chains. The β-amylolysis limit values of 21%DBPS1 was about 80%, indicating this debranched starch molecule still remained some of branching sites, which could be not hydrolyzed by the β-amylase enzyme. It suggested that debranching at a high solid concentration of starch containing amylose cannot be debranching completely due to the fact that a high strength form amylose gel would limit enzyme diffusion and accessibility to substrate, leading to low level of hydrolysis. As this reason, it cannot be prepare the completed-debranched starch from starches containing high amylose (i.e. PS2 and CN1) at a high concentration in this study.

Table A.2 Degree of hydrolysis and beta-amylolysis limit of debranched starches

sample	DH (%)	β-amylolysis limit (%)
10%DBRD6	4.5 ± 0.25	99.5 ± 2.10
10%DBPS1	4.2 ± 0.17	97.2 ± 2.30
10%DBPS2	4.3 ± 0.19	99.0 ± 1.60
10%DBCN1	4.4 ± 0.37	98.0 ± 4.23
21%DBRD6	4.7 ± 0.32	98.4 ± 1.99
21%DBPS1	3.7 ± 0.19	79.7 ± 2.78

A.3.3 Polymer chain distribution of debranched starch

The molecular size distribution of the debranched starch from four Thai rice varieties; waxy rice (RD6), low amylose rice (PS1), intermediate amylose rice and high-amylose rice (CN1) starches, as determined by HPSEC-MALLS-DRI, are shown in Figure A.1. The DRI elugram of DBRD6 displays 2 peaks at an elution volume (V_i) 17.7-19.0 ml (Fr. II), which corresponded to the long unit chains that interconnect the clusters of amylopectin and V_i 19.0-23.0 ml (Fr.III) representing short unit chain at DP up to approximately 36 (D. A. Koroteeva et al., 2007). The PS1 was a rice starch with a low amylose content, which corresponded to Fr. I (V_i 12.5-16.6 ml) in the HPSEC profile (Figure A.1B). A summary of the chain distribution is shown in Table A.1. The proportions of Fr. I between the PS2 and CN1 were similar. Since the PS2 was a rice starch with intermediate amylose content, it indicated that the amylopectin component of PS2 possessed super-long chain chains that eluted in the same volume (Fr. I) as the amylose. As a result of higher amounts of Fr. I, the amount of the short unit chains of amylopectin component became lower. In addition, the HPSEC profiles displayed an intermediated fraction that eluted at V_i 16.6-17.6 ml.

The PS2 possessed a higher intermediated fraction than CN1 and PS1, respectively. However, the weight ratios of Fr. III/II of all debranched starch were similar (3.0-3.4), suggesting the less structural differences of low molecular weight fraction between all these samples.

To confirm that the debranched samples prepared at high concentration (10%) were completely debranched, the freeze-dried debranched samples were further debranched by isoamylase. As shown in Figure A.1, the chromatograms of the DBRD6 were completely superimposed on the curve of the corresponding debranched starches with dual-debranching, thus showing that the DBRD6 were completely debranched and all chains of DBRD6 were linear. Compare with the dual-debranched starches, the DBPS1, DBPS2 and DBCN1 had a slightly lower proportion of high MW (Fr. I) and slightly higher proportion of low MW (Fr. III) than their corresponding dual-debranched starches. It was probably that amylose containing a few branched molecules was hydrolyzed during second debranching. This suggested that the amylose component possessed very lightly branched molecules with shorter chain length.

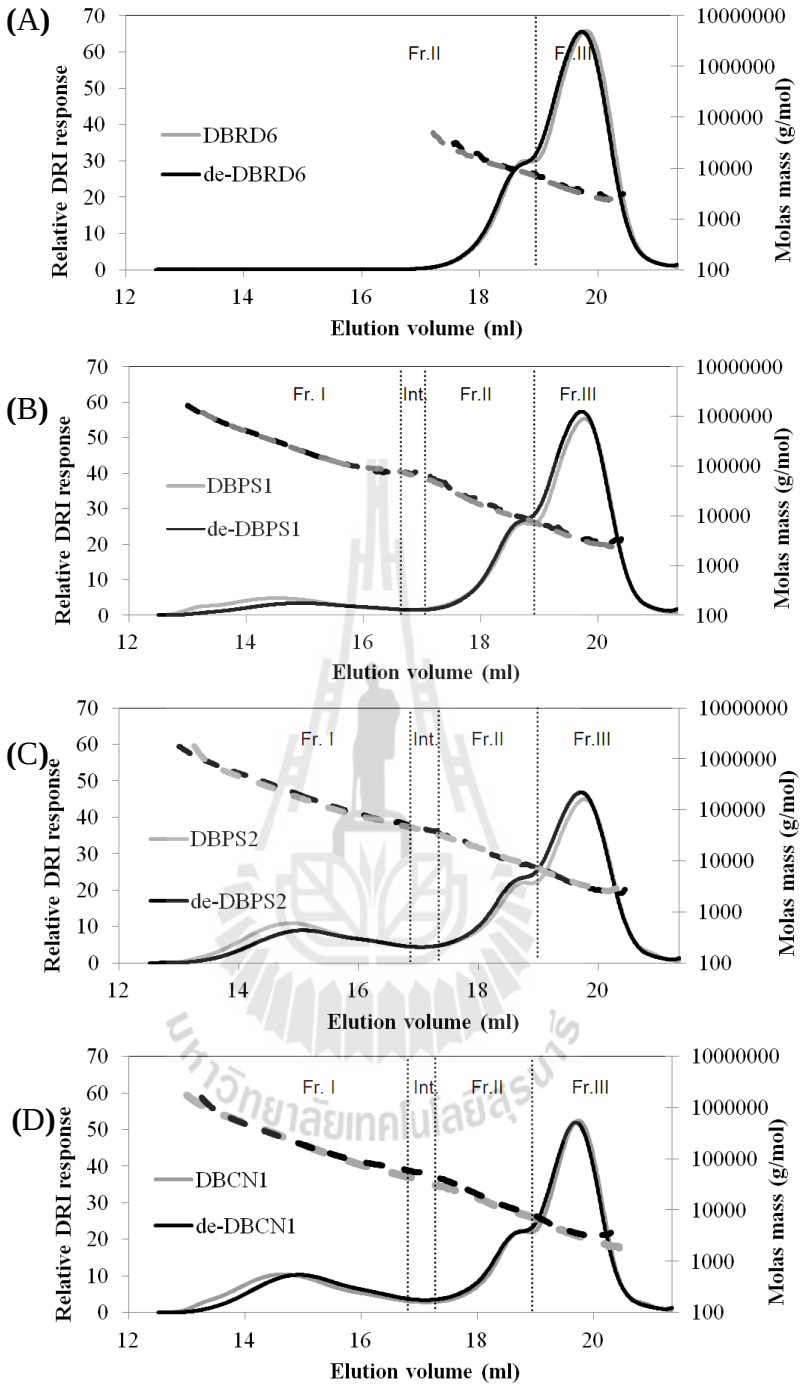

Figure A.1 Molecular size distribution of debranched starches (gray) and dual-debranched starch (black) as determined by HPSEC-MALLS-RI system. The DRI signal profile is shown throughout elution volume. The dash lines represent the molar masses. The chromatograms were divided into fractions as indicated.

Table A.3 Chain-length distribution of debranched starches as determined by HPSEC-MALLS-RI system.

sample	Fr. I	Int.	Fr. II	Fr. III	Ratio Fr. III/Fr. II
DBRD6	0	0	23.2	76.8	3.31
DBPS1	12.0	2.7	20.0	65.3	3.26
DBPS2	23.4	5.1	17.9	53.7	3.00
DBCN1	23.1	3.4	16.5	57.0	3.44

The chain-length distribution of the debranched starches with low DP<70 was analyzed in more detail by HPAEC-PAD. The chromatograms were show in Figure A.2 and A.3 and the change length distribution details were summarized in Table A.4. All debranched starch contained glucans with a high amount of chains of DP 10-24, amounting to >70% of the resolved chain lengths. As comparison the chain length distribution of debranched starches from different rice varieties, debranched starches from starch containing amylose content had a higher proportion of long chains with DP>18 and lower proportion of short chains with DP<12 than waxy starch (DBRD6). In addition, the CN1 with a high amylose contents had a higher proportion of DP 13-24 and lower proportion of short chains with DP 6-9.

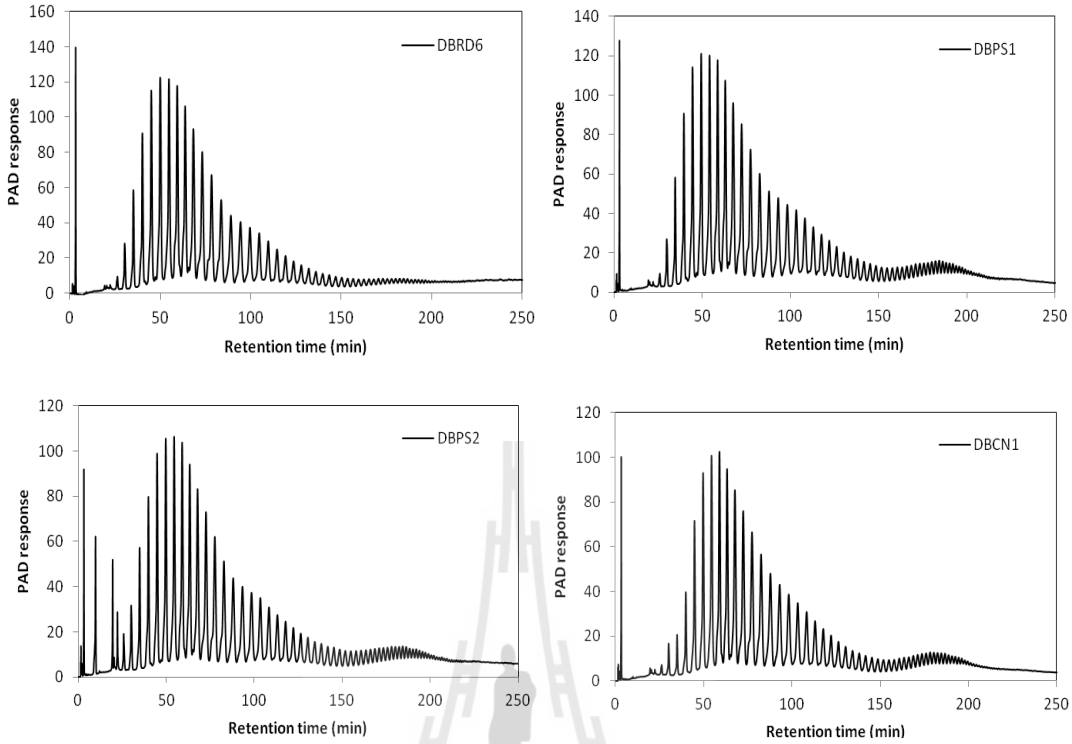

Figure A.2 The chromatograms of debranched starch as determined by by HPAEC-PAD.

Table A.4 The chain-length distribution of the debranched starches as determined by HPAEC-PAD.

sample	DP6-9	DP10-12	DP13-24	DP25-36	DP>37
DBRD6	15.52	23.98	50.38	7.04	3.07
DBPS1	13.31	20.54	50.13	9.68	6.34
DBPS2	14.09	20.41	48.86	9.88	6.76
DBCN1	7.79	20.55	56.18	9.15	6.33

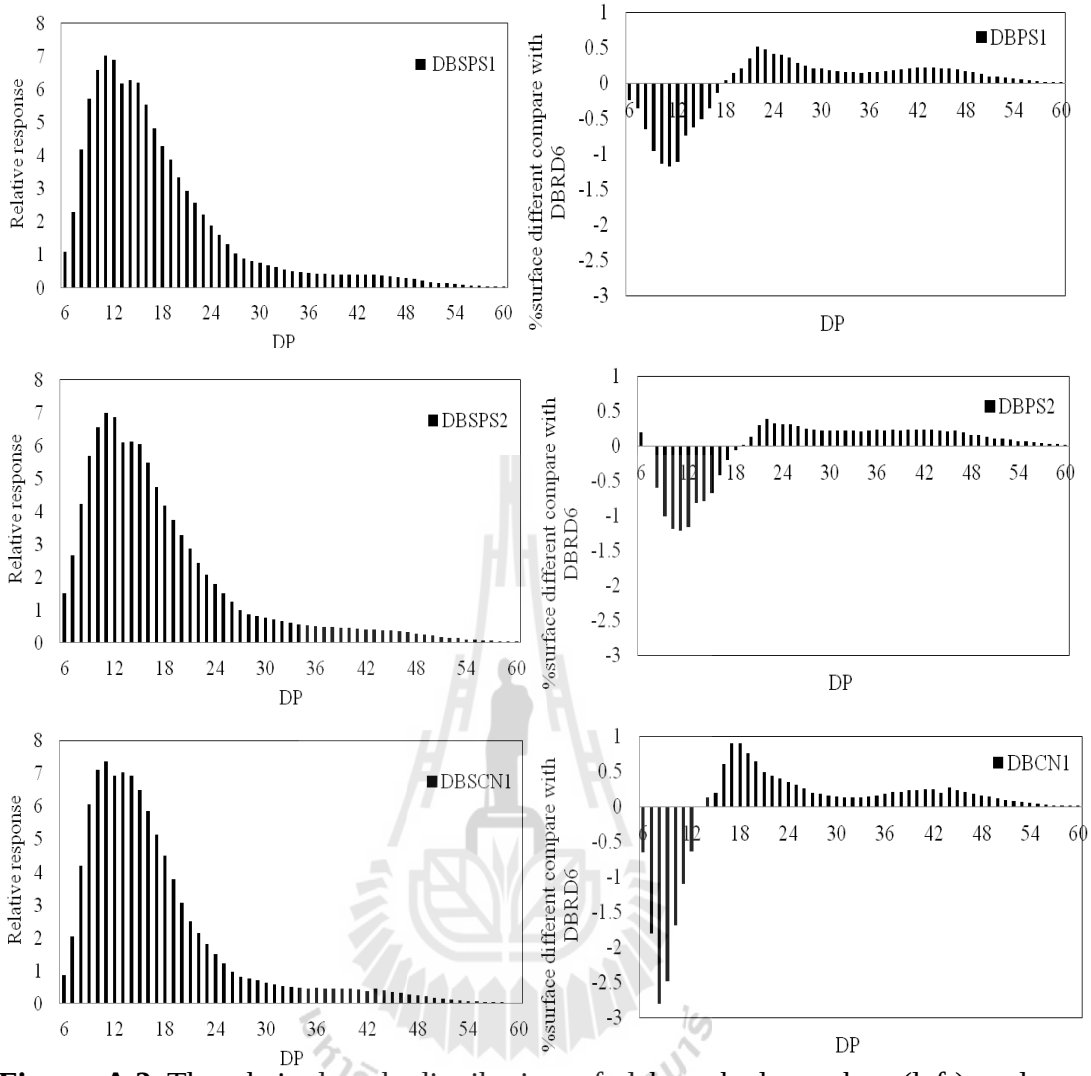

Figure A.3 The chain length distribution of debranched starches (left) and on a relative difference with the DBRD6 profile (right).

A.4 References

Ahmed, N., Maekawa, M., Tetlow, I. J (2008). Effects of low temperature on grain filling, amylose content, and activity of starch biosynthesis enzymes in endosperm of basmati rice. **Australian Journal of Agricultural Research.** 59(7): 599-604.

Buléon, A., Colonna, P., Planchot, V., and Ball, S. (1998). Starch granules: structure and biosynthesis. **International Journal of Biological Macromolecules.** 23(2): 85-112.

Cai, L., Shi, Y-C., Rong, L., and Hsiao, B. S. (2010). Debranching and crystallization of waxy maize starch in relation to enzyme digestibility. **Carbohydrate Polymers.** 81(2): 385-393.

Hoover, R. (2001). Composition, molecular structure, and physicochemical properties of tuber and root starches: a review. **Carbohydrate Polymers.** 45(3): 253-267.

Ju, Z., Hettiarachchy, N., and Rath, N. (2001). Extraction, denaturation and hydrophobic properties of rice flour proteins. **Journal of Food Science.** 66(2): 229-232.

Koroteeva, D. A., et al. (2007). Structural and thermodynamic properties of rice starches with different genetic background Part 1. Differentiation of amylopectin and amylose defects. **International Journal of Biological Macromolecules.** 41(4): 391-403.

Koroteeva, D. A., et al. (2007). Structural and thermodynamic properties of rice starches with different genetic background: Part 1. Differentiation of

amylopectin and amylose defects. **International Journal of Biological Macromolecules.** 41(4): 391-403.

Lawal, O. S., et al. Rheology and functional properties of starches isolated from five improved rice varieties from West Africa. **Food Hydrocolloids.** 25(7): 1785-1792.

Mutungi, C., Rost, F., Onyango, C., Jaros, D., and Rohm, H. (2009). Crystallinity, thermal and morphological characteristics of resistant starch type III produced by hydrothermal treatment of debranched cassava starch. **Starch-Stärke.** 61(11): 634-645.

Ozturk, S., Koksel, H., Kahraman, K., and Ng, P. K. (2009). Effect of debranching and heat treatments on formation and functional properties of resistant starch from high-amylose corn starches. **European Food Research and Technology.** 229(1): 115-125.

Pohu, A., Planchot, V., Putaux, J., Colonna, P., and Buleon, A. (2004). Split crystallization during debranching of maltodextrins at high concentration by isoamylase. **Biomacromolecules.** 5(5): 1792-1798.

Somogyi, M. (1952). Notes on sugar determination. **Journal of Biological Chemistry.** 195(1): 19-23.

Tester, R. F., Karkalas, J., and Qi, X. (2004). Starch—composition, fine structure and architecture. **Journal of Cereal Science.** 39(2): 151-165.

Appendix B

Supplementary data

CHAPTER 3

3.4.3.2 Effect of hydrothermal treatment on crystalline structure

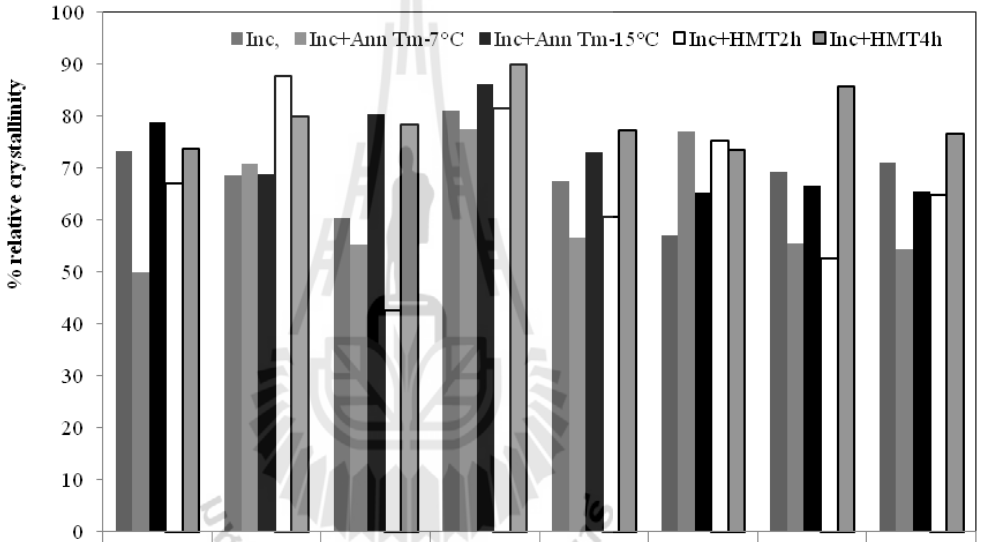

	10%DBR D6-LT	10%DBR D6-HT	21%DBR D6-LT	21%DBR D6-HT	10%DBPS 1-LT	10%DBPS 1-HT	21%DBPS 1-LT	21%DBPS 1-HT
Inc,	73	68	60	81	67	57	69	71
Inc+Ann Tm-7°C	50	71	55	77	56	77	55	54
Inc+Ann Tm-15°C	79	69	80	86	73	65	66	65
Inc+HMT2h	67	88	43	81	61	75	52	65
Inc+HMT4h	74	80	78	90	77	73	86	76

Figure B.1 Crystallinity of the annealed- and HMT-treated samples. Annealing was performed at 7 and 15 °C below the melting temperature of each incubated sample. HMT was performed at 130 °C for 2 and 4 h respectively.

CHAPTER 3

3.4.3.3 Effect of hydrothermal treatment on thermal properties

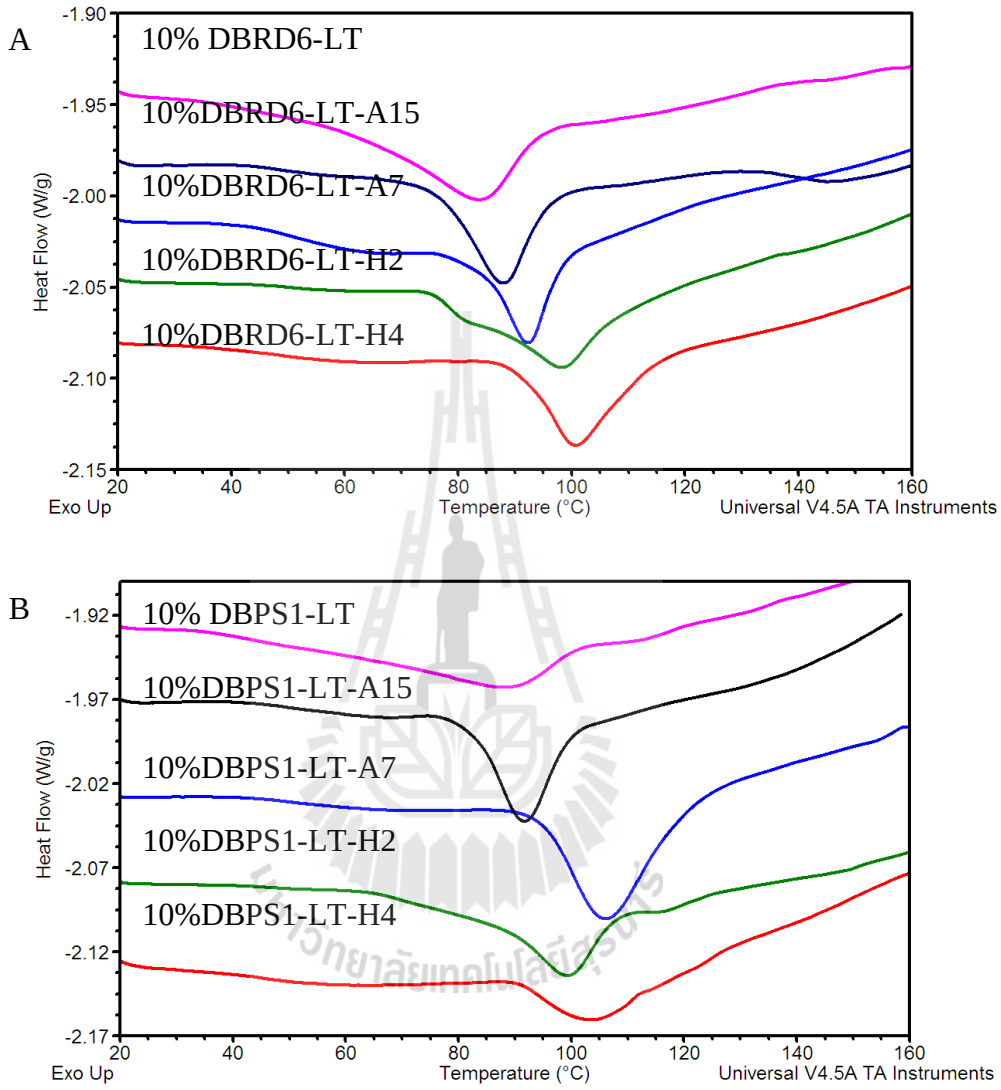

Figure B.2 DSC thermograms of the annealed- and HMT-treated samples obtained from (A) 10% incubated at low temperature (LT) and (B) 10% DBPS1 incubated at low temperature (LT). A7 and A15 represent an annealing at 7 and 15 °C below the melting temperature of each incubated sample respectively. H2 and H4 represent heat moisture treatment at 130 °C for 2 and 4 h respectively.

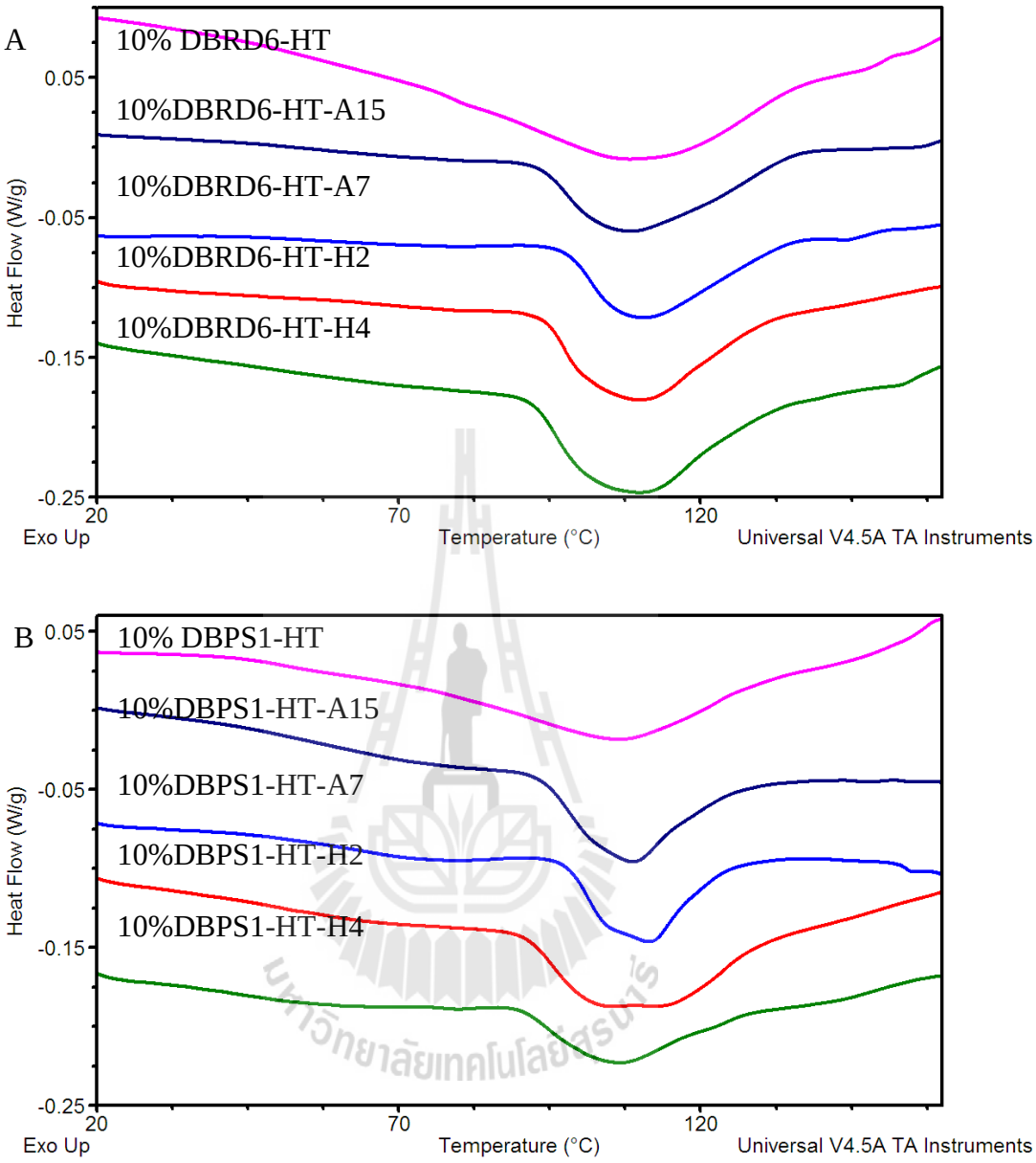

Figure B.3 DSC thermograms of the annealed- and HMT-treated samples obtained from (A) 10%DBRD6 incubated at high temperature (HT) and (B) 10% DBPS1 incubated at high temperature (HT). A7 and A15 represent an annealing at 7 and 15 °C below the melting temperature of each incubated sample respectively. H2 and H4 represent heat moisture treatment at 130 °C for 2 and 4 h respectively

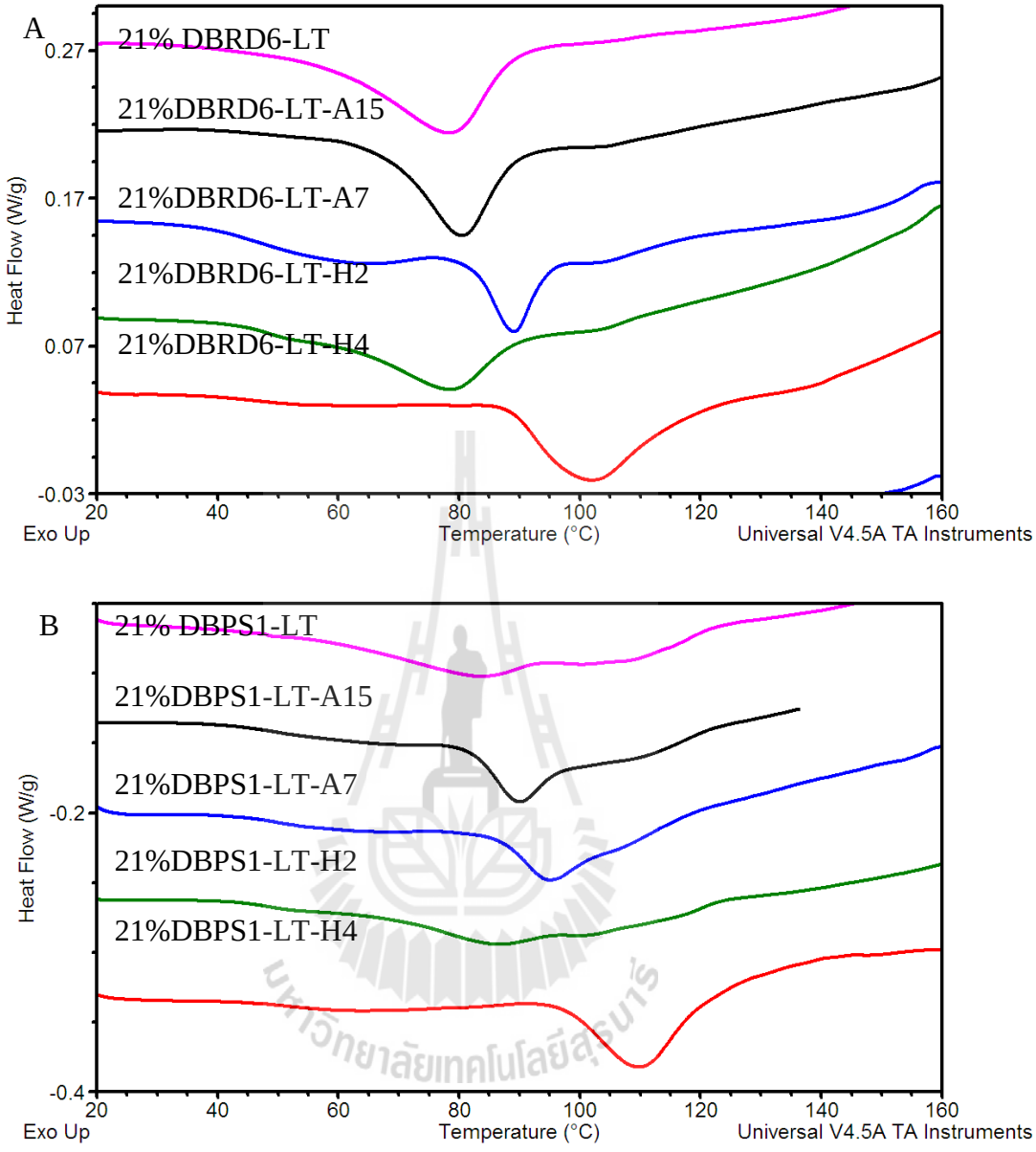

Figure B.4 DSC thermograms of the annealed- and HMT-treated samples obtained from (A) 21%DBRD6 incubated at low temperature (LT) and (B) 21% DBPS1 incubated at low temperature (LT). A7 and A15 represent an annealing at 7 and 15 °C below the melting temperature of each incubated sample respectively. H2 and H4 represent heat moisture treatment at 130 °C for 2 and 4 h respectively

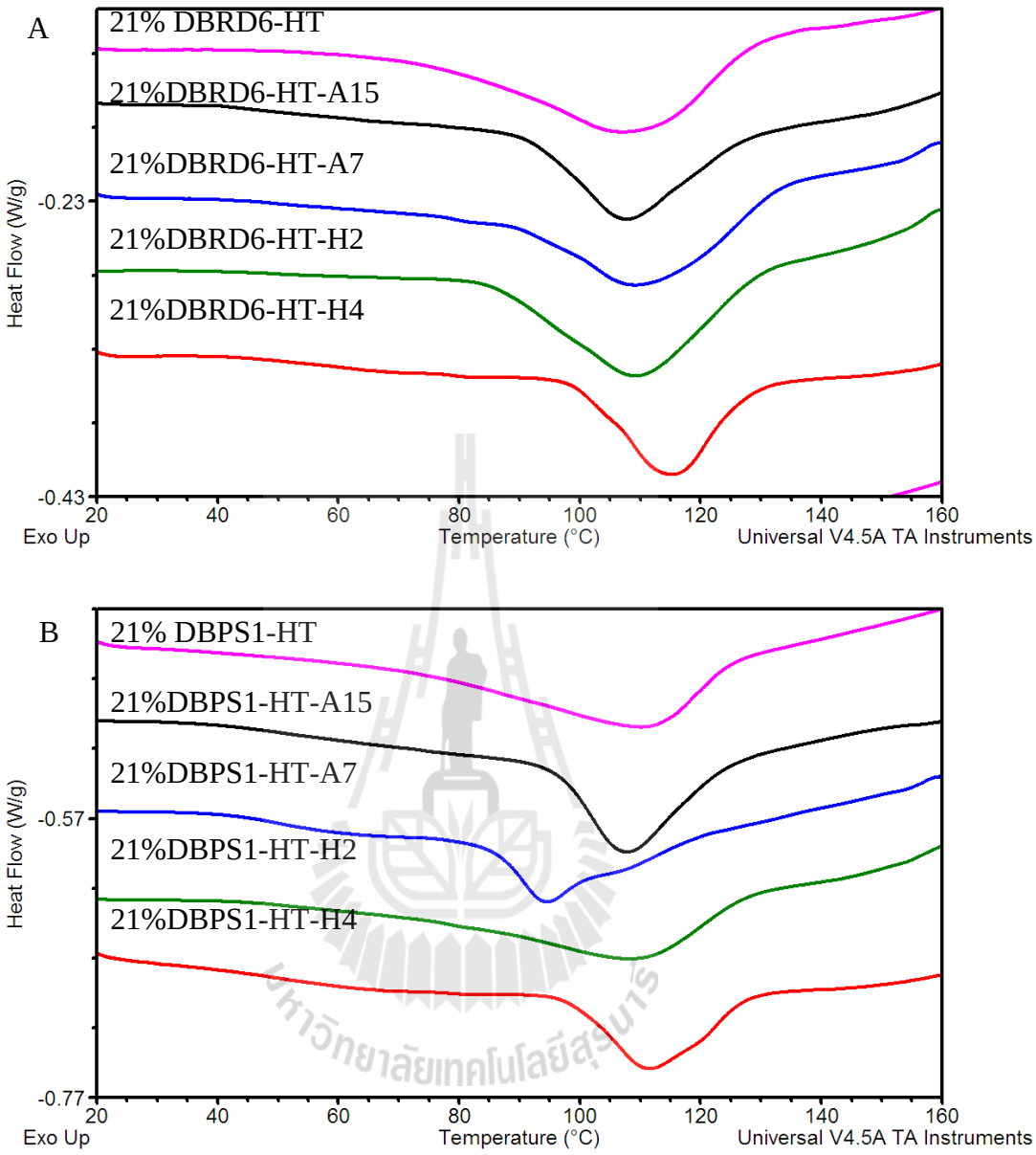

Figure B.5 DSC thermograms of the annealed- and HMT-treated samples obtained from (A) 21DBRD6% incubated at high temperature (HT) and (B) 21% DBPS1 incubated at high temperature (HT). A7 and A15 represent an annealing at 7 and 15 °C below the melting temperature of each incubated sample respectively. H2 and H4 represent heat moisture treatment at 130 °C for 2 and 4 h respectively

CHAPTER 4

4.4.2 Phase behavior and aggregation of rice starches during debranching and incubation

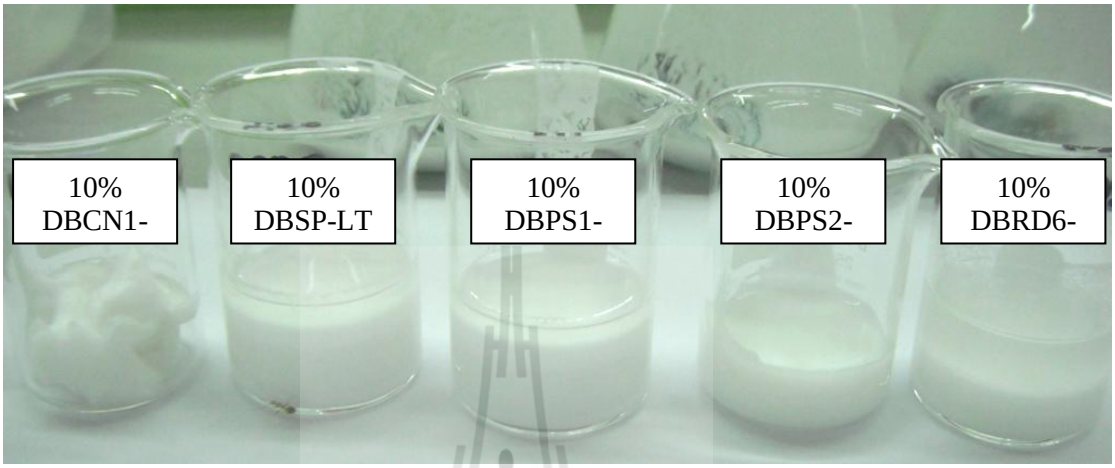

Figure B.6 The syneresis of gels and precipitation observed in the debranched starches after incubation at 25 °C for 24 h.

4.4.3 WAXS data evaluation and crystallinity determination

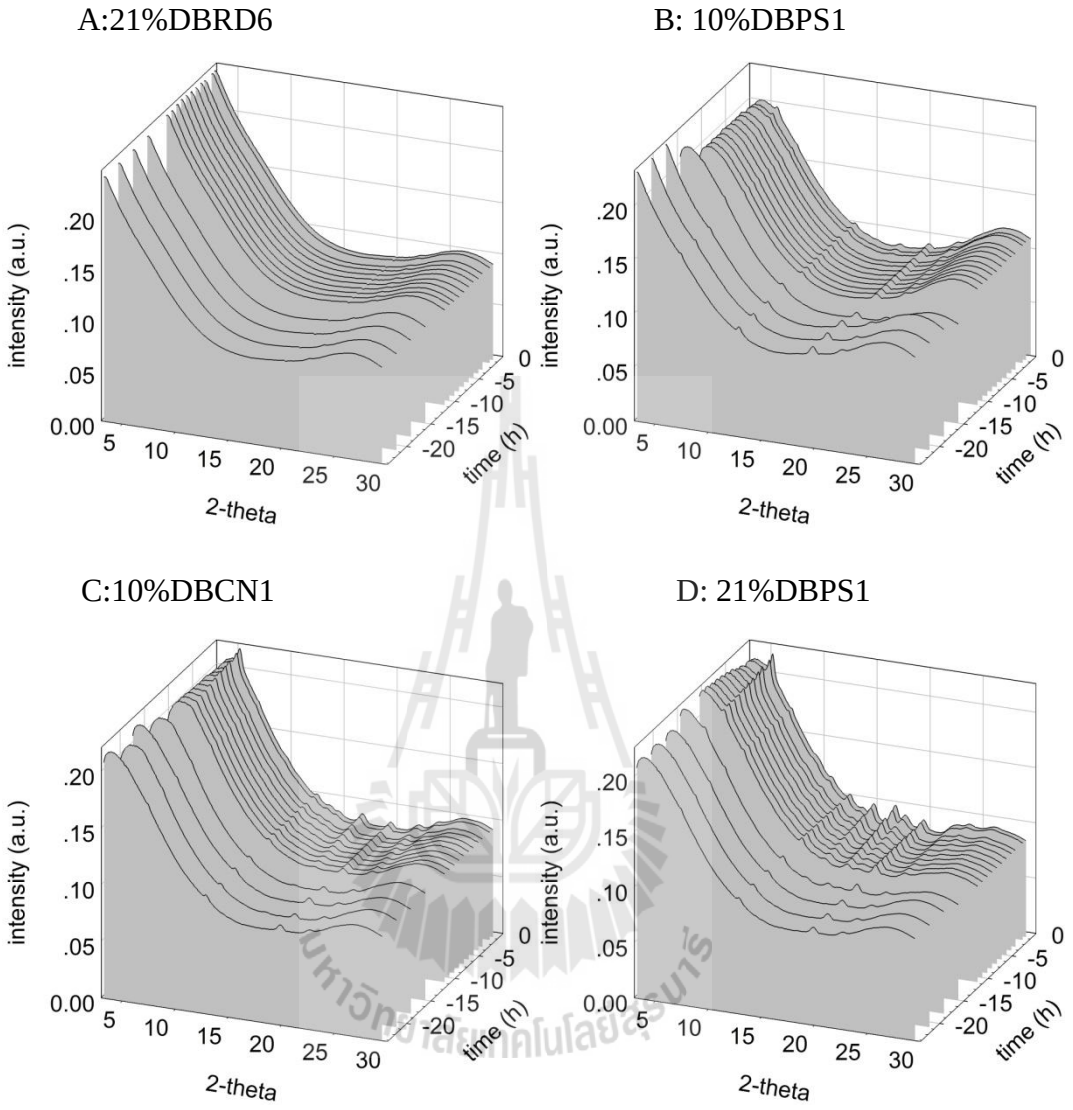

Figure B.7 Change in WAXS patterns as a function of time of the rice starches in aqueous suspension during debranching.

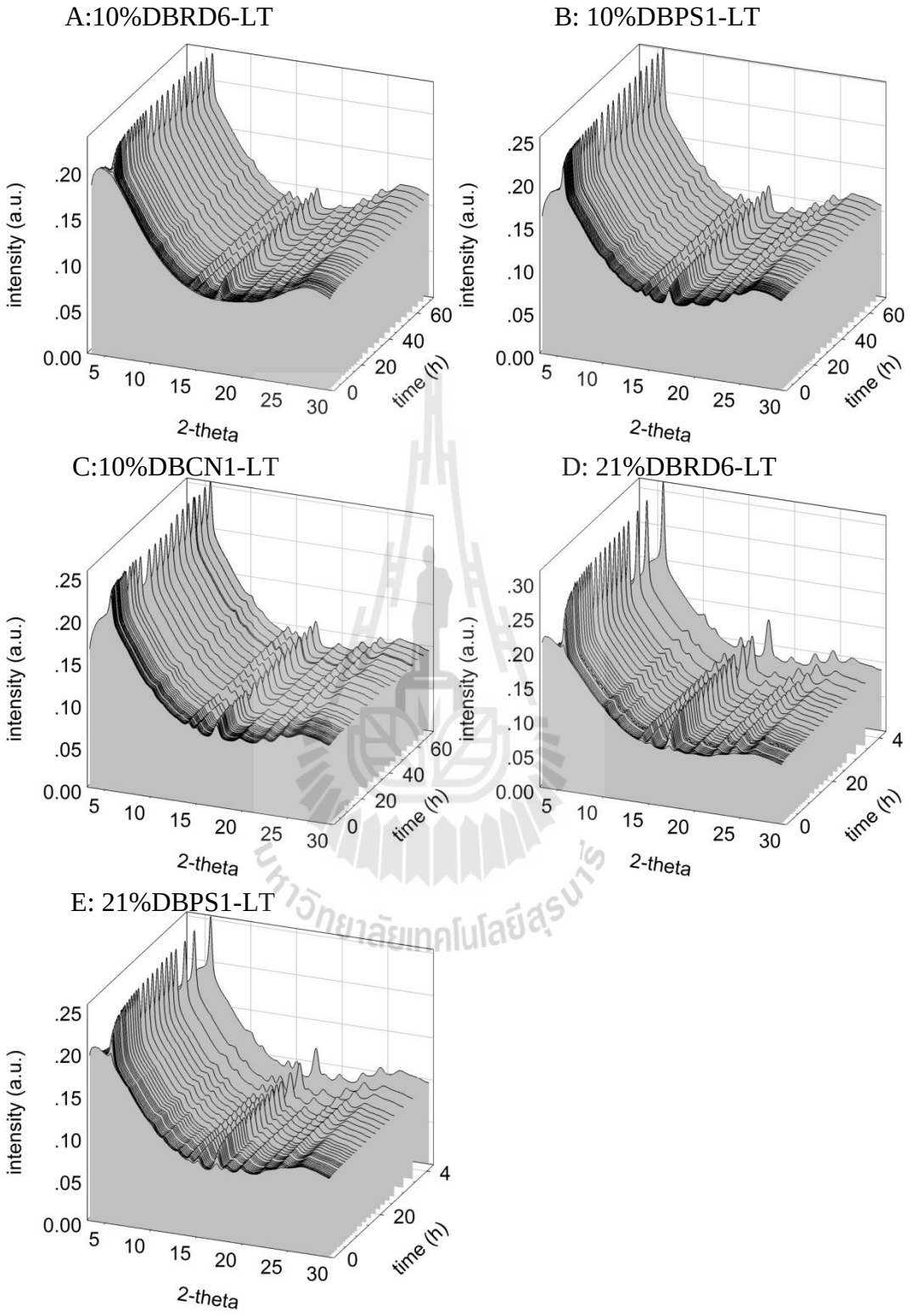

Figure B.8 Change in WAXS patterns as a function of time of the debranched starches in aqueous suspension during incubation at 25 °C.

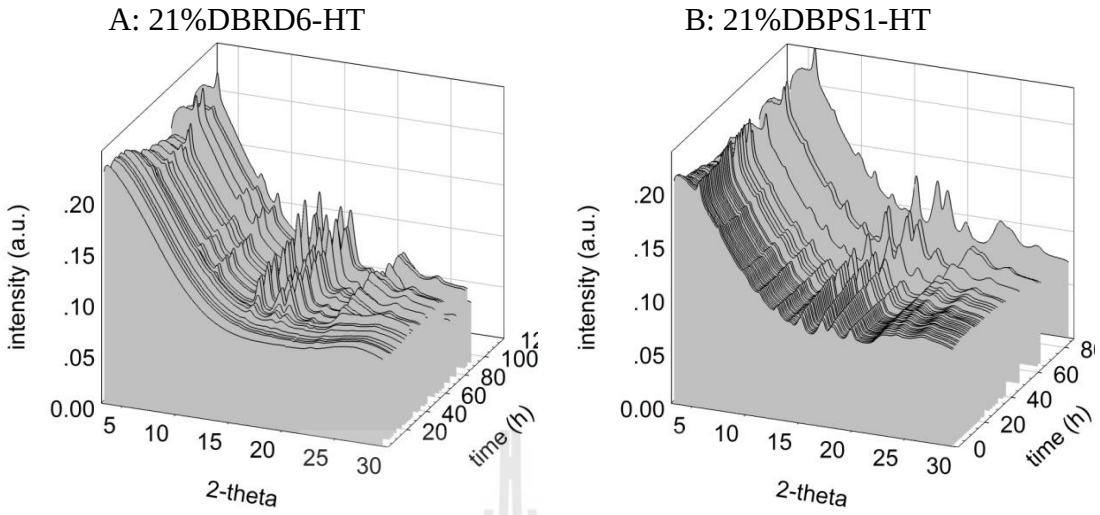

Figure B.9 Change in WAXS patterns as a function of time of the debranched starches in aqueous suspension during incubation at 50 °C.

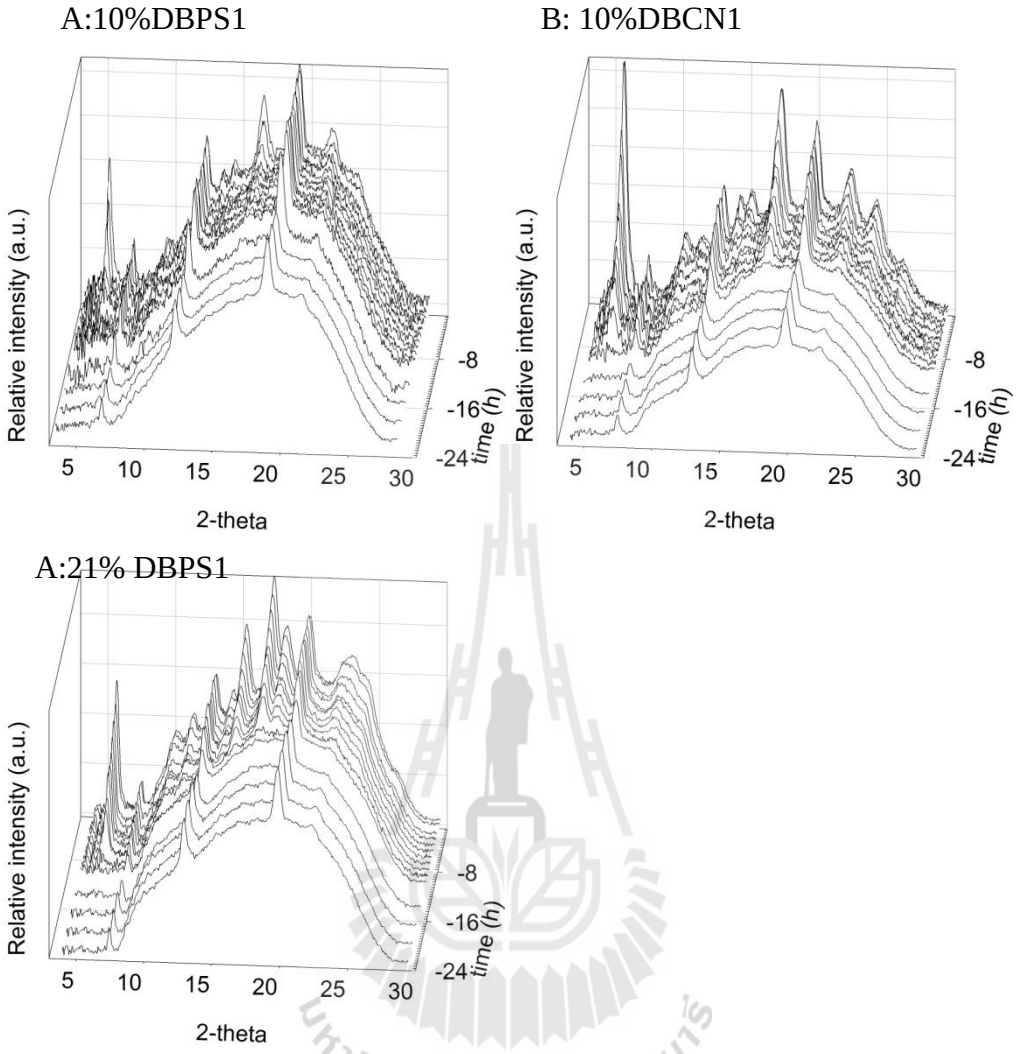

Figure B.10 Change in WAXS patterns as a function of time of the rice starches in aqueous suspension during debranching.

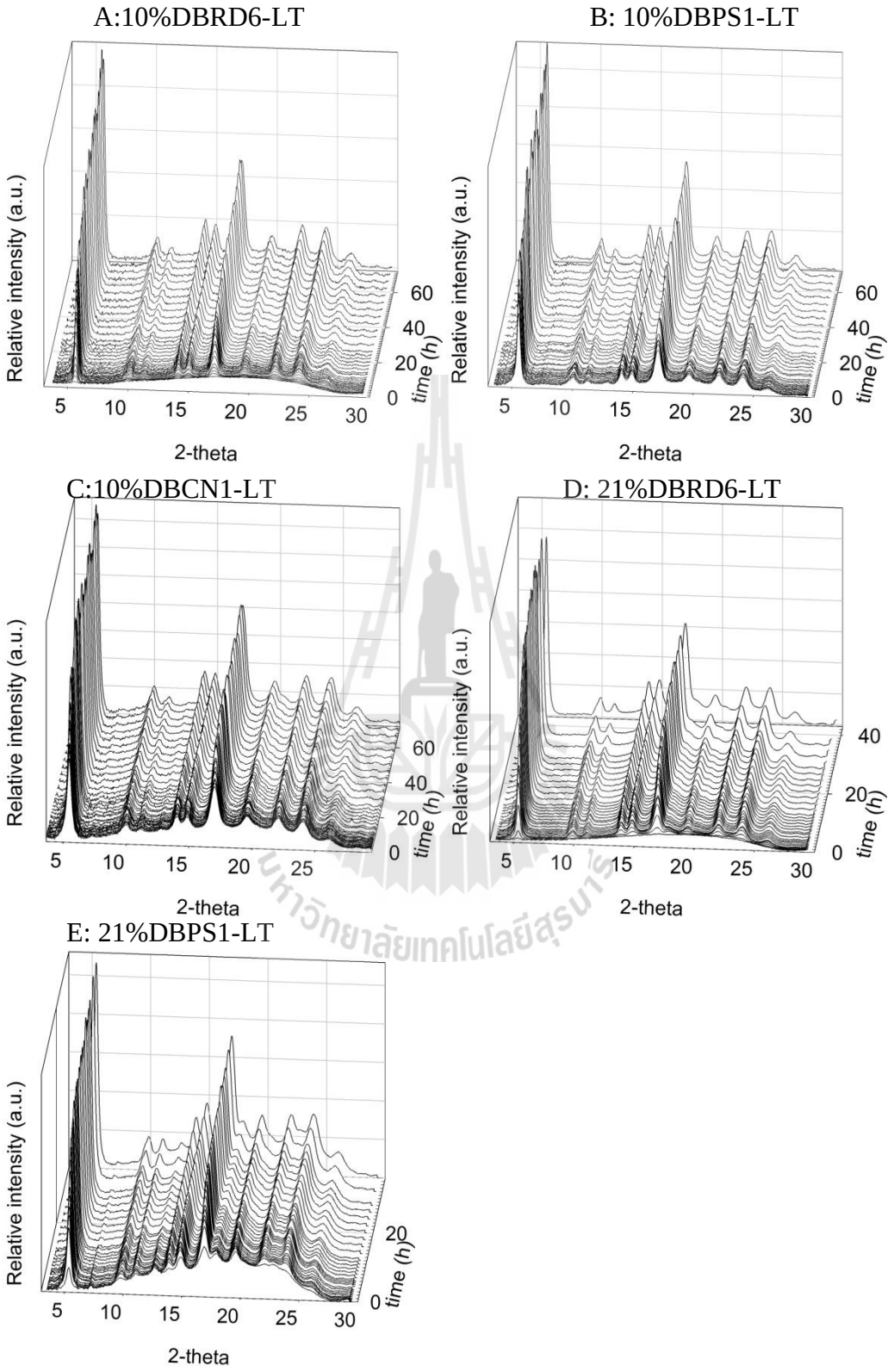

Figure B.11 Change in WAXS patterns as a function of time of the debranched starches in aqueous suspension during incubation at 25 °C.

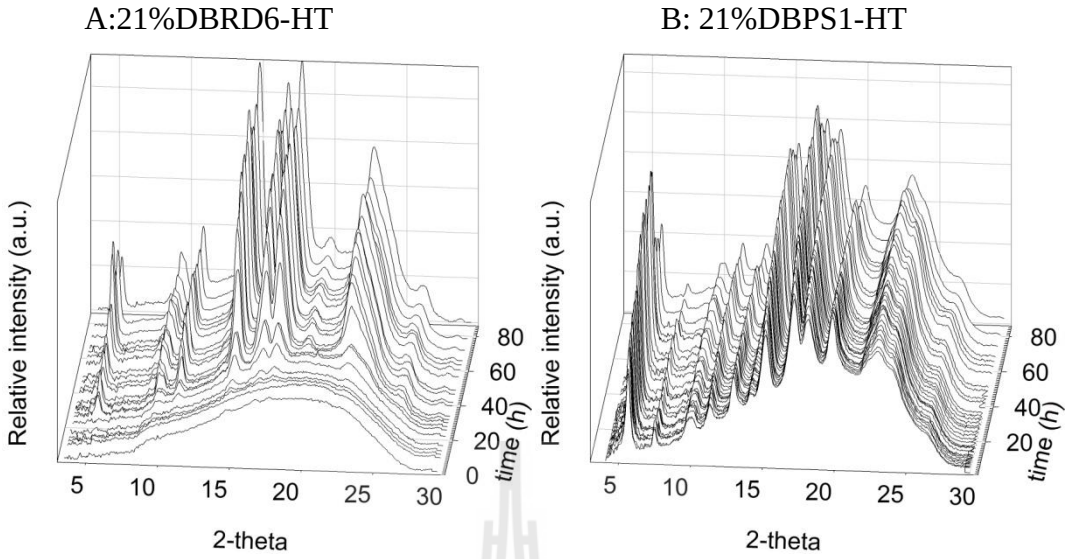

Figure B.12 Change in WAXS patterns as a function of time of the debranched starches in aqueous suspension during incubation at 50 °C.

BIOGRAPHY

Worawikunya Kiatponglarp was born in October 15, 1981 at Suphan Buri, Thailand. She studied for her high school diploma at Rachiniebourana School (1994-1997) and Satrirachinutit School (1998-1999). In 2003, she received the degree of Bachelor of Science (Food Technology) from Suranaree University of Technology. In 2007, she received the degree of Master of Science (Food Technology) from Suranaree University of Technology and she received scholarship from Thailand Research Fund (TRF) through TRF-MAG to financially support for her research. In 2010-2013, she received the Royal Golden Jubilee Scholarship from Thailand Research Fund to study for the degree of Doctor of Philosophy (Food Technology) at Suranaree University of Technology. During her Ph.D study, she obtained opportunities to present her research works including at Starch Update 2013: The 7th International Conference on Starch Technology (Bangkok, November 21-22th 2013), The RGJ-Ph.D. Congress XIV (Pattaya, Chonburi, April 5-7th 2013) and XIX International Starch Convention (Moscow, Russia, September 18-20th, 2012). She also published her researched work under the title "Crystallization and chain reorganization of debranched rice starches in relation to resistant starch formation" in Journal Carbohydrate Polymers (volume 122, page 108–114) in 2015.